# Effects of Stationary Wake on Turbine Blade Heat Transfer in a Transonic Cascade

by

Jamie Harold Hale

Thesis submitted to the Faculty of the
Virginia Polytechnic Institute and State University
in partial fulfillment of the requirements for the degree of

Master of Science

in

Mechanical Engineering

APPROVED:

Dr. Thomas E. Diller, Co-Chairman

Dr. Wing F. Ng, Co-Chairman

Dr. J. A. Schetz

April 1996

Blacksburg, Virginia

**Key Words:** Stationary Wake, Turbine Blade Heat Transfer, Transonic Cascade

# Effects of a Stationary Wake on Turbine Blade Heat Transfer in a Transonic Cascade

by

Jamie H. Hale

Dr. Thomas E. Diller and Dr. Wing F. Ng, Co-Chairmen

Mechanical Engineering

(ABSTRACT)

The effects of a wake generated by a stationary upstream strut on surface heat transfer to turbine blades were measured experimentally. Time-resolved and unsteady heat flux measurements were made with Heat Flux Microsensors (HFM) at three positions on the suction surface and one position on the pressure surface of a turbine blade. The experiments were conducted on a stationary cascade of blades for heated runs at transonic conditions

Methods for determining the adiabatic wall temperature and heat transfer coefficient are presented and the results are compared to computer predictions for these blades. Heat transfer measurements were taken with new HFM-6 insert gages. A strong influence on the heat transfer coefficient was seen from the relative position of the strut with respect to the leading edge of the test blades. As the strut approached the leading edge of the blade the heat transfer increased by 15% at gage location 2 on the suction surface. The largest increase in the heat transfer coefficient was seen on the pressure surface. Results at this location show a 24% increase in the overall heat transfer coefficient for one of the strut locations. The values obtained for the heat transfer coefficients for the no strut case did not compare well with computer predictions. The results did support the experimental results of other researchers, however. The fast time

response of the HFM illustrated graphically an increase in the frequency energy between the 0-10 kHz range when the strut was located near the leading edge of the instrumented blade. The heat flux turbulence intensity ($Tu_q$) was defined as another physical quantity important to turbine blade heat transfer, but no conclusions could be drawn from the results as to how this value compares to the turbulence intensity.

# Acknowledgments

First and foremost, I would like to thank the good Lord above for giving me strength to continue my education and knowledge to do so. Many times throughout this experience I know he has taken many burdens from my shoulders and carried them himself as he done so many years ago when he died on the cross so that we each may be saved.

I would also at this time like to thank the professors that comprised my committee- Dr. Diller, Dr. Schetz, and Dr. Ng. A special thanks to Dr. Ng and Dr. Diller my two co-chairmen. Dr. Diller was especially helpful during the analysis and writing stages showing great patience and a wealth of knowledge. Dr. Ng provided the guidance and support I needed, and was always there to ask the question "Why?" to keep me thinking.

I would like to thank the workers at Buchanan #1 Preparation Plant for allowing me the opportunity to work with them, and for showing me things about mechanical engineering that I would have never learned by reading books.

I would like to thank all the members on the team- Loren Johnson, David White, Tibor Kiss, Melissa Fasold, Angela Wesner, Terry Reid, Andrew Nix, and David Holmberg. I want to especially thank Loren and David. Loren was always there to help with the tunnel cleaning operations. David was always there to provide guidance in the analysis process and also in the data collection stages by helping to set-up and run the tunnel. A very special thank you must go to Dr. Todd Ninnemann. Todd was unique person. He was the one person who was always there when I had a problem and needed help. In most instances I need not ask for help he was there offering it. His generosity and friendship will not be forgotten.

I would like to thank the machinists in the Mechanical Engineering Machine Shop-- Mr. Johnny Cox, Mr. Jerry Lucas, Mr. Tim Kessinger, and Mr. Bill Songer. They were always there to lend advice, and allowed me to the use their facilities without

question. A special thanks to Timmy and Bill. I consider the time spent with these two individuals invaluable. They were there to discuss other interests in my life besides research, and I truly value their friendship.

I would like to thank my two room-mates Mr. Thomas Bunch and Mr. David Coppenhaver. They have truly been more than room-mates. They were always there offering assistance and have become great friends over the past few years.

I would also like to thank Mr. Gregory Harrell whom I met during my graduate studies here at Virginia Tech. He has become a special friend, and someone who I have grown to admire and respect.

I also wish to thank my parents, Harold and Loretta, for all of there prayers and continuous support throughout my engineering studies. My mother was always there showing her love for me and giving me the confidence I needed. My father has provided an excellent role model for me to follow, and I hope that one day I can fill his shoes.

Finally I want to thank my future wife, whom I look forward to marrying and growing old with. For the past two years, she has been my inspiration. She has endured both the good times and the bad times through this process, and has made this endeavor a worthwhile experience.

# Table of Contents

# List of Illustrations

# List of Tables

# List of Symbols

| | |
|---|---|
| a | free-stream strain rate |
| b | wake half width |
| c | blade chord |
| $C_D$ | drag coefficient |
| $c_p$ | specific heat |
| d | hot-wire diameter |
| D | diameter or thickness of strut |
| $E_T$ | Temperature sensor output |
| $E_q$ | heat flux sensor output |
| Fr | Frossling number- $Nu/Re^{1/2}$ |
| g | gravity |
| $G_q$ | gain heat flux |
| $G_T$ | gain temperature |
| h | heat transfer coefficient |
| I | current |
| k | thermal conductivity |
| l | hot-wire length |
| L | length scale |
| M | Mach number |
| Nu | Nusselt number- $hc/k$ |
| P | pressure |

| | |
|---|---|
| Pe | Peclet number |
| Pr | Prandtl number |
| q" | heat flux |
| r | recovery factor |
| R | universal gas constant |
| Re | Reynolds number-$U_\infty c/v$ |
| $R_{op}$ | resistance |
| S | gage sensitivity |
| t | time |
| T | temperature |
| $T_l$ | Integral time scale |
| $T_{aw}$ | adiabatic wall temperature |
| $T_R$ | recovery temperature |
| $T_{REF}$ | reference temperature |
| $Tu$ | Free-stream velocity turbulence intensity |
| $Tu_q$ | heat flux turbulence intensity |
| $\bar{u}$ | mean velocity |
| $u'$ | fluctuating component of velocity |
| $U$ | velocity |
| V | hot-wire voltage |
| x | axial position |

**Greek symbols**

| | |
|---|---|
| $\alpha$ | temperature coefficient of resistance |
| $\beta$ | coefficient of thermal expansion |
| $\gamma$ | specific heat ratio |

| | |
|---|---|
| $\lambda$ | Integral length scale |
| $\mu$ | dynamic viscosity |
| $\nu$ | kinematic viscosity |
| $\rho$ | density |
| $\rho(\tau)$ | auto-correlation coefficient |

**Superscripts**

| | |
|---|---|
| - | averaged |

**Subscripts**

| | |
|---|---|
| 1 | gage location 1 |
| 2 | gage location 2 |
| 3 | gage location 3 |
| 4 | gage location 4 |
| *a* | based on free-stream strain rate *dU/dx* |
| *amb* | based on ambient conditions |
| *atm* | based on atmospheric conditions |
| *c* | based on centerline or chord |
| *ds* | downstream |
| *f* | based on film temperature |
| *fs* | free-stream |
| *g* | based on gas temperature |
| *m* | based on mean temperature |
| *op* | operating conditions |

| | |
|---|---|
| $r$ | based on reference temperature |
| $s$ | static conditions |
| $sur$ | based on surface conditions |
| $t$ | total conditions |
| $us$ | upstream |
| $w$ | based on wire temperature |
| $\infty$ | free-stream conditions |

# Chapter 1.0

# Introduction

## 1.1 Background

There is a continuing drive to design more efficient and reliable gas turbine engines. This corresponds to an interest in understanding the flow characteristics in the turbine section. To achieve a more efficient gas turbine many researchers have looked into increasing the thrust to weight ratio of the gas turbine. While all of this looks good on paper, several things must be taken into consideration for this to become a reality. By increasing the thrust in the engine, it also increases the thermal loads that the turbine blade experiences. A reduction in the weight implies that lighter and stronger materials must be developed. Therefore, for these improvements to become a reality a better understanding of the flow field and the thermal stresses on the various components must be recognized.

An important tool in understanding the thermal stresses in a gas turbine engine is heat transfer. Heat transfer along a turbine blade is influenced by various effects such as turbulence, pressure gradient, surface temperature, temperature ratio, and periodic changes of the inflow. In an attempt to characterize and quantify the individual effects, theoretical and experimental work on gas turbine blades has been conducted in recent years. This work has led to a better understanding in the thermal stresses on the various components in the engine. This in turn allows better cooling schemes to be implemented.

A key area of interest inside the turbine engine is the turbine blades. The blades are subjected to high thermal loads which in turn increases the thermal stresses within the blade. Therefore, it is important to understand how to implement cooling schemes which will optimize the engine. Many of the advances in the design of highly efficient gas turbines over the last 40 years have been made possible with the

introduction of blade cooling schemes which were first implemented in the early 1950's. The use of cooled blades has made possible an increase of the gas turbine inlet temperature and hence an increase in the engine output power, thrust and thermal efficiency. Sieverding, (1982) states the use of blade cooling in conjunction with improved blade materials has allowed the gas temperature to increase from $\cong$ 1050 K in the 1950's to $\cong$ 1800 K in the 1980's.

As mentioned earlier several factors influence the heat transfer along a gas turbine blade. One of particular interest is turbulence. Several types of turbulence can be generated in a turbine engine. Two particular types of interest are turbulence from the combustor and turbulence generated by an upstream blade row or an inlet guide vane. The turbulence from the combustor can be simulated by free-stream turbulence. It is known from previous studies that free-stream turbulence augments the heat transfer to turbine blades. The wakes generated by an upstream blade row or inlet guide vane can be divided into three distinct areas of interest. The first is the unsteady flow created by the passing wake. The second is the wake defect and turbulence generated, and the third are shocks created by the disturbance. Several studies have been conducted studying these different effects on heat transfer to circular cylinders and turbine blading. However, little has been done in the area of measuring the time-resolved heat flux due to varying the turbulence intensity on an actual, modeled turbine blade in a heated transonic wind tunnel. One such study was conducted by Johnson and Diller, (1995). Several studies have been conducted studying the effect turbulence generated by an upstream airfoil or bar on the heat transfer to circular cylinders and turbine blades. However, little work has been done in the area of measuring the time-resolved heat flux due to turbulence generated by an upstream airfoil on an actual, modeled turbine blade in a heated transonic wind tunnel.

## 1.2 Objective

Tests in an actual turbine engine pose several problems, therefore, many researchers conduct tests in stationary turbine cascades. Virginia Tech constructed a unique cascade wind tunnel in order to simulate the flow conditions that exist in an actual turbine engine. The wind tunnel test facility provides a Reynolds number, a Mach number, and temperature ratios equivalent to those a turbine engine would encounter.

The focus of this thesis is the detailed measurement of the time-resolved heat flux due to a disturbance from an airfoil placed upstream in the inlet flow of the cascade using new and unique instrumentation. Heat transfer measurements were taken simultaneously at four different locations along the turbine blade. Three of these locations were along the suction side of the blade, while the fourth was located on the pressure side of the blade. The stationary upstream airfoil was located in a plane parallel to the cascade. Several locations of the airfoil were studied to determine the affect of the turbulence and velocity defect from the wake on the heat transfer. The experimental data can be compared with computer predictions and other experimental data. Hopefully, this process will bring a better understanding to blade surface heat transfer.

The heat flux and surface temperature of the blade were measured using new thin-film gages. One of the unique features of this particular gage is the ability to procure two independent measurements (heat flux and surface temperature). The Heat Flux Microsensor (HFM-6) manufactured by Vatell Corporations was used to acquire the time-resolved and unsteady heat transfer measurements. A more detailed description of the Heat Flux Microsensor is given in chapter 2.0. Chapter 2.0 also provides a background review into turbulence and the effects it has on heat transfer. Chapter 3.0 provides a description of the experimental set-up. The wind tunnel test facility is described in great detail. The experimental procedure is depicted in chapter

4.0. The experimental data is examined in chapter 5.0 and some final recommendation are made in chapter 6.0.

# Chapter 2.0

# Background

## 2.1 Turbulence

Most of today's technical society has a basic understanding of what turbulence is. However, it is not easy to define all the characteristics that make it up. According to "The Random House College Dictionary", turbulence means: a commotion or wild disorder, a violent irregular motion. This definition is a little general. A better definition was proposed by Taylor and Von Karman (1937). "Turbulence is an irregular motion which in general makes its appearances in fluids, gaseous or liquid, when they flow past solid surfaces or even when neighboring streams of the same fluid flow past or over one another." According to their definition, the flow has to satisfy some type of irregularity.

Due to this irregularity it is impossible to describe turbulent motion as a function of space and time coordinates alone. However, this irregular motion can be described by the laws of probability. it is possible to find discrete average values for quantities, such as velocity, pressure, and temperature.

All of this leads to the following definition given by Hinze (1959). He states the following: "Turbulent fluid motion is an irregular condition of flow in which the various quantities show a random variation with time and space coordinates, so that statistically distinct average values can be discerned."

As stated earlier, turbulence can be generated by friction forces at fixed walls or by the flow of layers of fluids with different velocities past or over one another. A distinct difference exists in the two types of turbulence. The turbulence generated by fixed walls is designated as "wall turbulence" and the turbulence generated in the absence

of walls is known as "free or free-stream turbulence". The focus in this paper will be on free-stream turbulence.

As pointed out earlier, average values of quantities exist with respect to time and space. These average values are thought to exist because of two reasons: 1). At a given point in the turbulent domain a distinct pattern is repeated more or less regularly in time. 2). At a given instant a distinct pattern is repeated more or less regularly in space, (Hinze, 1959). Therefore, to describe turbulent motion in detail, the idea of the scale of the turbulence can be introduced. A certain scale in time (integral time scale) and a certain scale in space (integral length scale) can be defined. The extent of these particular scales will be resolved by the dimensions of and the velocities within the test facility.

The integral time and length scale help to characterize turbulence by its space and time dimensions, but are inadequate in describing the violence of the motion. The mean flow velocity is not a measure of the violence. A good measure of this violence is the fluctuations in the velocity with respect to the mean flow velocity. The flow velocity component and a fluctuating component that changes in magnitude with respect to time.

$$u = \bar{u} + u' \qquad [2.1]$$

With this definition of the flow velocity, the violence or intensity of the flow can be defined. With the assumption of isotropy the following ratio is used to define the turbulence intensity,

$$Tu = \frac{\sqrt{\overline{u'^2}}}{\bar{u}} \qquad [2.2]$$

where $Tu$ is the turbulence intensity, $\bar{u}$ is the mean flow velocity and $u'$ is the fluctuating component.

The integral length scale, $\lambda$, can be determined from the auto-correlation coefficient,

$$\rho(\tau) = \frac{\lim_{t_o \to T} \frac{1}{t_o} \int_0^{t_o} u'(t)u'(t+\tau)dt}{\frac{1}{t_o} \int_0^{t_o} [u'(t)]^2 dt} \qquad [2.3]$$

where t is the time delay, T is the time record length and $u'$ is the fluctuating component of the velocity. The integral time scale $T_1$, can defined as

$$T_1 = \int_0^{\infty} \rho(\tau)d\tau \qquad [2.4]$$

The integral length scale equals the integral time scale multiplied by the mean flow velocity.

$$\lambda = T_1 \bullet \bar{u} \qquad [2.5]$$

## 2.2 Previous Studies

This section is broken into three areas. The first area to be covered is the effect of free-stream turbulence on heat transfer rates on flat plates and cylinders. The next topic to be discussed is the effect of free-stream turbulence upon heat transfer to turbine blading. The turbulence in this area was generated by some type of rotating disk or squirrel cage device to simulate a passing wake. The last topic discussed in this section is the effect of free-stream turbulence and wake characteristics on the heat transfer on a gas turbine blade. The turbulence and wakes were created by grids, cylindrical rods, and airfoils.

### 2.2.1 Flat Plate and Cylinders

In gas turbine blade design, the prediction of stagnation region heat transfer is critical due to the fact that the heat transfer rate is usually highest in this region. Flow in the stagnation region of a turbine blade can be simulated by a circular cylinder in crossflow.

Kestin (1966) summarizes previous studies on the effects of free-stream turbulence on heat transfer rates for flat plates and circular cylinder experiments. He concluded that heat transfer rates are affected by turbulence both locally and through an effect on the flow configuration. The most pronounced effect is on a laminar boundary layer near the stagnation point on a circular cylinder. He also showed there was very little effect from free-stream turbulence on a turbulent boundary layer for both flat plate and circular cylinder experiments. He concluded that heat transfer rates seem to increase with increasing levels of turbulence intensity. He was not confident that there was a consistent relationship between free-stream turbulence and heat transfer.

Kestin studied in detail the heat transfer through a laminar boundary layer on a circular cylinder. One particular area of interest was the stagnation point. Kestin (1971) was able to develop an equation for the heat transfer as a function of free-stream turbulence intensity answering the question he posed to himself years earlier.

$$Fr = \frac{Nu}{\mathrm{Re}^{1/2}} = 0.945 + 3.48\left[\frac{Tu\,\mathrm{Re}^{1/2}}{100}\right] - 4.0\left[\frac{Tu\,\mathrm{Re}^{1/2}}{100}\right]^2 \qquad [2.6]$$

Other studies were conducted on the effect of free-stream turbulence on heat transfer on the stagnation point of a circular cylinder. Lowery and Vachon (1975) conducted experiments using a circular cylinder with a laminar boundary layer. They showed that small increases in turbulence intensity (0.4-1.2) greatly increased the local rate of heat transfer. At the stagnation point on the circular cylinder they attained a 20% increase in

the heat transfer due to changes in the turbulence intensity. Their studies also showed that in the laminar boundary layer regime , the effect of increased turbulence intensity was to increase the local heat transfer by a constant factor which was dependent on the turbulence intensity and relatively independent of the Reynolds number over the range of their investigation. The augmentation factor was found to be approximately 1.6 for a turbulence intensity level of approximately 14%. Lowery and Vachon proposed a new equation for the Frossling number.

$$Fr = \frac{Nu}{\mathrm{Re}^{1/2}} = 1.010 + 2.624\left[\frac{Tu\,\mathrm{Re}^{1/2}}{100}\right] - 3.070\left[\frac{Tu\,\mathrm{Re}^{1/2}}{100}\right] \qquad [2.7]$$

More recent studies of the effect of normal vortices on stagnation region heat transfer were conducted by VanFossen and Simoneau (1987). They concluded that stagnation region heat transfer was a maximum where turbulent fluctuations were a minimum, and the heat transfer was minimal where the flow velocity was minimal. They also concluded that the boundary layer exhibited laminar characteristics in the presence of free-stream turbulence. O'Brien and VanFossen (1985) results were 10 to 15% lower than previous studies on stagnation point heat transfer of Lowery and Vachon. They concluded that heat transfer at the stagnation point of a cylinder in crossflow was augmented by free-stream turbulence, but a Reynolds number effect was also present. This Reynolds number effect was also observed by Smith and Kuethe (1966). Therefore, for a specific value of $Tu\mathrm{Re}^{1/2}$, if the Reynolds number is low and the turbulence intensity is relatively high a lower Frossling number will be produced. Gundappa and Diller (1991) concluded that as the turbulence intensity increased, the heat transfer increased at the stagnation point and in the boundary layer over the front of the cylinder.

Researchers are constantly striving to simulate actual engine operating conditions. One such study was conducted by Glezer et al. (1994). The equation for the Frossling

number developed by Lowery and Vachon was modified through their research. The new equation is given by

$$Fr = \frac{Nu}{\mathrm{Re}^{1/2}} = 1.01\left(\frac{\mathrm{Re}_D}{100000}\right)^{0.05} + 0.058\left(Tu\,\mathrm{Re}_D^{1/2}\right)^{0.65} \qquad [2.8]$$

### 2.2.2 Rotating rigs

Many researchers are constantly trying to emulate the unsteadiness of the flow within a turbine engine. To accomplish this they have placed rotating rigs in the flow. This accounts for the changes in flow angle and for the cutting of the wake by the passing rotor blades as found in the real rotating system.

Simoneau and Simon (1993) have provided an examination on the research conducted using rotating rigs to simulate appropriate flow conditions. The focus of their work was to provide an examination of the state of the art in the prediction of convective heat transfer in a turbine engine. From their research they determined that the most comprehensive research came from Dunn and his colleagues (Dunn and Stoddard, 1979; Dunn and Hause, 1982; Dunn, 1984; Dunn et al., 1984a,b; Dunn and Chupp, 1988; Dunn et al., 1989; Dunn, 1990).

Many other researchers have made significant contributions in this area also. Bayley and Milligan (1977) used a squirrel cage type generator to study the effect of turbulence on heat transfer to turbine blading. They concluded that the squirrel cage generator produced mainstream flow entering the cascade which possessed separately variable turbulence intensities and distinct frequency characteristics. They also showed that the low turbulence heat transfer on the blade followed trends associated with laminar boundary layers, especially on the pressure surface and along the leading edge. The last major conclusion drawn from their work was that the average heat transfer coefficient along the blade increased with increasing intensities. Bayley and Priddy (1981) also conducted research using a squirrel cage type generator to study the effect of free-stream

turbulence intensity and frequency on heat transfer on turbine blades. They concluded that the rotating squirrel cage technique was a reliable way of applying controlled disturbances to a cascade of turbine blades. They confirmed the previous study of Bayley and Milligan that perturbations applied to the flow enhance the heat transfer to all but the downstream half of the suction surface. They also confirm that the effect of the turbulence is greatest on the pressure surface and along the suction surface leading edge. They concluded that definite effects existed due to the frequency of the wakes passing, and a Reynolds number effect on the augmentation of heat transfer to the blade existed.

Doorly et al. (1985) developed a rotating rig to establish the correct relative unsteady velocity flow that the rotor would encounter. They accomplished this by rotating a row of cylindrical bars at the correct velocity in front of the cascade. This simulated the wake-passing and flow unsteadiness produced by nozzle guide vanes (NGV's) in an actual turbine engine. From their work they concluded that the primary effect of wake-passing on a laminar boundary layer was to promote an early, unsteady transition. This in turn caused an increase in the mean heat transfer and severe periodic fluctuations in the heat transfer rate.

Dullenkopf et al. (1991) used a rotating rig to study the effect of incident wake conditions on the mean heat transfer to an airfoil. Their results demonstrated a strong effect of unsteady wakes on the suction side boundary layer and heat transfer, whereas the pressure did not show similar behavior. The overall effect of the wakes was considerably less significant, and the increase in the heat transfer remained relatively constant over the majority of the pressure surface. Another important conclusion drawn from their research was the fact that the wake frequency is a dominant factor in the mean heat transfer.

Lui and Rodi (1994) used a squirrel cage type generator to create unsteady wakes and made various surface pressure and heat transfer measurements in a linear turbine cascade. They were able to deduce several conclusions from their work. The boundary layer remained laminar along the whole pressure surface under the influence of the unsteady wakes. The boundary layer was transitional on the suction surface under the

influence of unsteady wakes, and the starting point of the transition region moved upstream with increasing wake passing frequency. This caused an increase in the turbulence which in turn augmented the mean heat transfer on the suction and pressure surface. This was found to be true even though the pressure surface exhibited a laminar boundary layer.

Han et al. (1993) used a spoked wheel type generator with rods to study the influence of an unsteady wake on the heat transfer to a gas turbine blade. They concluded hat the inlet velocity (or Reynolds number) had the biggest effect on the heat transfer coefficient. For a given wake Strouhal number, the heat transfer coefficient was most influenced by a wake with a higher inlet flow velocity and higher rod speeds as opposed to lower velocities and lower rod speeds. This indicated the importance that the Reynolds and Strouhal numbers have in predicting the heat transfer coefficient under unsteady flow conditions.

Dullenkopf and Mayle (1994) incorporate previous studies on the effects of turbulence and moving wakes on laminar heat transfer in turbine blading into a correlation for the Nusselt number of cylinders and airfoils. The correlation assumes a constant free-stream strain rate,

$$a = {du}/{dx} \qquad [2.9]$$

with varying levels of turbulence intensity. The corrected Nusselt number for these flows was given by

$$Nu_a = \frac{h}{k}\sqrt{\frac{v}{a}} \qquad [2.10]$$

and the turbulence parameter is represented by

$$Tu_a = \frac{u'}{\sqrt{av}} \qquad [2.11]$$

where $u'$ is the turbulence intensity. They produced the following correlation for the cylinder and airfoil data studied.

$$Nu_a \, \mathrm{Pr}^{-0.37} = 0.571 + 0.0125 Tu_a \left\{ 1 + \frac{1.8}{\left[ 1 + \left( Tu_a / 20 \right)^3 \right]} \right\} \qquad [2.12]$$

They conducted an alternate investigation and developed a correlation that also incorporates the scale (integral length scale) of the turbulence. The new turbulence parameter was defined as

$$Tu_\lambda = \frac{Tu_a \sqrt{L_a}}{\left[ 1 + 0.004 {L_a}^2 \right]^{6/12}} \qquad [2.13]$$

where $L_a$ is the corrected dimensionless integral length scale. The following equation was used to calculate $L_a$

$$L_a = \frac{L}{\sqrt{v/a}} \qquad [2.14]$$

where L is the integral time scale.

The new correlation is described by the following equation

$$Nu_a \, \mathrm{Pr}^{-0.37} = 0.571 + 0.01 \cdot Tu_\lambda \qquad [2.15]$$

### 2.2.3 Grid and Airfoil disturbances

It is well known that convective heat transfer rates are affected by unsteady flow in a gas turbine engine. It is equally hard to discern the type of unsteadiness and its affect on the heat transfer rate. Two types of unsteadiness are of major importance. The first results from random fluctuation in the flow known as turbulence, and the latter is a more ordered fluctuation that could result from an upstream row of rotor blades or nozzle guide vanes. Both of these parameters have been argued to be of significant importance in characterizing an unsteady flow. The frequency of the fluctuations when they are of large amplitude has a distinct effect on the heat transfer as shown by Bayley and Milligan (1977), but the intensity or violence of the flow has emerged as the most important parameter of an unsteady flow.

Two basic methods are used to generate turbulence. One is by using grids to disrupt the flow and the other is by placing a cylindrical rod or airfoil in the flow to cause a disturbance. First, the case of varying the turbulence by employing grids or screens will be discussed.

Corrsin (1963) gives a detailed description on the effects different grid mesh sizes versus isotropy and boundary layer analysis. Uberoi and Wallis (1969) report on the effect of grid geometry on the decay of turbulence by measuring the energy spectra of the longitudinal, $\overline{u^2}$, and lateral, $\overline{v^2}$, turbulent velocity fluctuations. They also concluded that large scale turbulent eddies produce an anisotropic effect. Tan-Aticaht et al. (1982) studied the effects of free-stream turbulence with screens and grids. They determined the level, structure, and decay of turbulence generated by these devices was partially dependent upon their shear instabilities. They also concluded that the performance of the

screen was dependent upon characteristics such as the incoming flow velocity, turbulence level and energy spectra.

Young and Han (1988) studied the effect of jet grid turbulence on flat plate turbulent boundary layer heat transfer. The screen used produced levels of free-stream turbulence up to 15%. They attempted to distinguish how turbulence intensity, velocity (Reynolds number), and temperature affected the heat transfer from a flat plate.

Galassi et al. (1991) studied the effects of inlet turbulence scale on turbine blade surface heat transfer in a linear turbine cascade by placing a grid in the upstream flow. They developed methods of controlling the turbulent integral scale and microscale lengths at certain free-stream turbulence levels. They proved that the turbulent integral length scale corresponded closely with the outside diameter of the grid tubing. They also showed that high levels of free-stream turbulence could be produced which augmented the heat transfer to the blade surface.

Johnson and Diller (1995) studied the effects of grid generated free-stream turbulence on surface heat transfer to turbine blading. They measured time-resolved and unsteady heat flux at two locations on the suction surface, and saw a 15% increase in the average heat transfer coefficient from a 1 to 8 % increase in the turbulence intensity.

Now, a brief discussion will follow on turbulence and velocity defects by cylindrical rods and airfoils, and their effects on heat transfer. Wittig et al. (1988) studied the influence of wake flow on local heat transfer. A straight blade profile was placed in the inlet flow of the cascade. The blade was positioned at various axial distances from the entrance plane of the cascade, and was traversed in discrete steps in a plane parallel to the entrance of the cascade. This was an attempt to model the unsteadiness in an actual turbine engine, but it should be noted that changes in the flow vector, which occurs in the rotating system, were not present in this quasi steady model. They showed that a strong influence on the heat transfer coefficient on the relative position of the airfoil with respect to the test blade existed. They also concluded that there was a big increase in the heat transfer at large axial distances and lower heat transfer

rates were experienced at shorter axial distances except for a certain region around the stagnation point.

Wittig et al. (1986) showed that the wake generated by an airfoil causes an increase in the turbulence level as well as a decrease in the mean flow velocity. They also concluded the wake affects on the heat transfer to the pressure surface were of significant magnitude.

Suzuki and Suzuki (1991) studied heat transfer characteristics of a flat plate turbulent boundary layer disturbed by a circular cylinder. They conducted wall heat transfer measurements at a fixed streamwise location for different cylinder diameters and for different clearance ratios. They concluded that the most important factor in these experiments was the clearance-to-diameter ratio.

Engber and Fottner (1995) conducted pressure and thin-film measurements on a linear turbine cascade. They varied the following parameters in the inlet flow: inlet angle, Reynolds number, and turbulence intensity. They simulated oncoming wakes by placing a cascade of cylindrical bars in the flow which produced turbulence intensity levels up to 4%. They concluded that the impingement of the wake on the stagnation point caused the disappearance of a laminar separation bubble on the suction side and shifted the transition region upstream.

Through the tremendous amount of research, scientists are beginning to understand the flow in a turbine engine. They are using this data to develop prediction codes of the flow in a turbine blade passage. One of the first codes developed was the STAN5 code by Crawford and Kays (1976) which is a boundary layer analysis. This code was later modified by Gaugler (1981). There also exists a quasi-three-dimensional Navier-Stokes computer code. This code was modified by Chima (1986) such that heat transfer analysis could be conducted. Many other codes have been developed with each having its finer points. Two of these codes are TSONIC developed by Katsanis (1969) and MERIDL developed by Katsanis and McNally (1977).

The preceding has been a brief synopsis of the studies conducted in the past several years in the study of heat transfer. The intent of this thesis is to add to this collection by studying the affects that a wake defect and varying turbulence intensity has on heat transfer. This experiment is similar to the one conducted by Wittig et al. (1988). However, this experiment measures the actual time-resolved heat flux and does not use a finite element code to predict the heat transfer.

## 2.3 Heat Flux Microsensor

Throughout the study of heat transfer many advances have been made in the measurement techniques. One method of measuring heat flux is to measure the rate of change in the material temperature, and with proper modeling the heat flux that produced the temperature variation can be resolved. One of the most popular methods is assuming the material behaves as a one-dimensional semi-infinite model substrate (Diller, 1993). This method is used in short duration tests where this type of assumption is valid.

An extension of the above method was the creation of new thin-film gages on metal turbine blades that measured heat flux [Doorly and Oldfield, (1986,1987)]. The principle on which these gages would operate is as follows. A thermal resistance layer would be placed on a substrate to measure transient surface temperatures. If the properties of the two materials are known along with a suitable analytical model, then the surface heat flux could be determined.

The design of a new heat flux gage made from microfrabication techniques is discussed by Hager et al. (1991a). These gages consist of two separate sensors which are in close proximity of one another. This allows the simultaneous measurement of heat flux and surface temperature at a particular location.. The passive heat flux gage (Heat Flux Sensor) measures the temperature difference across a thin thermal resistance layer (Figure 2.1), and an active temperature gage (Resistance Temperature Sensor) measures the temperature from the sensor electrical resistance. The Heat Flux Sensor is contrived of many thermocouple pairs connected in a series configuration which amplifies the heat

flux signal to a measurable level. The output signal is also directly proportional to the heat flux. These particular gages have the capability of measuring high heat flux levels at a very fast response times. The Heat Flux Microsensor has a continuous readout due to its fast time response of 10μs (100 kHz), Holmberg and Diller (1995).

Several researchers have used thin film gages in their experiments and the results have been published in various papers. Hayashi et al. (1989) made transient heat transfer measurements in Mach 4 supersonic flow. Holmberg et al. (1994) measured the heat transfer from a shock wave through a turbine blade passage and confirmed a fast time response of 100 kHz. Simmons, Hager, and Diller, (1991) measured time-resolved surface heat flux with the HFM due to free-stream turbulence at a stagnation point on a circular cylinder. Johnson and Diller (1995) measured the heat transfer due to effect of free-stream turbulence in a stationary turbine cascade. Several other ideas on the uses of the HFM are mentioned by Hager et al. (1991b)

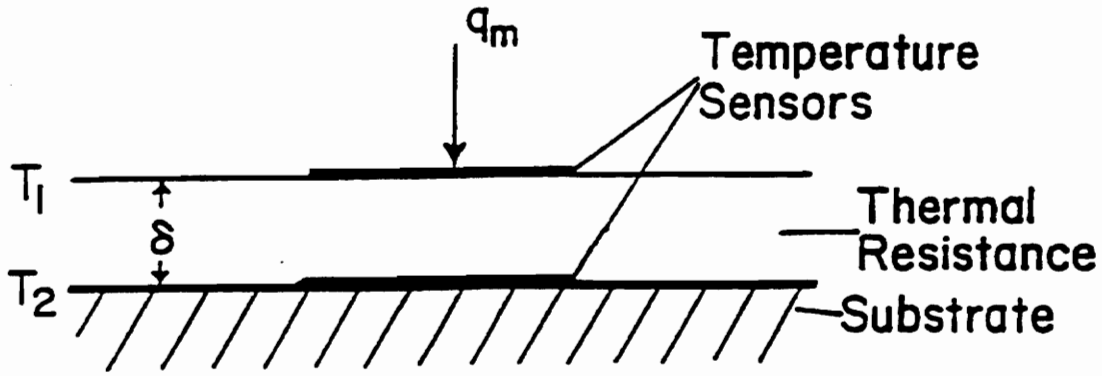


Figure 2.1 Cross Section of Resistance Layer of HFM

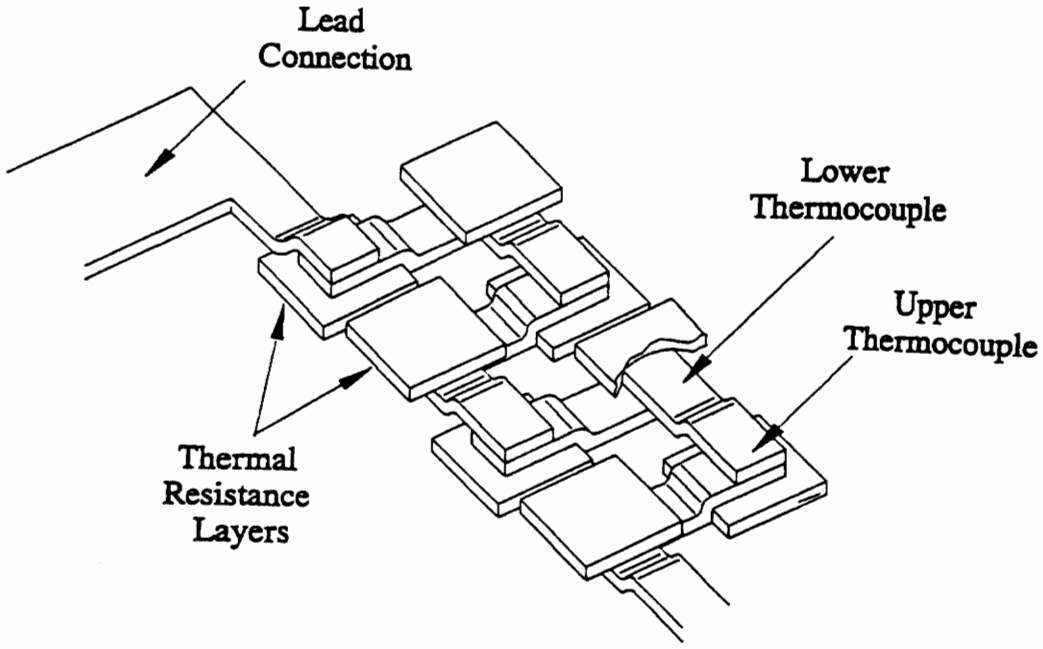


Figure 2.2 Detailed Section of HFM Thermopile

# Chapter 3.0

# Experimental Setup

This chapter provides an overview of the facilities used to conduct these experiments. Specifically discussed are the following: low speed tests, wind tunnel facility, test section and cascade, traversing mechanism, upstream survey, hot-wire probe, leading edge survey, HFM-6, and Kulite.

## 3.1 Low Speed Tests

The main objective of this experiment was to traverse a total pressure probe downstream of a strut at various axial locations and to map out the wake produced. With the aid of theoretical calculations and the experimental data a strut producing a particular wake width could be established. This strut would later be used in the transonic cascade wind tunnel..

The low speed tests were conducted in the 3 ft. Open Test Section Instructional Tunnel in the Aerospace and Ocean Engineering department at Virginia Tech (Figures 3.1 and 3.2). This tunnel is an open-throat return type. The tunnel is of circular cross section with the diameter varying from 39 inches to 72 inches. It is constructed of two layers of 1/4-inch waterproof plywood. There are four sets of straightening vanes located in the corners of the test facility (refer to Figure 3.1). They function to divert the air in the tunnel and to maintain a uniform velocity throughout the test section. This particular facility is a fan driven unit. The power is supplied by a 35 horsepower,D.C. motor (General Electric, 230 volts). The desired speed control is

# Low Speed Test Facility

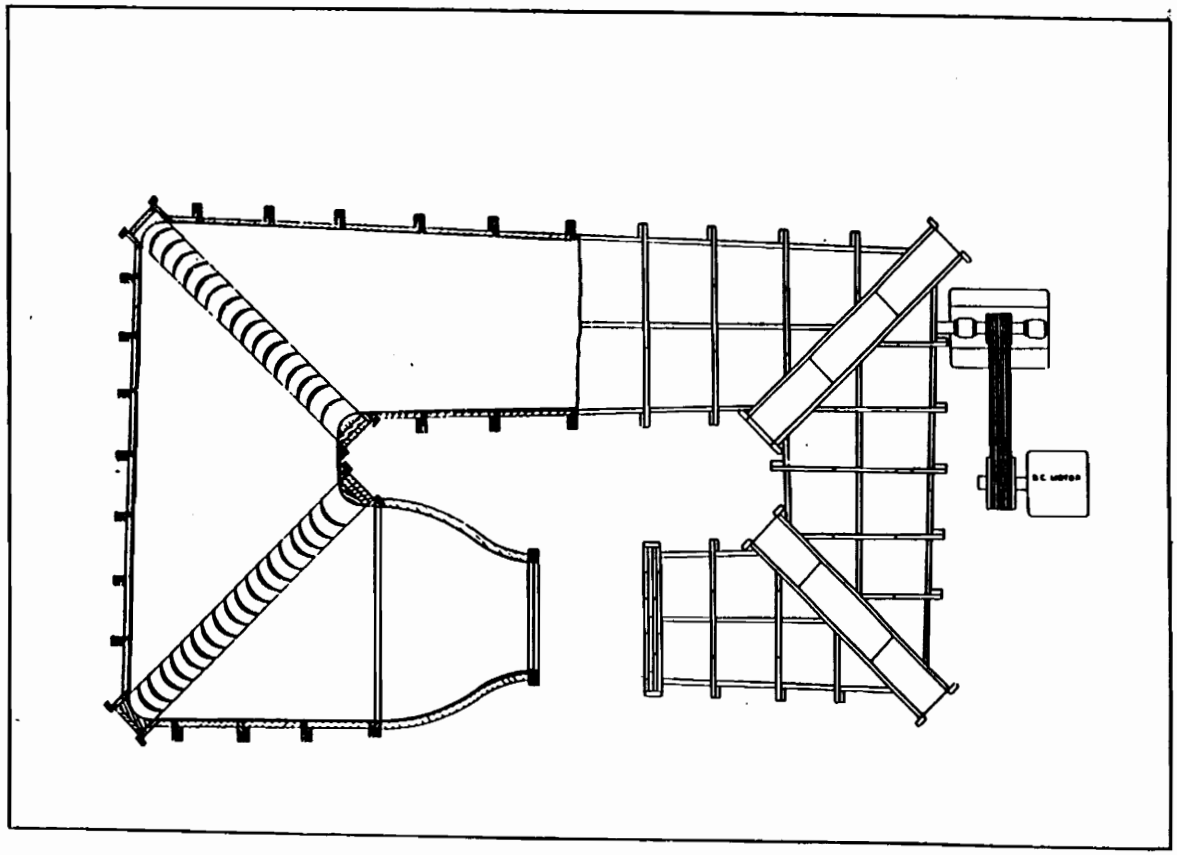

Figure 3.1 Student 3ft. Open Test Section Instructional Tunnel

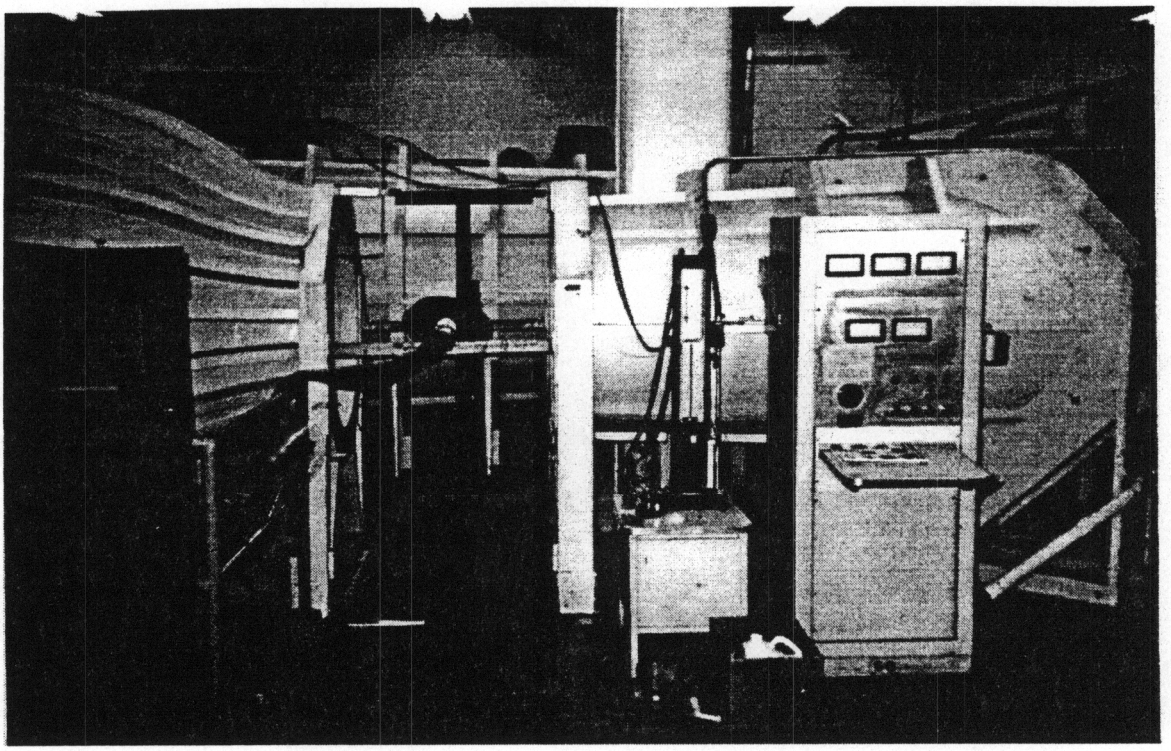

Figure 3.2 Low Speed Test Facility Test Section

attained by separate exciation furnished by a motor-generator set (General Electric 10 K.W., 80 amp generator, and 220 V, 60 cycle, 39 amp motor). The fan used is a four-bladed Hartzel propeller. The tunnel is capable of producing air speeds up to 150 miles per hour. The air speed is measured by two methods. A pitot-static probe connected to an inclined differential manometer graduated to read to .01 inches of water and static ports connected to a "setting" manometer yields the dynamic head. For a detailed description of the tunnel operation refer to the following document, Summary of Wind Tunnel Test Facilities.

The first step was to estimate the size of a strut which would produce a wake width and velocity defect comparable to that exiting the turbine cascade using a theoretical analysis. The following equations taken from Schetz (1993) were used to aid in this analysis:

$$\frac{\Delta U_c}{U_\infty} \approx 0.98\left(\frac{C_D D}{x}\right)^{1/2} \qquad [3.1]$$

$$b = 0.57\left(xC_D D\right)^{1/2} \qquad [3.2]$$

where

$U_c$ = centerline velocity

$U_\infty$ = free-stream velocity

$\Delta U_c$ = $U_\infty$ - $U_c$

$C_D$ = drag coefficient

$x$ = axial position behind wake

$D$ = diameter

$b$ = wake half width

Using the above equations a strut with the following dimensions was determined to yield an appropriate wake: 18.6 mm (0.732 in) in chord, 7.67 mm (0.302 in) in diameter, and 0.457 mm (0.018 in) in thickness. A strut measuring 91.44 cm (36.0 in) in span was located in the center of the 99.06 cm (39.0 in) open test facility with two 3.175 mm (0.125 in) allen screws. A manual traverse was secured to a bracket on the test section 10.6 cm (4.0 in) below the centerline of the strut. The traverse allows a probe to be moved in both a horizontal and vertical direction with respect to the trailing edge of the strut. A Keil probe, 15.24 mm (6.0 in ) in length and 1.65 mm (.065 in) in diameter, was secured to the traverse to collect the total pressure downstream of the strut.

## 3.2 Wind Tunnel Facility

The majority of the experiments were conducted in the Virginia Polytechnic Institute Cascade Wind Tunnel. It is a blow down wind tunnel which provides up to 40 second run times. This particular facility has an added feature. A heating loop was added to allow for heated runs (Figure 3.3). The following paragraphs explain in detail the process of generating the air used in this blow down facility. They also describe the inception of air into the tunnel and through the various sections of the tunnel.

A large four stage reciprocating compressor which is in-line with a heat exchanger (to cool the air) compresses the air. The air is then diverted through an activated-alumina drying unit which removes water vapor and other contaminates from the air. The air is then stored in two large reservoir tanks. The air leaves the storage tanks and enters the tunnel through 35.6 cm (14.0 in) diameter pipes. The air then flows through a safety valve and control valve which controls tunnel pressure. The control algorithm attempts to maintain a constant total pressure in the test section through manipulation of the control valve. A BASIC program on an IBM PC controls the

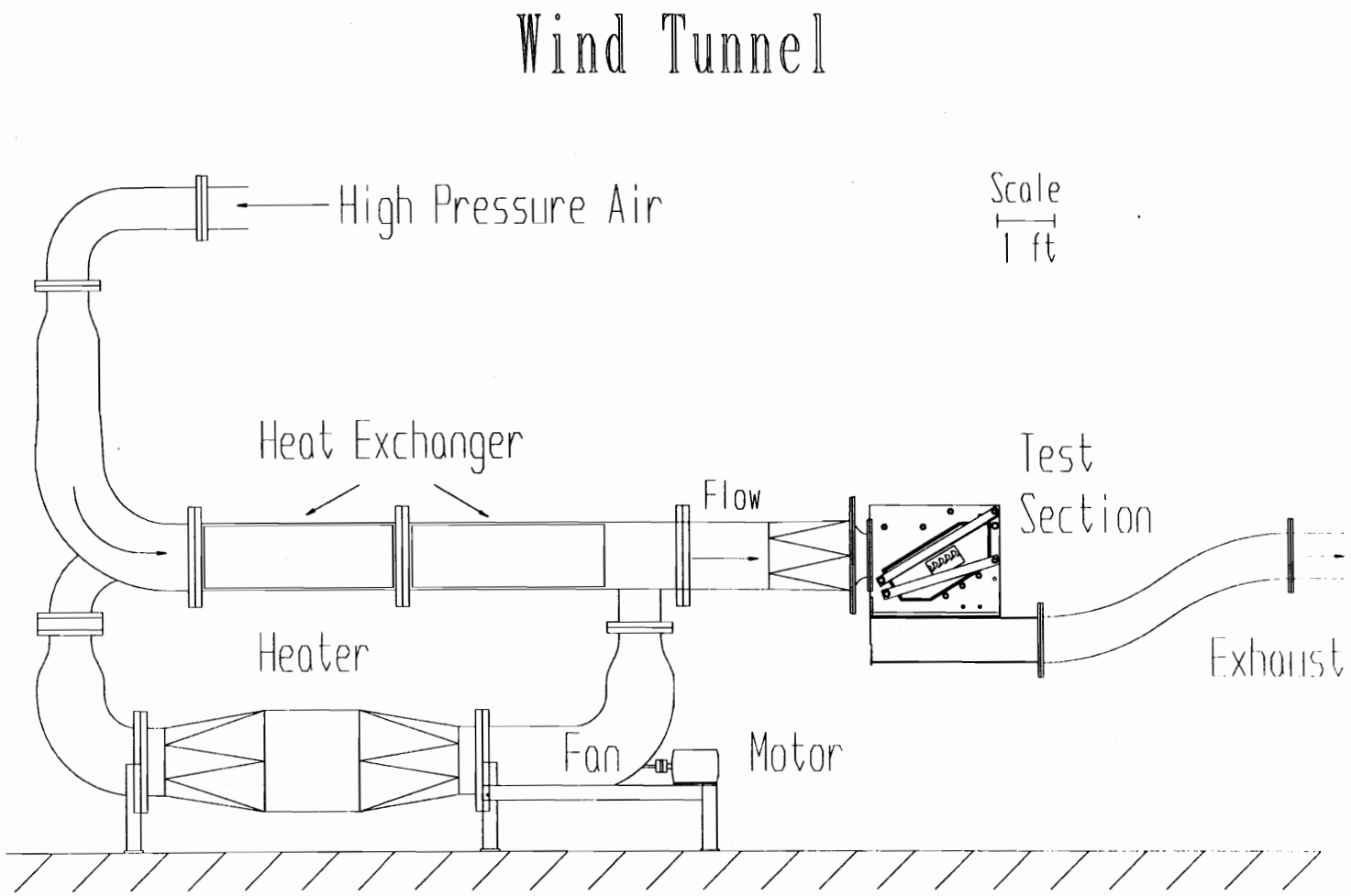


**Figure 3.3 Virginia Tech Cascade Wind Tunnel**

actuation of the valve based on feedback it is receiving from a pressure transducer measuring the flow's total pressure upstream of the cascade. The throttling process is achieved by using the BASIC program in conjunction with a compressed air-bottle, set at 138 kPa (20 psi). This actuation ensures a relatively constant tunnel pressure during a tunnel run. The safety valve is set to trip and shut down the tunnel operation if a gage pressure of 207 kPa (30psig) is attained. This is to ensure that no structural damage would occur to cascade test section. The flow coming from the valves passes through a 90 degree bend which is followed by a flow straightener (heat exchanger) consisting of an array of copper tubes before entering the wind tunnel test section. An inlet total pressure of 220 kpa (32 psia) can be maintained for around 30 - 40 seconds. As the air in the reservoir tanks starts decreasing the BASIC program actuates the control valve in such a manner that the inlet total pressure is maintained relatively constant. After each run of the tunnel approximately 5-10 minutes is required to recharge the supply tanks. The tanks are recharged to a pressure of 827 kPa (120 psig).

The cascade tunnel also consists of a heating loop which permits heated runs in the tunnel (Figure 3.4 and Figure 3.5). The heating loop consists of two bundles of heat exchanger tubes, an electric heater, and an axial flow fan. In between runs, the flapper valve is closed and the other valve is opened to construct the heating loop. A 36 KW electric heater is turned on, and a Dayton three-phase axial flow fan circulates air through the heating loop at approximately 2 m/s. The heat from the air is stored as thermal energy in the two bundles of copper tubes each weighing approximately 136 kg each. The 350 tubes are 1.59 cm in diameter and 1 m long, and are secured by stainless steel screens downstream of each bundle in the flow direction. This created an effective surface area of 70 $m^2$. The tube temperature is monitored by a surface mounted type K thermocouple. It is cemented to the end of a copper tube in the second bundle (44.5 cm [17.5 in] from the downstream flange). The hot gas temperature is monitored with a type K "air" thermocouple probe. This thermocouple (41.3 cm [16.25] from the downstream flange) is placed .3m (1ft) downstream of the tube bundle directly in the center of the passage.

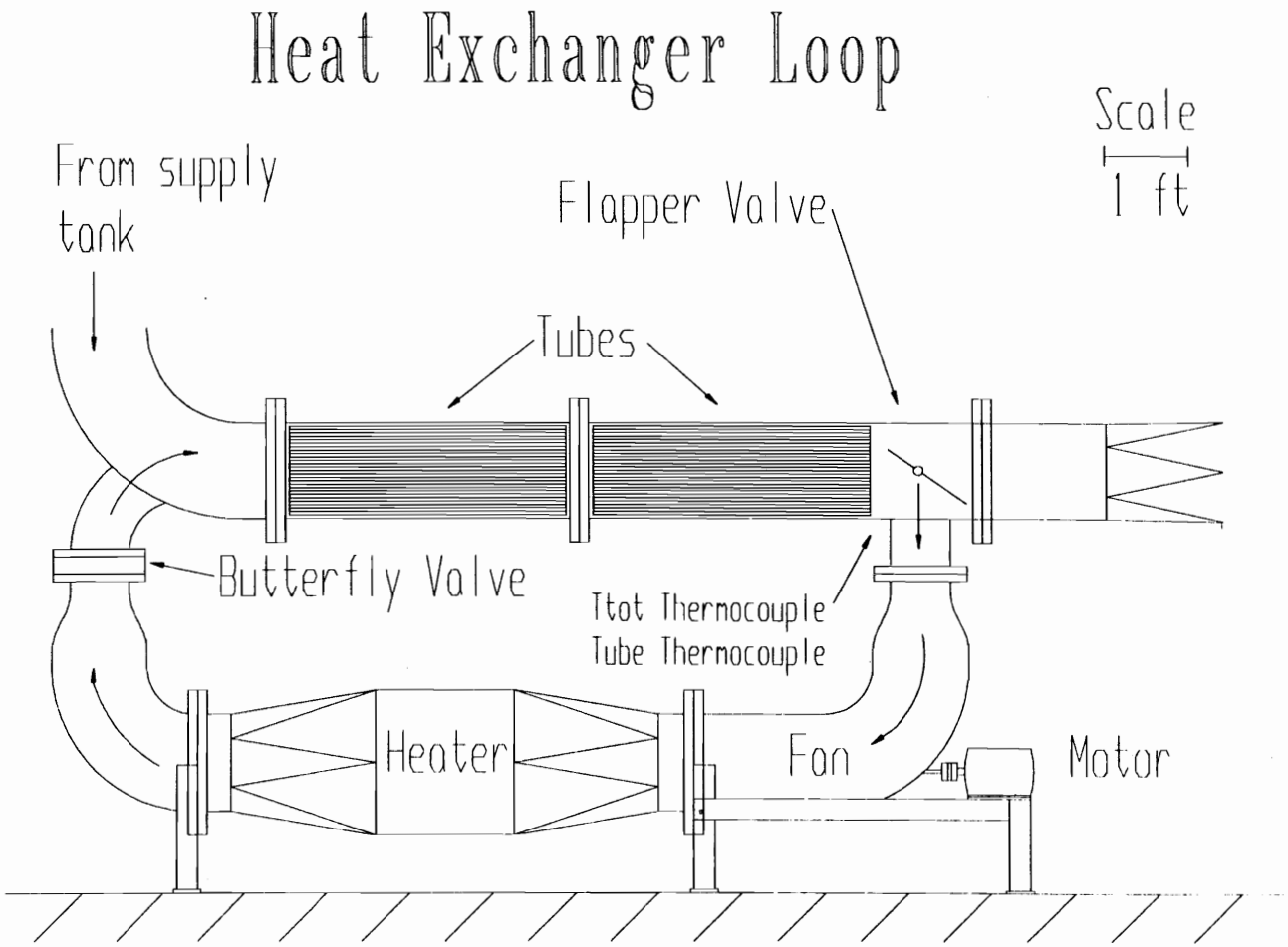


**Figure 3.4 Wind Tunnel Heat Exchanger Loop**

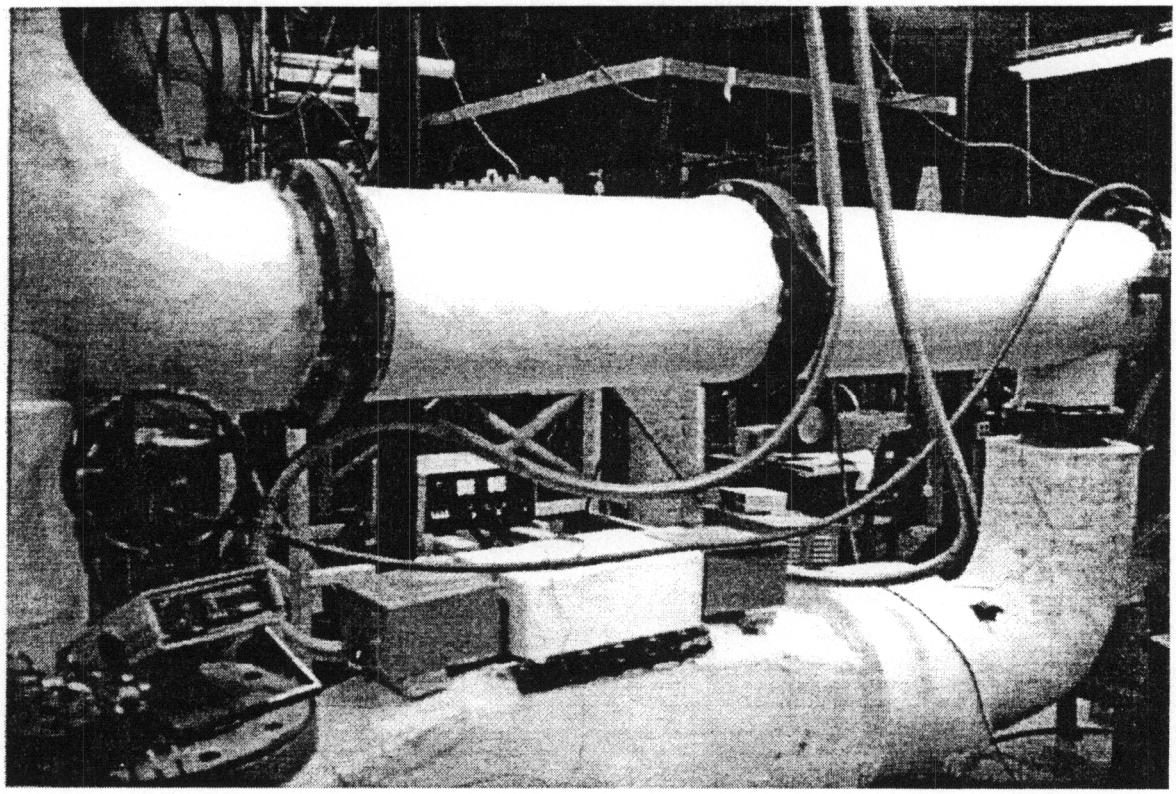

Figure 3.5 Wind Tunnel Heat Exchanger Loop Photo

The primary function of this particular probe is the measurement of total temperature during a run. A third thermocouple probe is installed to measure the electric heater temperature.

It takes approximately 30 minutes to initially heat the tubes to a temperature of 200°F (94°C). Subsequent heating between runs only require 10 to 15 minutes. After the tubes reach the desired temperature, the heater is turned off, and the fan is allowed to run for approximately five minutes to equalize the temperature throughout the flow field. The fan is then turned off, and the two valves are closed and opened, respectively. The tunnel is now ready for operation. With this particular setup flow temperatures up to around 85°C could be achieved. Upon exiting the heating loop, the air passes through a circular to rectangular transition piece and enters the test section.

The flow enters the test section at Mach 0.36 which allows for supersonic exit Mach numbers. The design average isentropic exit Mach number for these experiments is 1.26. The air then passes through the test section where it is turned by the turbine blades and enters the exhaust portion of the tunnel. Upon entering this section of the tunnel the air enters a diffuser and muffler before being vented to the atmosphere.

## 3.3 Test Section and Cascade

The cascade consists of eleven turbine blades, two end blocks, and two Plexiglass side plates. The blades are secured to the Plexiglass via a pin and screw combination (Figures 3.6 and 3.7), and the endblocks are secured to the Plexiglass side walls via allen screws. The cascade is secured in the test section by placing it in grooved slots located in the aluminum doors. The doors are secured by tightening two 1 1/4" nuts and two 3/4" nuts. The Plexiglass endwalls are transparent and allow for the collection of optical information such as shadowgraphs and flow visualization. The blades in the cascade have the following dimensions: 5.08 cm (2.0 in) in span and 4.5 cm (1.77 in) aerodynamic chord. The blades are spaced a distance of 3.81 cm (1.50 in) apart. The blades of primary interest are the blades located in the center of the passage.

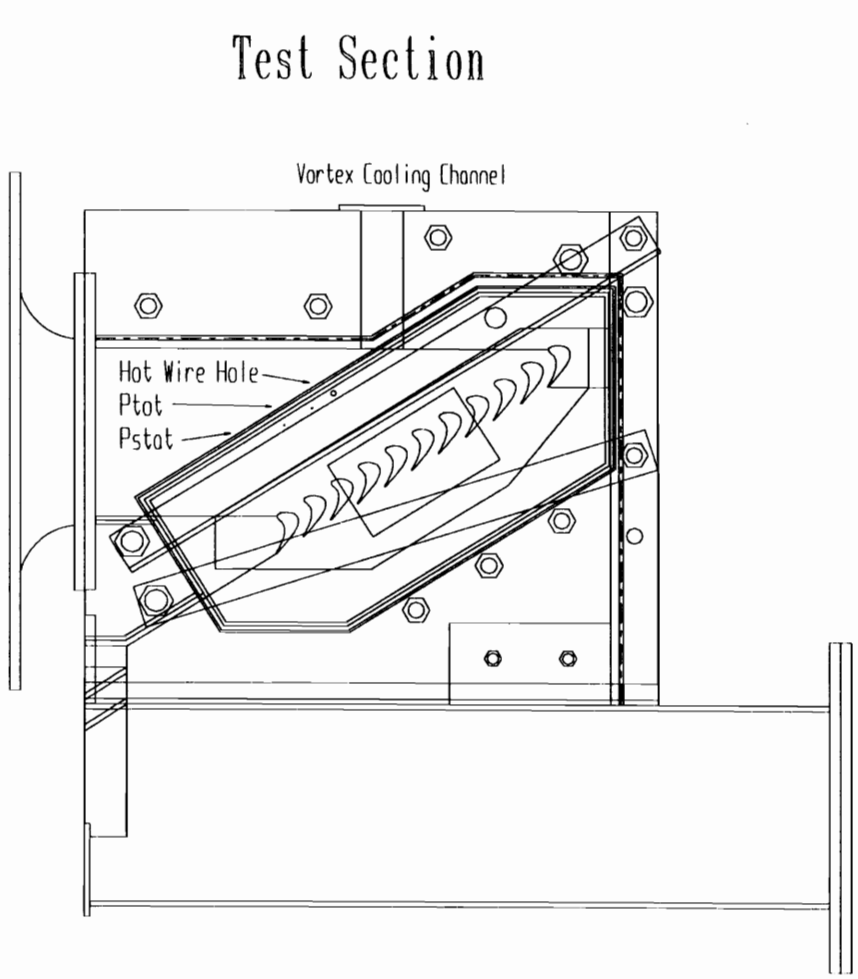


**Figure 3.6 Wind Tunnel Test Section and Cascade**

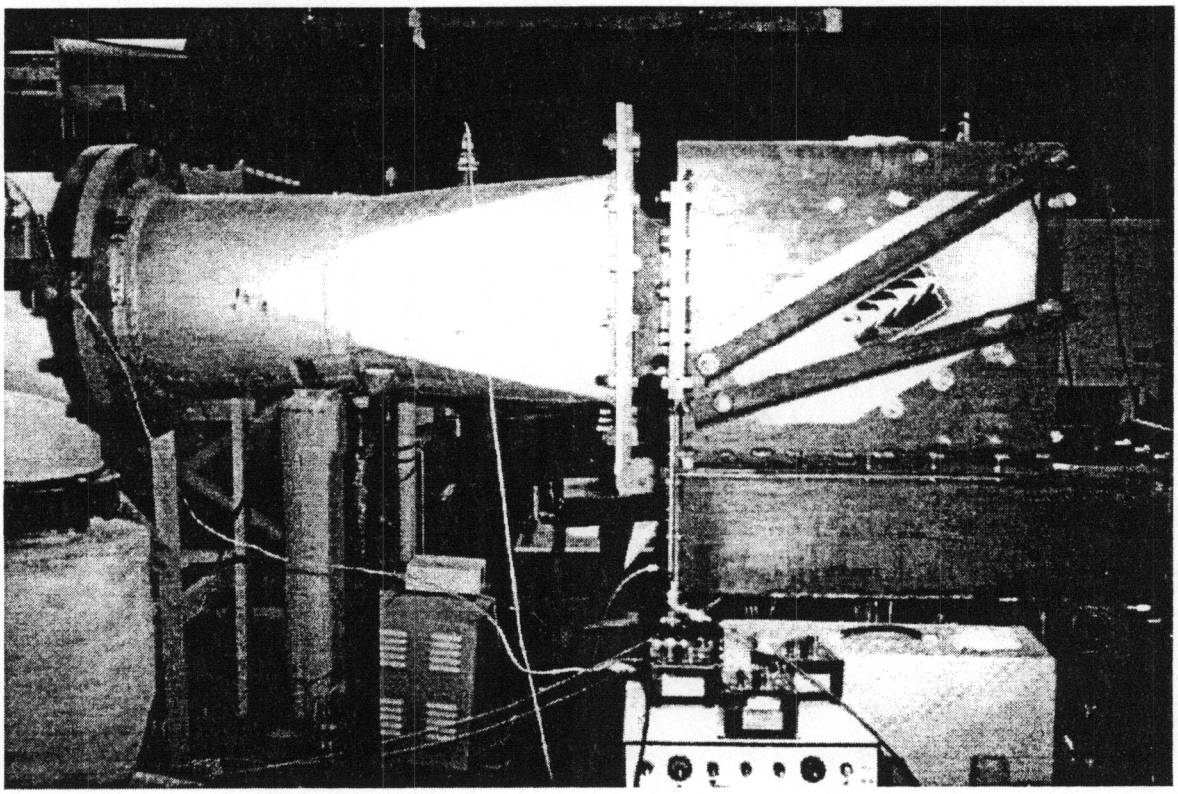

Figure 3.7 Wind Tunnel Test Section and Cascade Photo

## 3.4 Traversing Mechanism

The traversing mechanism consists of a stepper motor which drives a rack through a series of gear connections (refer to Figures 3.8 and 3.9). The traverse is controlled through a BASIC code run on an IBM PC (see Appendix B). This code controls the distance the traverse moves as well as the speed at which it moves. The traverse was used for two particular applications. It was utilized in the Upstream Survey experiments and the Leading Edge Survey experiments.

The position of a probe was recorded using a Linear Variable Displacement Transducer (LVDT). The voltage output was converted to a displacement through a calibration equation. Therefore, the position of the probe with respect to a reference point in the cascade was known at all times during the experiments.

## 3.5 Upstream Survey

The goal of the following experiment was to traverse a total pressure probe behind a strut in the transonic cascade wind tunnel and determine the wake profile at different positions behind the strut. This would also provide a check of the low speed results attained and another check of the analytical model.

The following experiment was conducted in the transonic cascade wind tunnel. Equations 3.1 and 3.2 were used to estimate the size strut needed to produce a wake similar to that exiting the turbine blades in the cascade. A thin hollow aluminum strut having the following dimensions was employed. The strut measured 18.6 mm (0.732 in) in chord, 7.67 mm (0.302 in) in diameter, and 0.457 mm (0.018 in). The strut was secured well upstream of the turbine blades in the test section endwall (refer to Figure 3.10). To secure the strut two pieces of 2.38 mm (0.09375 in) diameter all thread rod were soldered to a small flat piece of metal measuring approximately 3.175 mm (0.125 in) in thickness and 2.79 mm (0.110 in) in width. This was inserted through the hollow strut in a manner to assure that the incidence angle of the flow would be zero, and that the strut would remain stationary during tunnel operation. The all thread rods were inserted

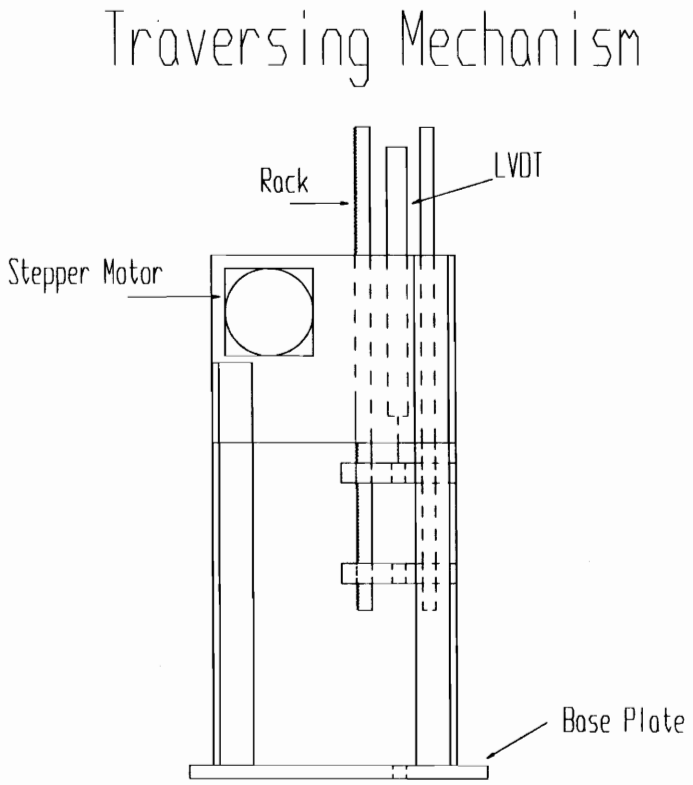


**Figure 3.8 Traversing Mechanism**

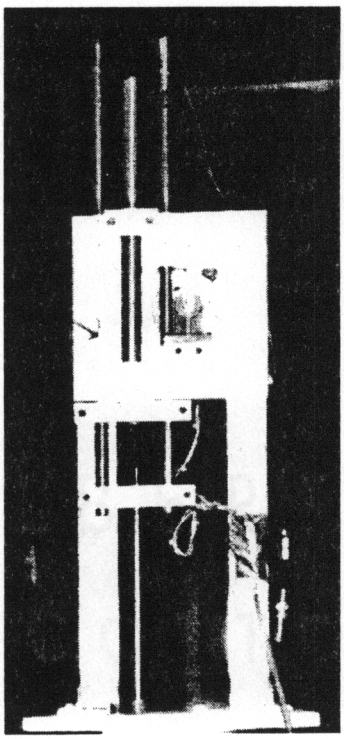

Figure 3.9 Traversing Mechanism Photo

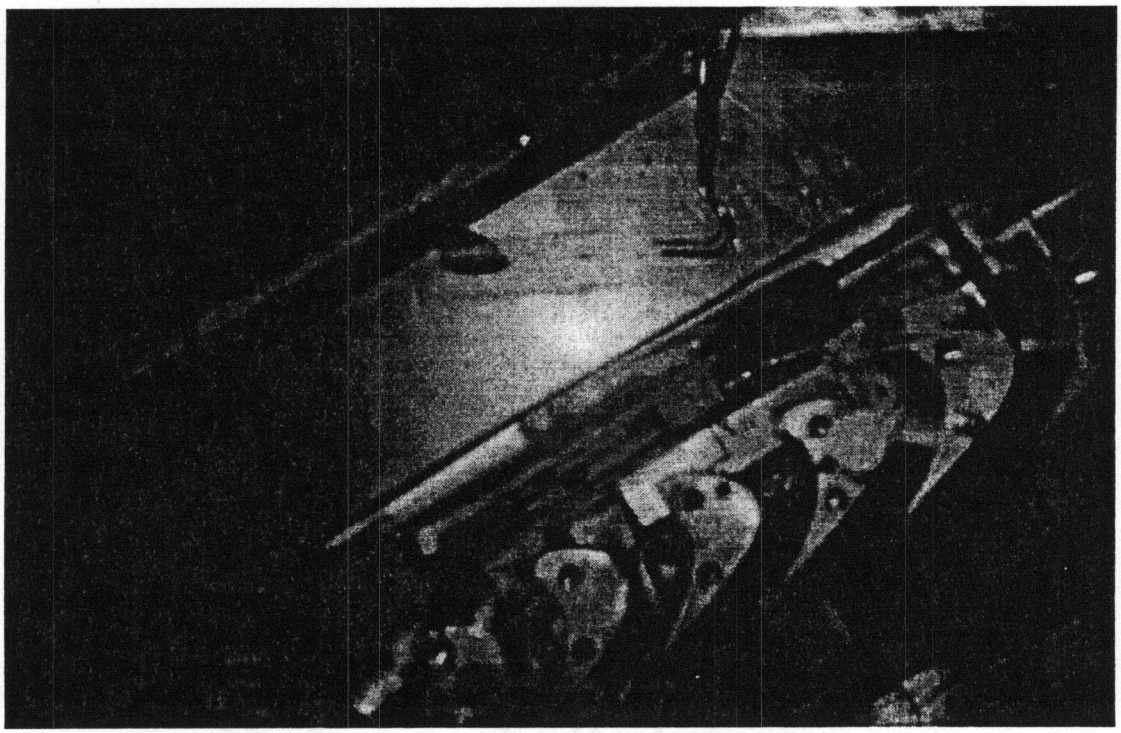

Figure 3.10 Strut and Probe Position

through the 25.4 mm (1.0 in) aluminum doors and were fastened by tightening a lock nut. This placed both of the rods in tension.

An upstream total pressure tap and an upstream static pressure tap were placed in the aluminum door to monitor the inlet (free-stream) pressure conditions. To monitor the static pressure at various locations behind the strut four static taps were drilled. One pair was placed at an axial location of 1.01" from the strut's trailing edge. One tap was drilled along the strut's centerline and the other was drilled 1.0" vertically above the strut's centerline. The other pair was placed in the same fashion except they were 1.614" from the strut trailing edge.

The traverse was secured to the test section's top with two 9.5 25 mm (0.375 in) allen screws (refer to Figures 3.11 and 3.12). The traverse baseplate is slotted such that the traverse can be manipulated to several locations. A total pressure probe was constructed with a 1.58 mm (0.0625 in) diameter and was 60.96 cm (24.0 in) in length, to acquire data at the two axial positions listed earlier. The probe was secured to the traverse with two set screws.

## 3.6 Hot Wire Probes and Anemometers

For the following experiments, a single wire, general purpose probe was used. The specific probe used was the TSI Model 1210-T1.5 (see Figure 3.13). Its small size and good frequency response makes it especially suitable for studying flow details, particularly in turbulent flow. Single sensor probes are general purpose probes for one dimensional flow measurements. This was adequate due to the believed isotropy of the test facility. This type of probe is ideal for velocity and turbulence measurements up to approximately 200 MPS (600 FPS) in air at temperatures from ambient conditions up to 150°C (TSI catalog).

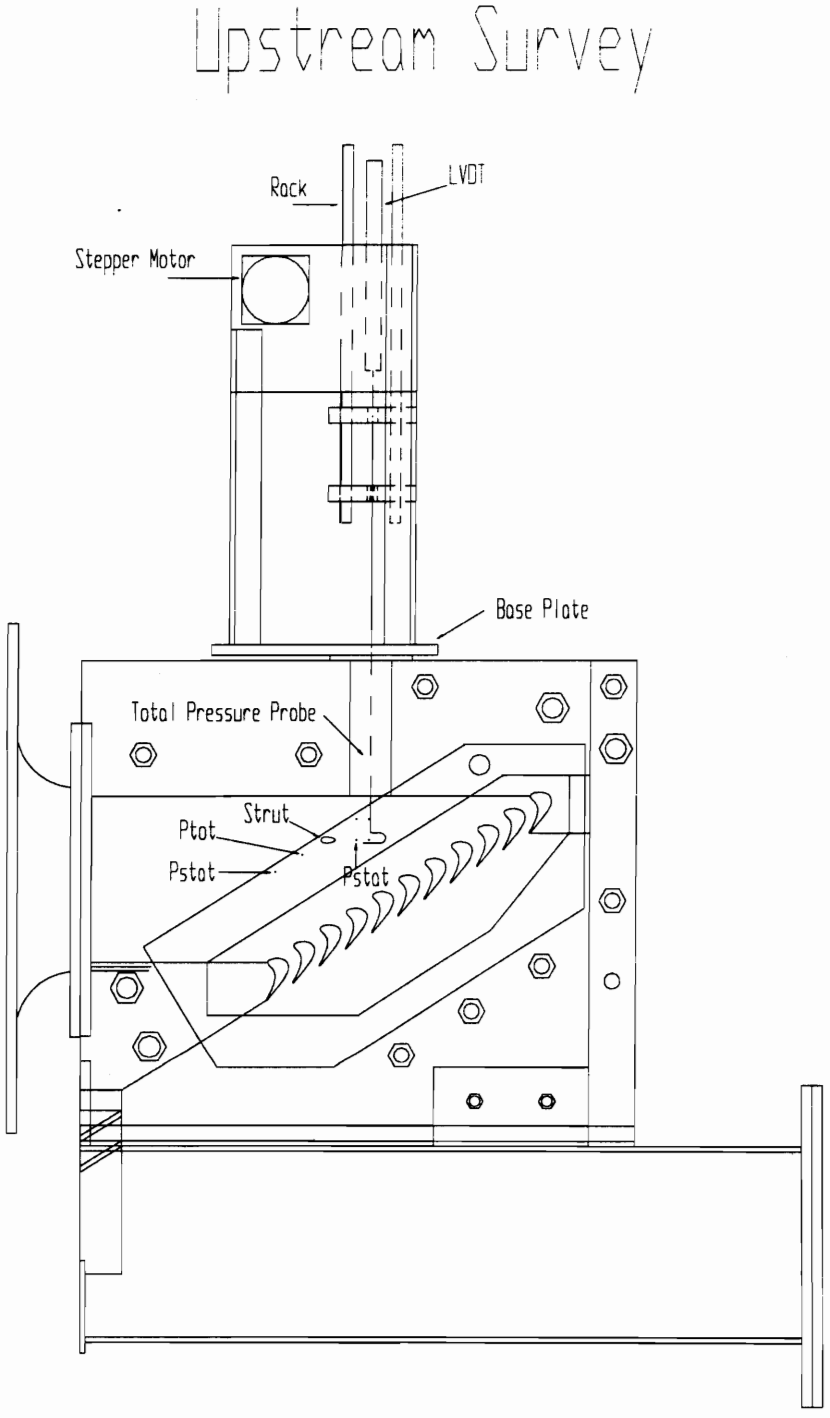


Figure 3.11 Upstream Survey Experimental Set-up

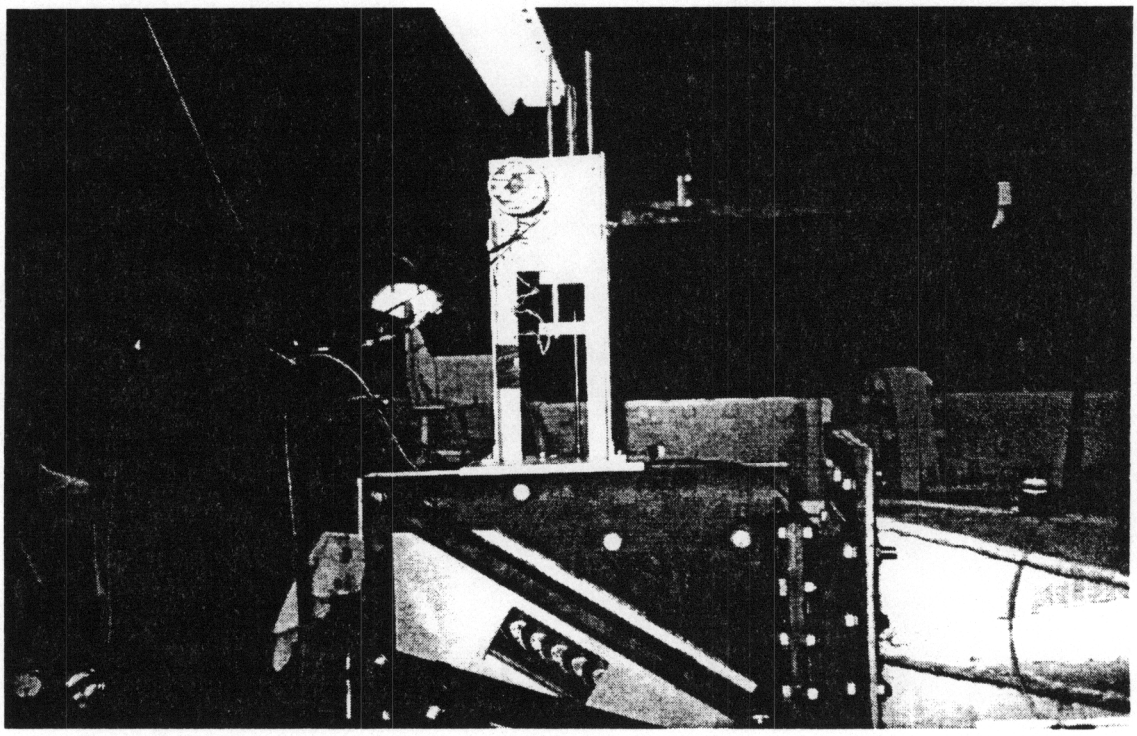

Figure 3.12 Upstream Survey Experimental Set-up Photo

### 3.6.1 Principles of Operation

The principle of operation of the anemometer is to measure the convective heat transfer from an electrically heated sensing element, in this case a platinum-coated tungsten wire five micrometers in diameter, to the surrounding fluid, the air in the tunnel. A constant temperature anemometer consists basically of a Wheatestone bridge with the probe serving as one of the arms (Figure 3.14). The probe is heated by passing an electric current through the circuit and is maintained at a constant temperature, implying a constant resistance. The voltage necessary to keep this constant resistance is measured and is proportional to convective heat loss.

Assuming a linear relationship between temperature and resistance, the resistance, $R_{op}$ of the sensor can be represented as:

$$R_{op} = R_r\left(1 + \alpha \cdot \left(T_m - T_r\right)\right) \qquad [3.3]$$

where:

$R_r$ = resistance at reference temperature, $T_r$

$T_m$ = average sensor temperature

$\alpha$ = temperature coefficient of resistance

Tungsten wires have a high temperature coefficient of resistance (0.0042 ohms/°C) which is an important property in obtaining good signals. A platinum coating provides oxidation resistance to improve the long term stability of the sensor. In Figure 3.14, if the resistance, of resistor R1 is large compared to that of the sensor (R), then the current, I, is nearly constant and any increase in heat transfer rate from the sensor to its surroundings will cause the sensor to cool. Because of the temperature coefficient of resistance, $\alpha$, this cooling will cause a decrease in R, a decrease in the voltage, $U_{12}$ (=IR), and a decrease in amplifier output U. When the changes in heat transfer are caused by changes in fluid velocity, the result is a thermal anemometer.

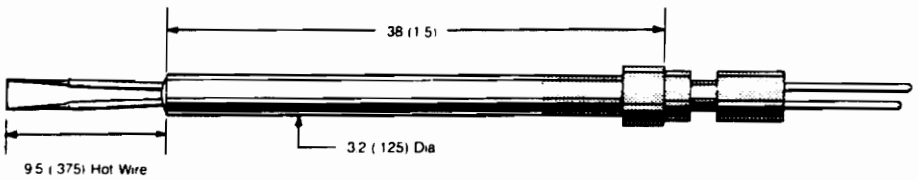


Figure 3.13 Hot Wire Probe

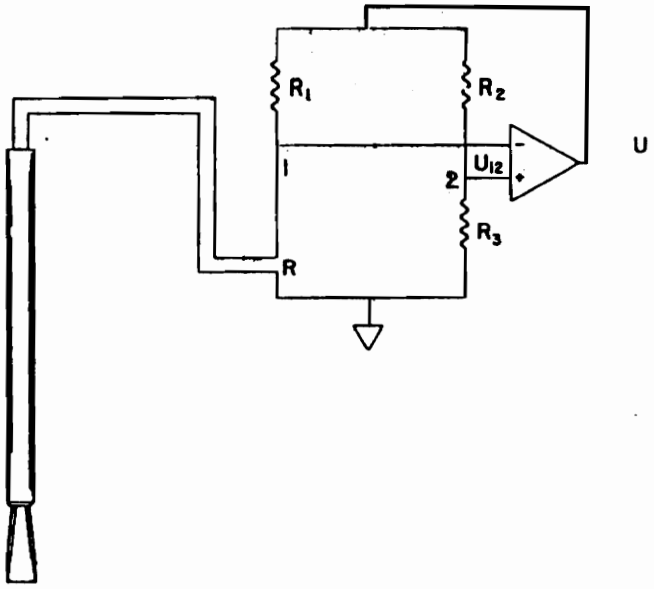


Figure 3.14 Hot Wire Circuit

The total amount of heat transferred depends usually on four particular items: the velocity of the flow; the temperature difference in the wire and the fluid; the physical properties of the fluid; and the properties and dimensions of the wire. In many cases the temperature difference between the wire and fluid, and the wire properties and dimensions are known. The other values can be determined, however. If the flow velocity is known or kept constant then the physical properties of the fluid can be measured or vice-versa.

The heat transferred from the wire to the gas from a wire of length $l$ and diameter $d$ is

$$q = h\pi dl \cdot \left(T_w - T_g\right) \cdot \qquad [3.5]$$

Where, $h$ is the heat transfer coefficient, $T_w$ is the wire temperature and $T_g$ is the gas temperature. The first law necessitates that thermal equilibrium conditions must prevail at steady state. This requires that the heat loss per unit time must be equal to the heat generated per unit time by the electric current through the wire. This conveys that the power ($I^2 R_w$), where $I$ is the electric heating current and $R_w$ the total electric resistance of the wire must equal the heat loss from the wire. To simplify some of the later analysis the dimensionless group of Nusselt is introduced,

$$Nu = hd/k_g \qquad [3.6]$$

where $k_g$ is the thermal conductivity of the gas at the temperature $T_g$. Performing an energy balance on the wire provides the following thermal equilibrium

$$I^2 R_w = hld\pi\left(T_w - T_g\right) = lk_g\pi\left(T_w - T_g\right) \cdot Nu \qquad [3.7]$$

The study of heat transfer has shown that several factors affect the heat transfer coefficient which in turn affects the Nusselt number. However, many of these parameters can be assembled into dimensionless groups to better understand each of the individual affects. The following equation exhibits how the Nusselt number is a function of several dimensionless groups

$$Nu = f\left[\mathrm{Re}, \mathrm{Pr}, Gr, \frac{\Delta T_w}{T_g}, \frac{U^2}{c_p \Delta T_w}, \frac{l}{d}, \varphi\right] \qquad [3.8]$$

where Re is the Reynolds number and is represented by the following equation

$$\mathrm{Re} = \rho_g U d / \mu_g \qquad [3.9]$$

The Reynolds number consists of the following physical and geometrical parameters: the gas density, $\rho_g$: the flow velocity, $U$; the wire diameter,$d$; and the dynamic viscosity, $\mu_g$. The Prandtl number, Pr, can be represented by the ensuing relationship

$$\mathrm{Pr} = c_p \mu_g / k_g \qquad [3.10]$$

where $c_p$ is the specific heat of the gas, and $k_g$ is the thermal conductivity of the gas. The last dimensionless group is the Grashof number which is described by

$$Gr = g \rho_g^2 d^3 \Delta T_w \beta / \mu_g^2 \qquad [3.11]$$

where $g$ is gravity, $\beta$ is the coefficient of thermal expansion, and $\Delta T_w$ is the difference between the wire temperature and the gas temperature.

This complex relationship, equation 3.8, appears to be to complicated, and as stated is. Therefore, to adopt this equation for hot wire use some simplifying approximations are made. These approximations are contingent upon the flow conditions encountered. One very important condition comes from the flow pattern that exists around the wire. This condition is influenced by certain dimensionless groups of which the Reynolds number is of primary importance. Since the flow pattern around a cylinder (representing the hot-wire) at very low values of the Reynolds number differs appreciably from the one at much higher Reynolds numbers, no single and simple relation between the Nusselt number and the Reynolds number can be expected.

Considering that the hot-wire can be modeled as a circular cylinder several relationships have been developed relating the heat transfer from cylinders to a fluid by forced convection.. One of the first relationships was proposed by King, (1914),

$$Nu = 1 + \sqrt{2Pe\pi} \qquad [3.12]$$

valid for Peclet number

$$\rho_g c_p U d \Big/ k_g \geq 0.08 \qquad [3.13]$$

He considered two dimensional flow theory around a circular cylinder for the derivation of the preceding relationship. The significance of this relationship is that is shows the square-root dependence of the Nusselt number on the Reynolds number considering the following

$$Pe = \mathrm{Pr} \cdot \mathrm{Re} \qquad [3.14]$$

This relation (equation 3.12) is still used today, but in a slightly modified form. The square-root dependence of the Reynolds number is prevalent and is left unchanged. However the 1 and $\sqrt{2\pi}$ are replaced by constants which are usually determined through experimentation. If compressibility affects are not a major concern then the constants are mainly functions of the Prandtl number

$$Nu = C_1(\mathrm{Pr}) + C_2(\mathrm{Pr})\mathrm{Re}^{1/2} \qquad [3.15]$$

A key concern is the temperature at which the gas properties are evaluated. In most instances gas properties are taken at the so-called "*film temperature*"

$$T_f = \frac{T_w + T_g}{2} = T_g + \frac{\Delta T_w}{2} \qquad [3.16]$$

Many researchers have diverged from the particular method above and have suggested a power-law relationship. This method has produced better results in applications where higher Reynolds numbers are encountered. Through experimentation they discovered a distinct difference when the Reynolds number was greater than 44. At $\mathrm{Re} \cong 44$ vortex shedding begins to take place. These relationships are as follows

$$Nu\left(\frac{T_f}{T_g}\right)^{-0.17} = 0.24 + 0.56\,\mathrm{Re}^{0.45} \quad \text{for } 0.02 < \mathrm{Re} < 44 \qquad [3.17]$$

$$= 0.48\,\mathrm{Re}^{.51} \quad \text{for } 44 < \mathrm{Re} < 140 \qquad [3.18]$$

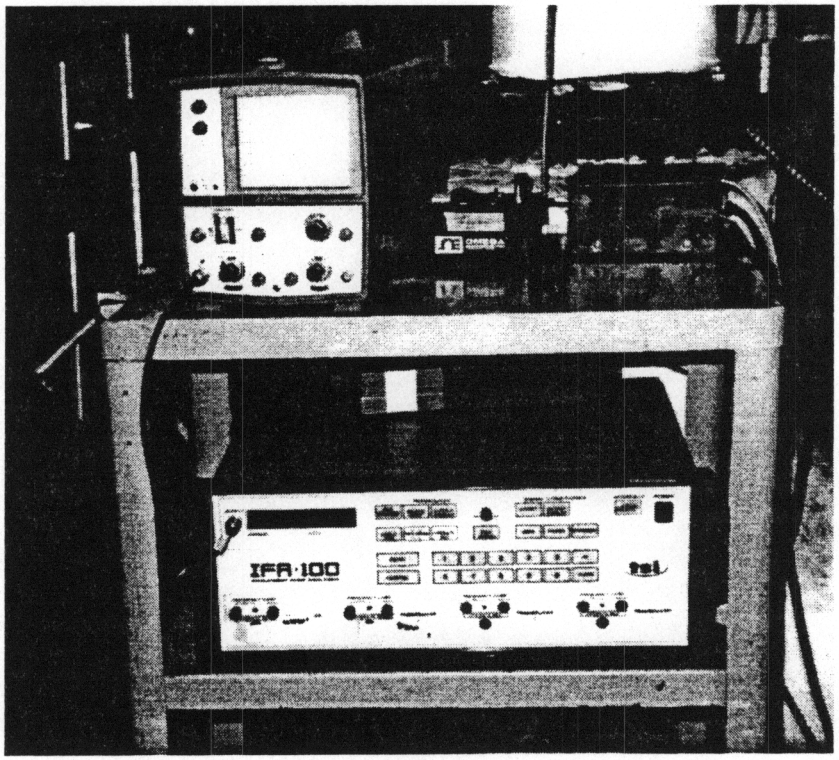


Figure 3.15 IFA 100 Flow Analyzer Photo

The first relationship refers to Reynolds number most frequently encountered in subsonic flow measurements. The second relationship was used for the calibration of the hot-wires used in the experimentation of this thesis.

### 3.6.2 Anemometer Frequency Response

The bridge ratio of the TSI-1210 hot-wire anemometer could be set to either Standard 1, Standard 2, Hi Power, or 1:1 on the IFA 100 Flow Analyzer (see Figure 3.15). The bridge ratio is the impedance ratio between the active and passive sides of the bridge. The 1:1 bridge ratio was used in these experiments, as this bridge provided a sufficient frequency response of 100 kHz.

To obtain this frequency response, several controls on the IFA 100 Flow Analyzer were adjusted. These controls were adjusted in such a manner to achieve the optimum frequency response to sudden changes in the flow field across the wire. To simulate this phonema, so the frequency response could be adjusted, the electric power to the probe was inputted in the form of a square wave signal. For a detailed description on tuning the hot-wire anemometer refer to the IFA Flow Analyzer Catalog.

## 3.7 Leading Edge Survey

The goal of the following experiment was to traverse a hot-wire anemometer in a plane parallel to the leading edge of the blades to characterize the inlet flow with the strut located at various positions.

The experiment was conducted in the transonic cascade wind tunnel. The strut described earlier was utilized. The strut was secured in the 12.7 mm (0.50 in) plexiglass endwalls using the same method as described in section 3.4 Upstream Survey. Slots were cut in the plexiglass endwalls to allow easy repositioning of the strut between runs. The slots measured 2.64 mm (0.10375 in) in width and 44.45 mm (1.75 in) in length. This

allowed the trailing edge of the strut to be 19.05 mm (.75 in) away from the leading edge of the instrumented blade.

The traverse was secured to the test section with a transition piece to obtain correct alignment with the plane of the blades (see Figure 3.16 and 3.17). The transition piece and traverse were fastened to the test section with four 6.35 mm (0.25 in) allen screws. Before the traverse was moved into position the hot-wire probe support was inserted into the test section through a half inch channel in the shock shaper plug. This particular probe support was not an on the shelf item. The probe support was fabricated in shop. It measures 6.502 mm (0.256 in) in diameter and 66.04 cm (26.0 in) in length. To position the hot-wire in close proximity to the leading edge, two turns were placed in the probe support starting at approximately 25.4 mm (1.0 in) from the end and ending at approximately 38.1 mm (1.5 in). This moved the hot-wire off the centerline of the probe support by 6.35 mm (0.25 in) (see Figure 3.18). The probe support is attached to the traverse with two set screws.

To assure that vibration of the probe would be minimized, the probe support was allowed to rest on the surface of the blades. An insert piece (50.8 mm (2.0 in) in length and 6.73 mm (0.265 in) in width and depth) was also placed in the shock shaper channel to reduce vibration. This positioned the hot-wire traverse 3.05 mm (0.120 in) from the surface of the blades.

## 3.8 HFM-6 Insert Gage

In the following experiments four HFM-6 Insert Gages were employed to measure heat flux and surface temperature at various locations on the turbine blade during a single run. The HFM-6 Insert Gage is shown in (Figure 3.19). These gages had to be inserted into bored holes in the turbine blade. Gages 1 through 3 are located on the suction surface of a blade and gage 4 is located on the pressure surface of a blade. The four heat flux gages possess the following dimensions: 8.74 mm (.344 in) in housing diameter

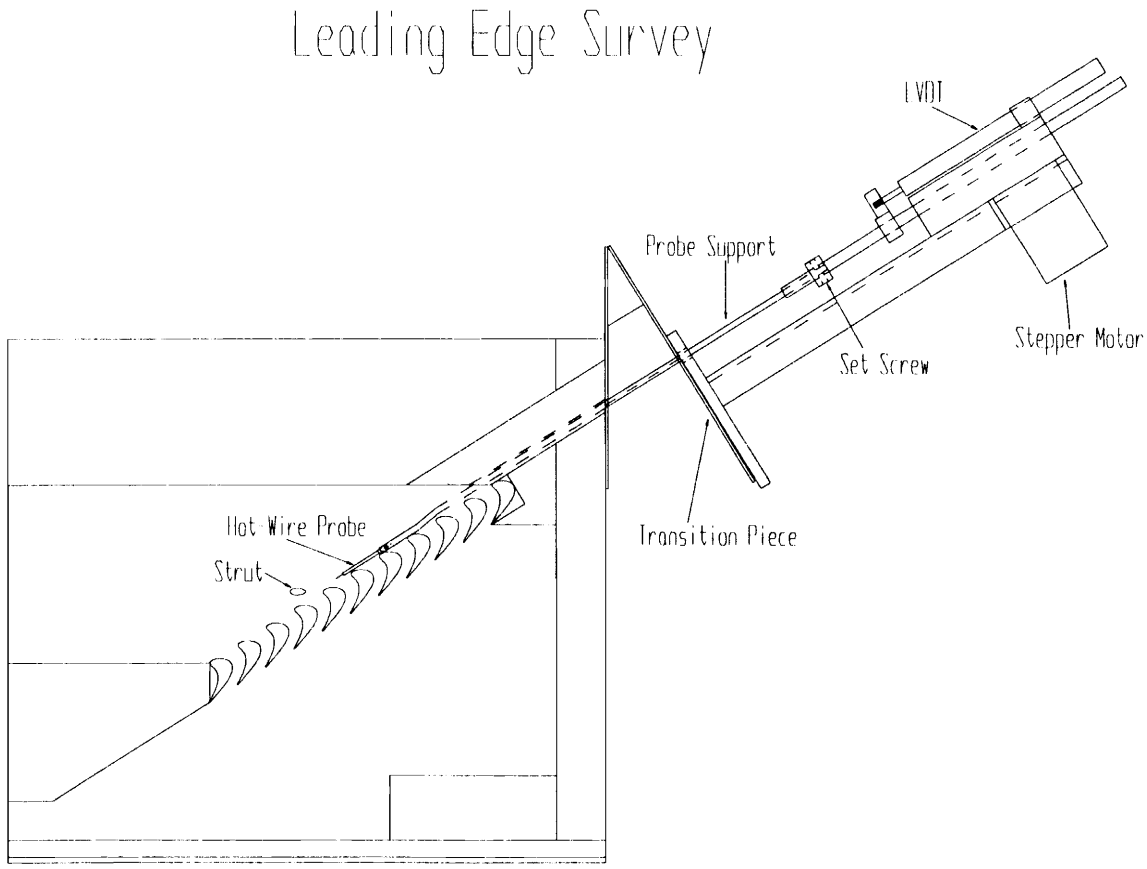


Figure 3.16 Leading Edge Survey Experimental Set-up

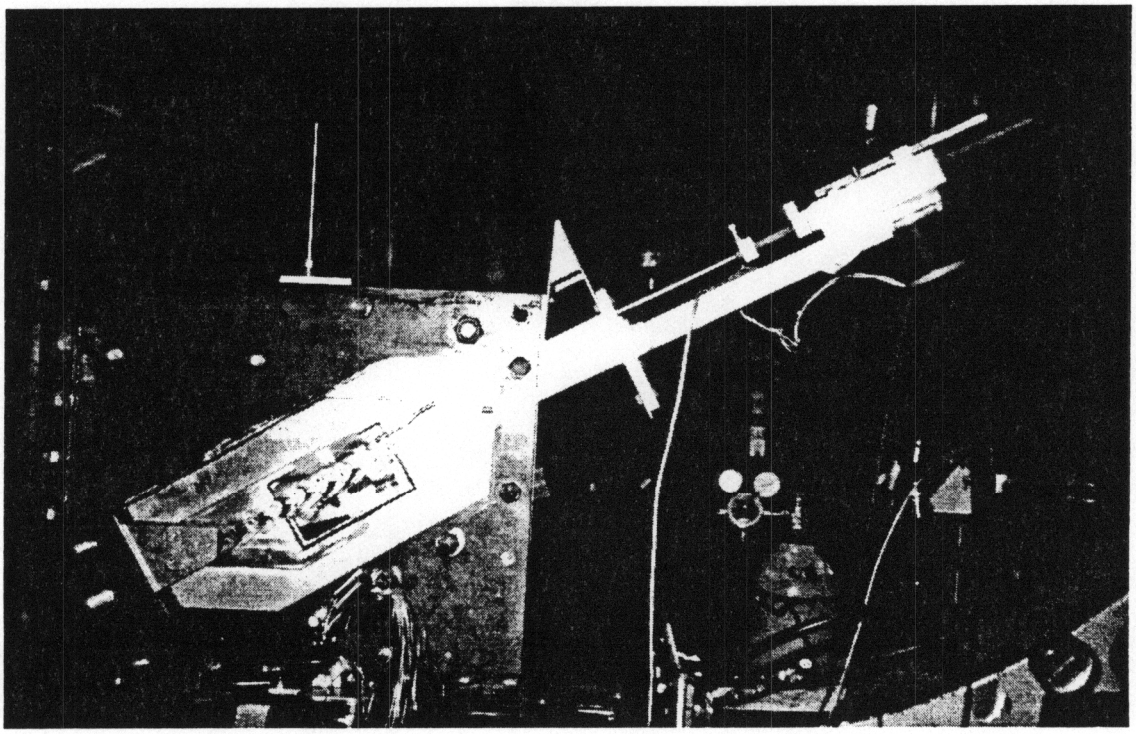

Figure 3.17 Leading Edge Experimental Set-up Photo

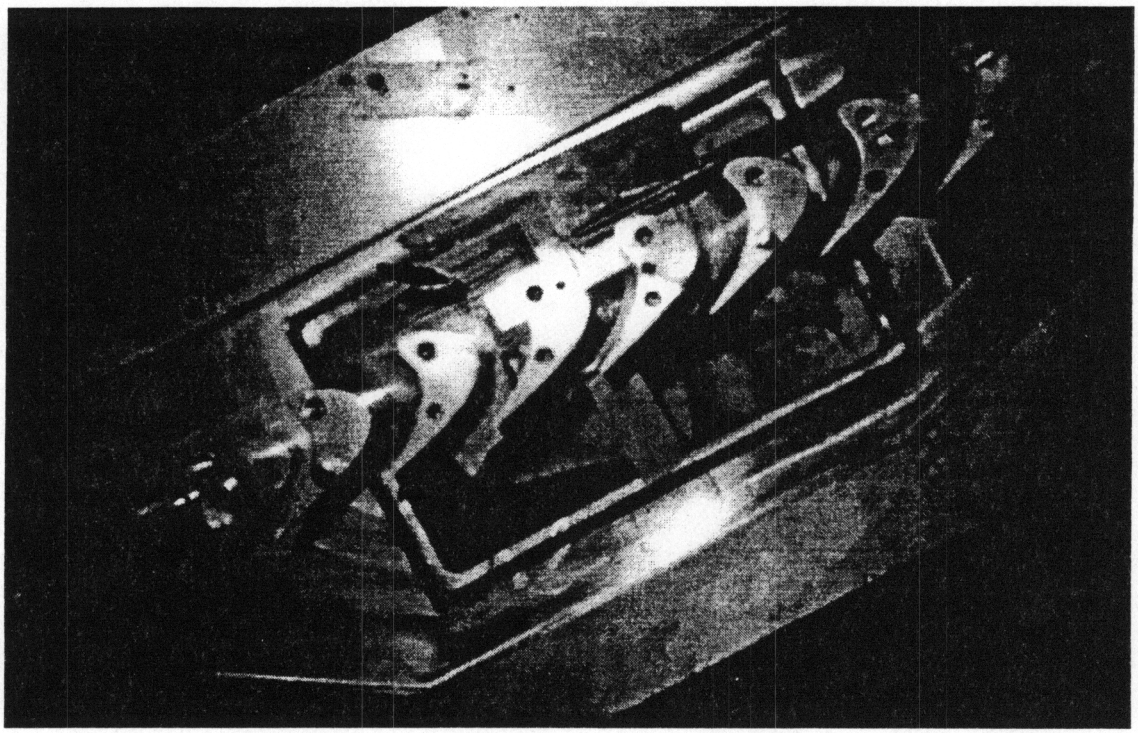

Figure 3.18 Strut and Hot Wire Probe Support Photo

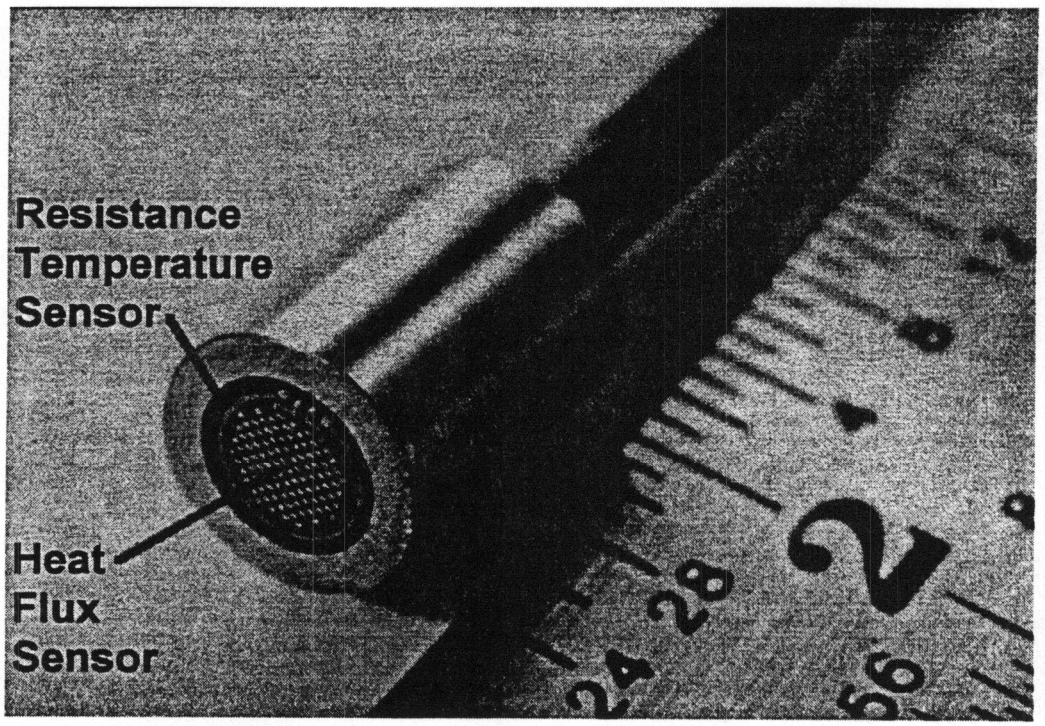


Figure 3.19 HFM-6 Insert Gage

and 24.5 mm (0.965 in) in length. The gage itself is 6.32 mm (.249 in) in diameter and 1.91 mm (0.075 in) in thickness.

HFM-6 gage 1 is located 6.7 mm (0.263 in) from the midspan of the blade to the center of the gage and 9.525 mm (0.34375 in) from the leading edge (refer to Figure 3.20). The gage is inserted into a bored hole of diameter 8.84 mm (0..348 in). A setscrew is inserted into bored hole with a diameter of 6.35 mm (0.240 in) and 15.875 mm (0.625 in) in depth to secure the heat flux gage in place. The setscrew is approximately 6.48 mm (0.255 in) in length and 6.10 mm (0.240 in) in diameter.

HFM-6 gage 2 is located 5.85 mm (0.230 in) from the midspan of the blade to the center of the gage and 18.256 mm (.71875 in) from the leading edge (refer to Figure 3.21). The gage is inserted into a bored hole possessing the same dimensions as the insertion hole of gage 1. A setscrew is inserted into a hole of diameter 4.32 mm (0.170 in) and 16.31 mm (0.642 in) in depth to secure the heat flux gage. The setscrew is approximately 9.78 mm (0.381 in ) in length and 4.11 mm (0.162 in ) in diameter.

HFM-6 gage 3 is located 1.76 mm (0.06925 in) from the midspan of the blade to the center of the gage and 41.275 mm (1.625 in) from the leading edge (refer to Figure 3.22). The gage is inserted into a bored hole occupying the same dimensions as the insertion hole of gage 1. A setscrew is inserted into hole of diameter 4.32 mm (0.170 in ) and 20.4 mm (0.803 in) in depth to secure the heat flux gage. A setscrew similar in dimensions to the one used to secure gage 2 was employed to secure gage 3.

HFM-6 gage 4 is located 18.85 mm (0.74225 in) from the midspan of the blade to the center of the gage and 15.08 mm (0.59375 in) from the leading edge (refer to Figure 3.23). The gage is inserted into a bored hole having the same dimensions as the insertion hole of gage 1. A setscrew is inserted into a hole having a diameter of 4.32 mm (0.170 in) and 15.61 mm (0.6145 in) in depth to secure the heat flux gage.

The wires from the three heat flux gages on the suction surface exit the blade through a 5.08 mm (0.200 in ) diameter channel drilled in the side of the blade. Four wires exeunt each gage, two for the heat flux signal (HFS) and two for the resistance

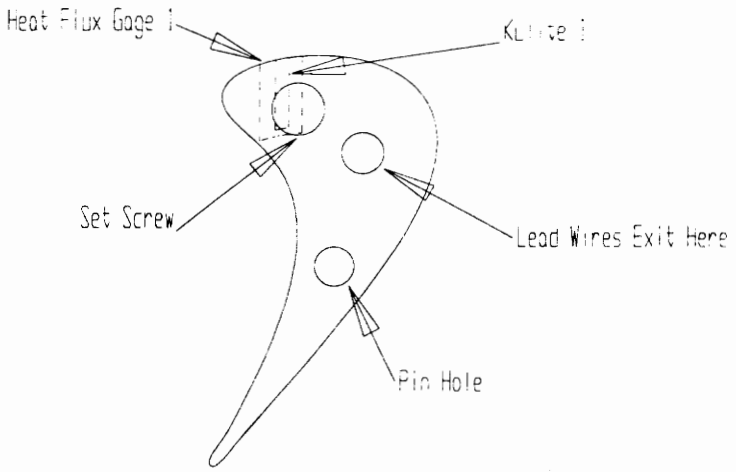


Figure 3.20 Heat Flux Gage and Kulite 1 Position in Turbine Blade

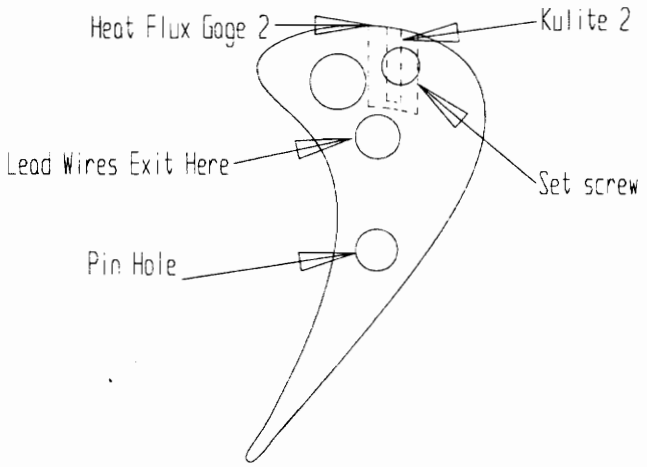


Figure 3.21 Heat Flux Gage and Kulite 2 Position in Turbine Blade

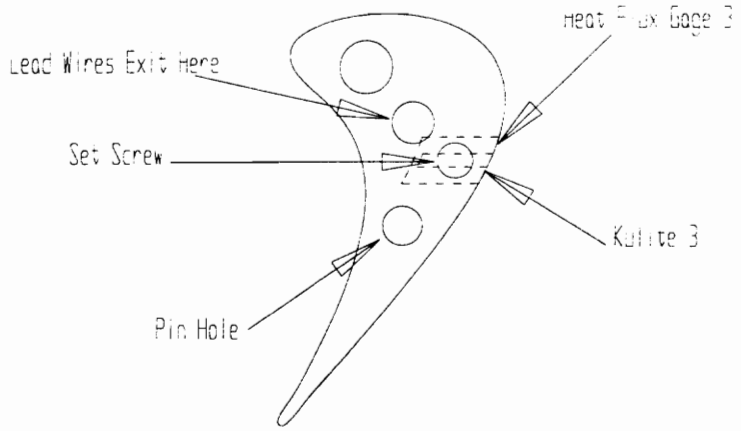


Figure 3.22 Heat Flux Gage and Kulite 3 Position in Turbine Blade

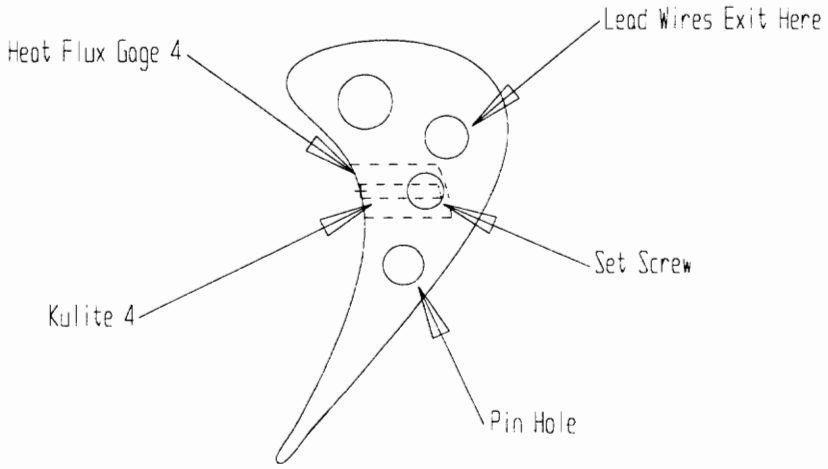


Figure 3.23 Heat Flux Gage and Kulite 4 Position in Turbine Blade

temperature signal (RTS). They then exit through a hole in the 12.7 mm (0.5 in) thick plexiglass endwalls having the same diameter of the blade channel. A bracket was configured to hold four female Lemo plugs and was secured to the side of the cascade using two of the allen screws which hold the blades in the cascade. The heat flux gages 0.076 mm (0.003 in) wires were soldered to the female Lemo plugs. A 91.4 cm (36.0 in) cable with two male Lemo plugs was used to make the connection between the female Lemo plugs and the HFM-6 amplifiers.

The heat flux gage on the pressure surface exits through the same process as the other three gages on the suction surface do. It connects to the fourth female Lemo plug and the same type of cable couples the female Lemo plug to the amplifier.

## 3.9 Kulite

In the following experiments four XCQ-062 Kulite miniature pressure transducers were employed to acquire blade surface pressure at various locations on the turbine blade during an individual run. The Kulites were inserted into bored holes along the same span as a corresponding heat flux gage. Gages 1 through 3 are located on the suction surface of a blade next to a parallel heat flux gage. Gage 4 is located on the pressure surface of a blade. The four Kulite pressure transducers retain the following dimensions: 1.63 mm (0.064 in) in diameter and 9.271 mm (.365 in) in length.

Kulite 1 is located 0.045 mm (.00175 in) from the midspan of the blade to the center of the gage and 9.525 mm (0.34375 in) from the leading edge (refer to Figure 3.20). The gage is inserted into a bored hole measuring 1.89 mm (0.0745 in) in diameter. The Kulite is secured by press fitting the gage into the hole, unlike the heat flux gages which were secured by setscrews.

Kulite 2 is located 0.527 mm (0.02075 in) from the midspan of the blade to the center of the gage and 18.256 mm (.71875 in) from the leading edge (refer to Figure 3.21). The gage is inserted into a bored hole possessing the same dimensions as the

insertion hole of Kulite 1. Again the Kulite is secured by press fitting the gage into the opening.

Kulite 3 is located 4.68 mm (0.18425 in) from the blade midspan to the gage center and 41.275 mm (1.625 in) from the leading edge (refer to Figure 3.22). The gage is inserted into a bored hole having the same dimensions as the opening used to inset Kulite 1. Kulite 3 is inserted into the hole in the same fashion as used to secure Kulite 1.

Kulite 4 is located 0.794 mm (0.03125 in) from the midspan of the blade to the center of the gage and 15.08 mm (0.59375 in) from the leading edge (refer to Figure 3.22). The gage is inserted into a bored hole occupying the same dimensions as the one used for Kulite 1. The same press fitting technique is used to secure the gage as was used to secure the other three gages.

The wires from the three Kulites on the suction surface exit the blade through a 5.08 mm (0.200 in ) diameter channel drilled in the side of the blade. Four wires exit each gage. They then exit through a hole in the 12.7 mm (0.5 in) thick plexiglass endwalls having the same diameter of the blade channel. The wires are then connected to an amplifier via a bridge board.

The Kulite on the pressure surface exits through the same process as the other three gages on the suction surface do. It also connects to the bridge board which couples the gage to an amplifier.

# Chapter 4.0

## Procedure

This chapter gives a detailed description of the instrumentation and data acquisition systems used to operate the transonic cascade wind tunnel, and collect the required data for the various experiments. It also discusses the procedures used to conduct the various experiments. Specifically discussed are the low speed tests, upstream survey, leading edge survey, and heat flux and Kulite measurements. In each section a brief discussion is given on the data reduction process.

### 4.1 Instrumentation and Data Acquisition

The following paragraphs give a brief description of the instrumentation and data acquisition needed to operate the transonic cascade wind tunnel. Properties monitored during tunnel runs were total temperature, static exit pressure, total pressure, and tube temperatures. Data was digitally recorded by computer or visually monitored and recorded by hand (tube temperatures).

A 780B Pressure Sensor Industries Machine was used to record gage pressure within the test section. A static pressure tap and Pitot probe were located in the aluminum doors upstream of the blades to monitor inlet pressure conditions. Approximately 12.7 mm (0.5 in) from the trailing edge of the turbine blades, twenty-one static pressure taps were drilled to monitor exit pressure conditions. These static taps were connected to an ESP-32 channel pressure transducer. The exit static taps were

designated as channels 1-21, while the upstream total and static pressure were labeled as channels 31 and 32, respectively. The signals from the transducer were recorded using an IBM PC running a BASIC program (NOPROB). Assuming an isentropic ideal gas relationship and using the upstream total pressure and an average trailing edge static pressure, an average exit Mach number could be calculated. A BASIC program (MSB) was used to calculate the exit Mach number, knowing atmospheric pressure which was recorded daily from a barometer.

Another IBM PC ran a BASIC program which controlled tunnel operation. The tunnel control was dependent upon two feedback signals within the tunnel. The first was the upstream total pressure which was collected with a Data Instruments Model ES pressure transducer, and the second was total temperature. The total temperature is measured with a type K thermocouple. The signal is amplified using an Omega Thermocouple D.C. millivolt amplifier set at a 100 gain. The mounted tube thermocouple and the heater thermocouple were visually monitored by a 10 channel, type K Omega 650 thermocouple readout.

Another IBM PC was used in conjunction with two 6810 LeCroy Waveform Recorders to collect data for the majority of the experiments conducted. The LeCroy allowed sampling rates as high as 1 MHz. The transient recorder sampled the analog signals, digitized the samples, and wrote them to digital memory. The files were then stored in a binary file which had to be converted to an ASCII file which could be manipulated on a PC.

Other instrumentation and data acquisition will be discussed in more detail in the appropriate sections later in this chapter.

## 4.2 Low Speed Tests

The goal of this particular experiment was to gain experience in conducting a strut experiment, and to determine an appropriate strut to be placed in the transonic cascade wind tunnel.

### 4.2.1 Procedure

After completion of the experimental set-up, the Kiel probe was located at a position exactly 25.4 mm (1.0 in) downstream of the strut centerline. The probe was manually traversed 2.54 mm (0.1 in) graduations above and below at this particular axial location. At the various intermittent locations in the vertical plane the differential pressure was recorded using a MKS differential pressure transducer connected to a digital readout. The differential pressure was allowed to stabilize before it was recorded. The differential pressure measured was the difference between atmospheric pressure and the pressure being measured from the Kiel probe. Atmospheric pressure was recorded using a barometer located near the test facility at the beginning of each run.

After the probe was traversed vertically at a particular axial location, it was then relocated to the strut centerline, zero position. The traverse was then moved to a new axial location. Six different axial locations were considered. They started 25.4 mm (1.0 in) and ended 88.9 mm (3.5 in) from the strut's trailing edge. The same procedure was conducted at each axial location.

### 4.2.2 Data Reduction

The next step was to analyze the data acquired. The differential pressure recorded had the following conversion factor.

$$1\ V = 1\ psia \qquad [4.1]$$

Atmospheric pressure is known for the various runs. The static air temperature was also recorded for the various runs with a type K "air" thermocouple probe mounted on the side of the test facility. Assuming that the static pressure in the closed loop open test facility was equal to atmospheric pressure, the density of the air flow could be determined as follows

$$\rho = \frac{P_s}{RT_s} \qquad [4.2]$$

where $P_s$ is static pressure (atmospheric pressure), $R$ is the universal gas constant, and $T_s$ is the static temperature. The free-stream velocity, $U_\infty$, can now be calculated knowing the differential pressure in the test facility, $\Delta P_{H_2O}$.

$$U_\infty = \sqrt{\frac{2\Delta P_{H_2O}}{\rho}} \qquad [4.3]$$

The next step is to calculate the Reynolds number, $\mathrm{Re}_c$ ,based on the strut's chord length

$$\mathrm{Re}_c = \frac{U_\infty C}{\nu} \qquad [4.4]$$

where $C$ is the chord and $\nu$ is the kinematic viscosity. The Reynolds number for the strut in this particular facility was found to be approximately 3.4 x $10^4$. Using figure 2 in section 6-2 of *Fluid-Dynamic Drag* in conjunction with the Reynolds number the drag coefficient for the strut could be estimated. The other information needed to accomplish this task is the ratio($t/C$) of the strut's thickness, $t$, to the strut's chord. For this particular strut the value was approximately 41%. This corresponds to a drag coefficient, $C_D$, of approximately 0.27. With the preceding information known the velocity defect and wake half width can be calculated using equations 3.1 and 3.2 respectively.

A comparison can be made between the calculated values and the measured values with some manipulation of the measured results. The centerline total pressure measured by the Kiel probe along with the static pressure (assumed atmospheric) will yield the centerline Mach number.

$$M_c = \left[ \left( \left( \frac{P_{tc}}{P_s} \right)^{\gamma - 1/\gamma} - 1 \right) \left( \frac{2}{\gamma - 1} \right) \right]^{1/2} \qquad [4.5]$$

The centerline velocity, $U_c$, can then be calculated from the following relationship

$$U_c = M_c \sqrt{\gamma RT} \qquad [4.6]$$

Now the velocity defect from the measured results can be compared to the calculated values.

## 4.3 Upstream Survey

The goal of this experiment was to map out the wake defect and wake half width produced by this particular strut and to compare these results with calculated values. The following experiment was conducted in the transonic cascade wind tunnel. The strut was placed well upstream of the cascade so no disturbances would be encountered from the blades during the trailing edge survey of the strut. Equations 3.1 and 3.2 were used as a comparison with the experimental results. To accomplish this goal the following procedures were carried out.

### 4.3.1 Procedure

After completing the experimental set-up the total pressure probe was located exactly 25.4 mm (1.0 in) above the centerline of the strut and 25.65 mm (1.01 in) from the trailing edge. The probe traversed through a distance of approximately 50. 8 mm (2.0 in) at this particular location.

An ESP-32 channel pressure transducer was utilized to acquire the pressure data in conjunction with the 780B Pressure Sensor Industries Machine which was controlled by a BASIC program (NEWOSR) run on an IBM PC. During a particular run the

following data was recorded: total pressure upstream ($P_{tus}$), static pressure upstream ($P_{sus}$), total pressure downstream ($P_{tds}$), static pressure downstream ($P_{sds}$), total temperature ($T_t$), and the voltage from the LVDT. The total and static pressure upstream of the strut were collected by a total pressure probe and a static tap located in the test section doors upstream of the strut (refer to Figure 3.11). The static pressures downstream were collected from static taps. The total pressure downstream of the strut was collected by traversing the Pitot probe in a vertical plane. The total temperature and the voltage from the LVDT was acquired using LABVIEW run on an IBM PC.

The BASIC program (NEWOSR) also controlled the sample rate of the 780 Pressure Sensor Industries Machine. For these particular experiments the program was modified to acquire 100 data points while traversing 50.8 mm (2.0 in) in approximately 20 seconds. This corresponded to a sampling frequency of approximately 5 Hz. This also conveyed that a data point would be collected every 0.51 mm (0.02 in). The LABVIEW sampling frequency was also set at 5 Hz. A complete instrumentation schematic is shown in (Figure 4.1).

After this particular location was traversed the traverse was positioned such that the total pressure probe was 40.74 mm (1.604 in) from the stut's trailing edge, and the same procedure was conducted as outlined before.

### 4.3.2 Data Reduction

The same basic procedure was employed to reduce this data as was used in section 4.2.2. The voltage from the LVDT was converted to inches by using the following calibration equation

$$x(in) = 0.88565 \cdot (Volts) - 0.019665 \qquad [4.7]$$

The following calibration equation was used to convert the voltage form the thermocouple to temperature in ($^{o}$C)

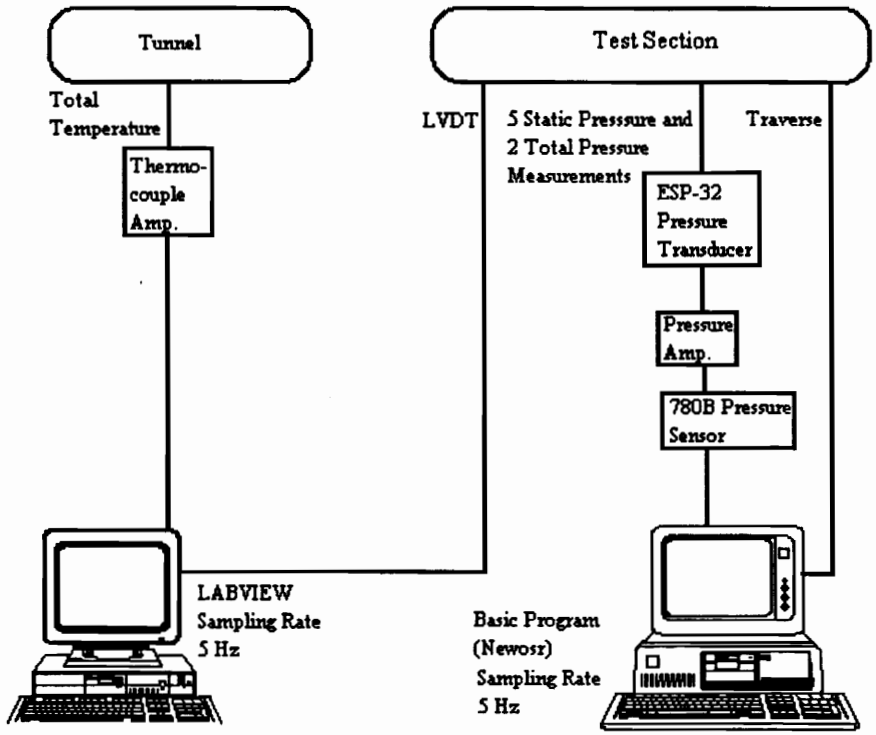


Figure 4.1 Instrumentation Schematic Upstream Survey

$$T_t(^{\circ}C) = 251.718 \cdot (Volts) + 2.040311 \qquad [4.8]$$

The final conversion which had to be made was to transform the pressure signal into actual pressure

$$P(psi) = 20(psig / volt) \cdot (Volts) + P_{atm} \qquad [4.9]$$

where $P_{atm}$ had to be added since the 780B Pressure Sensor Industry Machine measured gage pressure.

An average total and static pressure upstream was determined from the recorded data. Using isentropic flow parameters, $\gamma$ =1.4, the free-stream Mach number, $M_{fs}$ was determined from equation 4.5 with the appropriate substitutions made. The static temperature was determined from the following equation since the free-stream Mach number, and an average total temperature were known for the various runs.

$$T = \frac{T_t}{\left(1 + \frac{\gamma - 1}{2} M^2\right)} \qquad [4.10]$$

The procedure from this point is basically as that described in the procedure section (4.2.2) of the Low Speed Tests. The free-stream velocity was calculated, and was used with the other variables to calculate the dimensionless Reynolds number. The Reynolds number based on the chord was found to be 3.3 x $10^5$. This yielded a drag coefficient of approximately 0.04. Knowing this information, equations 3.1 and 3.2 were used to calculate the wake half width and velocity defect to compare with the experimental results.

## 4.4 Leading Edge Survey

The objective of this particular experiment was to characterize the inlet flow to the turbine blade cascade by traversing a hot-wire in a plane close to the leading edge of the blades while moving the upstream disturbance (strut) to different locations. Data acquisition could be separated into high frequency and low frequency sampled data. The low frequency sampled data was used to establish the velocity profile of the flow entering the turbine cascade and to calculate the turbulence intensity. The high frequency sampled data was used to calculate the integral length and time scales as well as the turbulence intensity.

### 4.4.1 Procedure

After securing the strut and the traverse to the side of the test section, the hot-wire was positioned such that the LVDT produced a zero voltage. This corresponded to the zero position of the hot-wire (refer to Figure 4.2). The hot-wire was traversed along the surface of the blades for approximately 38.1 mm (1.5 in) which corresponds to the blade spacing or pitch.

The following data was collected during the various traverses: hot-wire voltage, total pressure, differential pressure, total temperature, and LVDT voltage. The IFA 100 Flow Analyzer was used to operate the hot-wire. For a detailed description of the hot-wire operation refer to IFA 100 Flow Analyzer Manual. A Data Instruments Model ES pressure transducer was used in conjunction with a total pressure probe to collect the total pressure. The differential pressure was measured using a MKS pressure transducer. A type K "air" thermocouple measured the total temperature. The signal from the thermocouple was amplified using an Omega Thermocouple D.C. millivolt amplifier set at a 100 gain. The LVDT output was connected to channel 2 of the IFA 100 Flow Analyzer so the signal could be filtered.

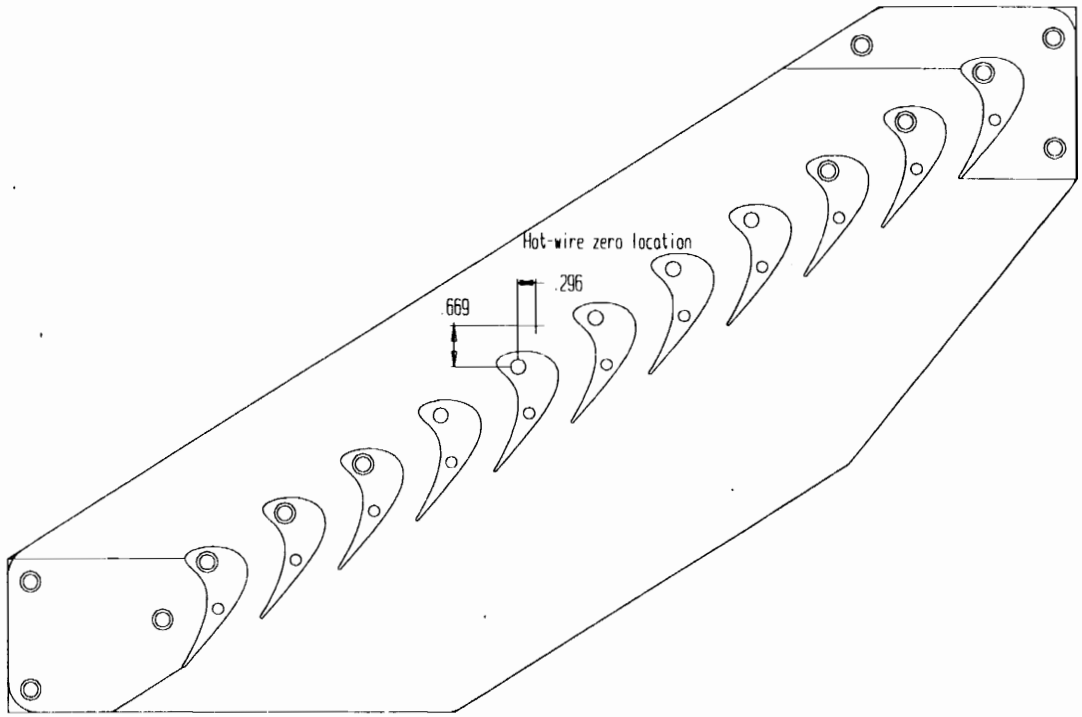


Figure 4.2 Hot-wire Start Location

The 6810 LeCroy Waveform recorder was connected to an IBM PC to acquire all of the above measurements. The sampling rate for these particular runs was 5 kHz, and the data was filtered at 2.5 kHz. Total pressure, total temperature, and differential pressure were low passed filtered using a Pressure Devices filter. The hot-wire and LVDT signal were low pass filtered using the IFA 100 Flow Analyzer filter. For a complete instrumentation schematic (refer to Figure 4.3).

The properties were measured during steady operation of the transonic cascade wind tunnel. This corresponded to a time in the run where the total pressure in the test section was relatively constant, making the inlet flow conditions constant. The traverse was controlled by the basic program (NEWOSR) run on an IBM PC. As the traverse started to move the voltage from the LVDT triggered the 6810 LeCroy Waveform recorder to acquire the other properties. Table 4.1 explains the LeCroy set-up for this particular experiment.

**Table 4.1 LeCroy Set-up, Leading Edge Survey**

| Sampling Frequency 5 kHz, Duration of run 13.1s | | |
|---|---|---|
| **Channel #** | **Name** | **Data** |
| 1 | HW | Hot-wire signal |
| 2 | DP | Differential |
| 3 | PT | Total pressure |
| 4 | TT | Total temperature |
| 5 | LVDT | LVDT signal |

After traversing the hot-wire for a particular location of the strut, the strut was repositioned and the same procedure was conducted again. Five different locations of the strut were considered. This data was utilized to establish the velocity profile of the incoming flow and the turbulence intensity from the strut at the five different locations.

The high sampling frequency part of the experiment was conducted in the same manner as the low frequency data acquisition portion. The data was sampled at 100 kHz for 2.61 seconds and low passed filtered at 50 kHz. Only one location of the strut was

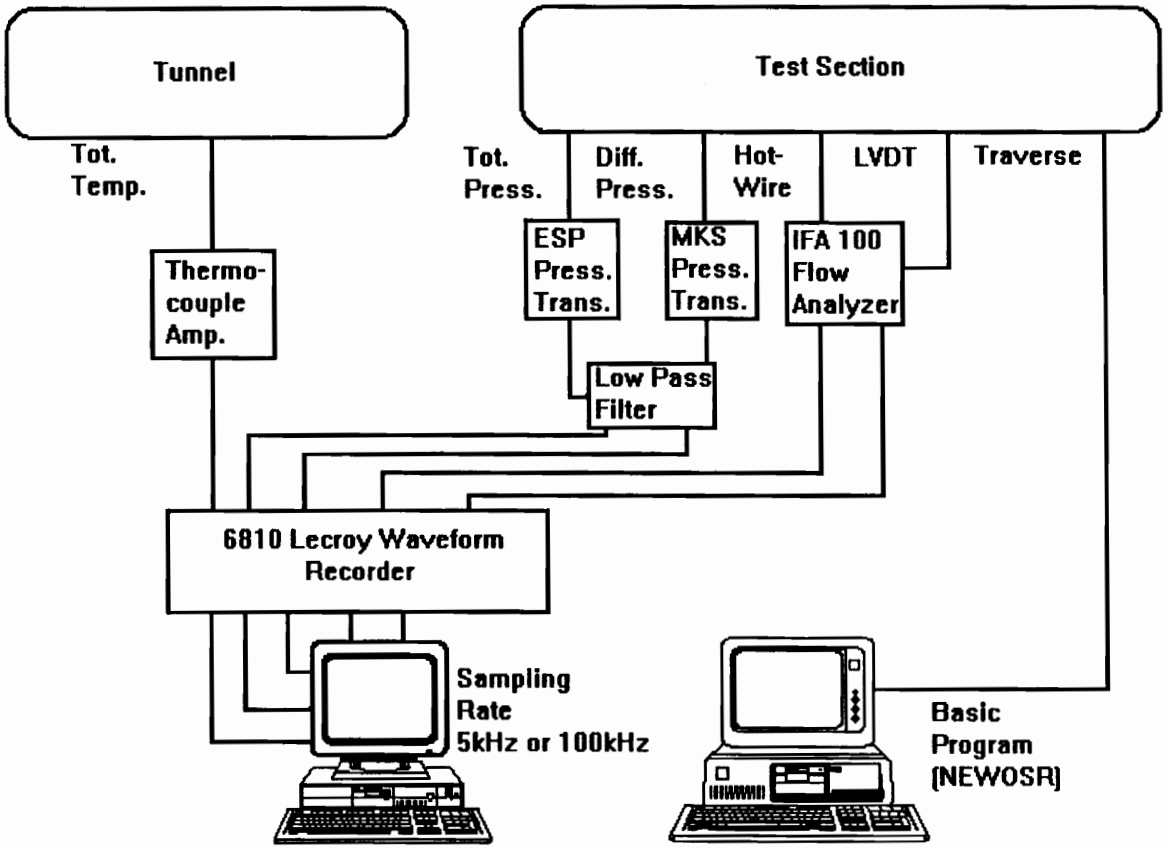


Figure 4.3 Instrumentation Schematic Leading Edge Survey

considered. It was a location near the leading edge of the turbine blade. The preceding data allowed the calculation of the integral length and time scales.

### 4.4.2 Data Reduction

The first step was to convert the total pressure, total temperature, differential pressure, and LVDT signal into meaningful data. The differential pressure, LVDT, and total temperature signals were converted using the following equations, respectively (4.1, 4.7, and 4.8). The following equation was used to convert the total pressure signal

$$P_t(psi) = 25.09389(psig/volt)\cdot(volts) - 25.19769(psig) + P_{atm} \qquad [4.11]$$

After the preceding conversions had been completed the actual hot-wire data could be analyzed. The same basic equations needed to calibrate the hot-wire are needed to reduce the hot-wire data. The hot-wire calibration procedure is outlined in Appendix C. The result of the calibration yielded an equation which was used to convert the hot-wire signal into meaningful data. After the low sampling frequency tests were concluded the hot-wire broke and was repaired to collect data for the high sampling frequency runs. Therefore, two calibration equations are needed to reduce the data. For the low sampling frequency (5 kHz) data acquisition, where the probe was traversed at the five different strut locations, the following equation was employed

$$\rho U = \mu\left(3012.718795\left(\frac{(V^2/k)}{(T_f - T_s)}\right)\left(\frac{T_f}{T_s}\right)^{-0.17} - 1165.61744\right)^{(1/0.51)} \qquad [4.12a]$$

and the ensuing equation was utilized in the data reduction where the data was sampled at a high sampling frequency (100 kHz).

$$\rho U = \mu\left(2794.964769\left(\frac{\left(V^2/k\right)}{\left(T_f - T_s\right)}\right)\left(\frac{T_f}{T_s}\right)^{-0.17} - 697.9084968\right)^{(1/0.51)} \qquad [4.12b]$$

To accomplish the actual data reduction a FORTRAN program was written (HWDAT), which was very similar to the hot-wire calibration program (HWCAL). These programs can be viewed in Appendix B.

The preceding equations (4.12a and 4.12b) calculate the product of the density and velocity since the flow is approaching the compressible range (Ma = 0.36) at the measurement location. After the combination of $\rho U$ had been calculated, the turbulence intensity was calculated using a modified equation 2.2.

$$Tu = \frac{\sqrt{\overline{\rho U'^2}}}{\overline{\rho U}} \qquad [4.13]$$

This was accomplished by using a FORTRAN program (VELTURB) which can be viewed in Appendix B.

The high sampling frequency data was reduced by using two LABVIEW programs (DGHSPCTM.VI and LORENHFM.VI) refer to Johnson (1995). The first program was used to determine the integral length and time scales. The program read in 2048 points in a 32 K file and used the auto correlation to determine the integral length and time scales. The entire file for this process was 256 K, therefore, the program calculated eight different values for the length and time scales for the different positions within the wake. The second program provided a spectral analysis of the data. The program is set-up to read 2048 points in a file of length 64 K. It then performs a Fast Fourier Tansform of the data. The same 256 K file was used for this analysis, therefore, the power spectra is calculated over four different time periods of the run. The results are then written to a file and the power spectra of the data can be plotted for a better understanding of the results.

## 4.5 Heat Flux and Kulite Measurements

The objective for this particular experiment was to measure the change in local heat transfer and surface pressure due to the impingement of a mean velocity defect and change in turbulence intensity at various locations along a turbine blade. The data acquisition could be separated into high frequency sampled data and low frequency sampled data. The low frequency sampled data was used to determine the average heat transfer coefficient and the high frequency sampled data allowed for a spectral analysis and a heat flux turbulence intensity measurement.

### 4.5.1 Procedure

The HFM-6 insert gage and Kulite tests consisted of measuring heat flux and surface pressure during heated runs with initial tube temperatures at 93°C (200°F) for the four particular locations of the strut. Specifically, measured during these runs were heat flux from the blade, the blade surface temperature, the blade surface pressure, total temperature and total pressure. The Heat flux Micosensors operated with an AMP #6 amplifier box manufactured by Vatell Corporation. The amplifier supplied a 0.1 mA current to provide the RTS measurement. The Kulites' signals were amplified by a Measurements Group 2310 Signal Conditioning amplifier. A Data Instruments Model ES pressure transducer was used in conjunction with a total pressure probe to collect the total pressure. A type K "air" thermocouple measured the total temperature. The signal from the thermocouple was amplified using an Omega Thermocouple D.C. millivolt amplifier set at a 100 gain.

The 6810 LeCroy Waveform recorder was connected to an IBM PC to acquire all measurements for both the high and low frequency sampled data. All of the signals were passed through a low pass filter at half the sampling rate. For a complete instrumentation schematic showing the high and low sampling frequency set-ups refer to (Figures 4.4 and 4.5).

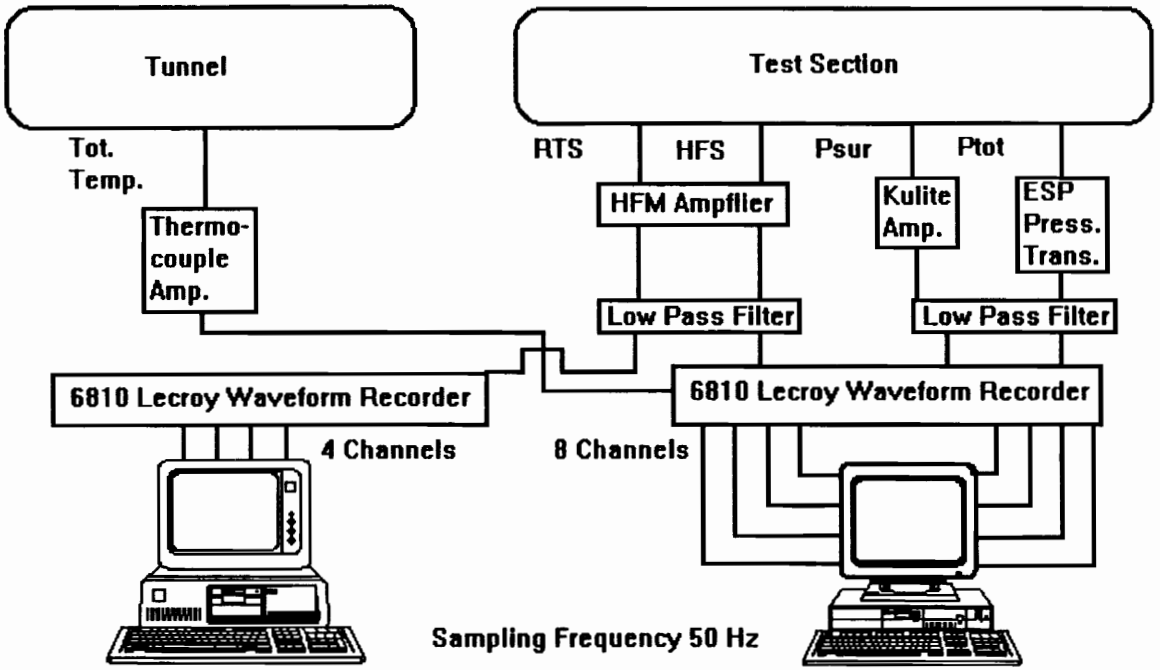


Figure 4.4 Instrumentation Schematic Low Sampling Frequency

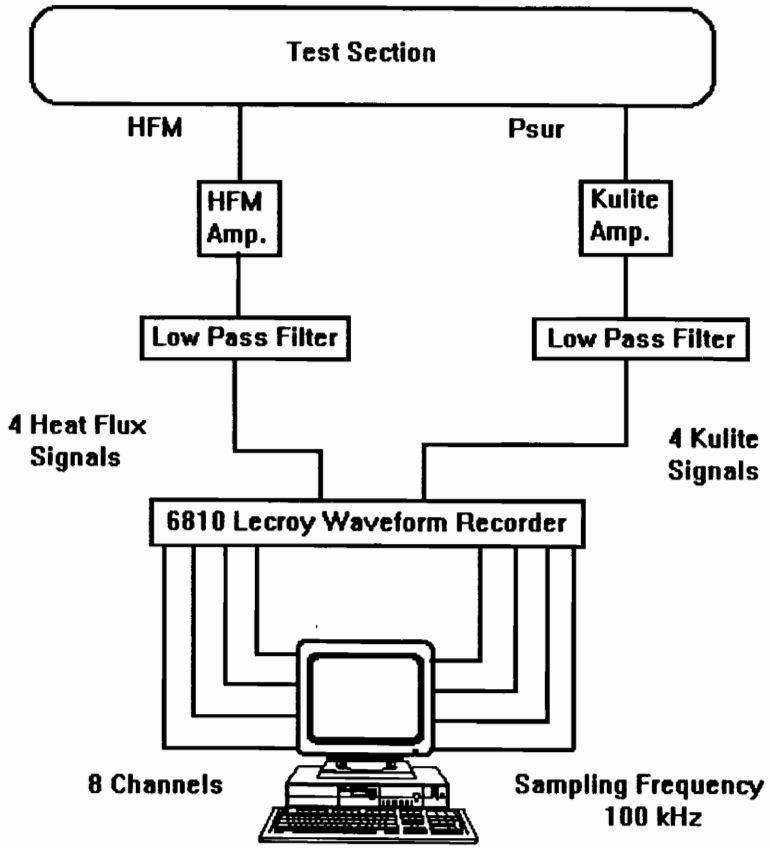


Figure 4.5 Instrumentation Schematic High Sampling Frequency

The low sampling frequency runs were conducted using the following procedures. Both the HFS and the RTS could be calibrated to zero level by turning small potentiometer knobs on the amplifier and connecting a voltmeter into the respective output channel. This was done at the beginning of each day at ambient conditions. Since no heat transfer was occurring, the heat flux was set to a zero value. The resistance of the RTS was measured using the voltmeter and was recorded as the ambient resistance. The RTS was then zeroed implying that the room temperature resistance became the zero volt level resistance offset. The temperature was also measured using a hand held thermocouple to verify the RTS calibration equations.

The HFS and RTS signals were acquired using the 6810 LeCroy Waveform Recorder, and the actual offsets were recorded. The copper tubes (heat exchanger) were heated next. Data acquisition was started, and after approximately 5 to 10 seconds the tunnel was operated. This allowed a short duration of time in the beginning of the run to check the zero level of the heat flux signal. Due to limitations in data acquisition, only two of the Kulite signals were collected during a particular run. The sampling frequency for these runs was 50 Hz, and all the signals were low pass filtered at 25 Hz. Table 4.2 shows the LeCroy set-up for this part of the experiment.

**Table 4.2 LeCroy Set-up, HFM and Kulite, Low Sampling Frequency**

| **LeCroy Module 1** | | | | | |
|---|---|---|---|---|---|
| **Sampling Rate 50 Hz** | | | **Duration 81 seconds** | | |
| Channel | Name | Data | Channel | Name | Data |
| 1 | HFS1 | q", heat flux | 5 | PSUR1 or 3 | surface pressure |
| 2 | HFS2 | q", heat flux | 6 | PSUR2 or 4 | surface pressure |
| 3 | HFS3 | q", heat flux | 7 | PTOT | Total pressure |
| 4 | HFS4 | q", heat flux | 8 | TTOT | Total temperature |
| **LeCroy Module 2** | | | | | |
| 1 | RTS1 | surface temperature | 3 | RTS3 | surface temperature |
| 2 | RTS2 | surface temperature | 4 | RTS4 | surface temperature |

After each run of the tunnel, the test section and blades were brought back to ambient conditions by the use of a vortex tube located in the top of the test section. The vortex tube's air was supplied by shop air at approximately 414 kPa (60 psi). This corresponded to an outlet air temperature between -1°C and 1.7°C ( 30°F and 35°F). The instrumented blade temperature was monitored by inserting a thermocouple into the screw hole of the blade. This ensured that the test section conditions were the same in the beginning of each run. At the same time the test section was being cooled to ambient conditions, the heat exchanger tubes were being heated. This process usually required approximately 15 minutes after the initial run.

Several runs were conducted at a particular strut location to establish some degree of confidence in the results and to check for repeatability. The strut was then moved to another location and the preceding operation was carried out.

The high sampling frequency runs were conducted using the same basic procedures except for a couple of differences in the data acquisition portion. Instead of acquiring data in the beginning of the run, data was collected only during steady operation of the tunnel for a short duration. The four HFS and the four Kulite signals were collected during these runs. Table 4.3 shows the LeCroy set-up for the high sampling portion of the experiment.

**Table 4.3 LeCroy Set-up, HFM and Kulite, High Sampling Frequency**

| **LeCroy Module 1** | | | | | |
|---|---|---|---|---|---|
| **Sampling Rate 100 kHz** | | | **Duration 2.62 seconds** | | |
| Channel | Name | Data | Channel | Name | Data |
| 1 | HFS1 | q", heat flux | 5 | PSUR1 | surface pressure |
| 2 | HFS2 | q", heat flux | 6 | PSUR2 | surface pressure |
| 3 | HFS3 | q", heat flux | 7 | PSUR3 | surface pressure |
| 4 | HFS4 | q", heat flux | 8 | PSUR4 | surface pressure |

This data was usually taken after the low sampling frequency runs before the strut was moved into a new location.

### 4.5.2 Data Reduction

The first step in the data analysis is to convert the signals from the various measurement devices into meaningful data. Equations 4.8 and 4.11 were used to convert the voltage to total temperature and total pressure, respectively. The formulas to convert voltage to surface pressure were provided by the manufacturer. They provided the following calibration equations for the Kulites

Kulite 1
$$P_{sur1}(psi) = \frac{2.680(psig/mvolts)\cdot(Volts)}{G_{sur}} + P_{atm} \qquad [4.13a]$$

Kulite 2
$$P_{sur2}(psi) = \frac{2.307(psig/mvolts)\cdot(Volts)}{G_{sur}} + P_{atm} \qquad [4.13b]$$

Kulite 3
$$P_{sur3}(psi) = \frac{1.541(psig/mvolts)\cdot(Volts)}{G_{sur}} + P_{atm} \qquad [4.13c]$$

Kulite 4
$$P_{sur4}(psi) = \frac{2.411(psig/mvolts)\cdot(Volts)}{G_{sur}} + P_{atm} \qquad [4.13d]$$

where $G_{sur}$ is the gain setting of the amplifier. The gain was set at 50 for all of the Kulites. The manufacturer of the heat flux microsensors also provided the formulas to convert voltage to a heat flux or surface temperature. They provided the following sensitivity equations for the heat flux signal

HFM-6 Gage 1
$$S(T)_1 = \frac{E_q}{G_q q''} = 0.029 \cdot T_{sur}(^{\circ}C) + 16.22\mu V/W/cm^2 \qquad [4.14a]$$

HFM-6 Gage 2 $$S(T)_2 = \frac{E_q}{G_q q''} = 0.0338 \cdot T_{sur}(^oC) + 15.55\mu V / W / cm^2$$ [4.14b]

HFM-6 Gage 3 $$S(T)_3 = \frac{E_q}{G_q q''} = 0.035 \cdot T_{sur}(^oC) + 21.33\mu V / W / cm^2$$ [4.14c]

HFM-6 Gage 4 $$S(T)_4 = \frac{E_q}{G_q q''} = 0.0355 \cdot T_{sur}(^oC) + 23.09\mu V / W / cm^2$$ [4.14d]

where $G_q$ is the gain setting on the HFM amplifier for the heat flux signal, $E_q$ is the amplified voltage from the sensor, q" is the heat flux. The gain was set at 1000 for all of the heat flux signals. The voltage conversion equations for the RTS are as follows

HFM-6 Gage 1 $$T_{sur_1}(^oC) = 2.9528(^oC/\Omega) \cdot \left(\frac{E_T}{I \cdot G_T} + R_{amb}\right) - 460.02^0C$$ [4.15a]

HFM-6 Gage 2 $$T_{sur_2}(^oC) = 2.80929(^oC/\Omega) \cdot \left(\frac{E_T}{I \cdot G_T} + R_{amb}\right) - 463.673^0C$$ [4.15b]

HFM-6 Gage 3 $$T_{sur_3}(^oC) = 3.2683(^oC/\Omega) \cdot \left(\frac{E_T}{I \cdot G_T} + R_{amb}\right) - 486.07^0C$$ [4.15c]

HFM-6 Gage 4 $$T_{sur_4}(^oC) = 4.8765(^oC/\Omega) \cdot \left(\frac{E_T}{I \cdot G_T} + R_{amb}\right) - 415.47^0C$$ [4.15d]

where $E_T$ is the amplified voltage from the RTS, $I$ is the current, $G_T$ is the RTS gain, and $R_{amb}$ is the ambient resistance measured at the beginning of each day. The gain for all of the RTS's was set at 500.

In determining the heat transfer coefficient for the various runs the adiabatic wall temperature is of major importance. The adiabatic wall temperature, $T_{aw}$, can be determined for long heated runs (>30s). As the surface temperature, $T_{sur}$, of the blade increases due to the heated flow, the total temperature, $T_t$, during the run decreases. At a certain point during the run the heat flux goes to zero (q"=0) refer to Figure 4.6. At this point the surface temperature, $T_{sur}$, should equal the adiabatic wall temperature, $T_{aw}$. An assumption is then made that the difference between $T_t$ and $T_{aw}$ is constant and this offset is used to recreate $T_{aw}$.

$$T_t - T_{aw} = \frac{rU_\infty^2}{2c_p} \text{ assumed constant} \qquad [4.16]$$

$$T_{aw} = T_t - \Delta T_{q"=0} \text{ where } \Delta T_{q"=0} = T_t - T_{sur} \text{ at q"=0} \qquad [4.17]$$

One of the major benefits of the HFM is the ability of the sensor to measure the heat flux without knowing the temperature field. This allows the recovery temperature and r to be calculated since the adiabatic wall temperature is already known

$$T_R = T_t + \frac{U_\infty^2}{2Cp}(r-1) = T_{aw} \qquad [4.18]$$

Once the adiabatic wall temperature is known, the heat transfer coefficient can be calculated from

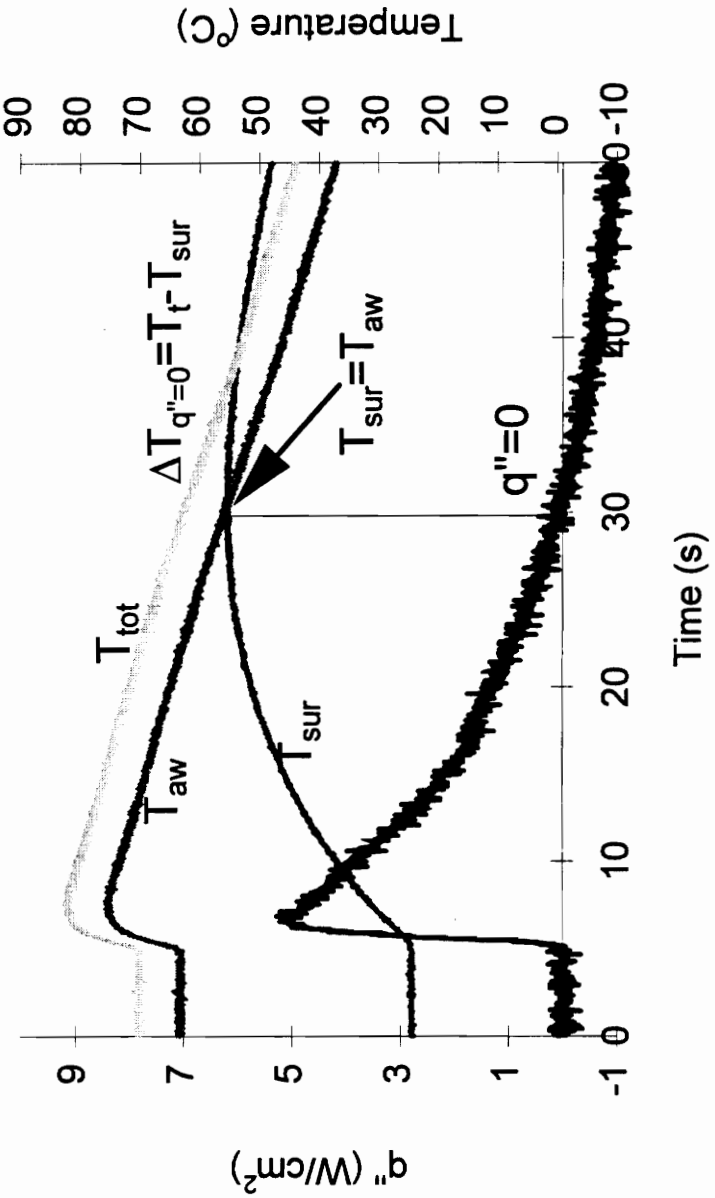


Figure 4.6 Example of Run Data for Heat Flux

$$h = \frac{q''}{T_{aw} - T_{sur}} \qquad [4.19]$$

since the heat flux, q", and the surface temperature, $T_{sur}$, are measured from the heat flux microsensor. Comparisons can then be made between these experimental heat transfer coefficients and other experimental heat transfer coefficients as well as computer predictions. The Nusselt number can be calculated next

$$Nu = \frac{hL}{k} \qquad [4.20]$$

where L is the blade chord length 38.1 mm (1.5 in) and $k$ is the thermal conductivity at the reference temperature

$$T_{REF} = 0.5 \cdot (T_{sur} - T_{\infty}) + 0.22 \cdot (T_{aw} - T_{\infty}) + T_{\infty} \qquad [4.21]$$

The 100 kHz data was manipulated in several ways in an attempt to understand what effects the strut wake were having on the overall heat transfer. A spectral analysis was performed using a LABVIEW program(LORENHFM.VI). The program could read a 64 K file. The 100 kHz data files were 256 K in length. The program was set up to read in 2048 data points of this 64 K file and perform a Fast Fourier Transform on the data. It would then read in 2048 more points and continue until the entire 64 K file had been read. At this point it would average all of the FFT's and write the results to a file. The program would then read in the next 64 K of the 256 K file. This was continued until the entire file had been analyzed. Another useful tool in evaluating the effect of the wake defect and turbulence on the heat transfer is the heat flux turbulence intensity. The definition of $Tu_q$ is based on the RMS of the heat flux divided by the mean heat flux value.

$$Tu_q = \frac{\sqrt{\overline{q''^2}}}{\overline{q''}} \qquad [4.22]$$

The value of $Tu_q$ was calculated every 2048 points and then an average of all these values was taken to determine the true value of $Tu_q$. This procedure was employed due to the small variation in the average heat flux over the run.

The pressure data was analyzed using the same basic procedures outlined above. The 100 kHz data was analyzed using the same spectral analysis. The 50 Hz data was graphed to see if there was any change in the surface pressure due to the strut wake.

# Chapter 5.0

## Results

The following sections report the results for the low speed experiments, upstream survey, leading edge survey, heat flux and Kulite measurements, and the heat flux turbulence intensity measurements. A detailed discussion of the results from these various experiments is provided in the individual sections. The intent of this chapter is to give explanations on the effects that a localized wake providing a varying turbulence intensity has on blade surface heat transfer.

### 5.1 Low Speed Results

The purpose of the low speed tests was to gain a better understanding of the wake shed by a small strut and how well it could be approximated. This was accomplished by placing the strut in a low speed (incompressible) test facility and measuring the velocity defect as well as the wake width at various axial locations behind the strut. The data was reduced and plotted as the normalized pressure versus the vertical position behind the strut. The normalized pressure is the total pressure, $P_t$, at a specific location divided by the total free-stream pressure, $P_{tfs}$. The results are shown in figures 5.1a through 5.1f. Notice how the velocity defect decreases as the axial measuring position increases. For example the centerline normalized pressure at an axial distance of 1.0" behind the strut is 0.9869 and at 3.5" it is 0.99054. The value at 3.5" corresponds to a higher centerline total pressure which in turn means that the velocity has increased at this position. The centerline velocity is approaching the free-stream velocity further downstream of the strut. Notice also how the wake half width increases as the axial measuring position increases. For example the wake half width at 1.0" is approximately 0.2" and at 3.5" it is approximately 0.5".

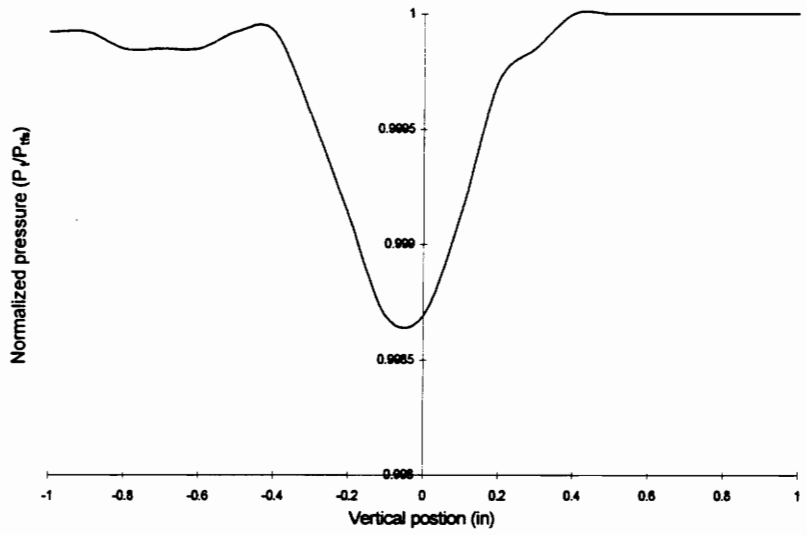


Figure 5.1a. Normalized pressure distribution 1.0" behind strut

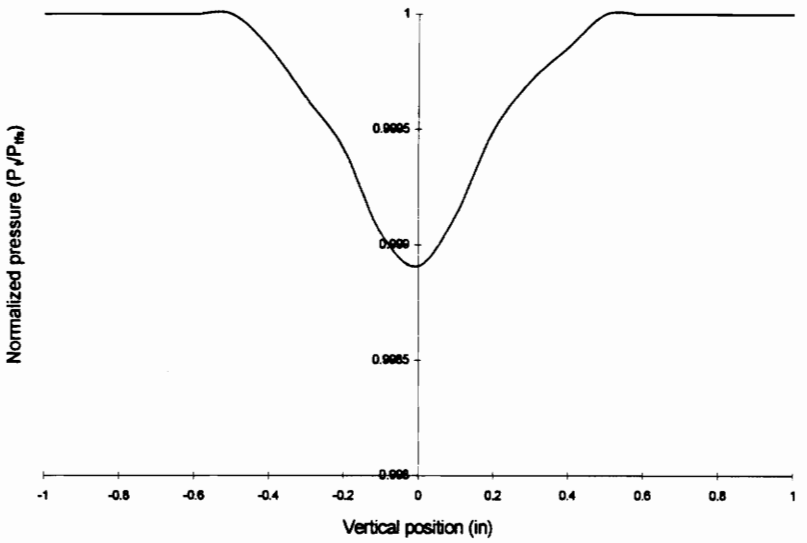


Figure 5.1b. Normalized pressure distribution 1.5" behind strut

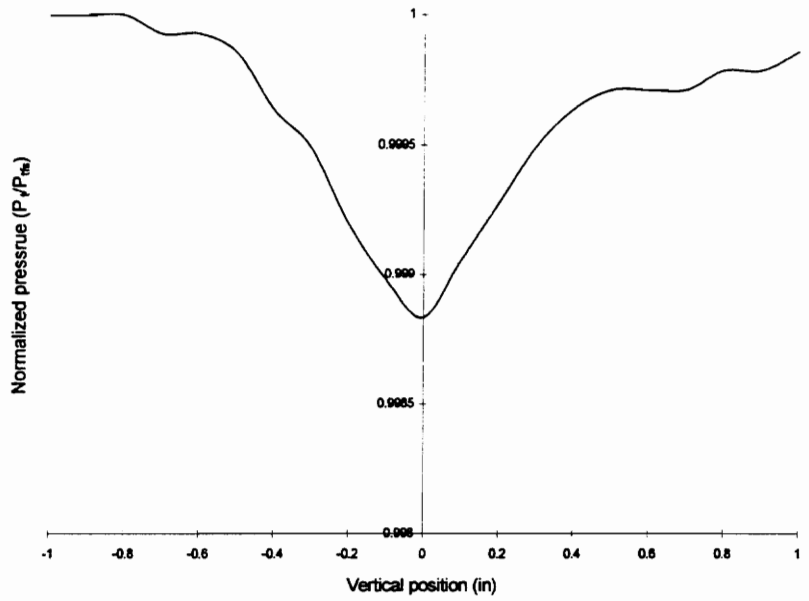


Figure 5.1c. Normalized pressure distribution 2.0" behind strut

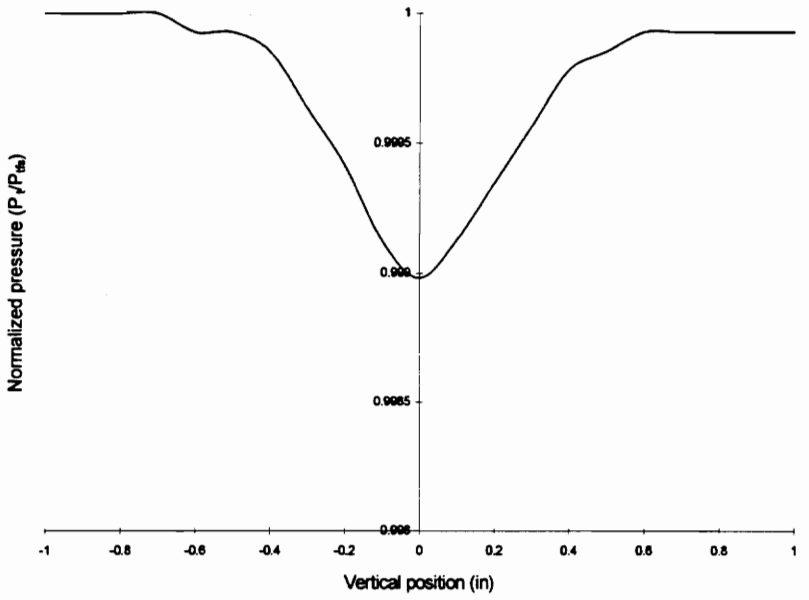


Figure 5.1d. Normalized pressure distribution 2.5" behind strut

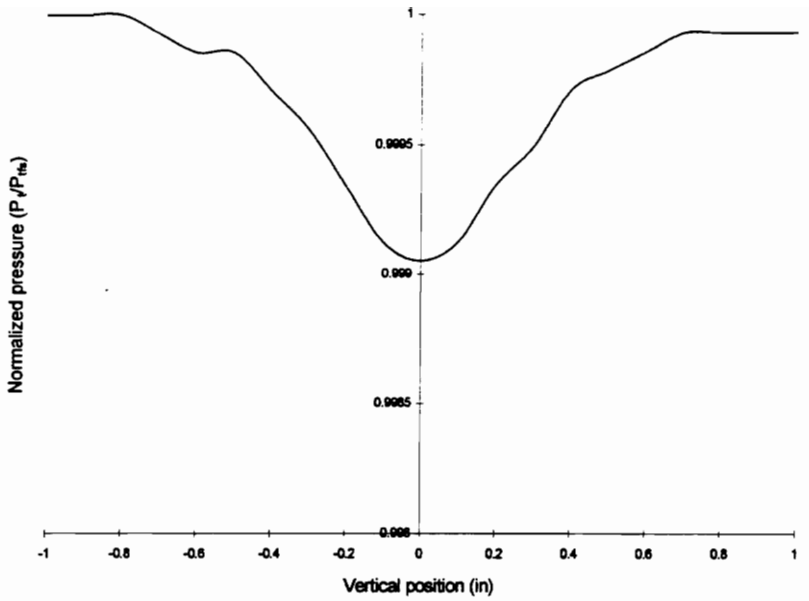


Figure 5.1e. Normalized pressure distribution 3.0" behind strut

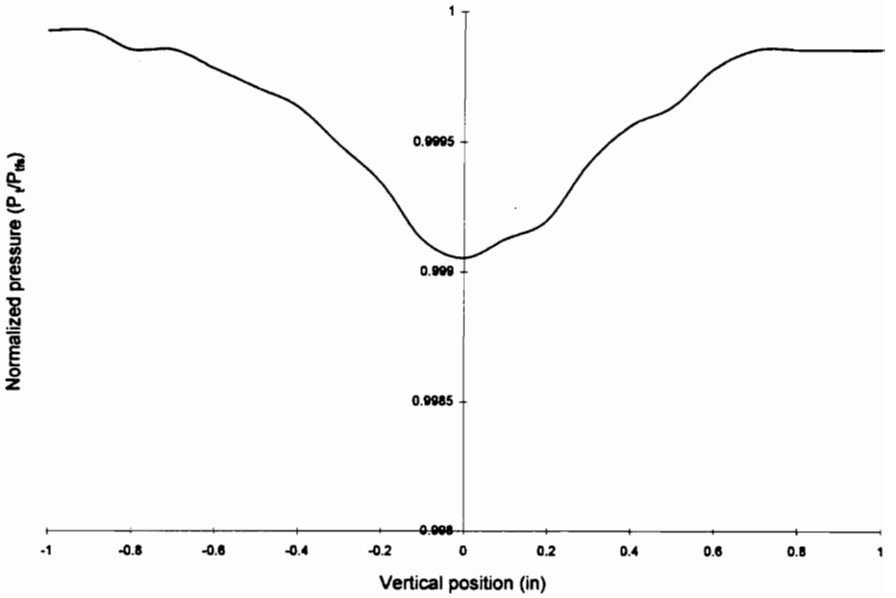


Figure 5.1f Normalized pressure distribution 3.5" behind strut

The next step in the process was to compare the measured data with the results produced by using equations 3.1 and 3.2. To accomplish this task the measured data was manipulated as described in section 4.2.1 [Low Speed Tests]. The goal for this endeavor was to check the experimental results using equations 3.1 and 3.2 with the measured experimental data. These results were tabulated and can be found in Table 5.1. The table does not list the experimental wake half width because the distance between the data points collected was not close enough to give an accurate representation of the wake half width. The plots give some indication of the approximate wake half width.

**Table 5.1 Low Speed Wind Tunnel (Wake Profile) Results**

| Axial Position (in) | $\Delta u_{cmeasured}$ (m/s) | $\Delta u_{ccalculated}$ (m/s) | $b_{calculated}$ (in) |
|---|---|---|---|
| 1.0 | 6.2945 | 8.8047 | 0.1628 |
| 1.5 | 5.5495 | 7.2010 | 0.1993 |
| 2.0 | 5.3070 | 6.2414 | 0.2302 |
| 2.5 | 5.3168 | 5.5928 | 0.2574 |
| 3.0 | 5.0717 | 5.1055 | 0.2819 |
| 3.5 | 5.0740 | 4.7290 | 0.3045 |

Notice how the calculated values agree better with the measured results as the axial position downstream of the strut increases. This was expected, the equations do not produce good results in the near wake due to approximations in the derivation. At the axial position of 1.0" there is approximately 39% difference in the measured and calculated velocity defect as compared to an approximate 6% difference at an axial position of 3.5".

The above table shows that equation 3.1 produces acceptable results at distances greater than 2.0" downstream of the strut. Therefore, equation 3.1 and 3.2 were used to estimate the wake half width and the velocity defect. This eliminated some of the experimentation needed in determining an appropriate sized strut to place in the transonic wind tunnel.

## 5.2 Upstream Survey

The purpose of the upstream survey was to confirm the analytical values for the wake velocity defect and wake half width obtained from using equations 3.1 and 3.2. This was accomplished by placing the strut upstream of the turbine cascade in the transonic wind tunnel, and traversing a total pressure probe at two axial locations downstream of the strut's trailing edge. The data collected was reduced and plots were generated to better quantify the results. The data was plotted as normalized pressure versus vertical position from the strut's centerline. The normalized pressure was defined as the total pressure downstream, $P_{tds}$, at a specific location divided by the total free-stream pressure, $P_{tfs}$. Three runs were conducted at location 1 (1.01" from the trailing edge) and two runs were conducted at location 2 (1.604" from the trailing edge). Figure 5.2a through 5.2c show the results at a location 25.64 mm (1.01 in) from the strut's trailing edge. Figures 5.3a and 5.3b show the results at a location 40.74 mm (1.604 in). Notice how the velocity defect decreases as the measuring position from the trailing edge increases. For example, the normalized centerline pressure at an axial distance of 1.01" behind the strut is approximately 0.98 and has increased to 0.99 at 1.604" from the trailing edge. The larger value corresponds to a higher centerline total pressure which in turn means that the velocity has increased downstream of the strut. The wake half width also increases as the measuring distance increases from the trailing edge. At 1.01" the wake half width is approximately 4.57 mm (0.18 in) and at 1.604" the wake width is 5.59 mm (0.22 in).

The experimental results were then compared with the analytical analysis using equations 3.1 and 3.2. The experimental data was reduced using the methods outlined in section 4.3.2 [Upstream Survey]. The results were tabulated and can be found in Table 5.2.

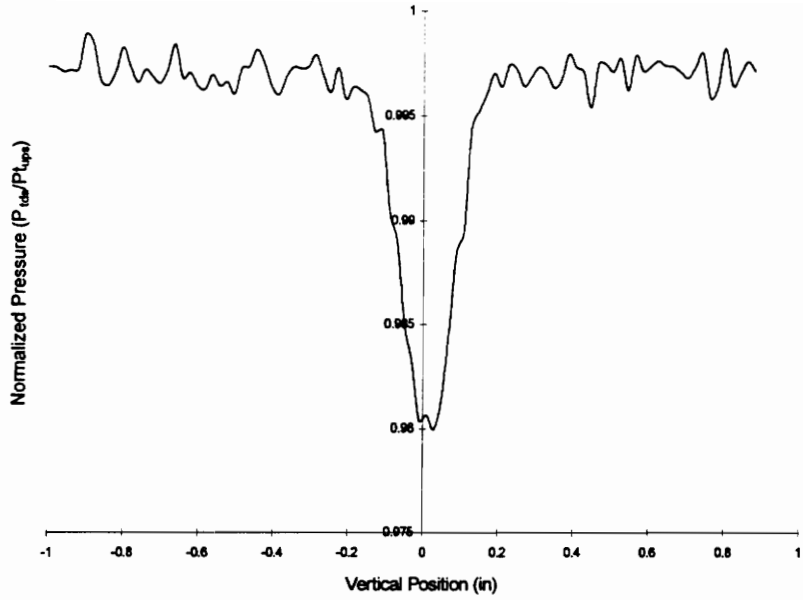


Figure 5.2a Normalized pressure distribution 1.01" from trailing edge

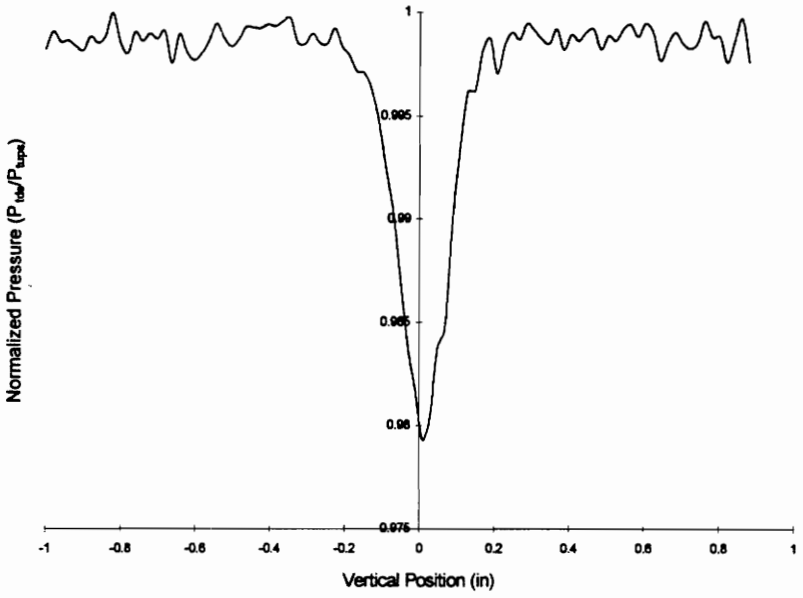


Figure 5.2b Normalized pressure distribution 1.01" from trailing edge

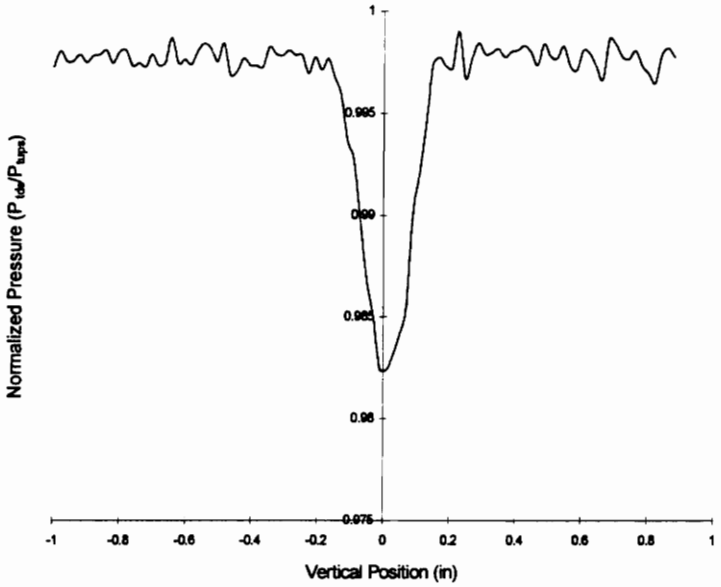


Figure 5.2c Normalized pressure distribution 1.01" from trailing edge

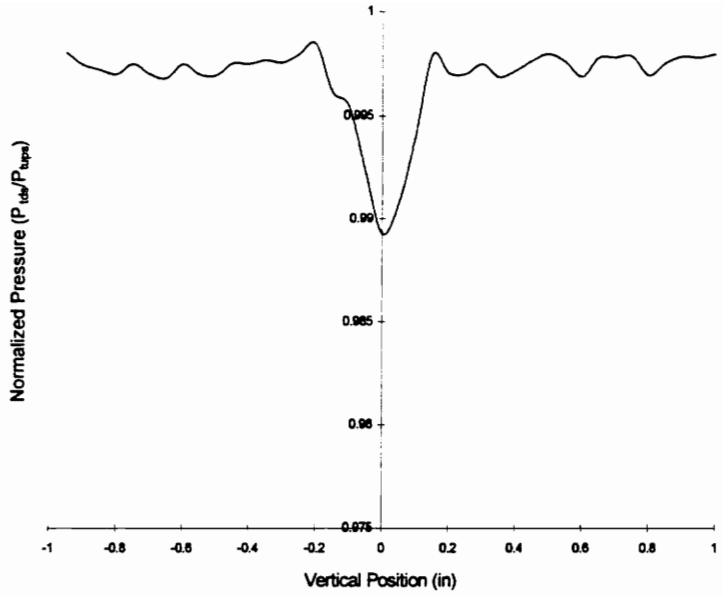


Figure 5.3a Normalized pressure distribution 1.604" from trailing edge

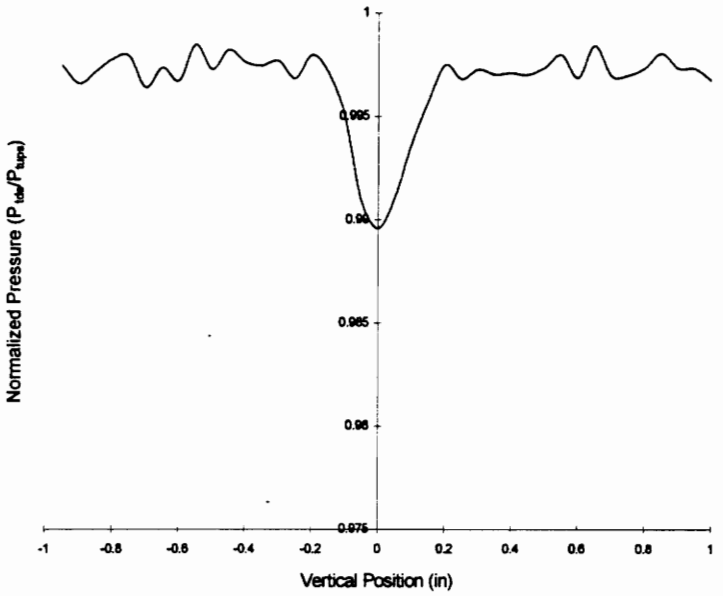


Figure 5.3b Normalized pressure distribution 1.604" from trailing edge

**Table 5.2 Upstream Survey Transonic Wind Tunnel (Wake Profile) Results**

| Axial Position (in) | $\Delta U_{ccalculated}$ (m/s) | $\Delta U_{cmeasured}$ (m/s) | $b_{calculated}$ (mm) | $b_{measured}$ (mm) |
|---|---|---|---|---|
| 1.01 | 14.45 | 12.63 | 1.52 | 3.81 |
| 1.01 | 15.01 | 12.84 | 1.52 | 4.32 |
| 1.01 | 13.63 | 12.21 | 1.52 | 3.56 |
| 1.604 | 10.96 | 9.87 | 2.02 | 5.08 |
| 1.604 | 10.96 | 9.96 | 2.02 | 5.33 |

The calculated values show better agreement with the measured results at location 2 (1.604" from trailing edge). This was expected since the accuracy of the equations is improved further downstream of the near wake. The calculated values change due to a change in the free-stream velocity for each run. At location 1 there is an average difference of 14.3% in the measured and calculated values for the wake deficit. The difference has decreased to 10.5% at location 2 further downstream. The wake half width is not approximated well by equation 3.2. There are large differences between the measured and calculated values for the wake half width. One possible reason for this large error could be the drag coefficient adopted. Although the results for the wake half width are different than expected, they are acceptable. The velocity defect and wake half width are adequate to create a small disturbance upstream of the turbine cascade.

## 5.3 Leading Edge Survey

The following experiment was conducted to characterize the inlet flow into the turbine cascade at the different strut locations. To accomplish this goal a TSI Model 1210 hot-wire was traversed in a plane 3.05 mm (0.12 in) from the surface of the blades. The probe was calibrated in the cascade wind tunnel. For specific calibration details, see Appendix C. Runs were made for five different strut locations. A system was used to maintain the various strut locations (refer to Figure 5.4). The strut moves in the direction z/p which is parallel to the turbine cascade. Here p is the blade spacing or pitch 38.1 mm

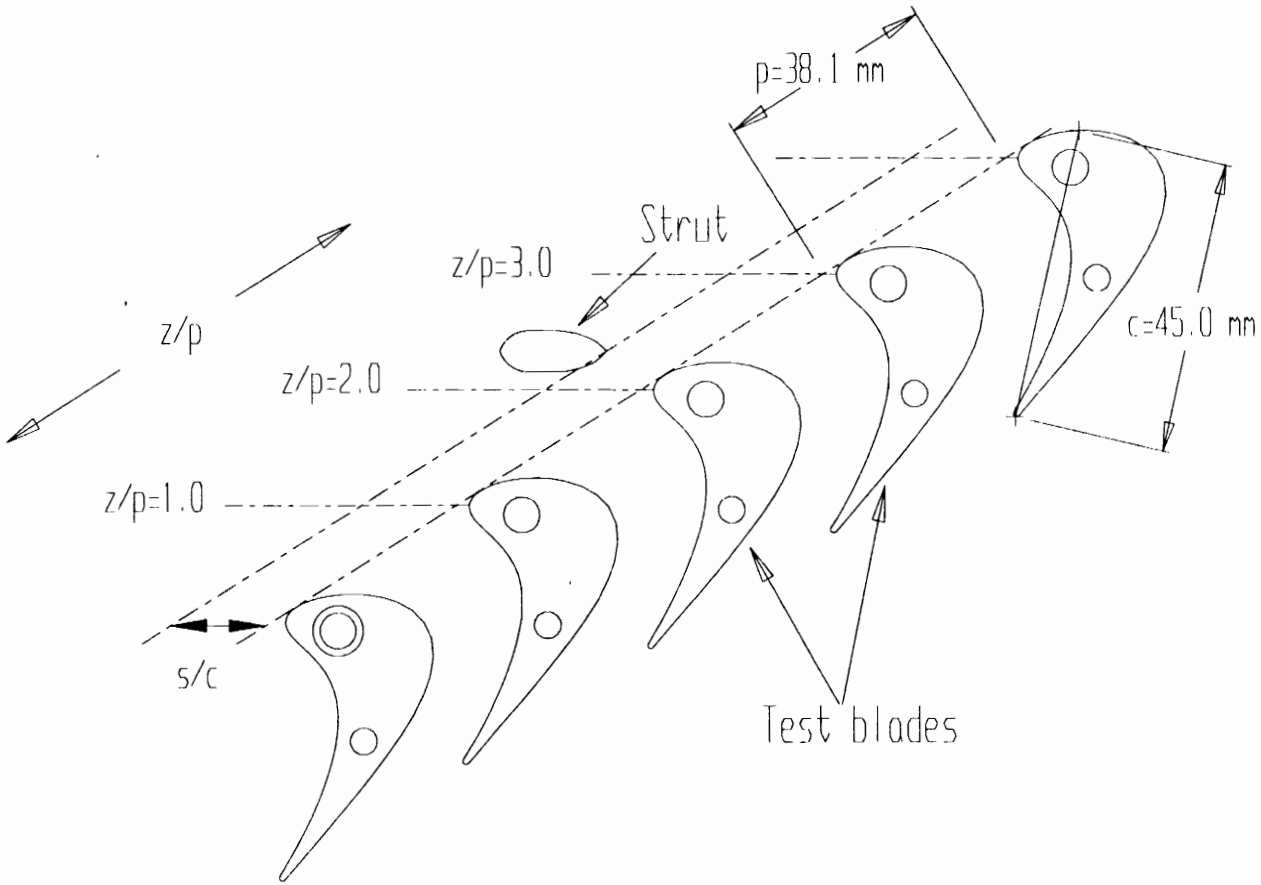


Figure 5.4 Positioning System used to Maintain Strut Location

(1.5 in). The hot-wire zero location was the same for all of the runs (z/p = 2.60). The distance the strut's trailing edge varies from the turbine blade's leading edge was measured by the quantity s/c, where s is the distance the strut's trailing edge to the leading edge of the turbine blade, and c is the turbine blade chord. For this experiment, s/c = .42 was utilized.

The low sampling frequency (5 kHz) hot-wire data was reduced using the appropriate calibration equation, and plots were generated which characterize the flow as a product of the density and velocity. The inlet Mach number for the various runs was approximately 0.36 which is in the compressible range, therefore no attempt was made to uncouple the density and velocity. For data manipulation purposes a FORTRAN program removed 19 out of 20 data points reducing the sampling rate to 250 Hz. The plots for only two of the strut locations will be considered within this section. The plots for the other locations are in Appendix A.

Location 5 will be considered first where z/p = 2.45 (refer to Figure 5.5). A distinct velocity defect exists from the strut (refer to Figure 5.6). In this region of the flow the fluctuations of $\rho U$ have increased and the mean flow velocity has decreased. Another interesting point is the effect in the flow field created by the turbine blades themselves. The mean flow field is reduced approaching the leading edge of blades. This is caused by the potential field around the turbine blade. Drastic changes occur in the flow field as the strut is moved to different locations. Location 2 is positioned at z/p = 2.05 (refer to Figure 5.7). At this particular strut location the flow field has dramatically changed. No distinct wake is shed from the strut, as was seen at location 5 (refer to Figure 5.8). The strut wake and potential effect of the blade have combined to create very large decrease in the mean flow as well as large fluctuations within the flow. The value of $\rho U$ drops to approximately 55 $kg/m^2s$ at location 2 as compared to 197 $kg/m^2s$ at location 5. This corresponds to a factor of almost 4 difference in the mean flow fields. The information obtained about the flow field thus far establishes only the mean

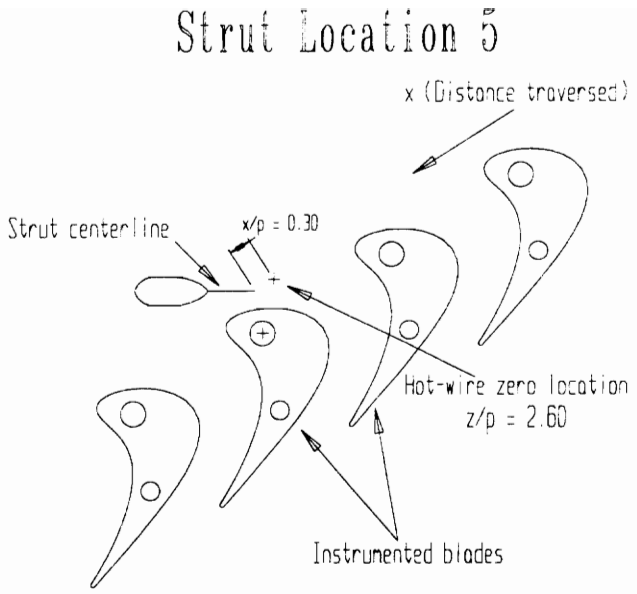


Figure 5.5 Position of Strut Relative to Hot-Wire Zero Location (z/p=2.45)

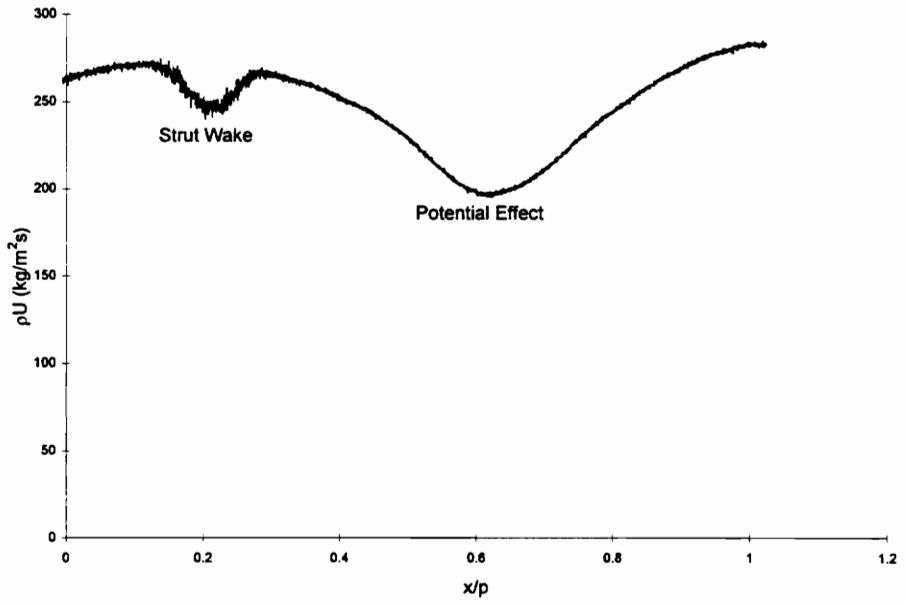


Figure 5.6 Profile of Inlet Flow into Cascade with Strut at z/p=2.45

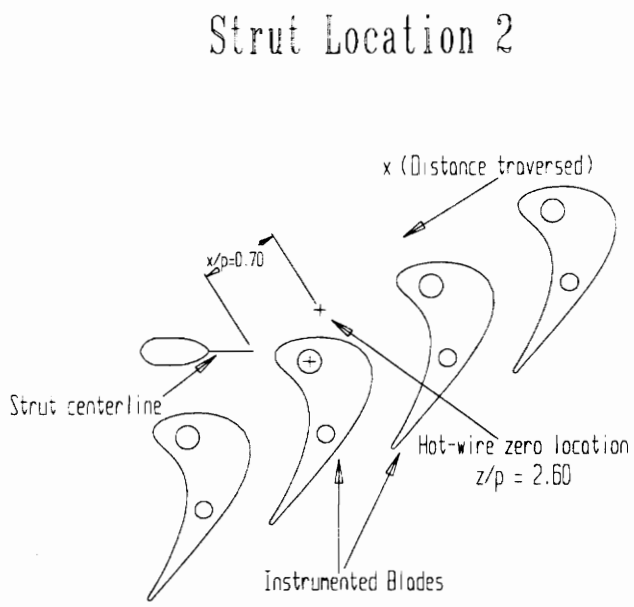


Figure 5.7 Position of Strut Relative to Hot-Wire Zero Location (z/p=2.05)

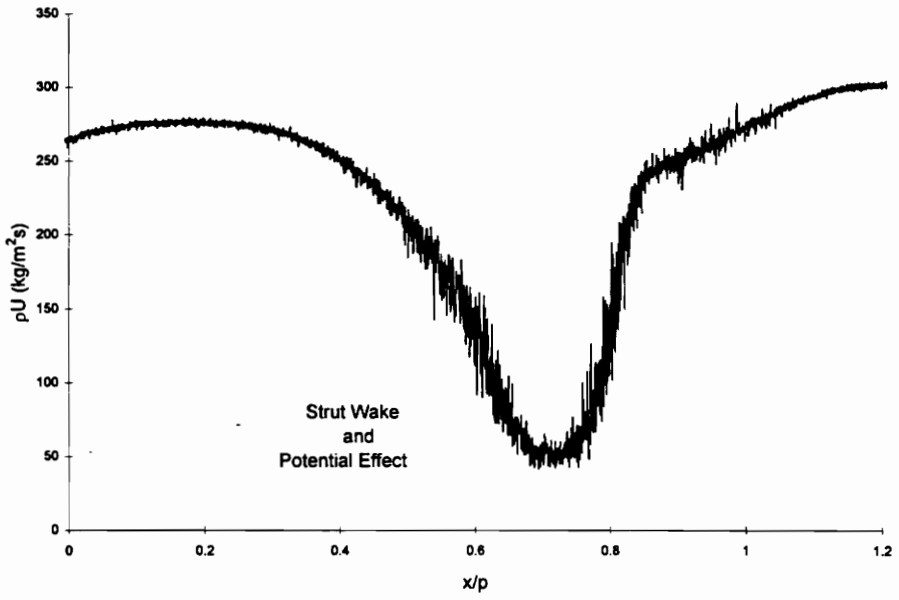


Figure 5.8 Profile of Inlet Flow into Cascade with strut at z/p=2.05

flow. To better characterize the flow environment, the fluctuations in the flow field need to be quantified.

This task was accomplished by calculating the turbulence intensity, as defined by equation 4.13 in section 4.4.2. The results were plotted to see the variations in turbulence intensity at the different strut locations as well as the variations in the free-stream turbulence. The maximum turbulence intensity value obtained at location 5 was 5.21 % and the maximum value calculated at position 2 was 51.4% (refer to Figures 5.9 and 5.10). A curious point to note is the two peaks present in the turbulence intensity in both of the two plots. It appears that the probe has detected the two shear layers present from the shedding wake. The turbulence is somewhat lower in the center of the wake. At location 5 the two peaks in the turbulence retain approximately the same values whereas at location 2 there is a 15% difference in the two peaks. The peak turbulence for both locations does not occur at a point where the mean flow is a minimum. The turbulence intensity actually declines where the mean flow field is a minima. This is expected since turbulence production is zero at a mean velocity extreme. It is hard to determine whether or not the reduction in the mean flow is the major cause for the high turbulence intensity values. In an attempt to understand the flow physics, the mean component was removed from the turbulence intensity equation. Removing the mean component produced the following equation for the RMS

$$\rho U_{rms} = \sqrt{\frac{\overline{\rho U'^2}}{n}} \qquad [5.1]$$

where n is the number of data points. Plots were created showing the fluctuations in the mean flow (RMS) and displaying the mean flow at the corresponding location. Figure 5.11 indicates that the fluctuations in the flow are 13.5 kg/m$^2$s at location 5 where there is little influence from the cascade. The RMS levels have increased sharply at location 2 (refer to Figure 5.12). The peak value in the RMS has increased to 58.3 kg/m2s which is

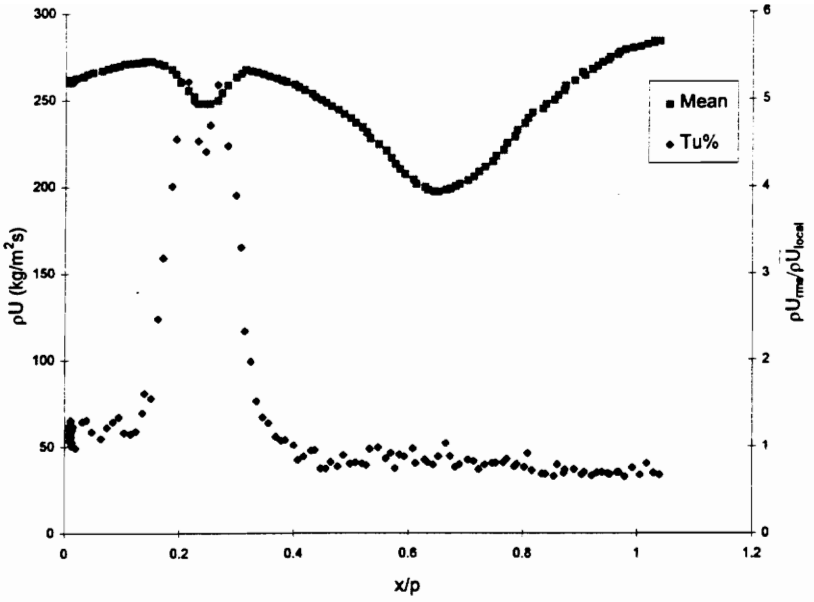


Figure 5.9 Mean and Turbulence Intensity Results of Hot-Wire with Strut at z/p=2.45

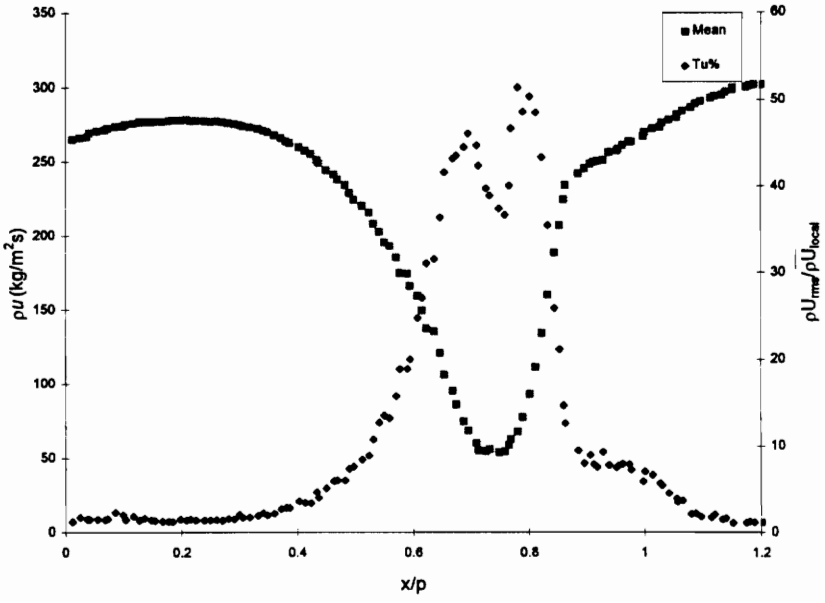


Figure 5.10 Mean and Turbulence Intensity Results of Hot-Wire with Strut at z/p=2.05

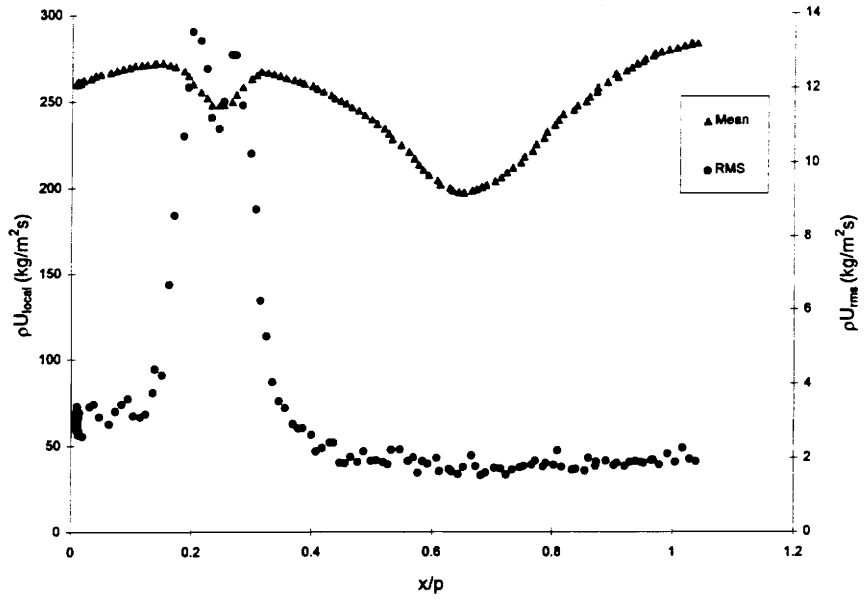


Figure 5.11 Mean and RMS Results of Hot-Wire with Strut at z/p=2.45

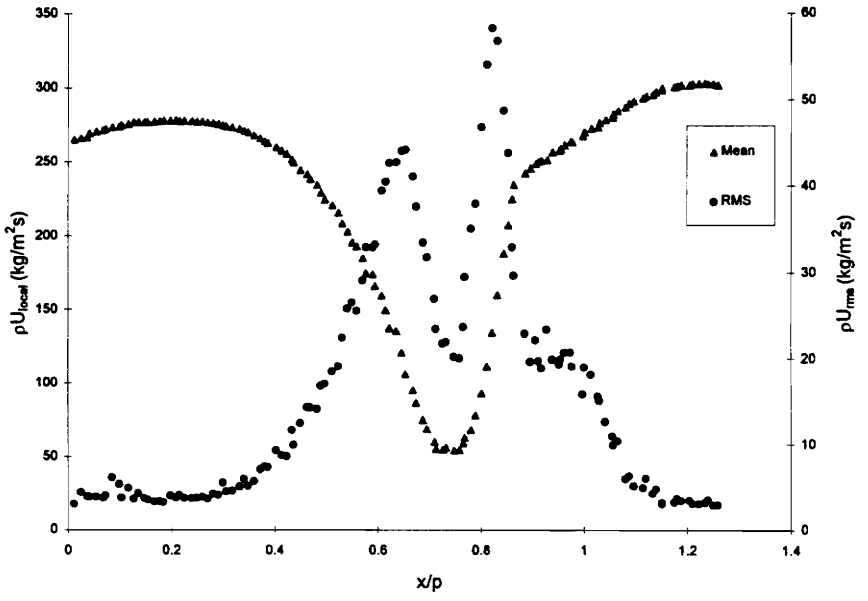


Figure 5.12 Mean and RMS Results of Hot-Wire with Strut at z/p=2.05

a factor of four higher than the level attained at position 5. Again the two peaks are noticed as was seen in the turbulence intensity plots. The maximum RMS values do not occur where the mean flow is a minimum. The RMS values actually decline in this region. Especially at location 2 where there is a factor of three difference in the peak value from this semi-turbulent region. The other strut locations were analyzed utilizing the same techniques as was used for locations 2 and 5. The results from this analysis are tabulated in Table 5.3.

**Table 5.3 Low Sampling Frequency Hot-Wire Results**

| Sampling Frequency (5 kHz) | | | | | |
|---|---|---|---|---|---|
| Loc. # | Free-stream RMS ($kg/m^2s$) | Wake RMS ($kg/m^2s$) | Free-stream Tu% | Wake Tu% | Minimum* $\rho U_{local}$ ($kg/m^2s$) |
| 1 | 3.0 | 20.6 | 1.4 | 9.8 | 203.0 |
| 2 | 4.2 | 58.3 | 1.1 | 51.4 | 54.8 |
| 3 | 3.8 | 47.8 | 1.6 | 50.0 | 72.2 |
| 4 | 4.2 | 28.0 | 0.9 | 12.5 | 219.5 |
| 5 | 2.9 | 13.6 | 1.3 | 5.2 | 247.7 |

* The minimum is measured behind the strut.

Locations 2 and 3 exhibit some of the same characteristics. The turbulence intensity is essentially the same for both locations, however, the fluctuations and the mean flow are quite different. The fluctuations have increased while the mean flow value has decreased. Therefore, it appears that the decrease in the mean flow has an affect on the turbulence, but it is very dependent upon the strut location being considered.

Location 2 (z/p = 2.05) produced results that were most interesting. Therefore, further data was collected to characterize this disturbance in the flow field. High sampling frequency (100 kHz) data was acquired to characterize the integral time and length scale being shed from the wake. Fast Fourier Transforms were performed on all the signals also. Several runs were made with the strut at location 2, but only two are shown in this thesis, due to the redundancy shown in the first two runs. A brief

explanation is needed in the data processing before an attempt is made to discuss the results.

Data was sampled continuously as the hot-wire probe was traversed so the length scale and the power spectra at a particular point in the flow could not be obtained. The integral length scale, integral time scale, and power spectra were calculated over a distinct region in the flow. This infers a smearing of the energy or an average of the energy in a particular region. The probe was traversed approximately 19.1 mm (0.75 in). The data file created was separated into different sections for the data analysis process. For the length and time scale calculations the file was divided into 8 segments of length 32 K. This implies that the length and time scale will be calculated over a 1.26 mm (0.05 in) region in the flow. The file was partitioned differently for the Fast-Fourier Transforms. The file was divided into 4 segments of length 64 K. Sixty Hertz noise was prevalent in all the hot-wire signals and was digitally filtered since it was below the frequency region of interest. The LABVIEW programs (DGHSPCTM.VI) and (LORENFFT.VI) digitally removed the 60 Hz noise with a bandstop filter and removed 5 subsequent multiples of 60 Hz from the data.

The power spectra graphs (Figures 5.13 and 5.14) produced from the Fast-Fourier Transforms indicate the presence of increased energy levels between 0 and 10 kHz. The energy increases as the probe approaches the strut wake. The first segment represents a region near the free-stream. The other segments are in or close to the wake. The results for the 100 kHz sampled data are listed in Table 5.4.

The integral time scale is small in the free-stream. A value of 0.03 milliseconds was determined which corresponds to a characteristic frequency of 33 kHz. As the probe enters the wake the time scale increases through the shear layers and declines in the centerline of the wake. For Run # 1 the integral time scale in the shear layer of the wake is 0.13 msec (7.6 kHz) and in the center it is 0.05 msec (20 kHz). The 7.6 kHz frequency is approximately twice the calculated characteristic shedding frequency of the strut. The

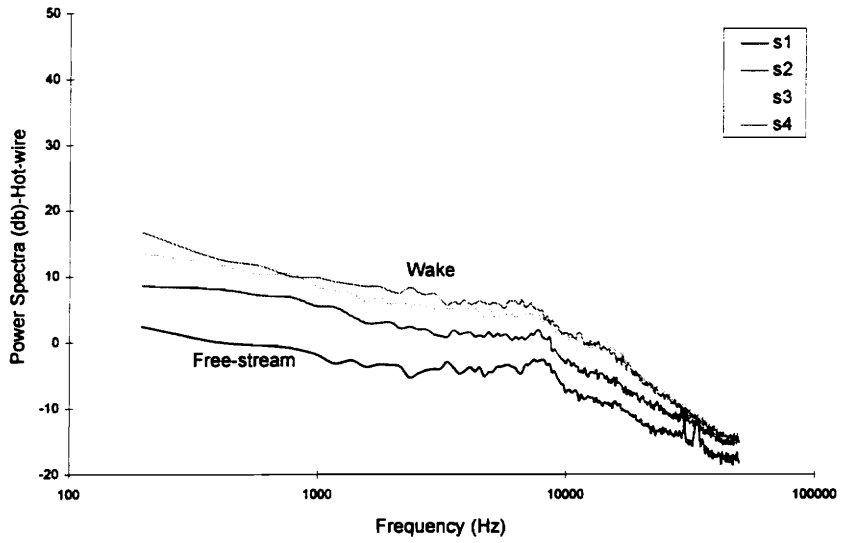


Figure 5.13 Power Spectra of Hot-Wire Signal with Strut at z/p=2.05 (Run #1)

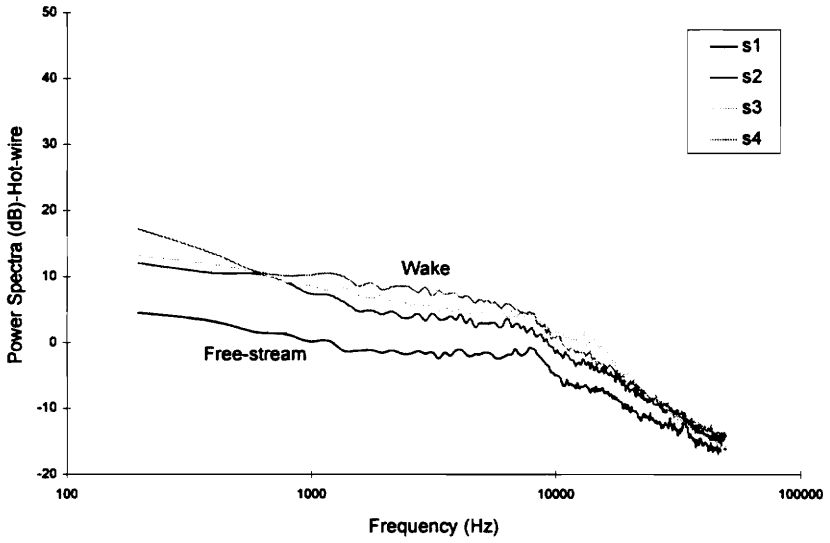


Figure 5.14 Power Spectra of Hot-Wire Signal with Strut at z/p=2.05 (Run #2)

characteristic shedding frequency was calculated to be 3.5 kHz using a Strouhal number of 0.2. The length scale behaves in a similar manner. The length scales are small in the free-stream ,3.0 mm, and become larger due to the influence of the shedding wake, 8.5 mm. The length scale has also decreased in the center of the wake to a value of 2.2 mm. The length scales measured in the wake appear to be the same as the thickness of the strut, 7.7 mm.

**Table 5.4 High Sampling Frequency Hot-Wire Results**

| Sampling Frequency 100 kHz, Location 2 (z/p = 2.05) | | | | | |
|---|---|---|---|---|---|
| Run #1 | | | Run #2 | | |
| Time Scale (msec) | Length Scale (mm) | Avg Velocity (m/s) | Time Scale (msec) | Length Scale (mm) | Avg Velocity (m/s) |
| 0.03 | 2.9 | 114.7 | 0.03 | 3.0 | 110.3 |
| 0.03 | 2.8 | 107.6 | 0.04 | 4.3 | 100.2 |
| 0.06 | 5.3 | 96.0 | 0.07 | 5.9 | 86.7 |
| 0.07 | 6.0 | 83.1 | 0.09 | 6.5 | 71.1 |
| 0.09 | 5.7 | 65.3 | 0.08 | 4.4 | 52.0 |
| 0.06 | 3.1 | 47.9 | 0.05 | 2.0 | 42.0 |
| 0.05 | 2.4 | 43.8 | 0.14 | 8.1 | 57.9 |
| 0.13 | 8.9 | 66.5 | 0.10 | 8.5 | 87.3 |

The results show a very interesting and complicated flow at location 2 of the strut. The change in the velocity defect is accompanied by variable turbulence intensity, integral length scales, and integral time scales across the wake. This type of disturbance creates an interesting flow regime in which to make heat transfer measurements.

## 5.4 Heat Flux and Kulite Measurements

Several runs were made with the HFM-6 insert gages and Kulites:two runs at each of the four different strut locations and with no strut. This was for the low frequency sampled data. Figures 5.15 through 5.22 show an example run for the no strut case (run

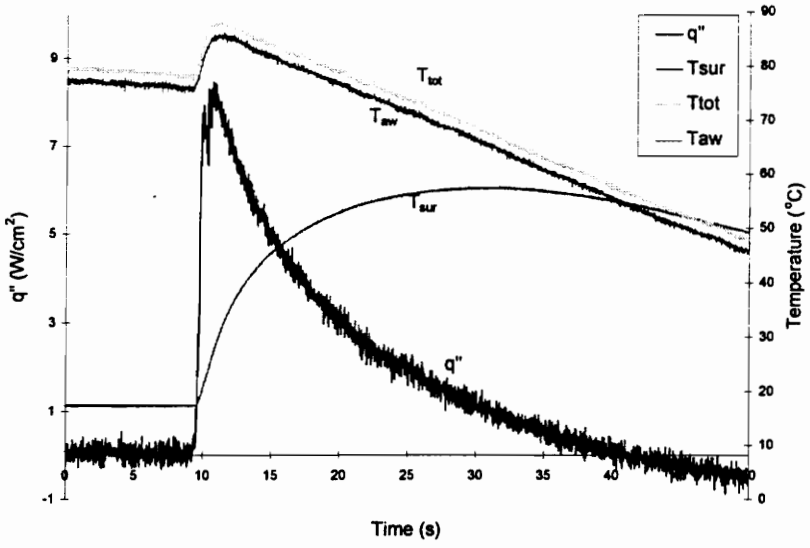


Figure 5.15 Example of Run for HFM-6 Gage 1-No Strut Case

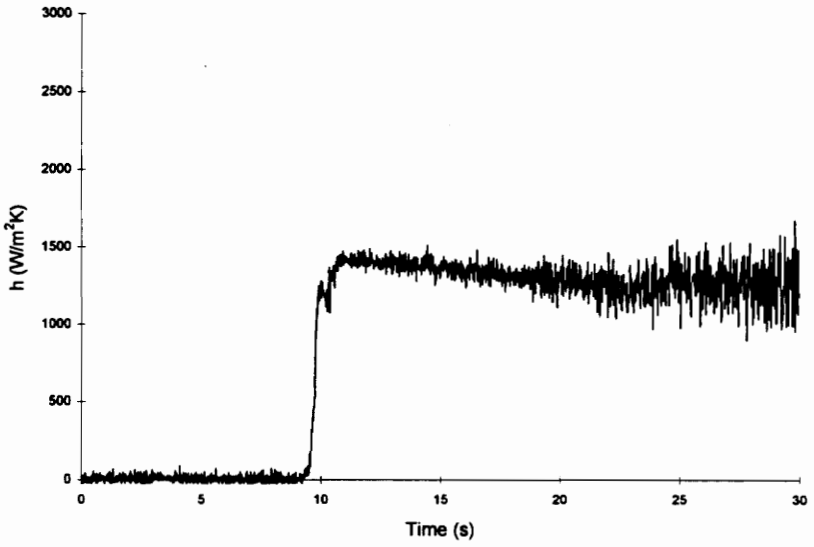


Figure 5.16 HTC Calculated From HFM-6 Gage 1 - No Strut Case

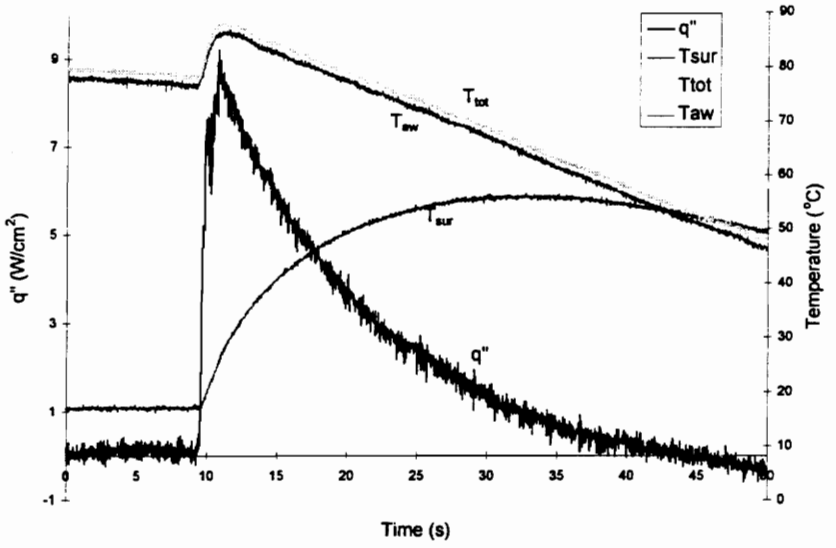


Figure 5.17 Example of Run for HFM-6 Gage 2-No Strut Case

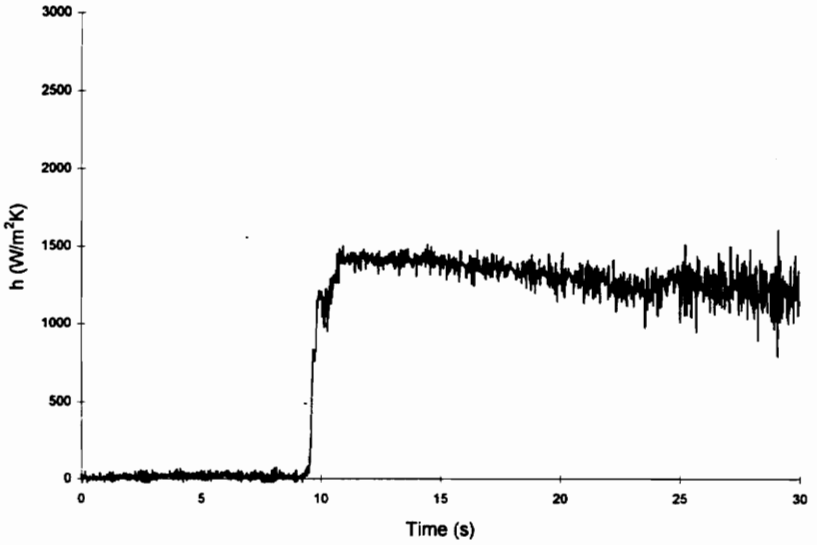


Figure 5.18 HTC Calculated From HFM-6 Gage 2 - No Strut Case

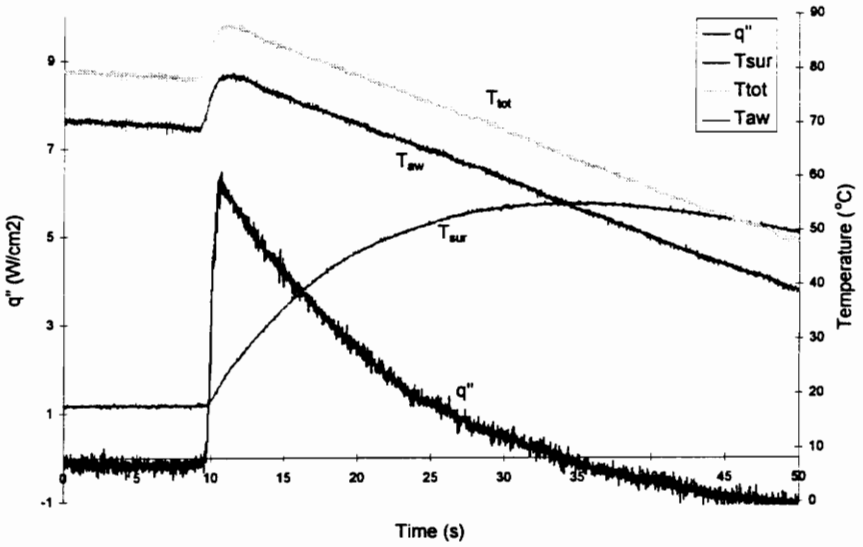


Figure 5.19 Example of Run for HFM-6 Gage 3 - No Strut Case

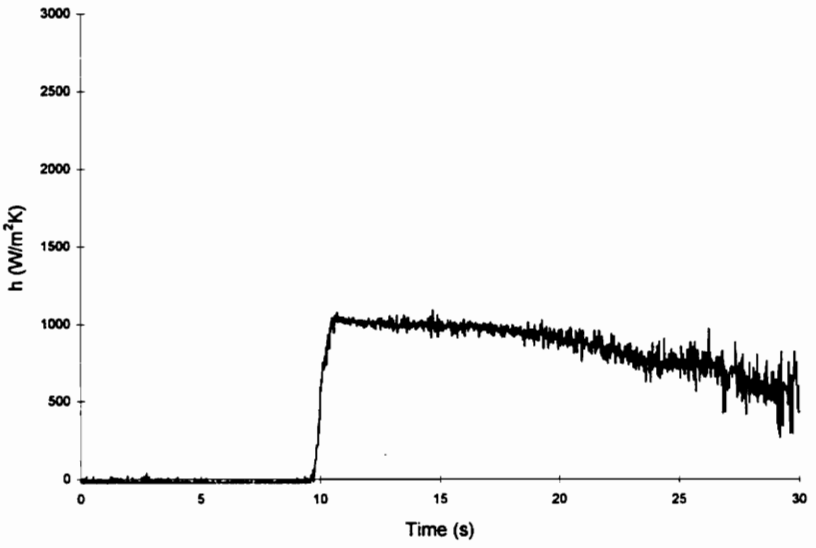


Figure 5.20 HTC Calculated From HFM-6 Gage 3 - No Strut Case

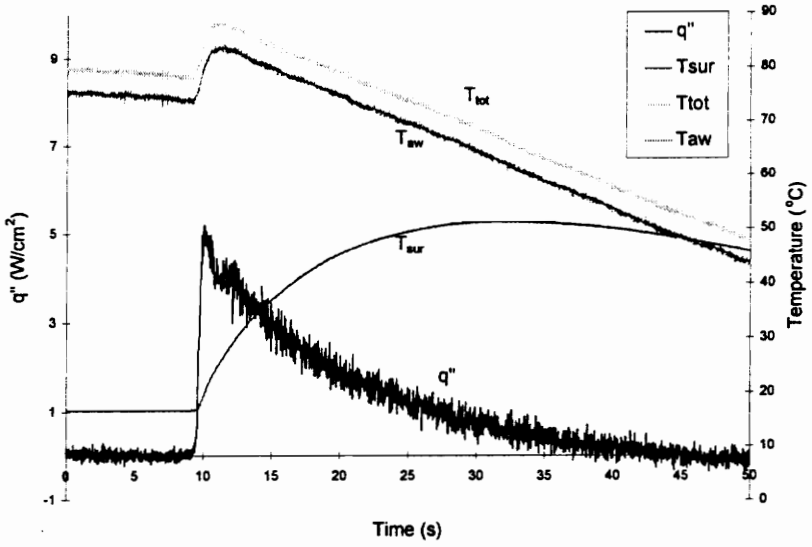


Figure 5.21 Example of Run for HFM-6 Gage 4 - No Strut Case

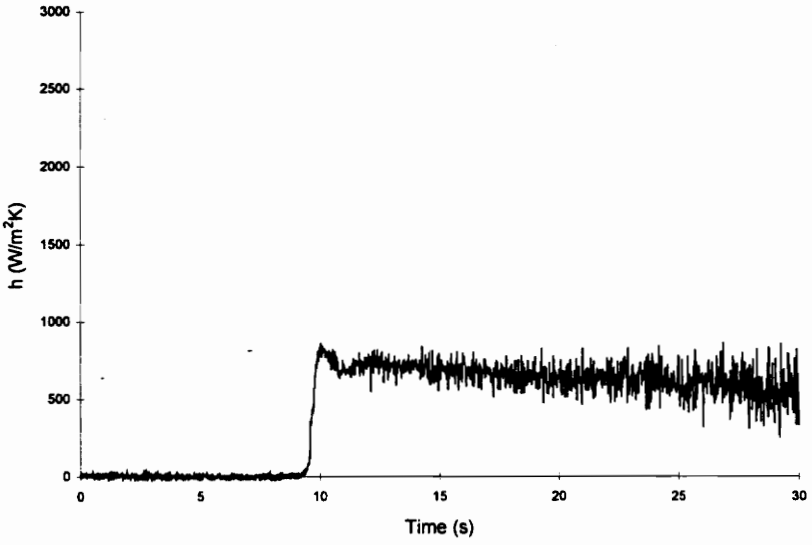


Figure 5.22 HTC Calculated From HFM-6 Gage 4 - No Strut Case

1). The corresponding heat transfer coefficient is plotted below the run data for each HFM-6 gage. Figures 5.23 through 5.30 show the run data and heat transfer coefficients for the four gages with the strut at location 2. For all of the runs the blades were not cooled during operation of the tunnel and the heat flux went to zero, thus allowing for a direct way to measure $T_{aw}$. A summary of the average heat transfer coefficients, at the various strut locations, with a 95% confidence interval calculated during a flat region of the run is shown Tables 5.5a through 5.5e.

**Table 5.5a Average Heat Transfer Coefficients and Nusselt Numbers for HFM-6 with No Strut**

| No Strut | | | | |
|---|---|---|---|---|
| | Run #1 | | Run #2 | |
| Gage Number | Heat Transfer Coefficient [W/(m$^2$C)] | Nusselt Number | Heat Transfer Coefficient [W/(m$^2$C)] | Nusselt Number |
| 1 | 1327 ±6 | 2046 ±10 | 1370 ±7 | 2044 ±12 |
| 2 | 1303 ±8 | 1915 ±13 | 1320 ±7 | 1976 ±11 |
| 3 | 992 ±8 | 1464 ±12 | 997 ±6 | 1531 ±9 |
| 4 | 649 ±6 | 1017 ±9 | 662 ±5 | 1046 ±7 |

**Table 5.5b Average Heat Transfer Coefficients and Nusselt Numbers for HFM-6 with Strut at z/p = 1.78**

| Strut at z/p = 1.78 (Location 1) | | | | |
|---|---|---|---|---|
| | Run #1 | | Run #2 | |
| Gage Number | Heat Transfer Coefficient [W/(m$^2$C)] | Nusselt Number | Heat Transfer Coefficient [W/(m$^2$C)] | Nusselt Number |
| 1 | 1257 ±5 | 1975 ±7 | 1216 ±8 | 1924 ±11 |
| 2 | 1332 ±7 | 2093 ±13 | 1314 ±6 | 2078 ±10 |
| 3 | 938 ±7 | 1472 ±11 | 944 ±7 | 1493 ±12 |
| 4 | 666 ±5 | 1046 ±8 | 734 ±7 | 1161 ±11 |

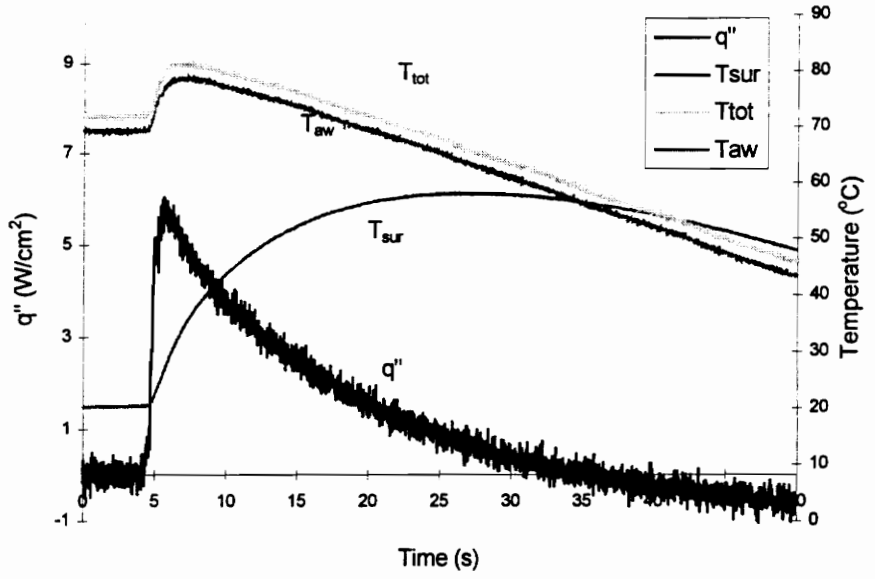


Figure 5.23 Example of Run for HFM-6 Gage 1 - Strut at z/p = 2.05

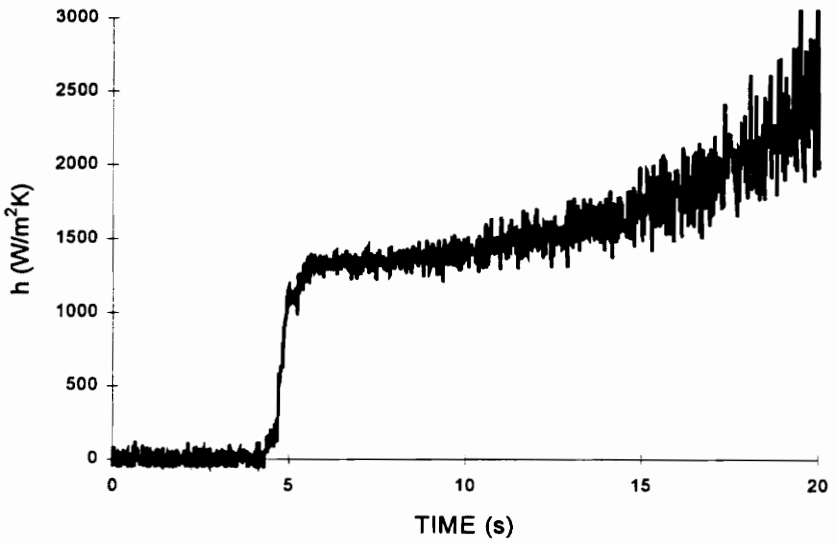


Figure 5.24 HTC Calculated From HFM-6 Gage 1 - Strut at z/p = 2.05

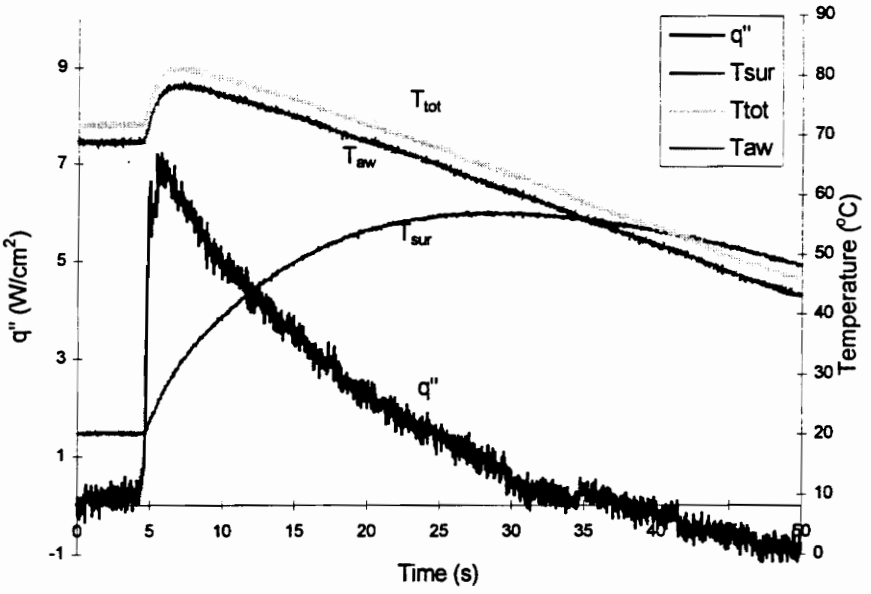


Figure 5.25 Example of Run for HFM-6 Gage 2 - Strut at z/p = 2.05

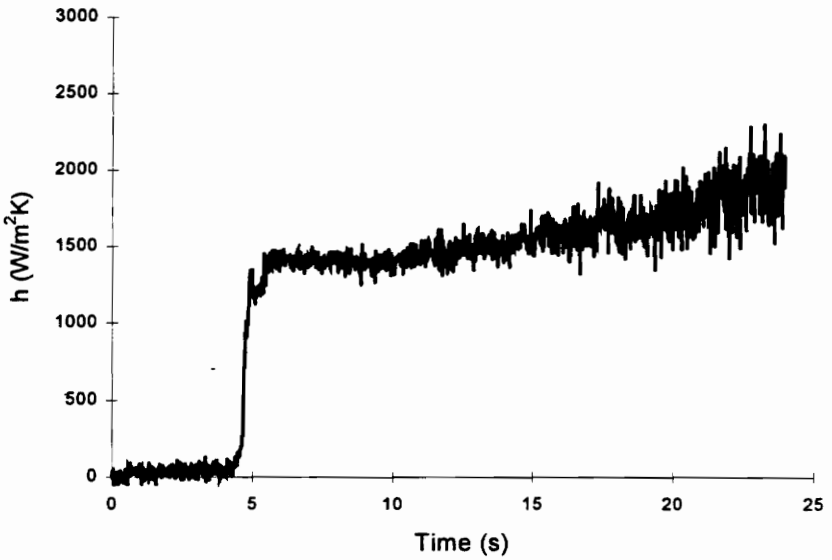


Figure 5.26 HTC Calculated From HFM-6 Gage 2 - Strut at z/p = 2.05

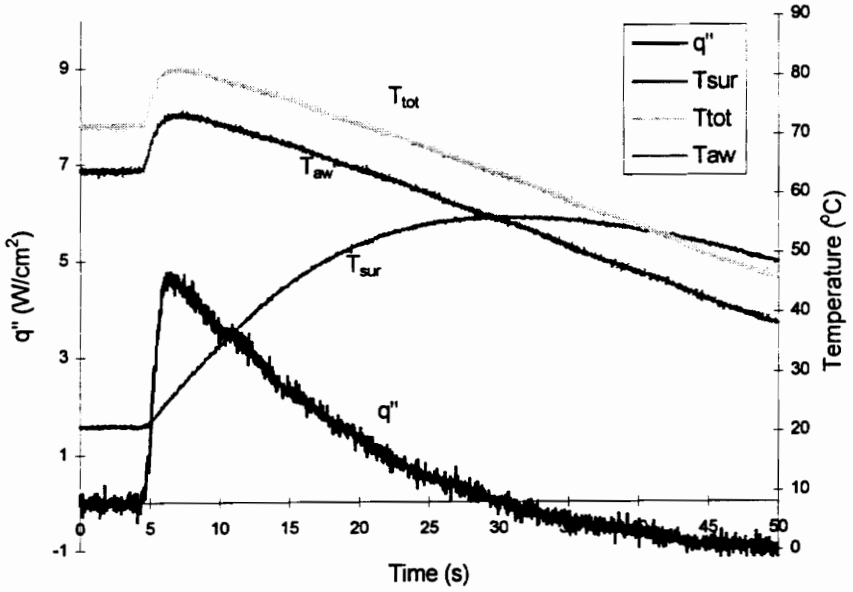


Figure 5.27 Example of Run for HFM-6 Gage 3 - Strut at z/p = 2.05

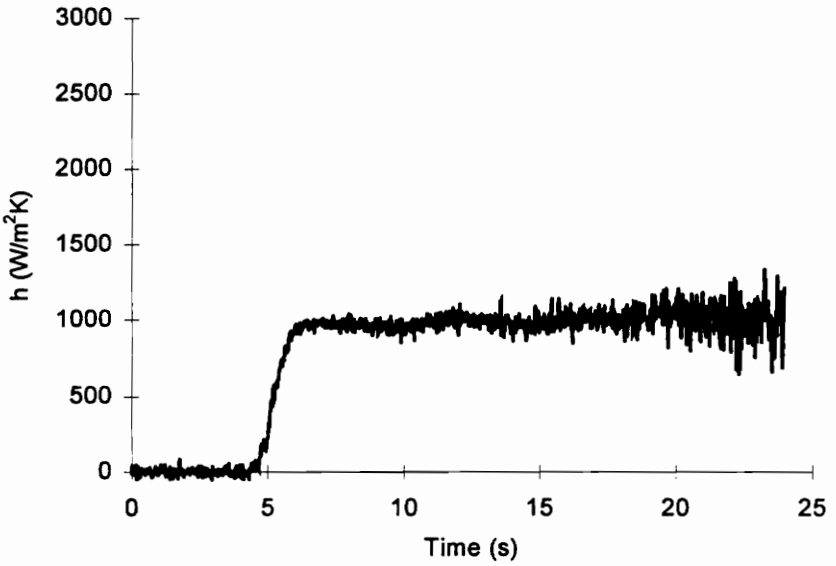


Figure 5.28 HTC Calculated From HFM-6 Gage 3 - Strut at z/p = 2.05

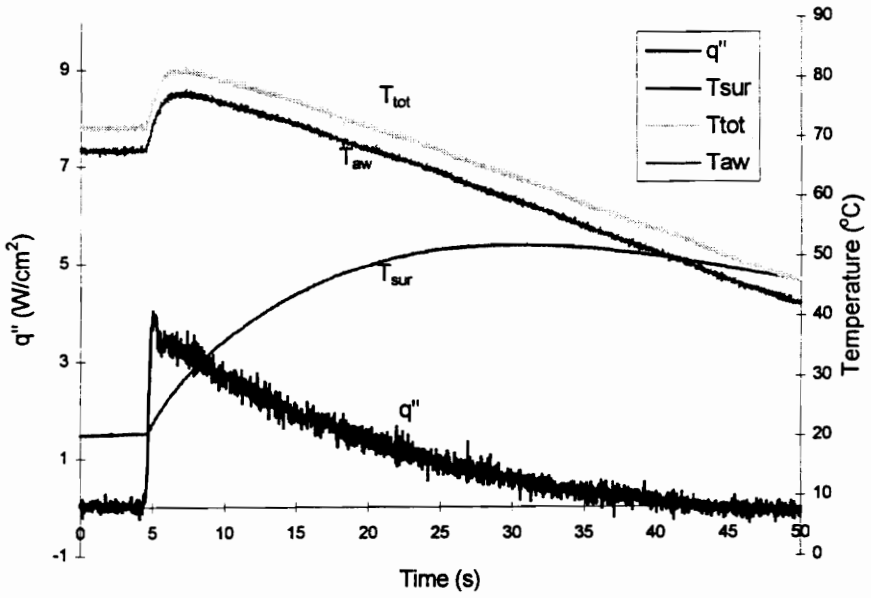


Figure 5.29 Example of Run for HFM-6 Gage 4 - Strut at z/p = 2.05

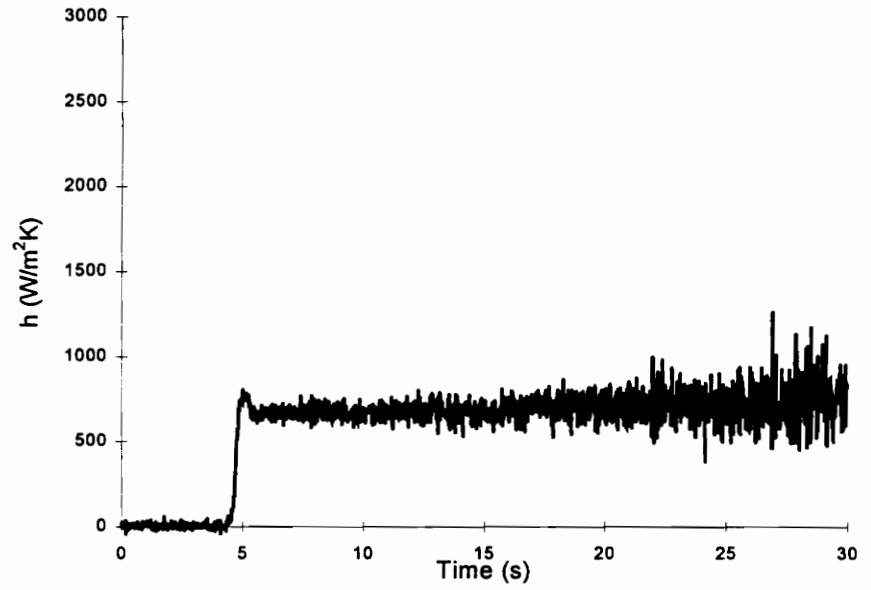


Figure 5.30 HTC Calculated From HFM-6 Gage 4 - Strut at z/p = 2.05

**Table 5.5c Average Heat Transfer Coefficients and Nusselt Numbers for HFM-6 with Strut at z/p =2.05**

| Strut at z/p = 2.05 (Location 2) | | | | |
|---|---|---|---|---|
| | Run #1 | | Run #2 | |
| Gage Number | Heat Transfer Coefficient [W/(m$^2$C)] | Nusselt Number | Heat Transfer Coefficient [W/(m$^2$C)] | Nusselt Number |
| 1 | 1538 ± 9 | 2446 ± 14 | 1481 ± 7 | 2338 ± 10 |
| 2 | 1557 ± 9 | 2477 ± 14 | 1464 ± 5 | 2310 ± 8 |
| 3 | 1088 ± 4 | 1732 ± 6 | 1033 ± 4 | 1631 ± 6 |
| 4 | 719 ± 5 | 1143 ± 9 | 673 ± 4 | 1062 ± 6 |

**Table 5.5d Average Heat Transfer Coefficients and Nusselt Numbers for HFM-6 with Strut at z/p =2.19**

| Strut at z/p = 2.19 (Location 3) | | | | |
|---|---|---|---|---|
| | Run #1 | | Run #2 | |
| Gage Number | Heat Transfer Coefficient [W/(m$^2$C)] | Nusselt Number | Heat Transfer Coefficient [W/(m$^2$C)] | Nusselt Number |
| 1 | 1432 ± 6 | 2227 ± 9 | 1470 ± 11 | 2309 ± 12 |
| 2 | 1465 ± 14 | 2279 ± 18 | 1504 ± 6 | 2363 ± 10 |
| 3 | 1074 ± 7 | 1671 ± 11 | 1073 ± 8 | 1684 ± 12 |
| 4 | 681 ± 4 | 1060 ± 6 | 695 ± 4 | 1092 ± 7 |

**Table 5.5e Average Heat Transfer Coefficients and Nusselt Numbers for HFM-6 with Strut at z/p =2.45**

| Strut at z/p = 2.45 (Location 4) | | | | |
|---|---|---|---|---|
| | Run #1 | | Run #2 | |
| Gage Number | Heat Transfer Coefficient [W/(m$^2$C)] | Nusselt Number | Heat Transfer Coefficient [W/(m$^2$C)] | Nusselt Number |
| 1 | 1252 ± 7 | 1991 ± 10 | 1318 ± 5 | 2097 ± 8 |
| 2 | 1336 ± 8 | 2125 ± 12 | 1301 ± 10 | 2068 ± 16 |
| 3 | 978 ± 7 | 1555 ± 10 | 946 ± 9 | 1504 ± 10 |
| 4 | 801 ± 6 | 1273 ± 9 | 820 ± 7 | 1303 ± 11 |

The average heat transfer coefficient values change for the various locations of the strut. The average heat transfer coefficients for the no strut case are 1348 [W/(m$^2$ °C)] for gage 1, 1311 [W/(m$^2$ °C)] for gage 2, 994 [W/(m$^2$ °C)] for gage 3, and 655 [W/(m$^2$ °C)] for gage 4. At location 2 (z/p=2.05) the following average heat transfer coefficients were obtained for the three suction surface gages: 1510 [W/(m$^2$ °C)] for gage 1, 1511 [W/(m$^2$ °C)] for gage 2, 1061 [W/(m$^2$ °C)] for gage 3. This corresponds to an increase of 12% for gage 1, 15 % for gage 2, and 7% for gage 3 in the average heat transfer coefficient. Location 3 (z/p=2.19) of the strut also caused increases in the heat transfer for the three suction surface gages. The heat transfer coefficient increased by 8% for gage 1, 13% for gage 2, and 8% for gage 3. The three suction surface gages are unaffected by the strut at position 5, however, an increase is seen at gage location 4. The average heat transfer coefficient increased 24%. There is no affect in the heat transfer coefficients for all four gages with the strut at location 1 (z/p=1.78). The calibration uncertainty for the HFM-6 gages was ± 10%. When comparing the relative values between the various heat tranfer coefficients this was not considered. The uncertainty in the measurements had to be considered. The uncertainty was determined to be ± 5%. The uncertainty analysis is located in Appendix D. The values obtained for the no strut case were compared with a computer prediction supplied by General Electric.

General Electric supplied results from their computer codes for the heat transfer coefficient distribution over the blade. These particular codes were modified from the KEP code [Zerkle,(1987)] which was a modification of the STAN5 code. General Electric's results along with the experimental results from this thesis are shown in Figure 5.31. Results from this thesis include the average heat transfer coefficients of the four gages for the no strut case. The computer predicted values were all smaller than the heat transfer coefficients measured. The following values were obtained from the computer prediction: 801 [W/(m$^2$ °C)] for gage 1, 788 [W/(m$^2$ °C)] for gage 2, 657 [W/(m$^2$ °C)] for gage 3, and 550 [W/(m$^2$ °C)] for gage 4. The heat transfer coefficients at gages 1 and 2 were approximately 1.6x greater than the predicted values, and the value of gage 3 was

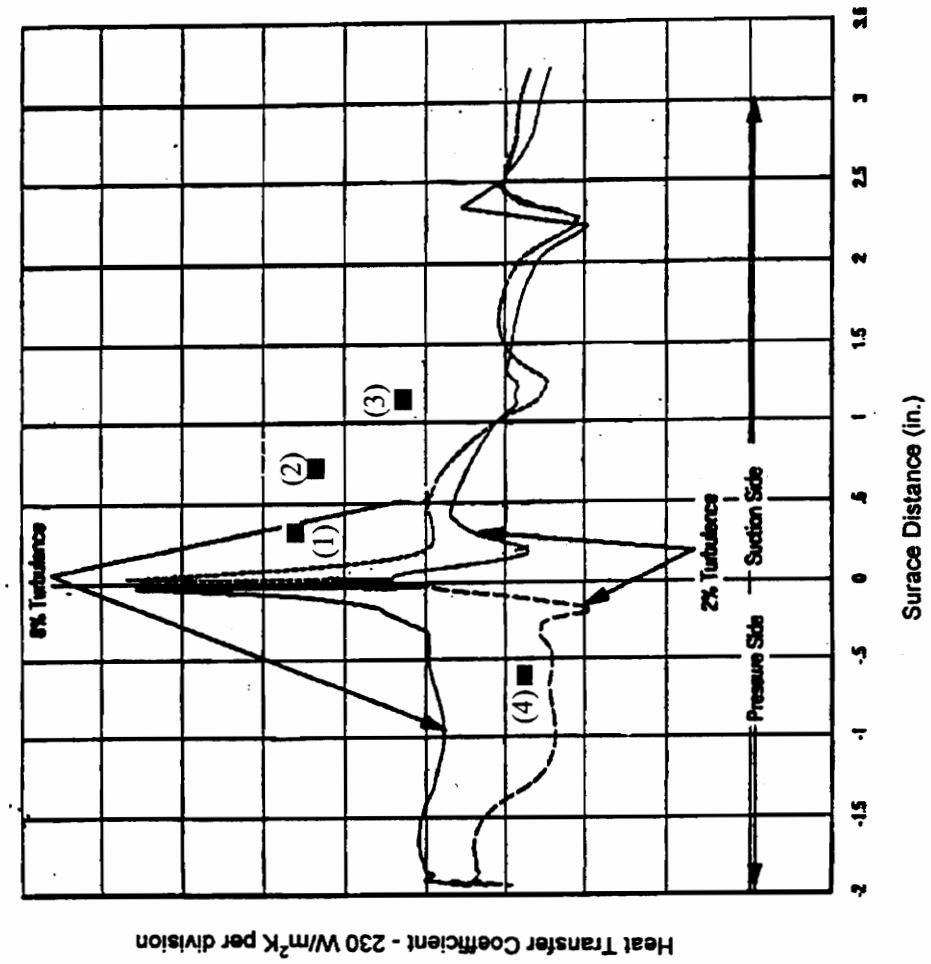


Figure 5.31 Experiment vs. Prediction for the Heat Transfer Coefficient

approximately 1.5x greater. Gage 4 showed the best agreement with the computer prediction being only 1.2 x higher. The heat transfer coefficient for gage 1 compared well with the results from Johnson, (1995) at this location using the same type insert gage. Johnson experimentally determined the heat transfer coefficient to be 1300 [W/($m^2$ $^{o}$C)] for the location of gage 1.

There appears to be a strong influence on the heat transfer coefficient distribution depending on the relative position of the strut with respect to the test blade. The position of the strut wake with respect to the leading edge of the turbine blade appears also to be of major importance. Positioning the strut such that the wake would impinge on the suction surface near the leading edge of the blade increased the heat transfer coefficient for the three suction surface gages. One possible answer for the increase in the heat transfer coefficients along the suction surface might be that the boundary layer has transitioned causing most of the suction surface to experience a turbulent boundary layer. It is believed through previous research and shadowgraphs that the boundary layer on the suction surface of the blade is laminar until the trailing edge shock from an upstream blade impinges on the surface. The largest increase in the heat transfer coefficient occurred on the pressure surface (24%) when the strut wake was impinging on the blade pressure surface near the leading edge (location 5). At this location the strut was approximately 39.16 mm (1.54 in) from the pressure surface gage. These results confirmed the results of Wittig et al, (1985). Wittig determined the heat transfer from the blade from measurements of the temperature distribution on the blade. With the aid of a finite element program, the local heat transfer coefficients along the cooled blades were derived from surface and coolant temperature measurements. The results from Wittig's experiment were also compared with computer predictions. In several regions of the blade on both the pressure and suction surface the computer calculations underpredicted the heat transfer coefficients. Wittig's results also showed that the largest increases occurred on the pressure surface of the blade and that the ratio of s/c had a dramatic effect on the heat transfer. For larger values of s/c the heat transfer increased.

In this thesis only one axial position was examined (s/c=0.42), but the axial distance the strut trailing edge deviated from any particular gage varied.

The static pressure measured by the Kulites at each gage location enabled the calculation of the isentropic Mach number. Again during any run only two of the Kulite signals were acquired due to limitations in data acquisition. These experimental values were then compared with other experimental values and computer predictions (Figure 5.32) [Wesner,(1994)] and used as a basis for determining the free-stream velocity at the four gage locations. The experimental results closely matched the curve provided by General Electric for this blade design. Figure 5.33 and 5.34 show the total pressure and normalized pressure ($P_{sur}/P_t$) for the two runs with the strut at location 2. The pressure data for the two runs of the no strut case are plotted in Figures 5.35 and 5.36. The plots for the other runs are located in Appendix A. The plots show that the pressure remains constant over most of the run. The normalized pressure was averaged to determine the isentropic Mach number. Table 5.6 lists the average normalized pressure and Mach number for the various runs for each gage. The different locations of the strut appears to have no affect on the average normalized pressure or the isentropic Mach number. The Mach number at Kulites 1, 2, and 4 seems to decrease slightly when the strut is placed upstream of the cascade at the different locations compared to the no strut case, but gage 3 shows a slight increase in the Mach number. The variations are relatively small and could be attributed to deviations in the flow due to tunnel control, therefore, from this data there is no detectable change in the surface pressure along the surface of the blade for the various locations of the strut.

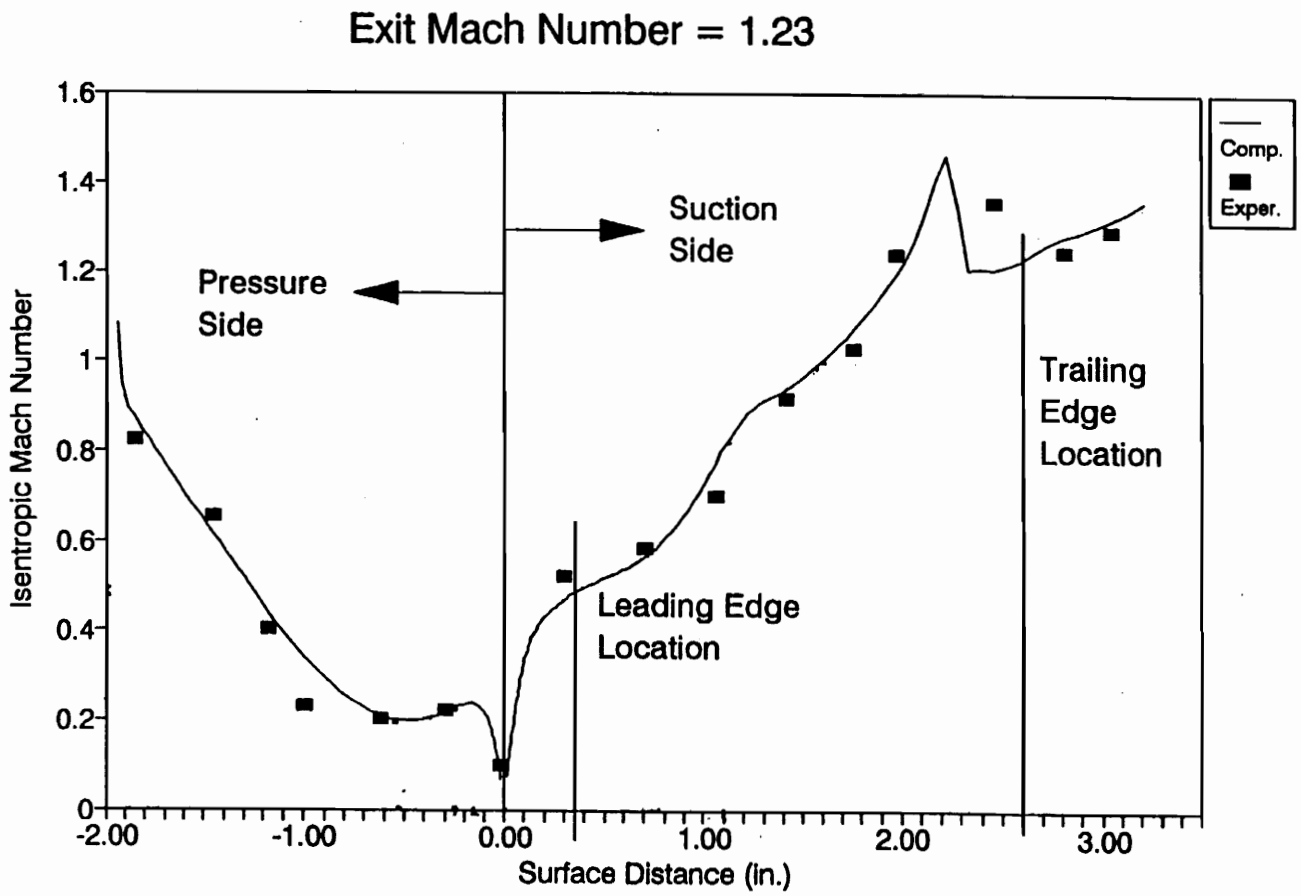


Figure 5.32 Isentropic Mach Number Distribution on Blade - Experimental and Prediction

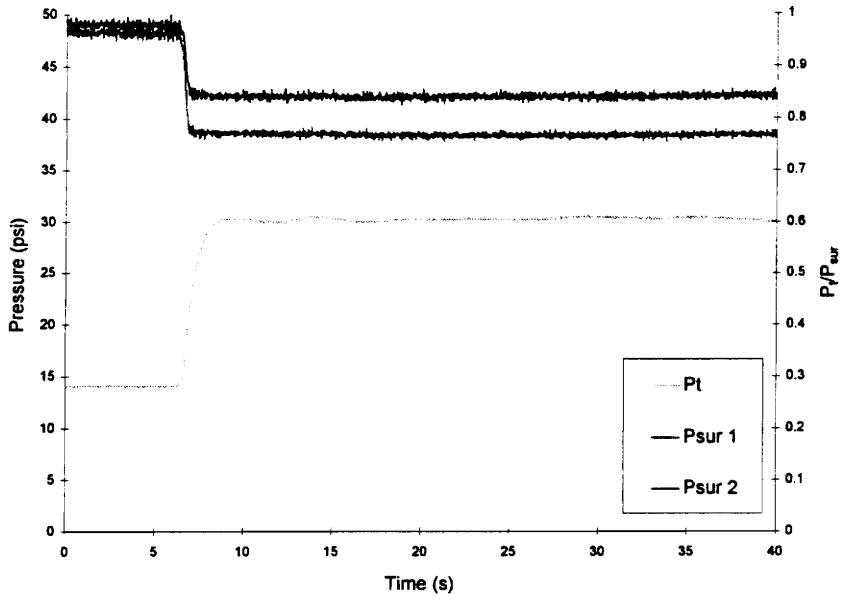


Figure 5.33 Total Pressure and Normalized Pressure for Strut at z/p=2.05 (Run #1)- Kulite 1 and Kulite 2

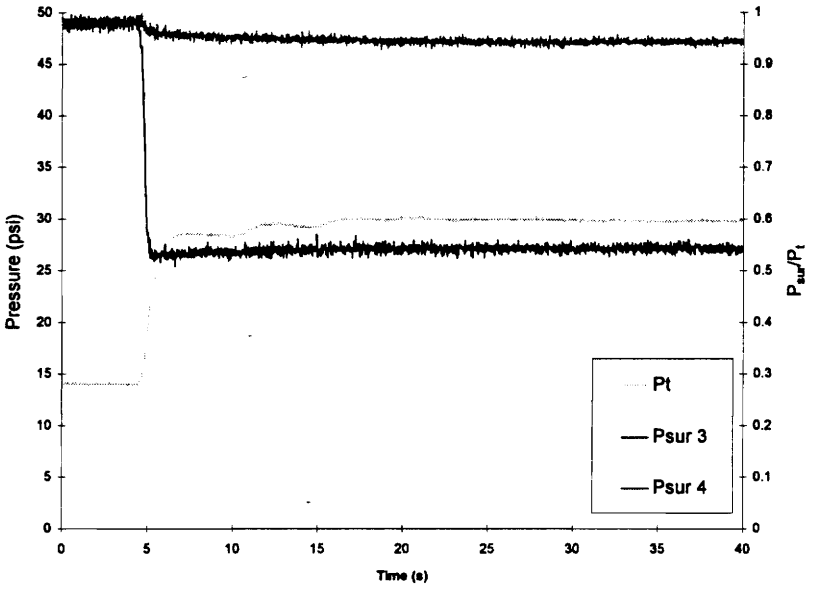


Figure 5.34 Total Pressure and Normalized Pressure for Strut at z/p=2.05 (Run #2)- Kulite 3 and Kulite 4

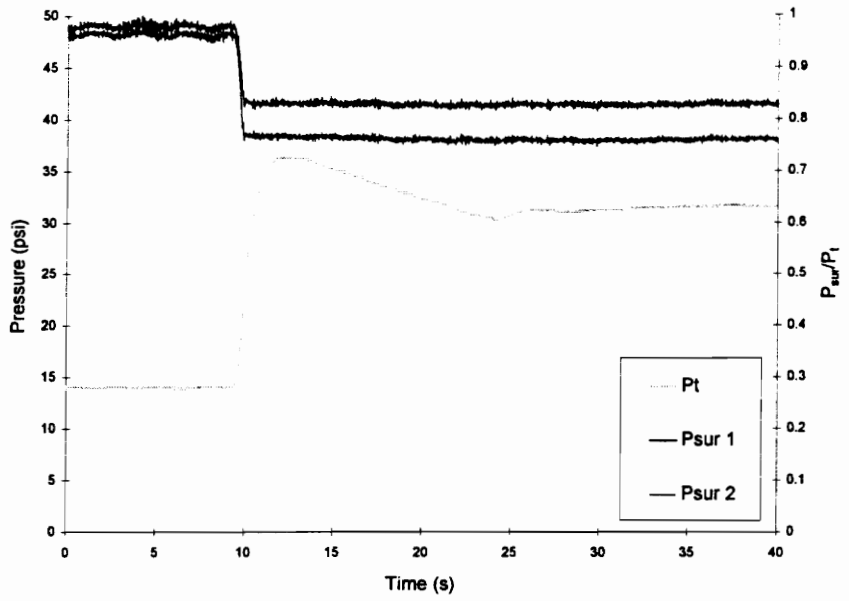


Figure 5.35 Total Pressure and Normalized Pressure for No Strut Case (Run #1)- Kulite 1 and Kulite 2

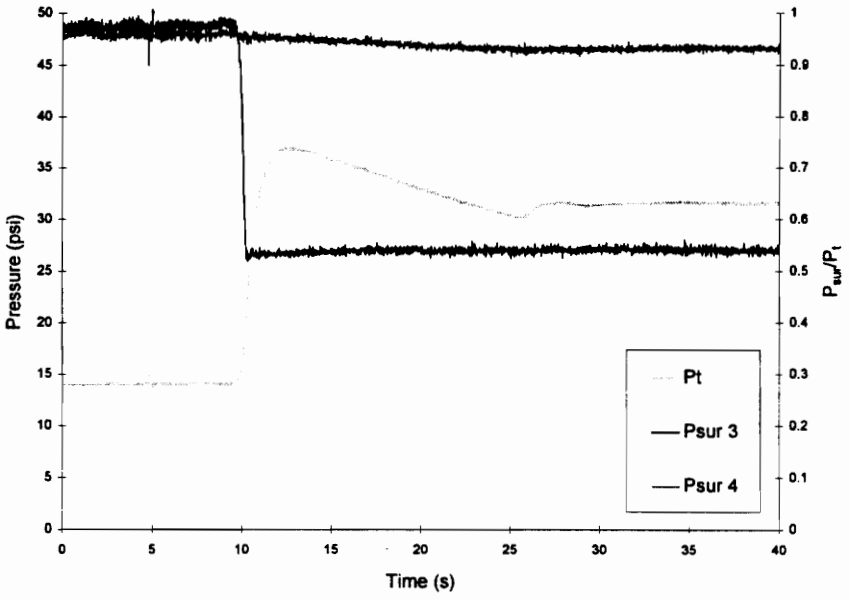


Figure 5.36 Total Pressure and Normalized Pressure for No Strut Case (Run #2)- Kulite 3 and Kulite 4

**Table 5.6 Average Normalized Pressure and Mach Numbers for Various Strut Locations**

| | Kulite 1 | | Kulite 2 | | Kulite 3 | | Kulite 4 | |
|---|---|---|---|---|---|---|---|---|
| | $P_{sur}/P_t$ | Ma | $P_{sur}/P_t$ | Ma | $P_{sur}/P_t$ | Ma | $P_{sur}/P_t$ | Ma |
| | Run #1 | | | | Run #2 | | | |
| **N. S.** | .8290 | 0.5247 | .7614 | 0.6365 | 0.5404 | 0.9805 | 0.9353 | 0.3106 |
| **Loc. 1** | 0.8413 | 0.5030 | 0.7648 | 0.6309 | 0.5384 | 0.9836 | 0.9447 | 0.2861 |
| **Loc. 2** | 0.8417 | 0.5023 | 0.7680 | 0.6259 | 0.5416 | 0.9784 | 0.9451 | 0.2853 |
| **Loc. 3** | 0.8473 | 0.4923 | 0.7711 | 0.6208 | 0.5351 | 0.9889 | 0.9436 | 0.2891 |
| **Loc. 5** | 0.8390 | 0.5060 | 0.7745 | 0.615 | 0.5368 | 0.9863 | 0.9422 | 0.2929 |

Knowing the isentropic Mach number, the free-stream velocity was calculated, and was this used in conjunction with the heat flux and temperature measurements to determine the recovery factor, r at the four gage locations. The recovery factors varied from values of 0.28 to 0.95. Table 5.7 summaries the recovery factors calculated at the four gage locations for the various runs.

**Table 5.7 Recovery Factors for Various Strut Locations**

| | Run #1 | | Run #2 | |
|---|---|---|---|---|
| | Gage 1 (r) | Gage 2 (r) | Gage 3 (r) | Gage 4 (r) |
| **N. S.** | 0.85 | 0.94 | 0.87 | 0.60 |
| **Loc. 1** | 0.88 | 0.85 | 0.91 | 0.55 |
| **Loc. 2** | 0.88 | 0.93 | 0.89 | 0.57 |
| **Loc. 3** | 0.88 | 0.95 | 0.84 | 0.51 |
| **Loc. 5** | 0.96 | 0.93 | 0.88 | 0.28 |

The recovery factor for the 3 suction surface gages remains relatively constant with respect to the position of the strut, and matches reasonable well with the recovery factor for the case of turbulent flow over a flat plate which is typically taken to be $Pr^{1/3}$=0.89. The recovery factor for the pressure side gage (gage 4) is considerably less for all the positions of the strut, especially for location 5 where the strut wake impinges on the pressure surface. For this case the recovery factor has decreased by a factor of 2. The mean free-stream velocity over gage 4 for this particular run is comparable to that of

the other runs. For example when the strut was positioned at location 3 the free-stream velocity over gage 4 was determined to be 107 m/s and when the strut was positioned at location 5 the free-stream velocity was 108 m/s. The cause of the recovery factor being so low during this particular run is due to the large difference in the total temperature and adiabatic wall temperature. For the other strut locations this difference was approximately 2.55°C as compared to 5.12°C for location 5 of the strut. The strut has augmented the heat transfer causing the blade surface temperature to heat up faster while the total temperature has decreased at the same rate as in previous runs.

Possible reasons for the low recovery factors of the pressure surface gage are the curvature of the blade in this region and the relatively high acceleration of the flow near the leading edge. However, this cannot be proven since the suction surface gages were not affected. The flow acceleration is extremely high over gages 1 and 2 on the suction surface.

The HFM-6 gages have great frequency response (>100 kHz) and can show a great deal of resolution in the actual heat flux signals. The power spectra graphs of the HFM-6 gages show an increase in frequency energy levels in the 0-10 kHz range for the three suction surface gages with the strut at location 2 compared to the no strut and no flow cases (refer to Figures 5.37 through 5.40). The frequency energy remains unchanged for the pressure surface gage (gage 4) at this location of the strut (location 2). At this time the large spikes in the spectra above 10 kHz are believed to be caused by electrical noise. To remove this noise a low pass filter (<10 kHz) was constructed using MATLAB. Figures 5.41 through 5.44 show the filtered results. The results are the same up to 10 kHz, then the filter cuts off all of the high frequency energy "noise". With the strut in location 3 the frequency energy increased for the three suction side gages, and no affect was seen with the strut in location 1. The graphs for these two locations are located in Appendix A. Location 5 of the strut showed an affect on the pressure surface gage. The frequency energy levels increased between 0 and 10 kHz (refer to Figures 5.45 and 5.46). The graphs for the suction surface gages are located in Appendix A.

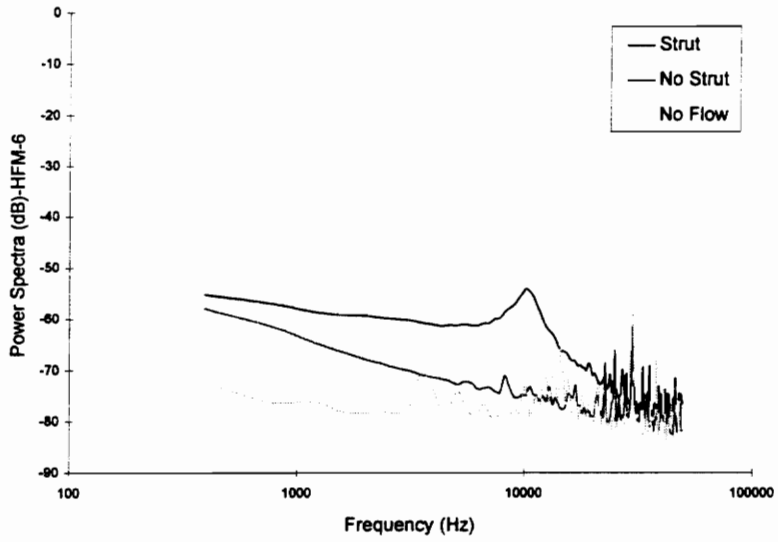


Figure 5.37 Power Spectra of No Strut and Strut at z/p=2.05 of Heat Flux Signal Sampled at 100 kHz (Gage 1)

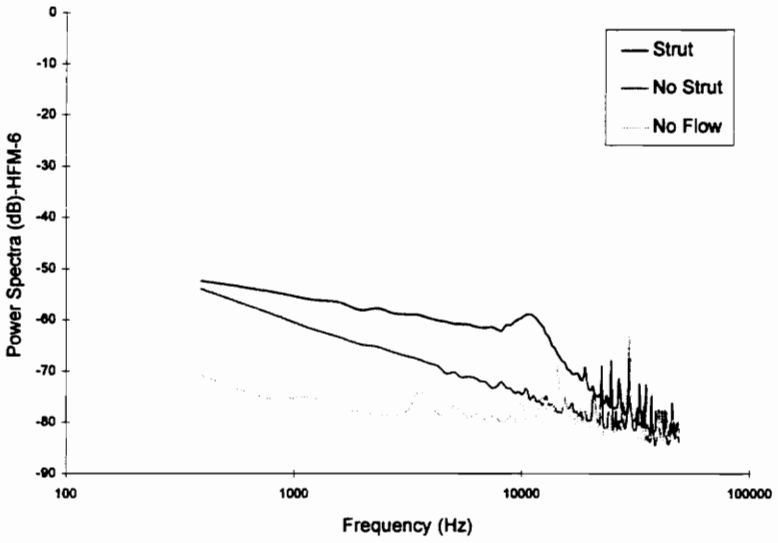


Figure 5.38 Power Spectra of No Strut and Strut at z/p=2.05 of Heat Flux Signal Sampled at 100 kHz (Gage 2)

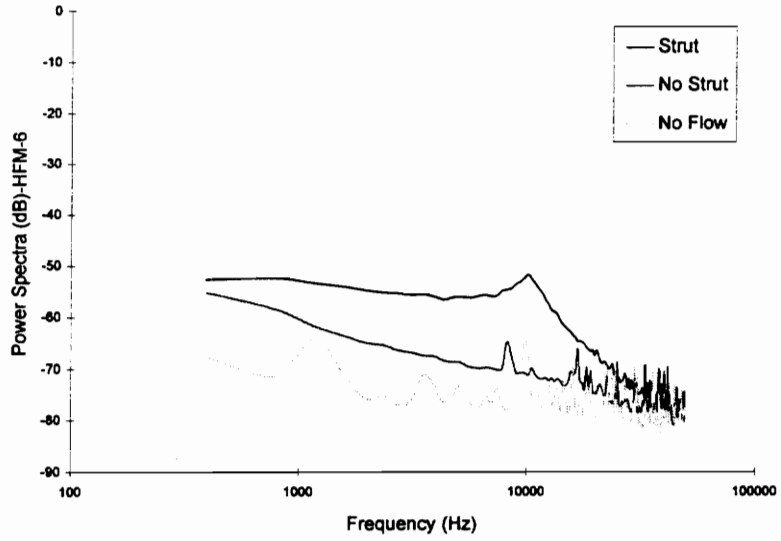


Figure 5.39 Power Spectra of No Strut and Strut at z/p=2.05 of Heat Flux Signal Sampled at 100 kHz (Gage 3)

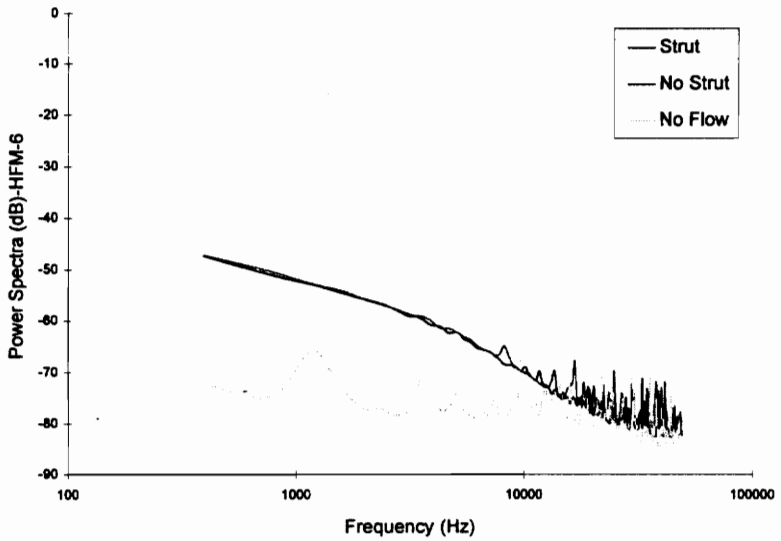


Figure 5.40 Power Spectra of No Strut and Strut at z/p=2.05 of Heat Flux Signal Sampled at 100 kHz (Gage 4)

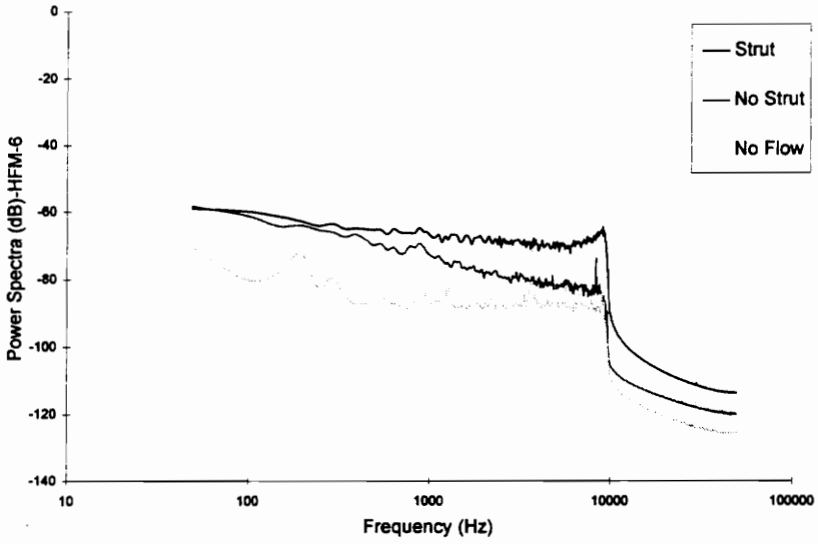


Figure 5.41 Filtered Power Spectra of No Strut and Strut at z/p=2.05 of Heat Flux Signal Sampled at 100 kHz (Gage 1)

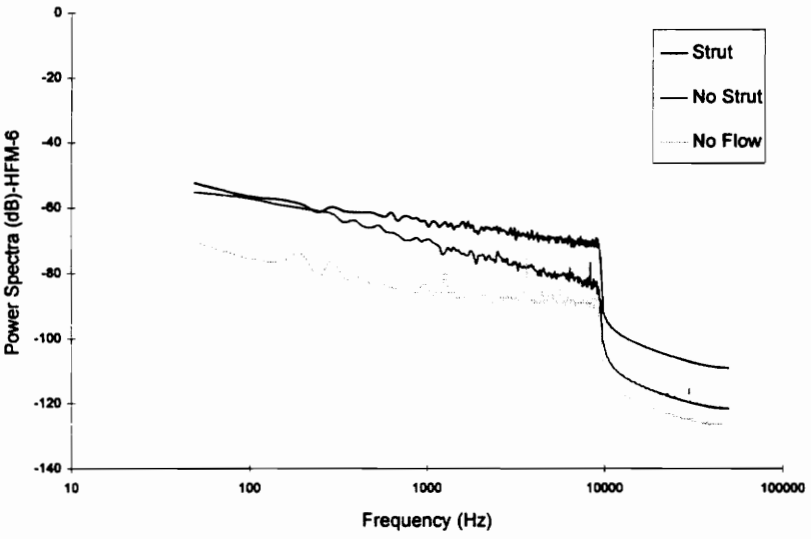


Figure 5.42 Filtered Power Spectra of No Strut and Strut at z/p=2.05 of Heat Flux Signal Sampled at 100 kHz (Gage 2)

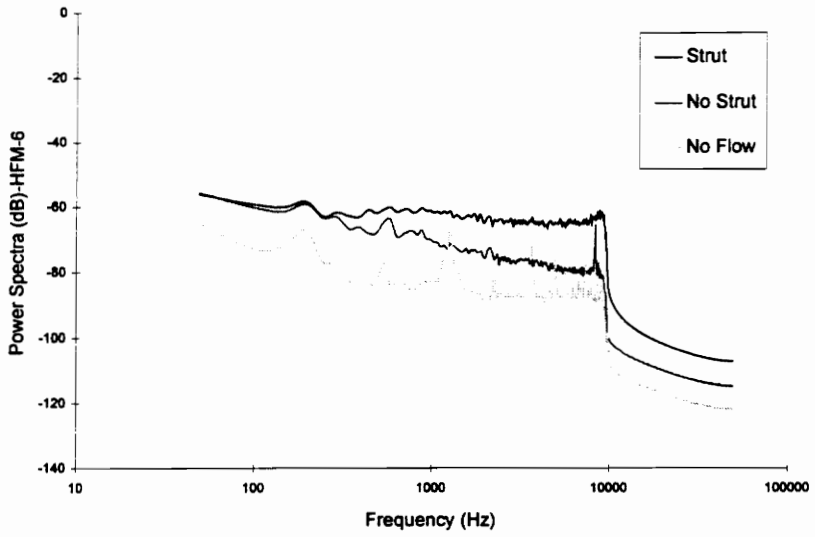


Figure 5.43 Filtered Power Spectra of No Strut and Strut at z/p=2.05 of Heat Flux Signal Sampled at 100 kHz (Gage 3)

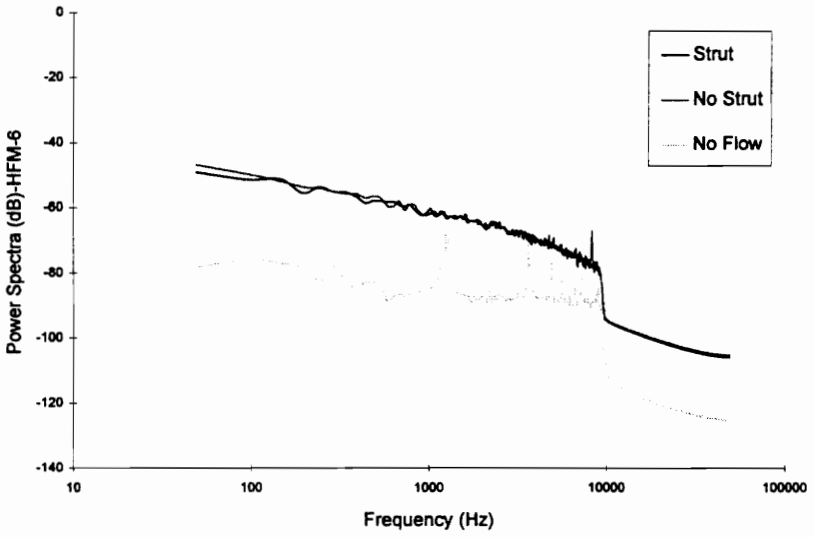


Figure 5.44 Filtered Power Spectra of No Strut and Strut at z/p=2.05 of Heat Flux Signal Sampled at 100 kHz (Gage 4)

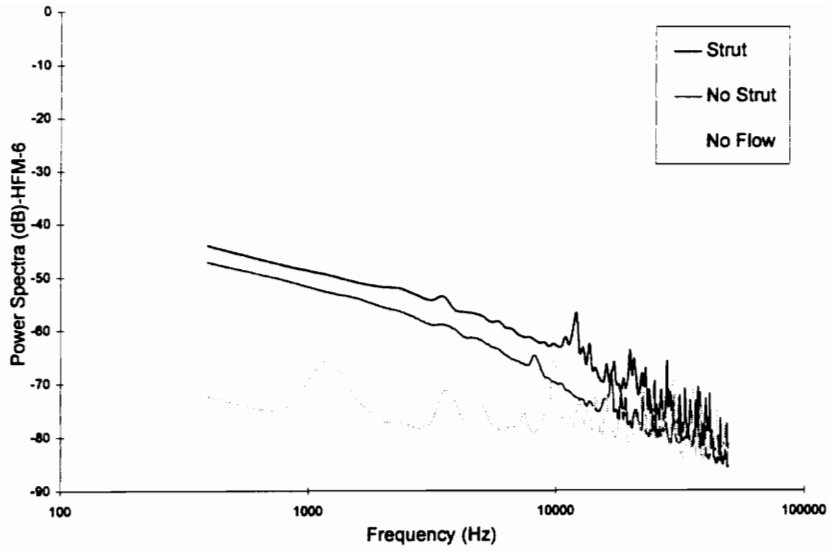


Figure 5.45 Power Spectra of No Strut and Strut at z/p=2.45 of Heat Flux Signal Sampled at 100 kHz (Gage 4)

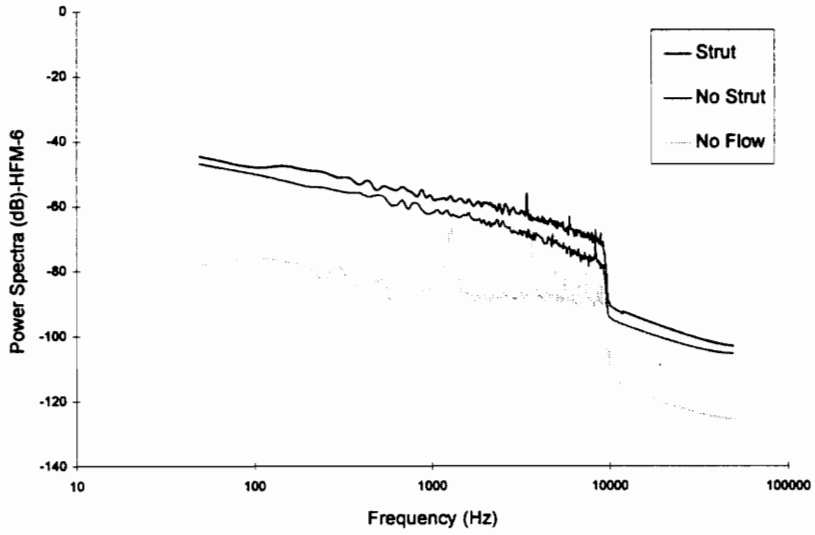


Figure 5.46 Filtered Power Spectra of No Strut and Strut at z/p=2.45 of Heat Flux Signal Sampled at 100 kHz (Gage 4)

The Kulites also possess a good frequency response (35 kHz). The power spectra graphs of the Kulites show an increase in the frequency energy between 2 - 10 kHz for the three suction surface gages when the strut is in location 2 (refer to Figures 5.47 through 5.50). The frequency energy of the pressure surface gage (Kulite 4) remains unchanged with the strut in this position. The suction surface Kulites do not pick up the lower frequency energy levels (< 2 kHz) as do the HFM-6 gages. The signals do not appear to have the "electrical noise" that was experienced by the HFM-6 gages, therefore, no attempt at this time was made to filter the data. The same trends were noticed with the Kulites as was seen with the heat flux gages at locations 1 and 3 of the strut (refer to Appendix A). However, with the strut at location 5 the frequency energy of the pressure surface Kulite was not increased as was the frequency energy of the heat flux gage (refer to Figure 5.51).

## 5.5 Heat Flux and Kulite Turbulence Intensity

Turbulence intensity measurements based on heat flux is a relatively new concept. This was used by Johnson and Diller (1995) for a turbine blade. This new technique could be achieved due to the fast time response of the Heat Flux Microsensor. These results are another attempt to help understand the effect that a localized velocity defect and increased turbulence intensity has on blade surface heat transfer. The heat flux turbulence intensity ($Tu_q$) was performed on all of the runs at the different strut locations sampled at 100 kHz. A $Tu_q$ value was calculated every 2048 points (.02 seconds), and then these were averaged to determine the average $Tu_q$ value for the run. The values were calculated over short time periods due to the average heat flux changing during the run. This produced a more accurate representation of the heat flux turbulence intensity. The RMS values were calculated using the same procedure. As mentioned earlier there appeared to be "electrical noise" present in the signals above 10 kHz, therefore, the filtered and unfiltered results are presented for comparison. Tables 5.8a through 5.8f show these results. $Tu_q$ at 0 is undefined because the mean heat flux is zero (no flow

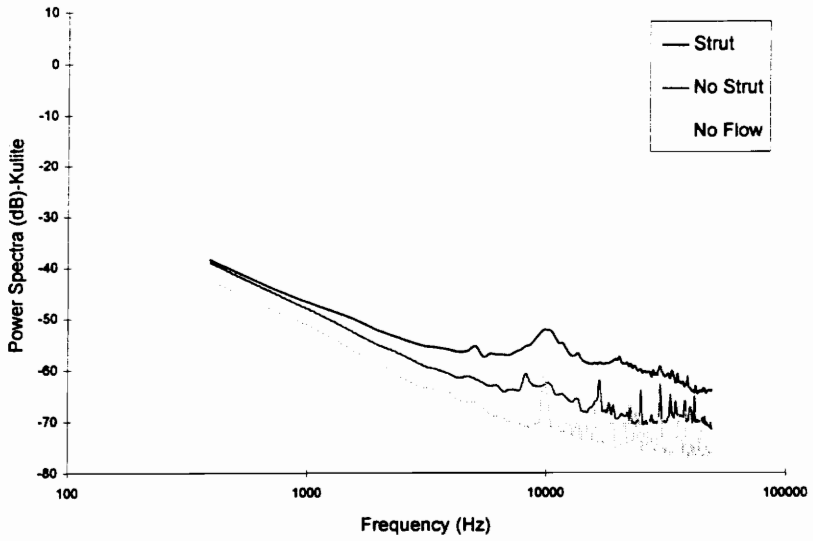


Figure 5.47 Power Spectra of No Strut and Strut at z/p=2.05 of Kulite Signal Sampled at 100 kHz (Gage 1)

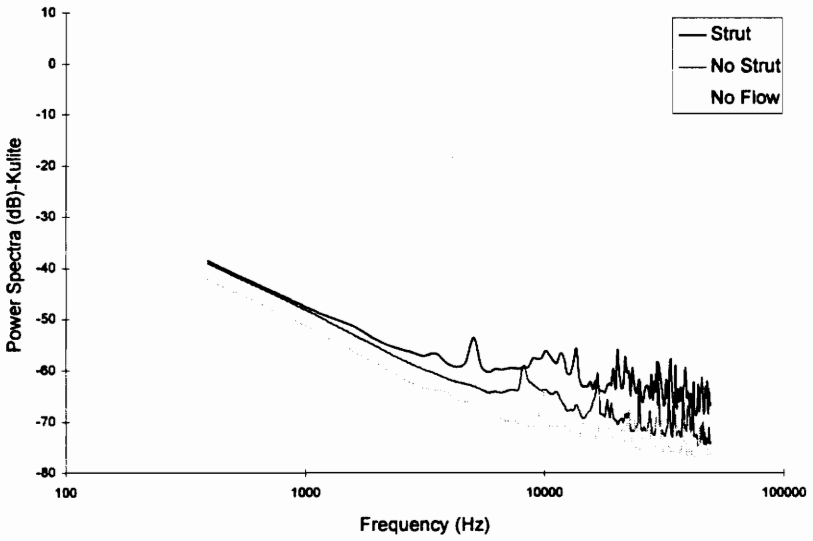


Figure 5.48 Power Spectra of No Strut and Strut at z/p=2.05 of Kulite Signal Sampled at 100 kHz (Gage 2)

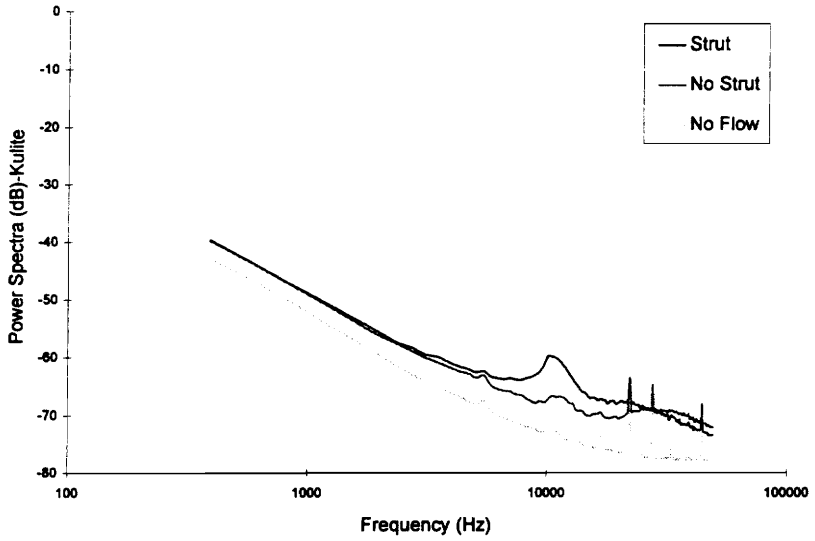


Figure 5.49 Power Spectra of No Strut and Strut at z/p=2.05 of Kulite Signal Sampled at 100 kHz (Gage 3)

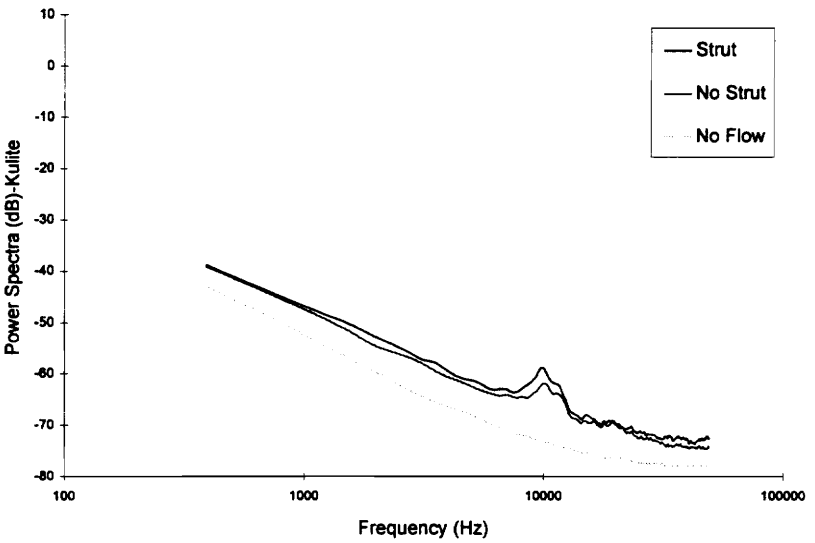


Figure 5.50 Power Spectra of No Strut and Strut at z/p=2.05 of Kulite Signal Sampled at 100 kHz (Gage 4)

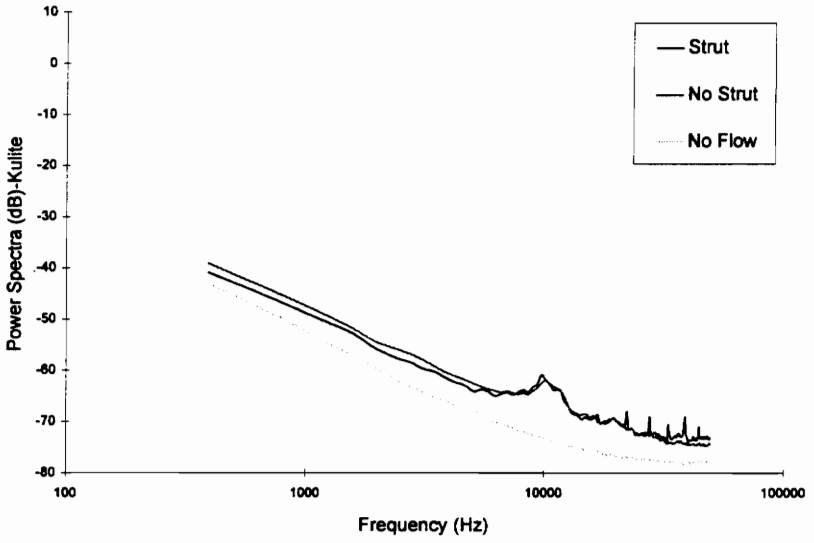


Figure 5.51 Power Spectra of No Strut and Strut at z/p=2.45 of Kulite Signal Sampled at 100 kHz (Gage 4)

case). Comparing the no flow (Table 5.8a) with the baseline case (no strut Table 5.8b) it is apparent that the noise level of the gage is relatively small, therefore, no attempt was made to remove the noise from the other runs. Filtering has varied effects on the data. For example, filtering the data has little affect on the mean, RMS, and $Tu_q$ for the no strut case, and locations 1 and 5. However, an affect is seen when the strut is positioned at location 2. The mean remains approximately constant while the RMS and $Tu_q$ values for the three suction surface gages drop by an average of 20%. There is little to no change in the pressure surface gage. The same trend is noticed when the strut is placed in location 3.

**Table 5.8a Mean, RMS, and $Tu_q$ (Unfiltered and Filtered) for No Flow**

| No Flow | | | | | | |
|---|---|---|---|---|---|---|
| | Unfiltered | | | Filtered | | |
| Gage # | Mean HFS (V) | RMS (V) | $Tu_q$ (%) | Mean HFS (V) | RMS (V) | $Tu_q$ (%) |
| HFM-6, 1 | 0.0 | 0.002277 | N/A | 0.0 | 0.000825 | N/A |
| HFM-6, 2 | 0.0 | 0.001742 | N/A | 0.0 | 0.000784 | N/A |
| HFM-6, 3 | 0.0 | 0.002234 | N/A | 0.0 | 0.001336 | N/A |
| HFM-6, 4 | 0.0 | 0.001792 | N/A | 0.0 | 0.000942 | N/A |

**Table 5.8b Mean, RMS, and $Tu_q$ (Unfiltered and Filtered) for No Strut**

| No Strut | | | | | | |
|---|---|---|---|---|---|---|
| | Unfiltered | | | Filtered | | |
| Gage # | Mean HFS (V) | RMS (V) | $Tu_q$ (%) | Mean HFS (V) | RMS (V) | $Tu_q$ (%) |
| HFM-6, 1 | 0.104355 | 0.003051 | 2.93 | 0.104207 | 0.002473 | 2.38 |
| HFM-6, 2 | 0.084456 | 0.003048 | 4.62 | 0.084324 | 0.003603 | 4.27 |
| HFM-6, 3 | 0.092971 | 0.004169 | 4.52 | 0.092844 | 0.003631 | 3.94 |
| HFM-6, 4 | 0.077740 | 0.009617 | 12.47 | 0.077625 | 0.009489 | 12.3 |

**Table 5.8c Mean, RMS, and $Tu_q$ (Unfiltered and Filtered) with Strut at z/p=1.78**

| Strut at z/p=1.78 (Location 1) | | | | | | |
|---|---|---|---|---|---|---|
| | Unfiltered | | | Filtered | | |
| Gage # | Mean HFS (V) | RMS (V) | $Tu_q$ (%) | Mean HFS (V) | RMS (V) | $Tu_q$ (%) |
| HFM-6, 1 | 0.078561 | 0.002717 | 3.47 | 0.078449 | 0.002006 | 2.57 |
| HFM-6, 2 | 0.112854 | 0.002932 | 2.61 | 0.112688 | 0.002527 | 2.26 |
| HFM-6, 3 | 0.066509 | 0.003932 | 5.94 | 0.066418 | 0.003270 | 4.94 |
| HFM-6, 4 | 0.094318 | 0.005548 | 5.91 | 0.094182 | 0.005548 | 5.69 |

**Table 5.8d Mean, RMS, and $Tu_q$ (Unfiltered and Filtered) with Strut at z/p=2.05**

| Strut at z/p=2.05 (Location 2) | | | | | | |
|---|---|---|---|---|---|---|
| | Unfiltered | | | Filtered | | |
| Gage # | Mean HFS (V) | RMS (V) | $Tu_q$ (%) | Mean HFS (V) | RMS (V) | $Tu_q$ (%) |
| HFM-6, 1 | 0.094282 | 0.007308 | 7.76 | 0.094153 | 0.005368 | 5.71 |
| HFM-6, 2 | 0.134770 | 0.007328 | 5.45 | 0.134578 | 0.006360 | 4.74 |
| HFM-6, 3 | 0.091323 | 0.011023 | 12.07 | 0.091198 | 0.008744 | 9.59 |
| HFM-6, 4 | 0.074437 | 0.008824 | 11.94 | 0.074334 | 0.008755 | 11.86 |

**Table 5.8e Mean, RMS, and $Tu_q$ (Unfiltered and Filtered) with Strut at z/p=2.19**

| Strut at z/p=2.19 (Location 3) | | | | | | |
|---|---|---|---|---|---|---|
| | Unfiltered | | | Filtered | | |
| Gage # | Mean HFS (V) | RMS (V) | $Tu_q$ (%) | Mean HFS (V) | RMS (V) | $Tu_q$ (%) |
| HFM-6, 1 | 0.057135 | 0.004379 | 7.67 | 0.057052 | 0.003308 | 5.80 |
| HFM-6, 2 | 0.057998 | 0.005741 | 10.00 | 0.057917 | 0.005135 | 8.97 |
| HFM-6, 3 | 0.046475 | 0.006322 | 13.7 | 0.046412 | 0.005494 | 11.92 |
| HFM-6, 4 | 0.083040 | 0.006818 | 8.47 | 0.080278 | 0.006652 | 8.28 |

**Table 5.8f Mean, RMS, and $Tu_q$ (Unfiltered and Filtered) with Strut at z/p=2.45**

| Strut at z/p=2.45 (Location 4) | | | | | | |
|---|---|---|---|---|---|---|
| | Unfiltered | | | Filtered | | |
| Gage # | Mean HFS (V) | RMS (V) | $Tu_q$ (%) | Mean HFS (V) | RMS (V) | $Tu_q$ (%) |
| HFM-6, 1 | 0.070784 | 0.002858 | 4.05 | 0.070683 | 0.002328 | 3.31 |
| HFM-6, 2 | 0.134356 | 0.003169 | 2.37 | 0.134160 | 0.002837 | 2.12 |
| HFM-6, 3 | 0.053879 | 0.004483 | 8.40 | 0.053879 | 0.003695 | 6.93 |
| HFM-6, 4 | 0.088018 | 0.008946 | 10.19 | 0.087886 | 0.008463 | 9.63 |

The results for the pressure surface gage are more confusing than those for the suction surface gages. With the strut at location 5, the RMS values for gage 4 are less than those for the no strut case, however, with the strut in this position a 24% increase in the overall heat transfer coefficient was seen. There appears to be some variation in the data for gage 4 (pressure surface) on a day to day basis. The no strut and location 2 data were collected one day and the other three locations were collected another. From the hot-wire traverses and the Fast Fourier Transform performed on the heat flux and Kulite signals, no noticeable changes could be quantified in the flow field of the instrumented passage with the strut at location 1. Therefore, using this as the baseline case for gage 4 the same trends are noticed as with two suction surface gages (1 and 2). The RMS levels increase as does the overall heat transfer coefficient. The preceding analysis of gage 4 is pure conjecture, and more runs should be conducted for a better understanding of the pressure surface gage.

The turbulence intensity values based on the heat flux, $Tu_q$, for each of the strut locations was plotted with the corresponding average heat transfer coefficient. This was an attempt to see if any coherence existed between the value of $Tu_q$, and the average heat transfer coefficient as is believed to exist between $h$ and $Tu$. The results are shown in Figures 5.52 through 5.55. The results for gage 1 show a slightly upward trend. The results for the other three gages are scattered and no trend can be distinguished. From these results it appears there is no relationship between the value of $Tu_q$ and $h$.

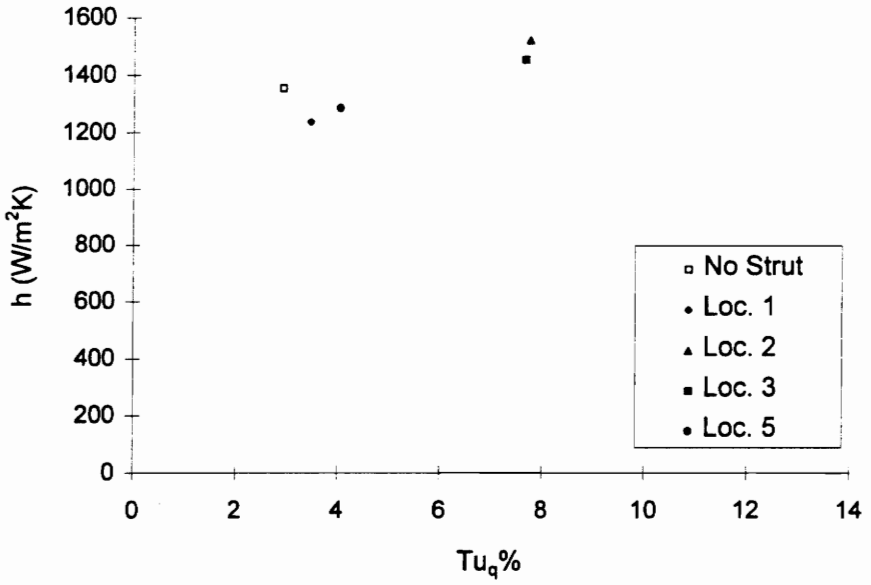


Figure 5.52 $Tu_q$ vs. HTCfor No Strut Case and 4 Strut Locations (Heat Flux Gage 1)

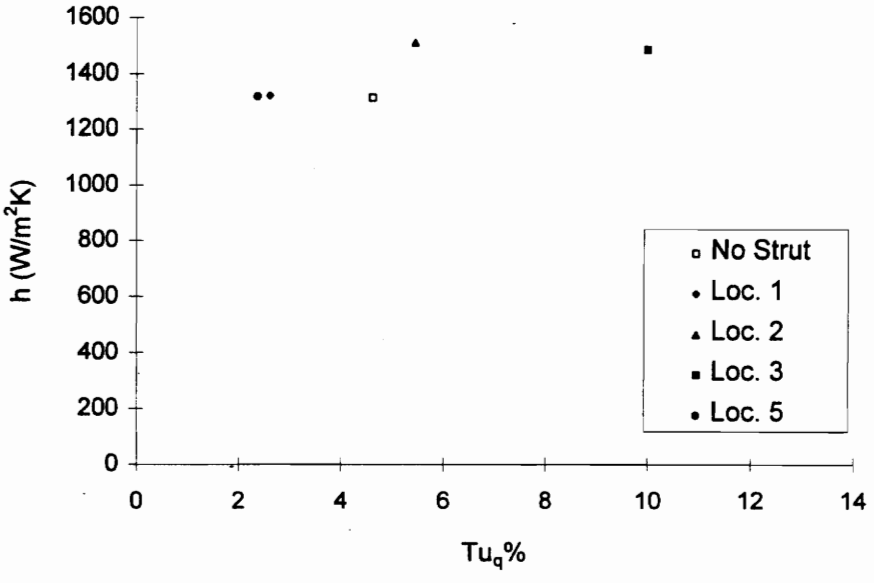


Figure 5.53 $Tu_q$ vs. HTC for No Strut Case and 4 Strut Locations (Heat Flux Gage 2)

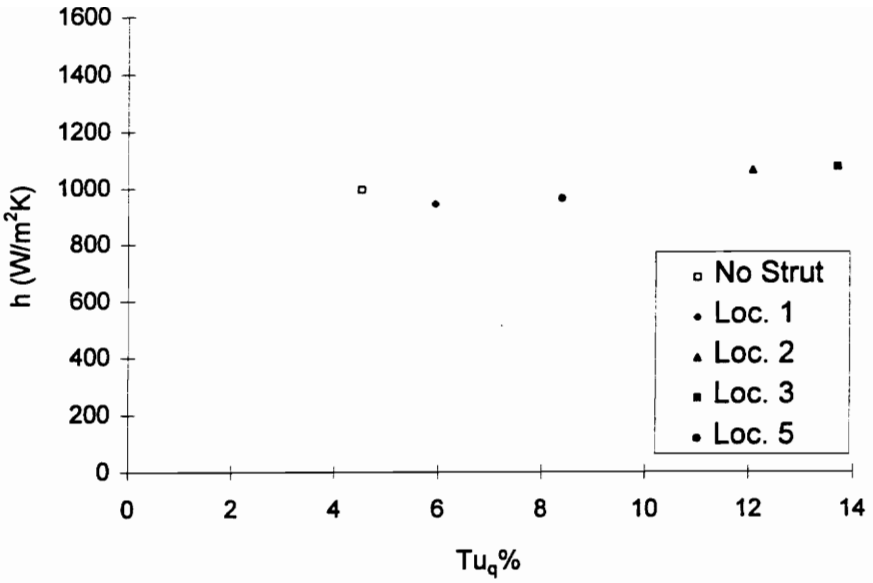


Figure 5.54 $Tu_q$ vs. HTC for No Strut Case and 4 Strut Locations (Heat Flux Gage 3)

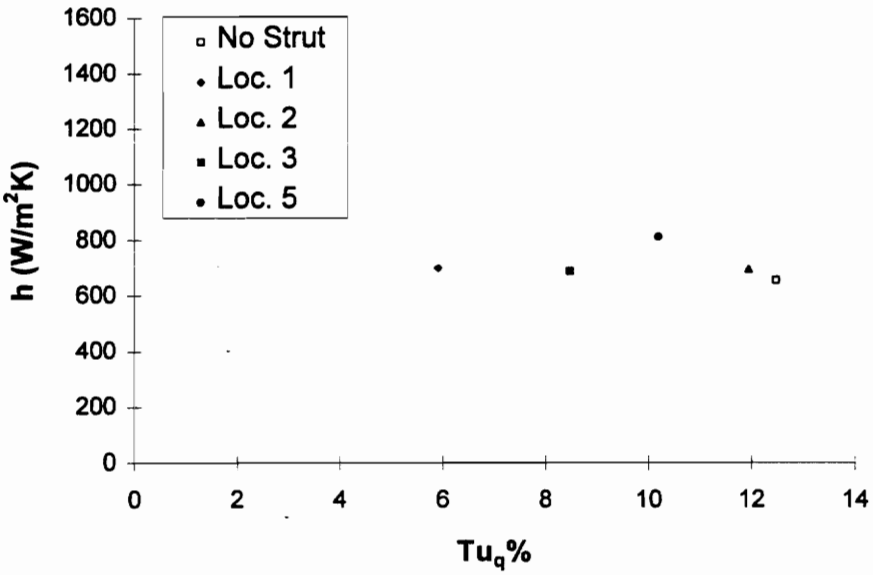


Figure 5.55 $Tu_q$ vs. HTC for No Strut Case and 4 Strut Locations (Heat Flux Gage 4)

The same type of analysis used for the HFM-6 gages was used for the pressure signals from the Kulites. The results were inconclusive, however. No distinct increases or decreases could be distinguished between the RMS and turbulence values for the strut cases and the no strut cases. Only one position of the strut will be considered in this thesis since the results from the other positions were redundant. Table 5.9a through 5.9b show some of the results for the pressure data collected. Notice how the average values differ for the two runs (two locations). This again is believed due to variations in the pressure tunnel control causing the data to be collected during different times after the tunnel is initially started. There is very little difference between the filtered and unfiltered results. The RMS values for the no strut case differ only slightly from the RMS values with the strut at z/p = 2.05 (location 2). This was true for all of the gages, both suction and pressure surface. No change was expected from the pressure surface Kulite. The pressure turbulence intensity values for Kulites 1 and 2 on the suction surface and for Kulite 4 on the pressure surface remain approximately constant for the strut at location 2 and the no strut case. Some deviation does exist between the values obtained for Kulite 3 on the suction surface. The values for $Tu_p$ vary significantly for the no strut and strut case, with the no strut case being the higher of the two. The RMS values are nearly the same for the two locations. The difference in the two turbulence values for this case can be attributed to the mean values.

**Table 5.9a Mean, RMS, and $Tu_p$ (Unfiltered and Filtered, Kulites) for No Strut**

| No Strut | | | | | | |
|---|---|---|---|---|---|---|
| | Unfiltered | | | Filtered | | |
| Gage # | Mean KLS (V) | RMS (V) | $Tu_p$ (%) | Mean KLS (V) | RMS (V) | $Tu_p$ (%) |
| **Kulite 1** | 1.776627 | 0.023450 | 1.32 | 1.773957 | 0.023122 | 1.30 |
| **Kulite 2** | 1.282690 | 0.023107 | 1.80 | 1.280765 | 0.022817 | 1.78 |
| **Kulite 3** | 0.297100 | 0.020799 | 7.02 | 0.296650 | 0.020539 | 6.93 |
| **Kulite 4** | 2.090880 | 0.022648 | 1.08 | 2.08774 | 0.022486 | 1.08 |

**Table 5.9b Mean, RMS, and $Tu_p$ (Unfiltered and Filtered, Kulites) with Strut at z/p=2.05**

| Strut at z/p=2.05 (Location 2) | | | | | | |
|---|---|---|---|---|---|---|
| | Unfiltered | | | Filtered | | |
| Gage # | Mean KLS (V) | RMS (V) | $Tu_p$ (%) | Mean KLS (V) | RMS (V) | $Tu_p$ (%) |
| Kulite 1 | 2.190674 | 0.026488 | 1.21 | 2.187290 | 0.024165 | 1.10 |
| Kulite 2 | 1.593107 | 0.024487 | 1.54 | 1.591655 | 0.023082 | 1.45 |
| Kulite 3 | 0.430470 | 0.020385 | 4.74 | 0.429820 | 0.019961 | 4.64 |
| Kulite 4 | 2.457810 | 0.022751 | .93 | 2.454020 | 0.022536 | .92 |

An attempt was made to correlate the turbulence effects on the surface heat transfer along a turbine blade with the effects of turbulence at the stagnation point on a circular cylinder and portions of airfoils possessing constant strain rates. Dullenkopf and Mayle (1994) incorporate previous studies on the effects of turbulence and moving wakes on laminar heat transfer in turbine blading into a correlation for the Nusselt number of cylinders and airfoils. They extend their analysis to include portions of the airfoil that exhibit a constant strain rate, $a$. They assume that since the strain rate $a = dU/dx$ is nearly constant over a particular section of the airfoil that this flow is similar to that found for stagnation flow or flow on the forward portion of a circular cylinder, except for magnitude. It follows then that the effect of free-stream turbulence and the turbulence within moving wakes on the heat transfer in an accelerating laminar boundary layer of an airfoil must be related to that for a similar flow on the forward portion of a circular cylinder. From this analysis they determined the following correlation to fit existing cylinder and airfoil data

$$Nu_a \, \mathrm{Pr}^{-0.37} = 0.571 + 0.0125 \cdot Tu_a \left\{ 1 + \frac{1.8}{\left[ 1 + (Tu_a/20)^3 \right]} \right\} \qquad [5.2]$$

where $Tu_a$ is evaluated using the absolute incident turbulence level and not percent. The free-stream strain rate was determined using the computer predictions provided by General Electric since the prediction for the isentropic Mach number compared well with the experimental results by Wesner (1994). Figures 5.56 and 5.57 show the isentropic Mach number and free-stream strain rate along the pressure and suction surfaces of the blade. The free-stream strain rate is approximately constant over the majority of the suction surface, especially for the region in which the three suction surface gages are located. The free-stream strain rate varies over the pressure surface.

The results for the no strut case and the strut at z/p = 2.05 (location 2) were used to compare with the prediction from the correlation. The results are tabulated in Tables 5.10 and 5.11.

**Table 5.10 Experimental Results vs. Dullenkopf and Mayle's correlations for No Strut Case**

| No Strut | | | | | |
|---|---|---|---|---|---|
| **Gage #** | **$Tu_{inlet}$** | **$Tu_{decay}$** | **$Tu_a$** | **$Nu_a$ (Exp.)** | **$Nu_a$ (Theory)** |
| 1 | 0.031 | 0.023 | 14.35 | 1.65 | 0.87 |
| 2 | 0.031 | 0.019 | 14.53 | 1.59 | 0.87 |
| 3 | 0.031 | 0.011 | 11.35 | 1.36 | 0.82 |
| 4 | 0.031 | 0.051 | 37.58 | 1.52 | 1.01 |

**Table 5.11 Experimental Results vs. Dullenkopf and Mayle's correlation for Strut at z/p = 2.05**

| No Strut | | | | | |
|---|---|---|---|---|---|
| **Gage #** | **$Tu_{inlet}$** | **$Tu_{decay}$** | **$Tu_a$** | **$Nu_a$ (Exp.)** | **$Nu_a$ (Theory)** |
| 1 | 0.212 | 0.158 | 98.69 | 1.83 | 1.61 |
| 2 | 0.212 | 0.131 | 99.90 | 1.90 | 1.62 |
| 3 | 0.212 | 0.076 | 77.86 | 1.52 | 1.38 |
| 4 | 0.212 | 0.353 | 258.389 | 1.59 | 3.35 |

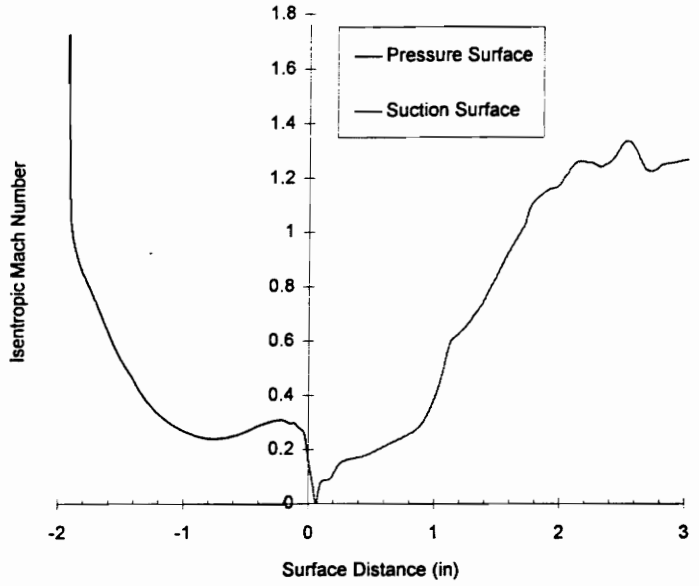


Figure 5.56 Isentropic Mach Number Distribution on Blade - Prediction

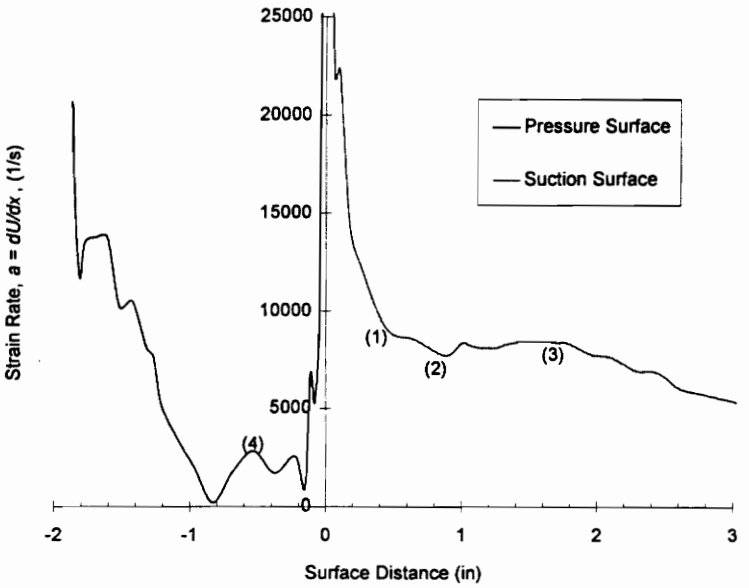


Figure 5.57 Free-stream Strain Rate Distribution on Blade - Prediction

The turbulence intensity decay values were determined from a plot provided by General Electric. These values were used to determine $Tu_a$ from equation 2.11. The experimental results from the three suction surface gages compare reasonably well with the correlation for the strut at z/p = 2.05 (location 2). The correlation over predicts for the pressure surface gage (4) by a factor of 2. Dullenkopf and Mayle's correlation underpredicts for all of the gages for the no strut case.

Dullenkopf and Mayle also derived a correlation based on the effects of turbulence as well as length scale to fit the airfoil and cylinder data. From their analysis they determined the following correlation

$$Nu_a \, \mathrm{Pr}^{-0.37} = 0.571 + 0.01 \cdot Tu_\lambda \qquad [5.3]$$

where $Tu_\lambda$ is defined by equation 2.13. The results for the no strut and strut case (z/p = 2.05) are located in Table 5.12.

**Table 5.12 Experimental Results vs. Dullenkopf and Mayle's Length Scale Correlation for No Strut and Strut at z/p = 2.05**

| | No Strut | | | Strut at z/p = 2.05 | | |
|---|---|---|---|---|---|---|
| **Gage #** | **$Tu_\lambda$** | **$Nu_a$ (Exp.)** | **$Nu_a$ (Theory)** | **$Tu_\lambda$** | **$Nu_a$ (Exp.)** | **$Nu_a$ (Theory)** |
| 1 | 20.79 | 1.65 | 0.88 | 142.9 | 1.83 | 2.27 |
| 2 | 19.89 | 1.59 | 0.88 | 136.8 | 1.90 | 2.20 |
| 3 | 13.36 | 1.36 | 0.80 | 91.8 | 1.52 | 1.69 |
| 4 | 66.4 | 1.52 | 1.40 | 456.5 | 1.59 | 5.8 |

Again this correlation does not predict the no strut case very well. The experimental results for the three suction surface gages compare reasonably well with the correlation for the strut case. This correlation also underpredicts the modified Nusselt number. An answer to this might be the length scale used in the calculations. Only one

measure of the length scale was obtained and this was used in the calculations even though the scale of the turbulence is stretched as it advances through the flow passage.

Finally, a comparison was made between the $Tu_q$ values calculated for the no strut case and for the strut at z/p = 2.05 with the turbulence intensity (decay) values measured by the hot-wire. The results are tabulated in Table 5.13.

**Table 5.13 $Tu_q$ and Tu (decay) Comparison for No Strut and Strut at z/p = 2.05**

| | No Strut | | Strut at z/p = 2.05 | |
|---|---|---|---|---|
| **Gage #** | **$Tu_q$** | **$Tu_{decay}$** | **$Tu_q$** | **$Tu_{decay}$** |
| 1 | 2.93 | 2.23 | 7.76 | 15.76 |
| 2 | 2.36 | 1.91 | 5.45 | 13.13 |
| 3 | 4.52 | 1.10 | 12.07 | 7.59 |
| 4 | 12.5 | 5.13 | 11.94 | 35.3 |

For the no strut case, the $Tu_q$ values compare well with the turbulence intensity decay values for gages 1 and 2. There is approximately 20% difference in the values. The turbulence intensity decay values for the strut case are approximately 2 times greater than the $Tu_q$ values for gages 1 and 2. There is 74 % difference and a 34 % difference in the values for the no strut and strut case for gage 3 on the suction surface. These large differences could possibly be from transition of the boundary layer at gage 3. To achieve a better comparison of $Tu_q$ with the turbulence intensity, it should have been measured with a hot-wire over each gage.

# Chapter 6.0

## Conclusions and Recommendations

### 6.1 Conclusions

Several conclusions can be made about the effects of a stationary wake on turbine blade surface heat transfer.

A major accomplishment with this project was the measurements of time averaged and unsteady heat flux with a HFM inserted into the blade. Three gages were located on the suction surface and one gage on the pressure surface.

A strong influence on the mean heat transfer coefficient was seen from the relative position of the strut with respect to the test blades. In particular the position of the strut with respect to the leading edge of the blade had significant importance. At location 2 (z/p = 2.05) the time-averaged heat transfer coefficients for the three suction surface gages was increased by 12%, 15%, and 7%, respectively. Increases were also seen with the strut at location 3 (z/p = 2.19). The time-averaged heat transfer coefficient increased by 8% for gage 1, 13% for gage 2, and 8% for gage 3. The largest increase in the time-averaged heat transfer coefficient, 24%, was seen on the pressure surface with the strut at location 5 (z/p= 2.45).

The mean heat transfer coefficients determined for the no strut or baseline case did not match well with the computer predictions provided by General Electric. The results did support the experimental results of Wittig (1987), however. He showed increases in the heat transfer coefficient depending on the relative position of the strut with respect to the test blade. He also showed the largest increases in the heat transfer coefficient on the pressure surface.

When compared to Dullenkopf and Mayles's correlation's (equations 5.1 and 5.2) on the effects of free-stream turbulence and length scale on heat transfer to an airfoil, the experimentally determined values were slighty higher than those determined from the two different correlations for the three suction surface gages with the strut at x/p = 2.05. The two correlations did not compare well with the experimental results for the no strut case.

The fast time response of the HFM gages allowed for a spectral density analysis and showed a definite increase in the energy at the 0 - 10 kHz range for z/p = 2.05 and z/p = 2.19 (locations 2 and 3) for the three suction surface gages. An increase in the energy level was noticed for the pressure surface gage with the strut at z/p = 2.45 (location 5). Results using turbulence intensity based on heat flux, $Tu_q$, showed a higher $Tu_q$ value for the three suction surface gages with the strut at the two leading edge locations. The value also increased for the pressure surface with the strut at location 5.

A comparison of the turbulence intensity, *Tu*, was made with the turbulence intensity based on $Tu_q$. The turbulence intensity values, *Tu*, were calculated from the hot-wire results and the turbulence intensity decay plot provided by General Electric. There appears to be no distinct correlation between the two values.

The spectral analysis conducted on the Kulites showed a definite increase in the energy above 2 kHz for locations 2 and 3 for the three suction surface Kulites.

## 6.2 Recommendations

Recommendations for future research include the following ideas.

More strut locations around the leading edge of the test blade should be considered. The axial position of the strut should also be varied. In this thesis a value of s/c = 0.42 was utilized.

This was a first attempt in measuring heat flux on the pressure surface of the turbine blade. More research should be conducted on the pressure surface. Presently, for

this project, heat flux measurements have been made at five locations on the suction surface.

Heat flux and velocity should be measured simultaneously at the surface of the blade to compare the two signals and power spectra during heated tunnel runs. By measuring the velocity and heat flux together at a particular location along the blade it may be possible to determine if there is any coherence in the two signals. A direct correlation may exist between free-stream turbulence, Tu, and turbulence intensity based on heat flux, $Tu_q$.

# References


Bayley, F. J., and Milligan, R. W., "The Effect of Free-Stream Turbulence Upon Heat Transfer to Trubine Blading," *AGARD PEP on High Temperature Problens in Gas Turbine Engines*, 1977,CP 229, Paper No. 37.

Bayley, F. J., and Priddy, W. J., "Effects fo Free-Stream Turbulence Intensity and Frequency on Heat Transfer to Turbine Blading," *ASME Journal of Engineering for Power*, Vol. 103, January 1981, pp. 60-64.

Chima, R. V., "Development of an explicit Multigrid Algorithm for Quasi-Three-Dimensional Flows in Turbomachinery,: AIAA Paper No. 86-00032; NASA TM-87128, 1986.

Corrsin, S., "Turbulence: Experimental Methods," Encyclopedia of Physics, Ed. S. Flugge, Vol. VIII/2. Fluid dynamics II., 1963, pp. 524-590.

Crawford, M.E. and Kays, W.N., "STAN5 - A Progran for Numerical Computation of 2-D Internal and External Boundary Layer Flows," NASA CR2742, 1976.

Diller, T. E., "Advances in Heat Flux Measurements," Advances in Heat Transfer, Vol. 23, Academic Press, New York, 1993, pp. 279-368.

Doorly, D. J., Oldfield, M. L. G., and Scrivener, C. T. J., "Wake Passing in a Turbine Rotor Cascade," AGARD Symposium on Heat Transfer and Cooling in Gas Turbines, 1985.

Doorly, J. E., and Oldfield M. L. G., "New Heat Transfer Gages for Use on Multilayered Substrates," *ASME Journal of Turbomachinery*, Vol. 108, July 1986, pp. 153-160.

Doorly, J. E., and Oldfield M. L. G., "The Theory of Advanced Mulit-Layer Thin Film Heat Transfer Gauges," *International Journal of Heat Mass Transfer*, Vol. 30, No. 6, 1987, pp. 1159-1168.

Doorly, D. J., Oldfield, M. L. G., and Scrivener, C. T. J., "Wake Passing in a Turbine Rotor Cascade," AGARD Symposium on Heat Transfer and Cooling in Gas Turbines, 1985.

Dullenkopf, K., Schultz, A., and Wittig, S., "The Effecto of Incident Wake Conditions on the Mean Heat Transfer of an Airfoil," *Journal of Turbomachinery*, Vol. 113, 1991, pp. 412-418.

Dullenkopf, K., and Mayle, R. E., "An Account of Free-stream Turbulence Length Scale on Laminar Heat Transfer," ASME Paper 94-GT-174.

Dunn, M. G., and Stoddard, F. J., "Measurements of Heat-transfer Rate to a Gas Turbine Stator," *Journal of Engineering for Power*, Vol. 101, 1979, pp. 275-280.

Dunn, M. G., and Hause, A., "Measurement of Heat Flux and Pressure in a Turbine Stage, *Journal of Engineeing for Power*, Vol. 104, 1982, 215-223.

Dunn, M. G., Rae, W. J., and Holt, J. L., "Measurement and Analyses of Heat Flux Data in a Turbine Stage: Part I - Description of Experimental Apparatus and Data Analysis," *Journal of Engineering for Gas Turbines and Power*, Vol. 106, 1984a, pp. 229-233.

Dunn, M. G., Rae, W. J., and Holt, J. L., "Measurement and Analyses of Heat Flux Data in a Turbine Stage: Part II - Discussion of Results and Comparison with Predictions," *Journal of Engineering for Gas Turbines and Power*, Vol. 106, 1984b, pp. 234-240.

Dunn, M. G., "Turbine Heat Flux Measurements: Influence of Slot Injection on Vane Trailing Edge heat Transfer and Influence of Rotor on Vane Heat Transfer," ASME Paper 84-GT-175.

Dunn, M. G., and Chupp, R. E., "Time-averaged Heat Flux Distributions and Comparison with Prediction for the Teledyne 702 HP Turbine Stage," *Journal of Turbomachinery*, Vol. 110, 1988, pp. 51-56.

Dunn, M. G., Seymour, P. J., Woodward, S. H., George, W. K., and Chupp, R. E., "Phase-resolved Heat Flux Measurements on the Blade of a Full-Scale Rotating Turbine," *Journal of Turbomachinery*, Vol. 111, 1989, pp. 8-19.

Dunn, M. G., "Phase and Time-Resolved Measurements of Unsteady Heat Transfer and Pressure in a Full-Stage Rotating Turbine," *Journal of Turbomachinery*, Vol. 112, 1990, pp. 531-538.

Engber, M. and Fotner, L., "The Effect of Incoming Wakes on Boundary Layer Transition of a Highly Loaded Turbine Cascade," AGARD Conference 1995.

Galassi, L., King P. I., and Elrod, W. C., "Effects of Inlet Turbulence Scale on Turbine Blade Surface Heat Transfer in a Linear Cascade," AIAA Paper No. 91-3178.

Gaugler, R. E., "Some Modifications to , and Operating Experiences With the Two-Dimensional Finite-Difference, Boundary-Layer Code STAN5," ASME Paper No. 81-GT-89.

Glezer, B., Moon, H. K., Zhang, L., and Camci, C., "Application of a Heat Flux/Calorimeter Based Method to Asses the Effect of Turbulence on Turbine Airfoil Heat Transfer," *International Gas Turbine and AeroEngine Congress and Exposition*, The Hague, Netherlands, June 1984.

Gundappa, M., and Diller, T. E., "The Effects of Free-stream Turbulence and Flow Pulsation on Heat Transfer from a Cylinder in Crossflow," *ASME Journal of Heat Transfer*, Vol. 113, 1991, pp. 766-769.

Hager, J. M., Simmons, S., Smith, D., Onishi, S., Langley, L. W., and Diller, T. E., "Experimental Performance of a Heat Flux Microsensor," *ASME Journal of Engineering for Gas Turbines and Power*, Vol. 113, 1991a, pp. 246-250.

Hager, J. M., Terrell, J. P., Langley, L. W., Onishi, S., and Diller, T. E., "Measurements with the Heat Flux Microsensor," *Proceedings of the 37th International Instrumentation Symposium*, ISA, Research Triangle Park, 1991b, pp. 551-561.

Han, J. C., Zhang, L., and Ou, S., "Influence of Unsteady Wakes on Heat Transfer Coefficient from a Gas Turbine Blade," *Transactions of ASME*, Vol. 115, November 1993, pp. 904-911.

Hayashi, H., Aso, S., and Tan, A., "Fluctuation of Heat Transfer in Shock Wave/Turbulent Boundary-Layer Interaction," *AIAA Journal*, Vol. 27, 1989, pp. 399-404.

Hinze, J. O., Turbulence, Magraw-Hill, New York, New York, 1959.

Holmberg, D. G., Reid, T., Kiss, T., Moses, H. L., Ng, W. F., and Diller, T. E., "Effects of Shock Wave Passage on heat Transfer in a Transonic Turbine Cascade," *International Gas Turbine and Aeroengine Congress and Exposition*, The Hague, Netherlands, June 1994.

Holmberg, D. G., and Diller, T. E., "High Frequency Heat Flux Sensor Calibration and Modeling," *Journal of Fluids Engineering*, Vol. 117, December 1995, pp. 659-664.

Holmberg, D.G., Modified Labview VI's - LORENHFM.VI, DGHSPCTM.VI, Virginia Tech, 1996.

IFA 100 Intellignet Flow Analyzer Instructional Manual, Revision A. P/N 1990237, copyright 1983 by TSI, Inc.

Johnson, L. P., "Effects of Free-Stream Turbulence on Turbine Blade Heat Transfer in Trasonic Flow", M. S. thesis, Virginia Tech, Blacksburg, 1995.

Johnson, L. P., and Diller, T. E., "Measurements with a Heat Flux Sensor Deposited on a Transonic Turbine Blade," 16th International Congress on Instrumentation in Aerospace Simulation Facilities, June 18-21, Wright Patterson AFB.

Katsanis, T., "FORTRAN Program for Calculating Transonic Velocities on a Blade-to-Blade Stream Surface of a Trubomachine," NASA TN D-5427, 1969.

Katsanis, T., and McNally, W. D., "Revised FORTRAN Program for Calculating Velocities and Streamlines on the Hub-Shroud Mid-channel stream Surface of an Axial-, Radial-, or Mixed-Flow Turbomachine or Annular Duct," Vol. I, User's Manual, Vol. II, Programmer's Manual, NASA TN D-8430, 8431, 1977.

Kestin, J., "The Effect of Free-stream Turbulence on Heat Transfer Rates," *Advanced Heat Transfer*, Vol. 3, Academic Press, New York, 1966, pp.1-32.

Kestin, J., and Wood, R., "The Influence of Turbulence on Mass Transfer from Cylinders," *Journal Heat Transfer*, Vol. 93, No. 4, 1971, pp. 321-327.

Lowery, G. W., and Vachon, R. I., "The Effect of Turbulence on Heat Transfer from Heated Cylinders," *International Journal Heat Mass Transfer*, Vol. 18, November 1975, pp. 1229-1242.

Lui, X., and Rodi, W., "Surface Pressure and Heat Transfer Measurements in a Trubine Cascade with Unsteady Oncoming Wakes," *Experiments in Fluids*, Vol.17, 1994, pp. 171-178.

Mason, W. H., "Summary of Wind Tunnel Test Facilities,", Virginia Tech, May 1989.

O'Brien, J. E., and VanFossen, Jr., G. J., "The Influence of Jet-Grid Turbulence on Heat Transfer from the Stagnation Region of a Cylinder in Crossflow," *National Heat Transfer Conference*, Denver, Colorado, August, 1985.

Schetz, J. A., Boundary Layer Analysis, Prentice Hall, Englewood Cliffs, New Jersey, 1993.

Sieverding, C. H., and Cicatelli G., "A Review of the Research on Unsteady Turbine Blade Wake Characteristics," AGARD Conference 1995.

Simmons, S. G., Hager, J. M., and Diller, T. E., "Simultaneous Measurements of Time-Resolved Surface Heat Flux and Freestream Turbulence at a Stagnation Point", *ASME Journal of Engineering for Gas Turbines and Power*, Vol. 112, 1990, pp. 375-380.

Simoneau, R. J., and Simon F. F., "Progress Towards Understanding and Predicting Heat Transfer in a Gas Turbine Path," *International Journal Heat and Fluid Flow*, Vol. 14, No. 2, June 1993, pp. 106-128.

Smith, M. C., and Kuethe, A. M., "Effects of Turbulence on Laminar Skin Friction and Heat Transfer," Physics of Fluids, Vol. 9, No. 12, December 1966, pp. 2337-2344.

Suzuki, H. and Suzuki, K., "Heat Transfer and Skin Friction of a Flat Plate Turbulent Boundary Layer Distrubed by a Cylinder," *Trans. JSME*, 55(519), 1989, 3333-3340.

Tan-Atichat, J., Nagib, H. M., and Loerke, R. I., "Interaction of Free-Stream Turbulence with Screens and Grids; A Balance Between Turbulence Scales," *Journal Fluid Mechanics*, Vol. 114, 1982, pp. 501-528.

Taylor and VonKarman, *J. Roy. Aeronaut. Soc.*, 41, 1109, 1937.

Uberoi, M. S., and Wallis, S., "Spectra of Grid Turbulence," The Physics of Fluids, Vol. 12, No. 7, July 1969, pp. 1355-1358.

VanFossen, Jr., G. J., and Simoneau, R. J., "A Study of the Relationship Between Free-stream Turbulence and Stagnation Region Heat Transfer," *Journal of Heat Transfer*, Vol. 109, February 1987, pp. 10-15.

Wesner, A. L., Personal Communication, March 10, 1996, Virginia Tech, Blacksbrug.

Wittig, S., Dullenkopf, K., Schultz, A., and Hesterman R., "Laser-Doppler Studies of the Wake-Effected Flow Field in a Turbine Cascade," ASME Paper No. 86-GT-160.

Wittig, S., Schultz, A., Dullenkopf, K., and Fairbank, J., "Effects of Free-stream Turbulence and Wake Characteristics on Heat Transfer Along a Cooled Gas Turbine Blade," ASME Paper No. 88-GT-179.

Young, C. D., and Han, J. C., "Effect of Jet Grid Turbulence on Turbulenct Boundary Layer Heat Transfer," *ASME Winter Annual Meeting*, Chicago, Illionois, November, 1988.

# Appendix A

## Data Runs

The following appendix contains the data runs for the Leading Edge Survey experiments, Heat Flux measurements, and Kulite measurements. The results for the Leading Edge experiments are presented first, followed by the heat flux results, and finally the data runs for the Kulite measurements.

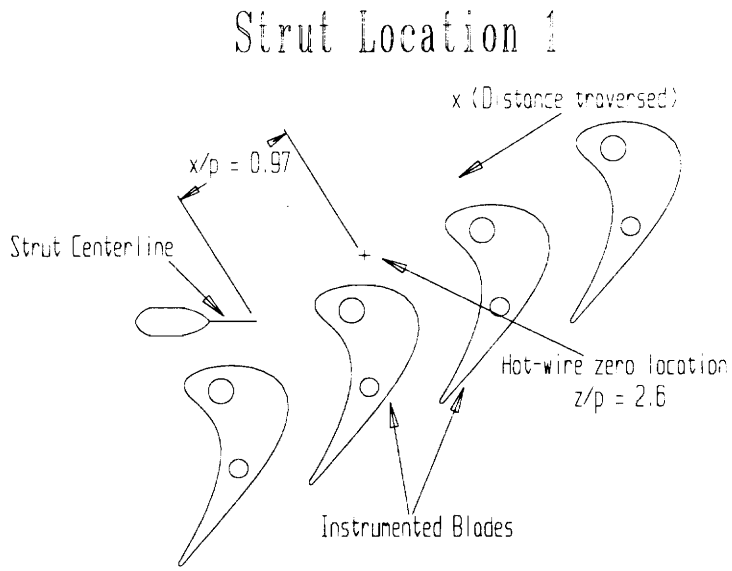


Figure A1 Position of Strut Relative to Hot-Wire Zero Location (z/p=1.78)

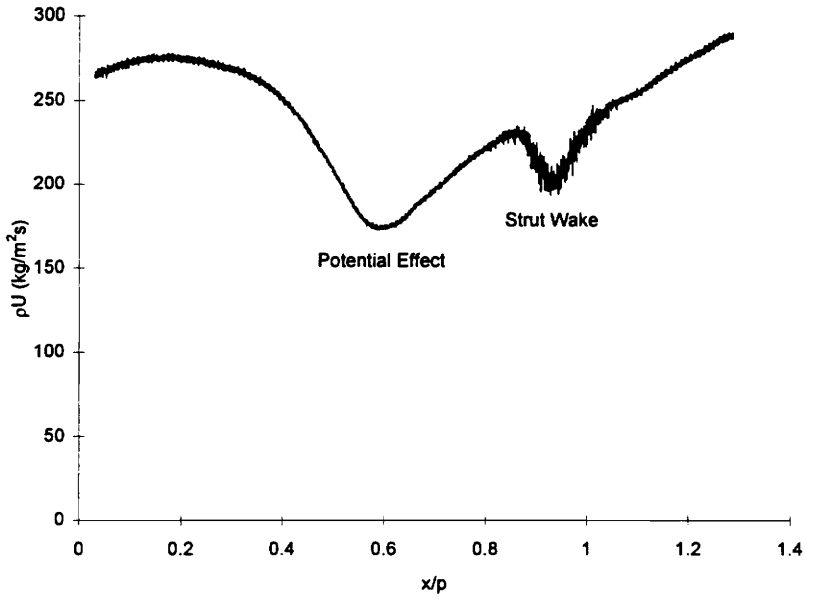


Figure A2 Profile of Inlet Flow into Cascade with strut at z/p=1.78

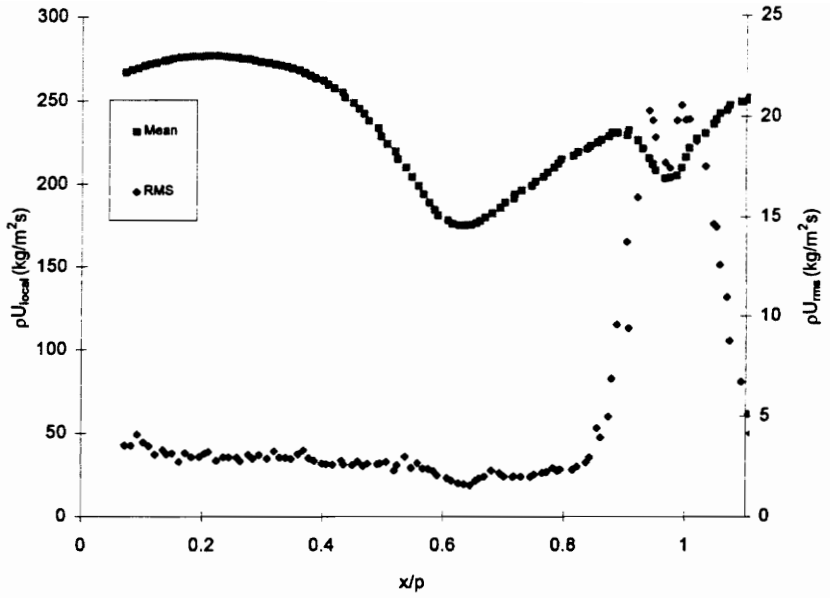


Figure A3. Mean and RMS Results of Hot-Wire with Strut at z/p=1.78

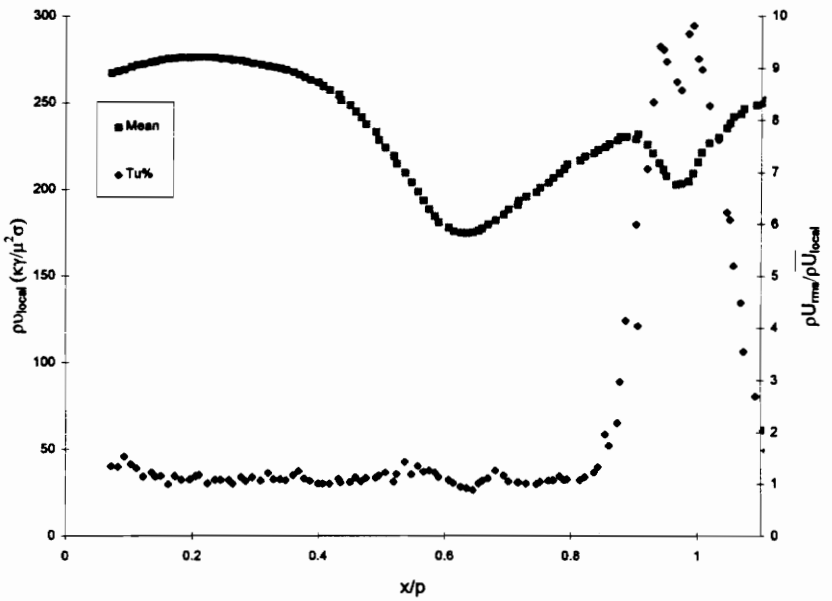


Figure A4. Mean and Turbulence Intensity Results of Hot-Wire with Strut at z/p=1.78

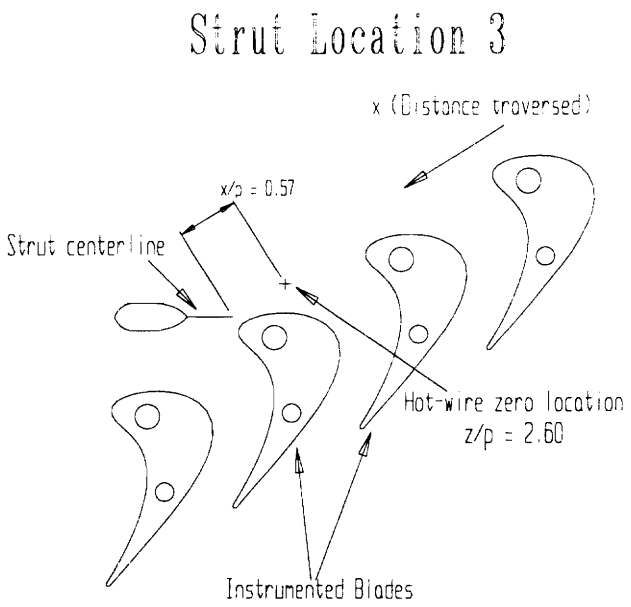


Figure A5. Position of Strut Relative to Hot-Wire Zero Location (z/p=2.19)

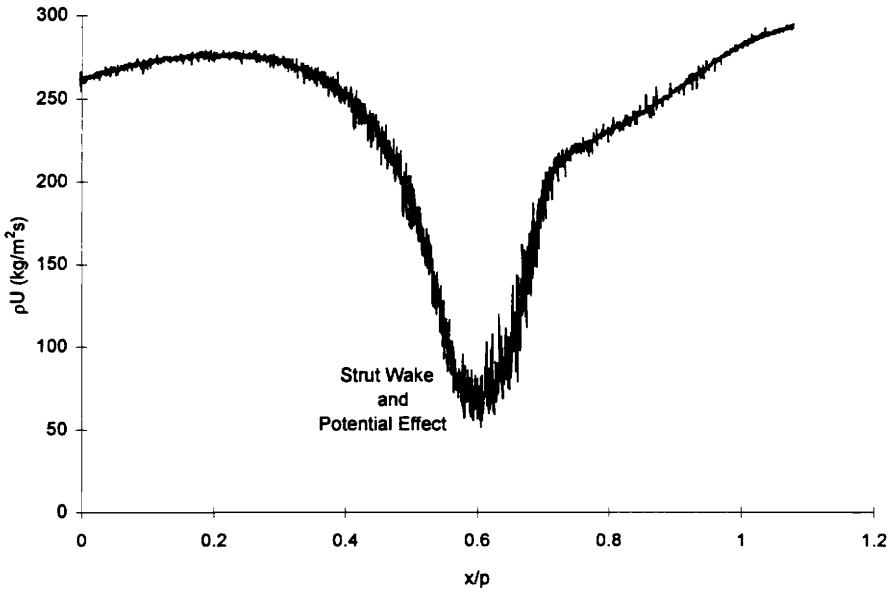


Figure A6. Profile of Inlet Flow into Cascade with strut at z/p=2.19

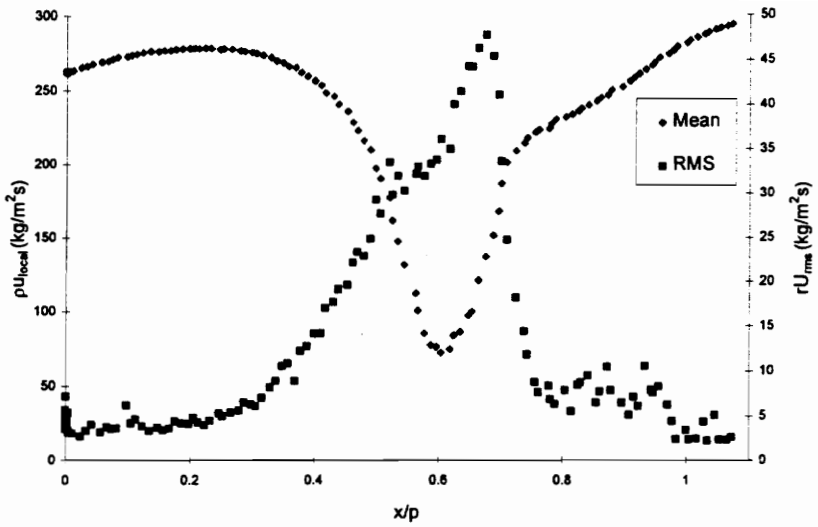


Figure A7. Mean and RMS Results of Hot-Wire with Strut at z/p=2.19

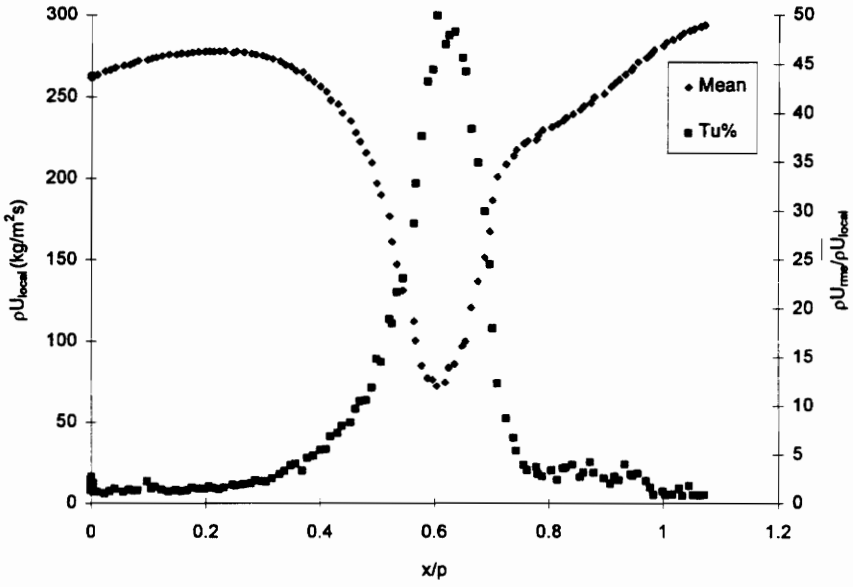


Figure A8. Mean and Turbulence Intensity Results of Hot-Wire with Strut at z/p=2.19

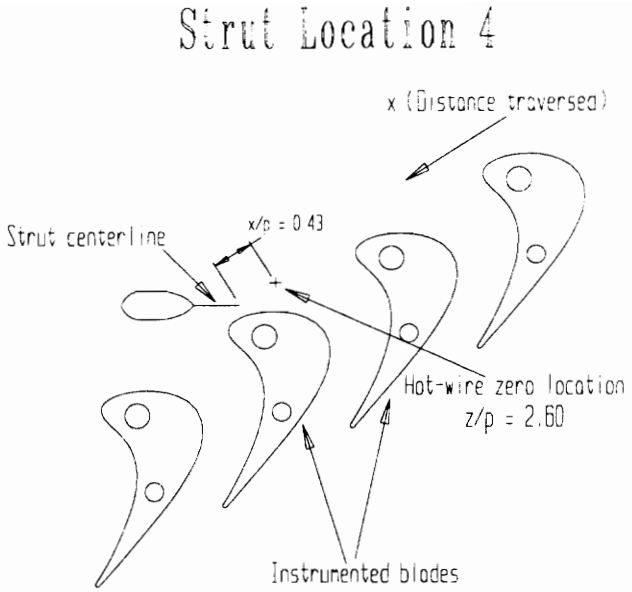


Figure A9. Position of Strut Relative to Hot-Wire Zero Location (z/p=2.32)

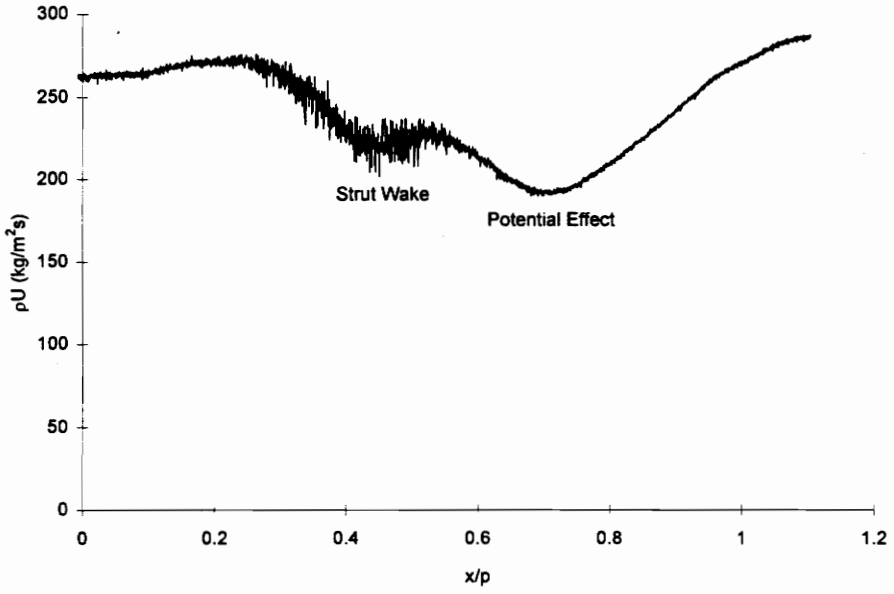


Figure A10. Profile of Inlet Flow into Cascade with strut at z/p=2.32

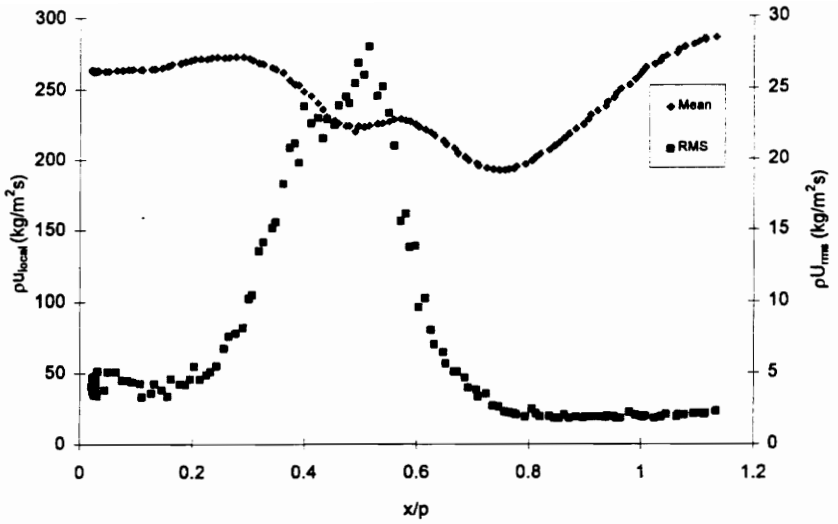


Figure A11. Mean and RMS Results of Hot-Wire with Strut at z/p=2.32

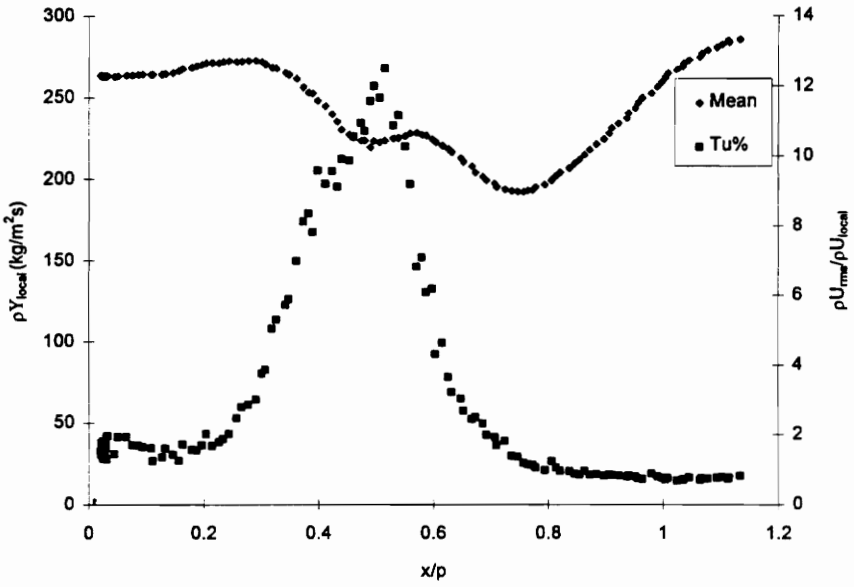


Figure A12. Mean and Turbulence Intensity Results of Hot-Wire with Strut at z/p=2.32

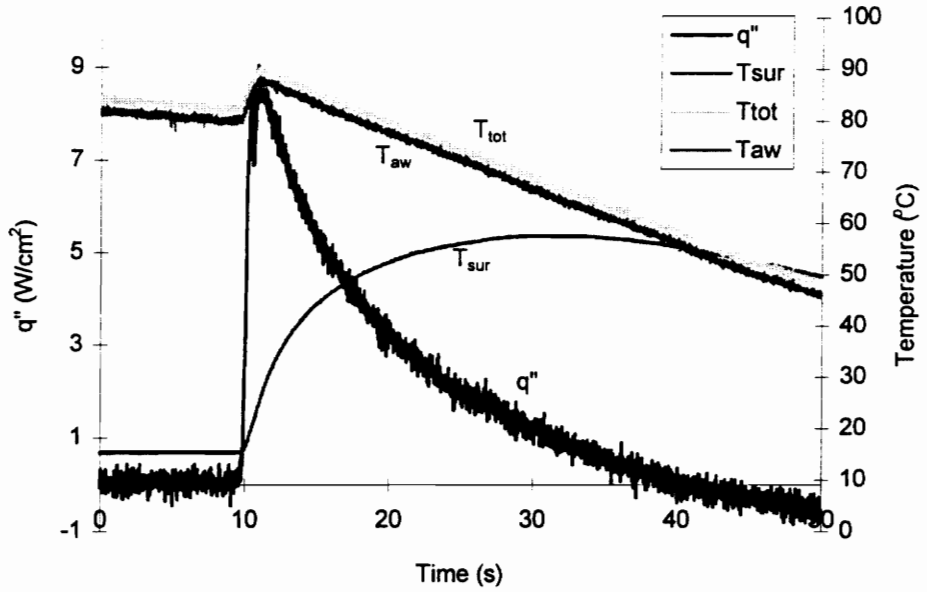


Figure A13. Example of Run For HFM-6 Gage 1 - No Strut - Run #2

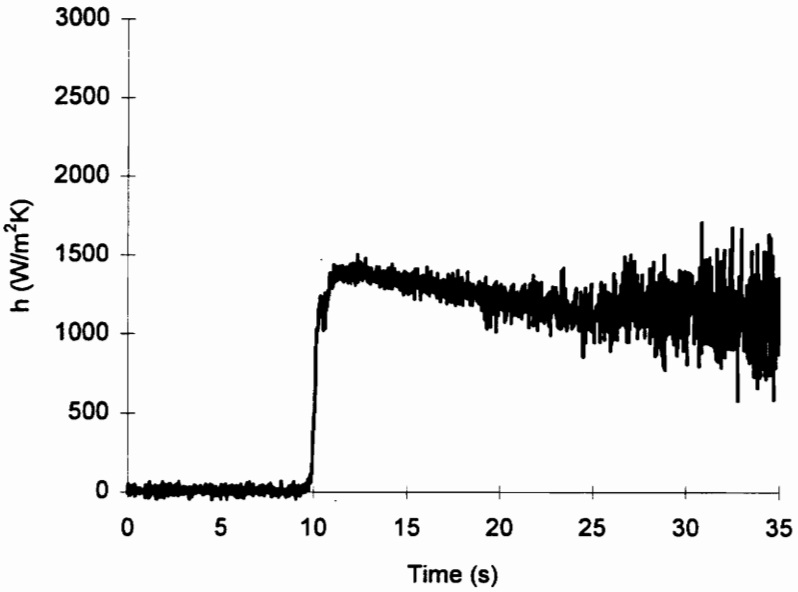


Figure A14. HTC Calculated From HFM-6 Gage 1 - No Strut - Run #2

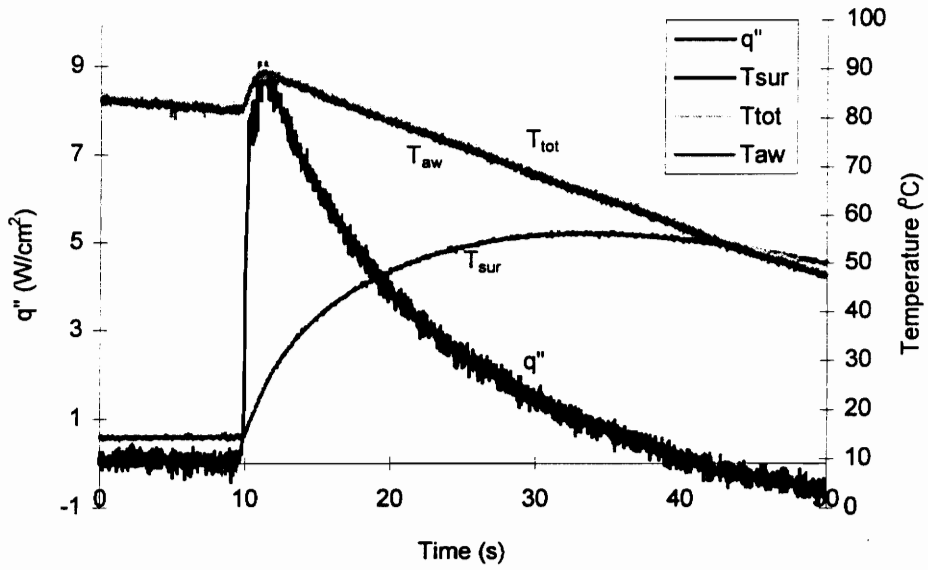


Figure A15. Example of Run For HFM-6 Gage 2 - No Strut - Run #2

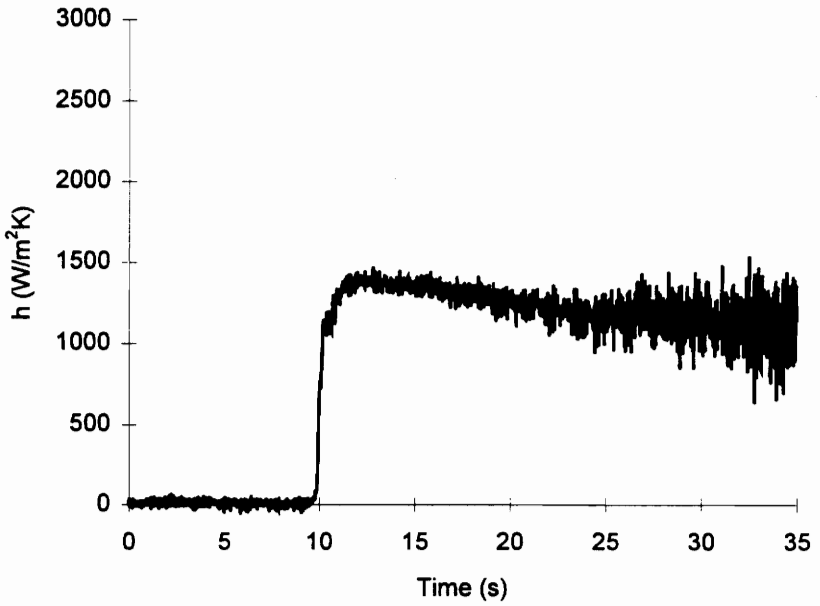


Figure A16. HTC Calculated From HFM-6 Gage 2 - No Strut - Run #2

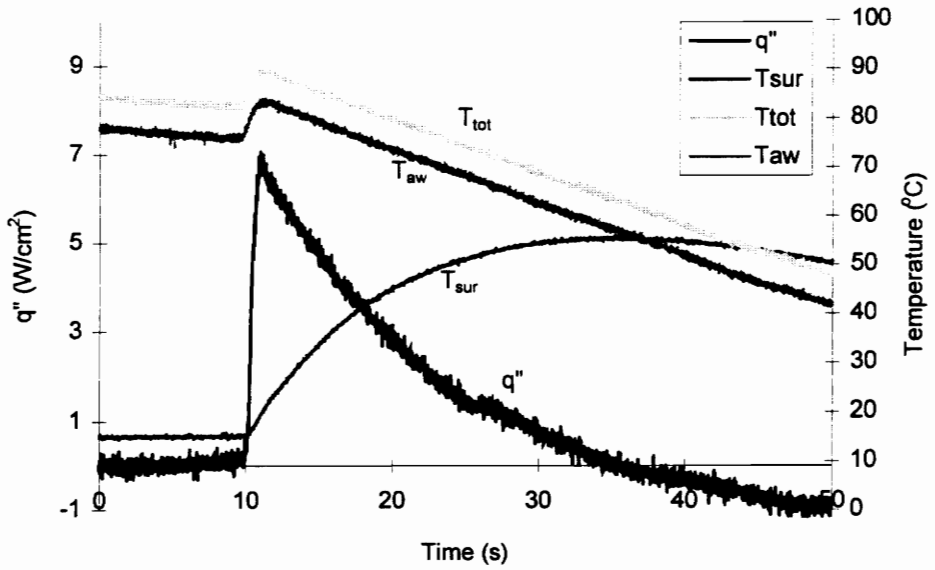


Figure A17. Example of Run For HFM-6 Gage 3 - No Strut - Run #2

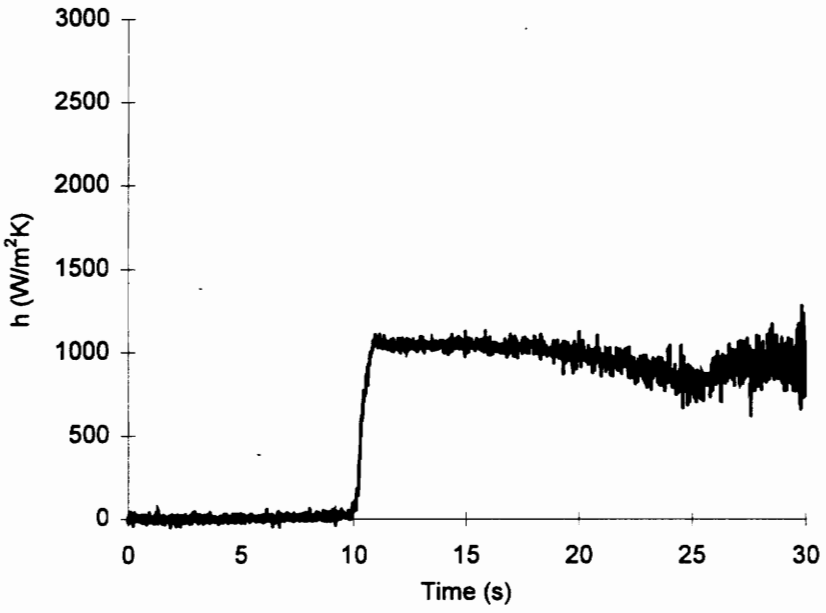


Figure A18. HTC Calculated From HFM-6 Gage 3 - No Strut - Run #2

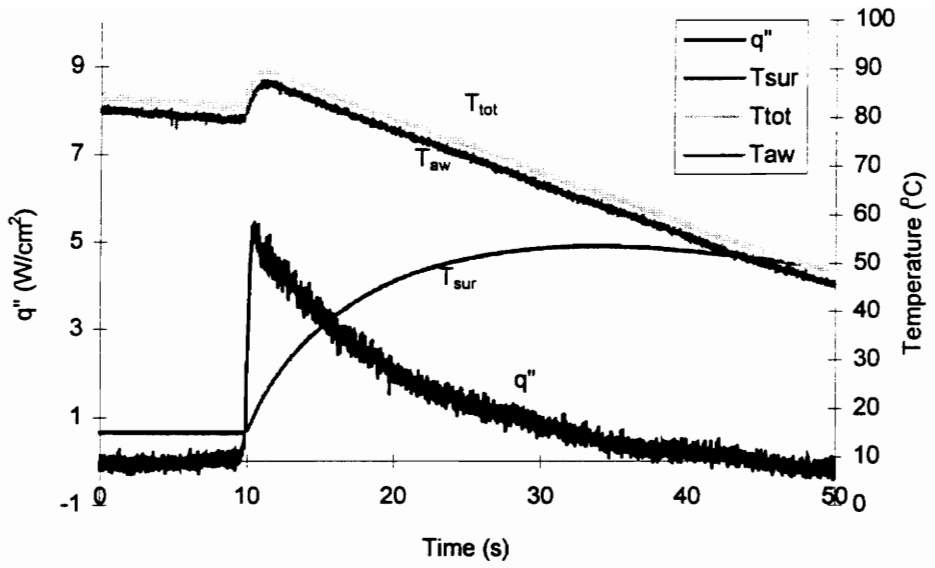


Figure A19. Example of Run For HFM-6 Gage 4 - No Strut - Run #2

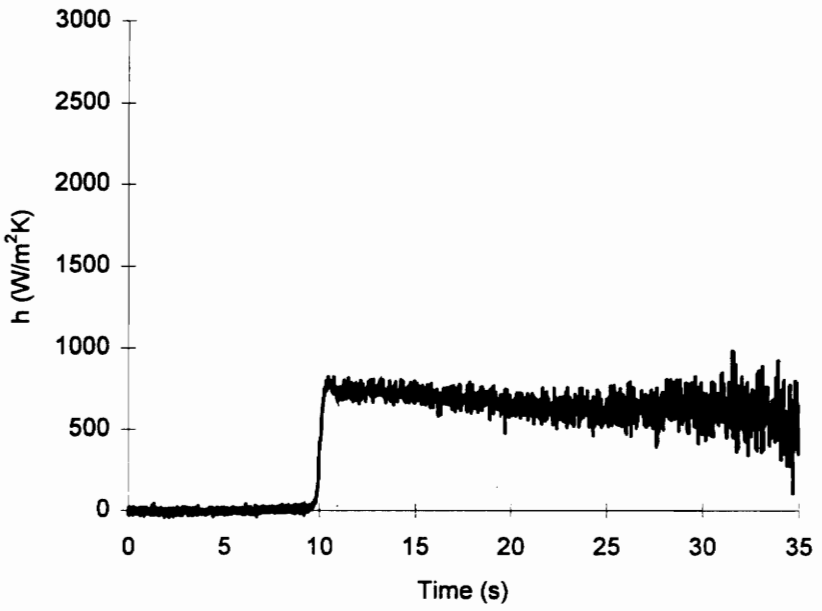


Figure A20. HTC Calculated From HFM-6 Gage 4 - No Strut - Run #2

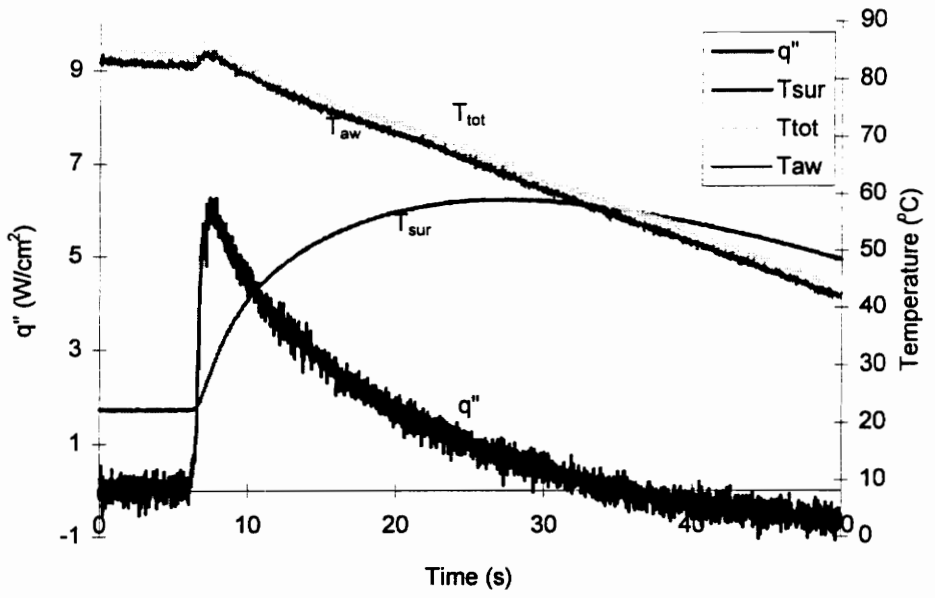


Figure A21. Example of Run For HFM-6 Gage 1 - Strut at Location 2 - Run #2

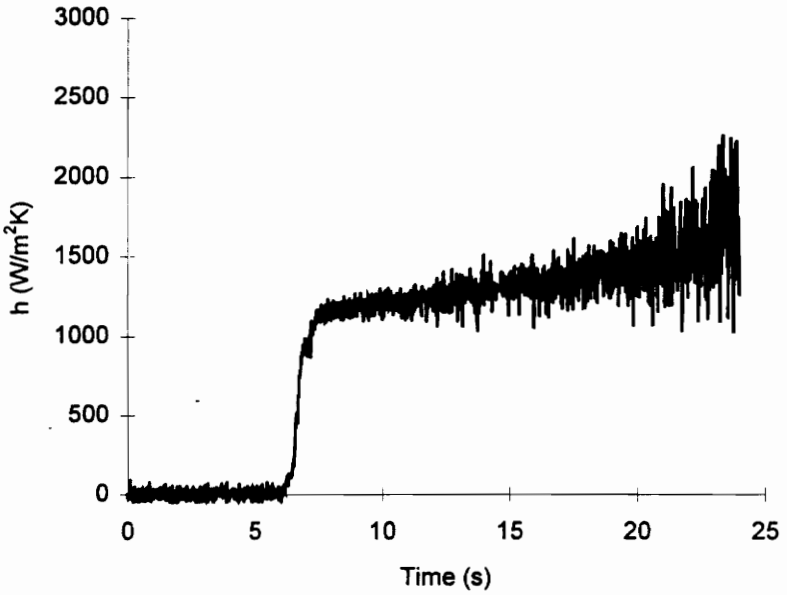


Figure A22. HTC Calculated From HFM-6 Gage 1 - Strut at Location 2 - Run #2

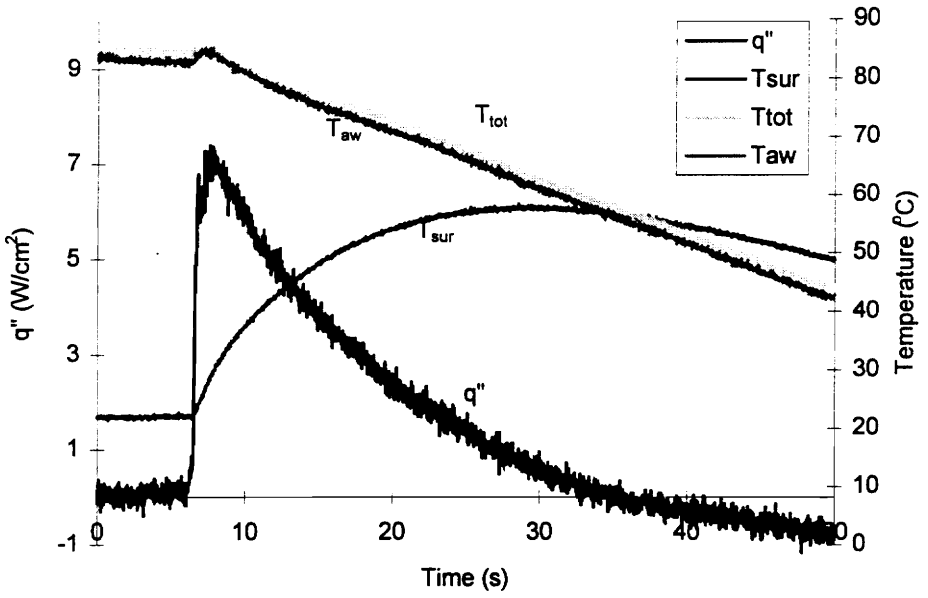


Figure A23. Example of Run For HFM-6 Gage 2 - Strut at Location 2 - Run #2

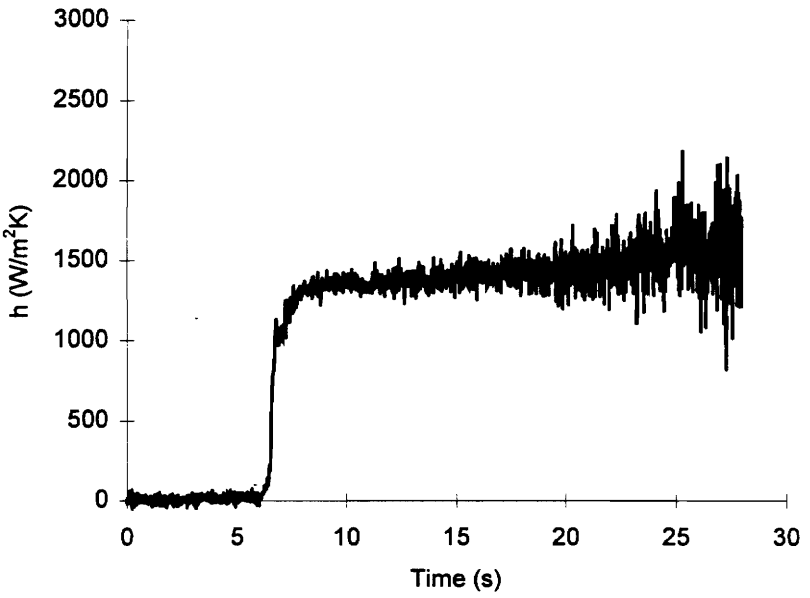


Figure A24. HTC Calculated From HFM-6 Gage 2 - Strut at Location 2 - Run #2

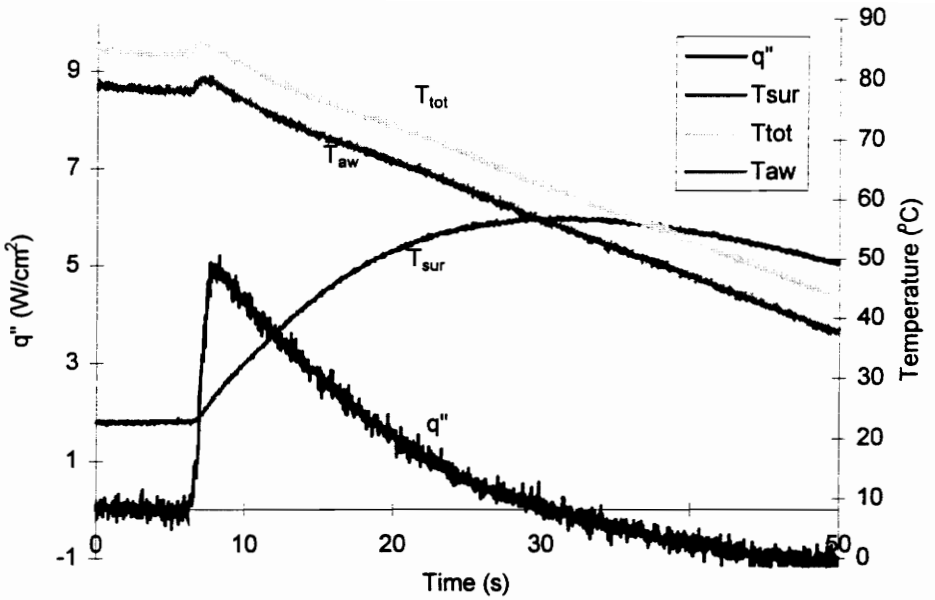


Figure A25. Example of Run For HFM-6 Gage 3 - Strut at Location 2 - Run #2

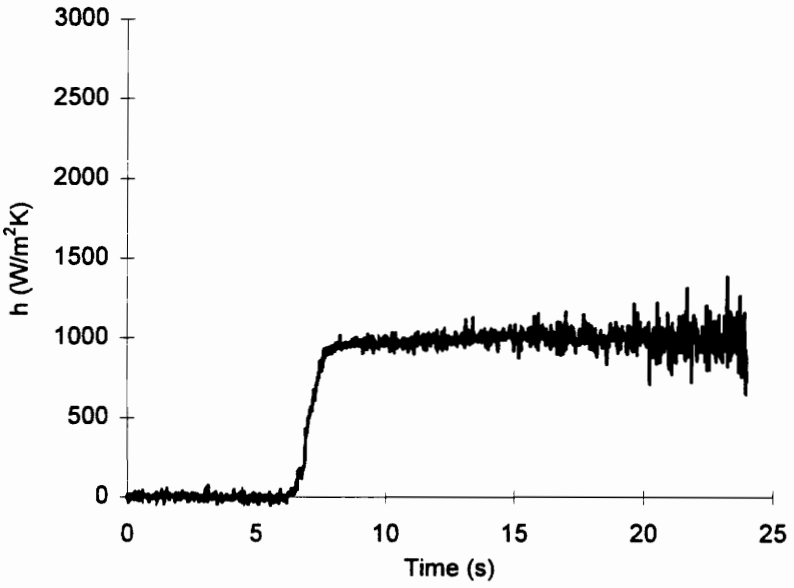


Figure A26. HTC Calculated From HFM-6 Gage 3 - Strut at Location 2 - Run #2

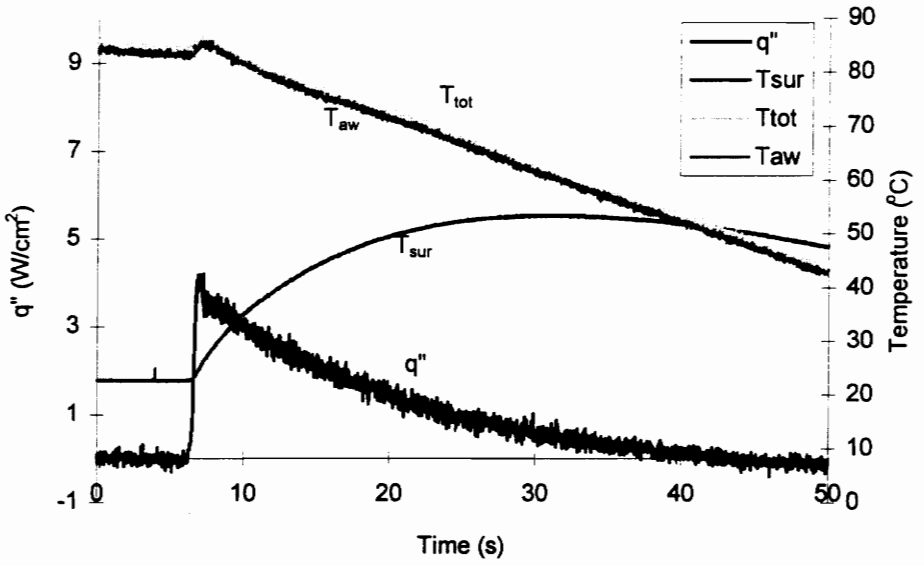


Figure A27. Example of Run For HFM-6 Gage 4 - Strut at Location 2 - Run #2

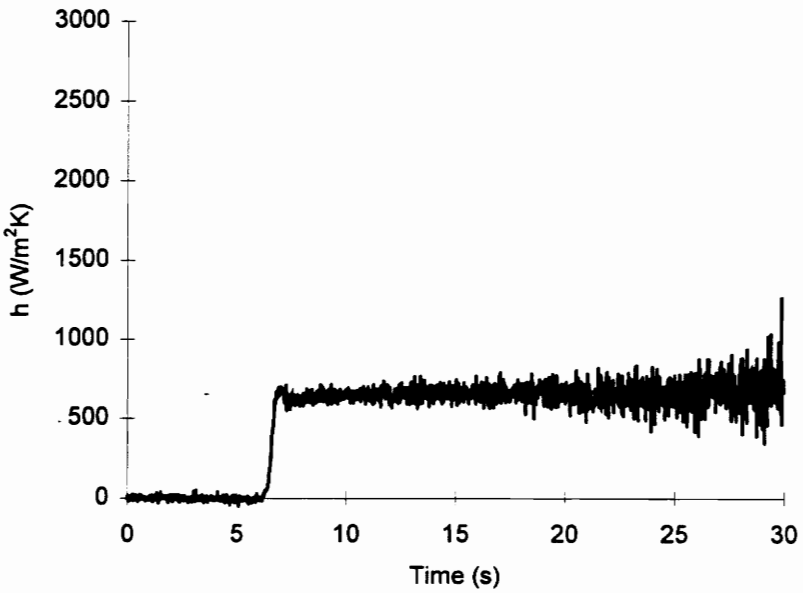


Figure A28. HTC Calculated From HFM-6 Gage 4 - Strut at Location 2 - Run #2

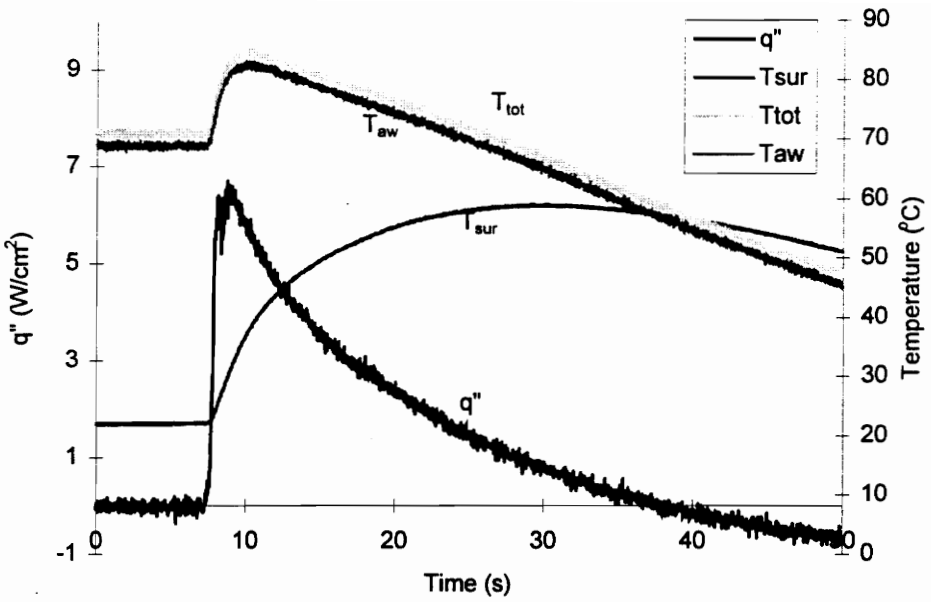


Figure A29. Example of Run For HFM-6 Gage 1 - Strut at Location 1 - Run #1

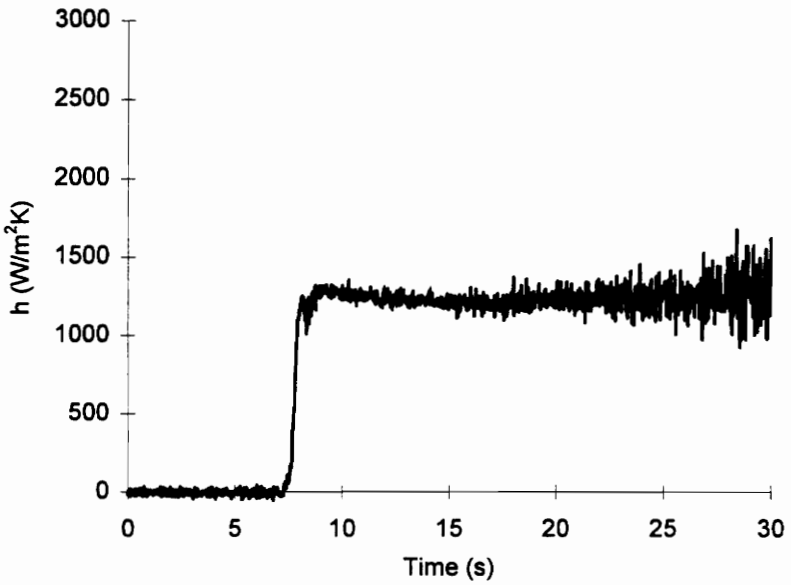


Figure A30. HTC Calculated From HFM-6 Gage 1 - Strut at Location 1 - Run #1

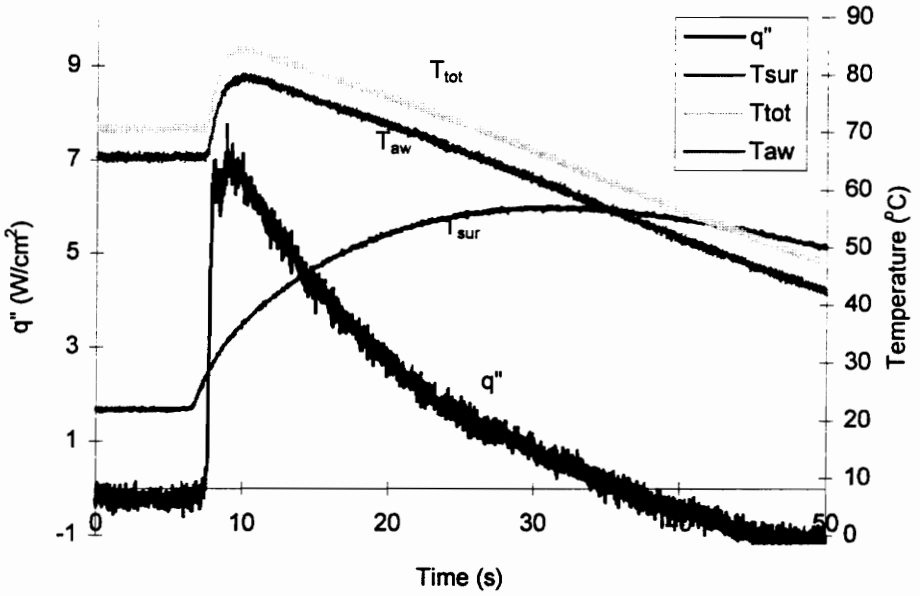


Figure A31. Example of Run For HFM-6 Gage 2 - Strut at Location 1 - Run #1

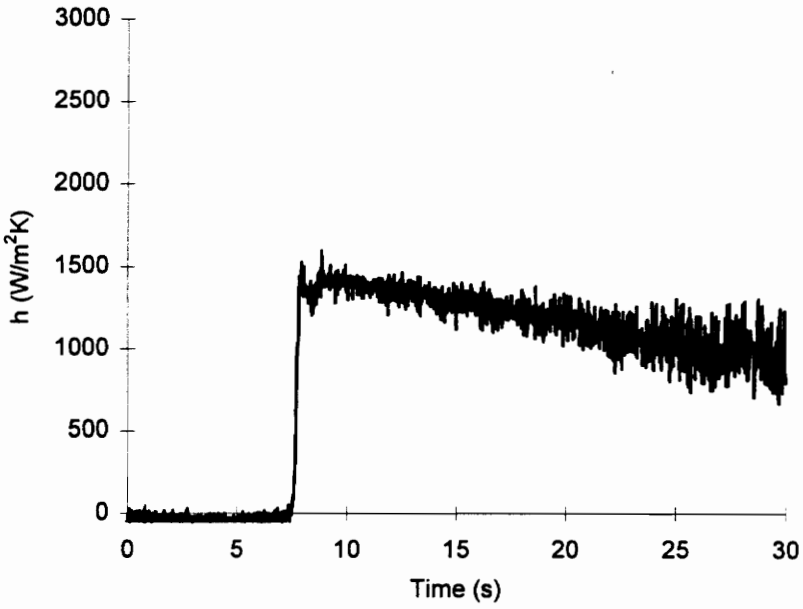


Figure A32. HTC Calculated From HFM-6 Gage 2 - Strut at Location 1 - Run #1

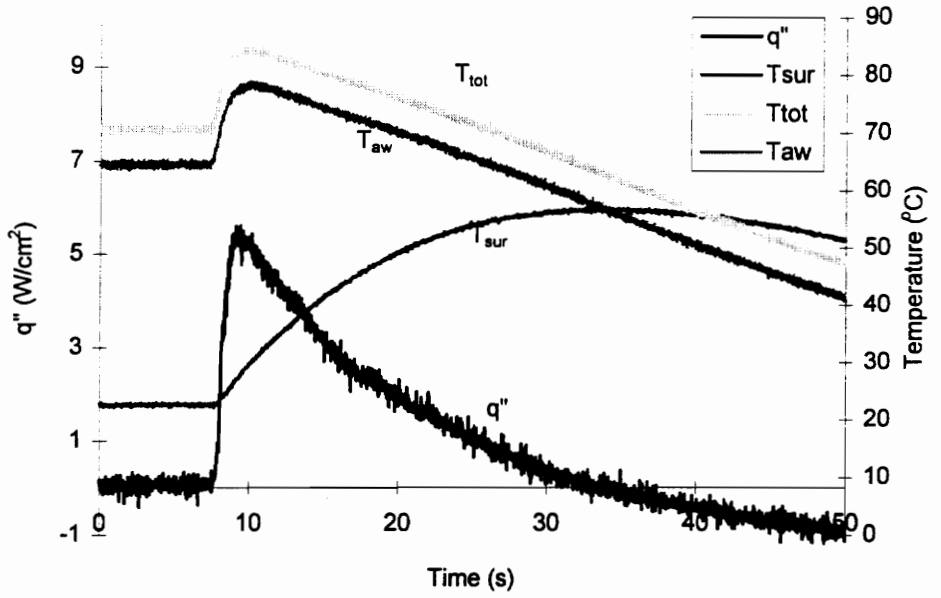


Figure A33. Example of Run For HFM-6 Gage 3 - Strut at Location 1 - Run #1

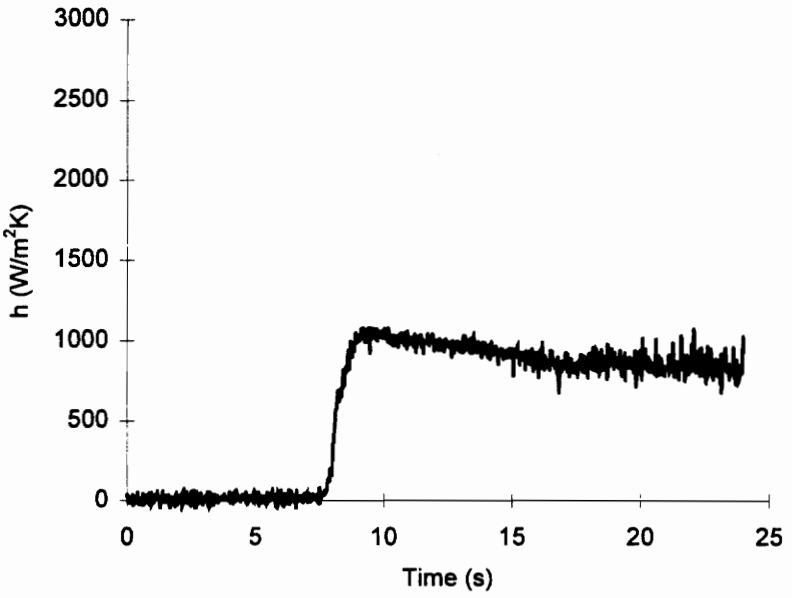


Figure A34. HTC Calculated From HFM-6 Gage 3 - Strut at Location 1 - Run #1

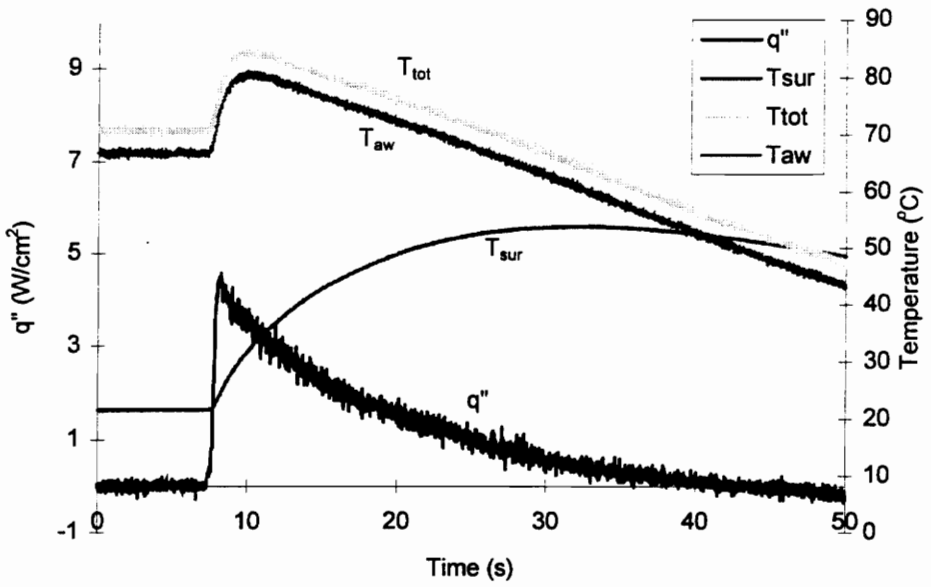


Figure A35. Example of Run For HFM-6 Gage 4 - Strut at Location 1 - Run #1

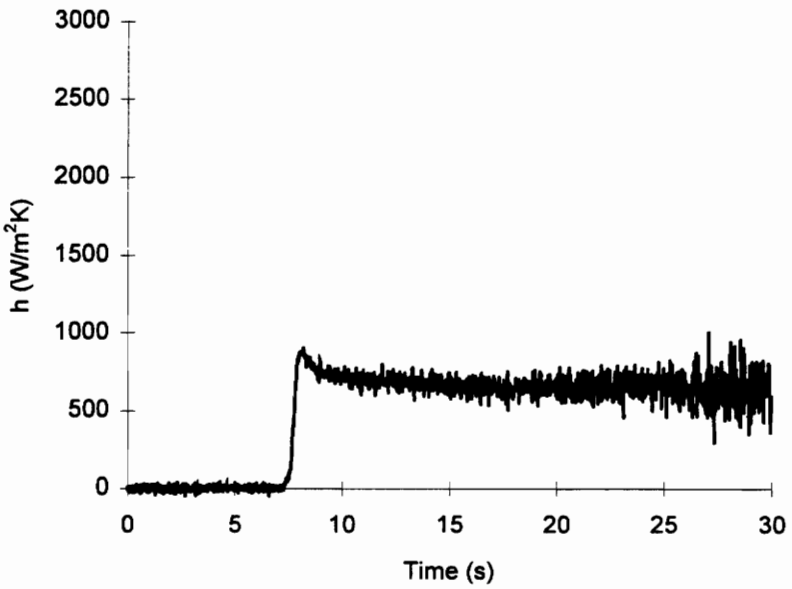


Figure A36. HTC Calculated From HFM-6 Gage 4 - Strut at Location 1 - Run #1

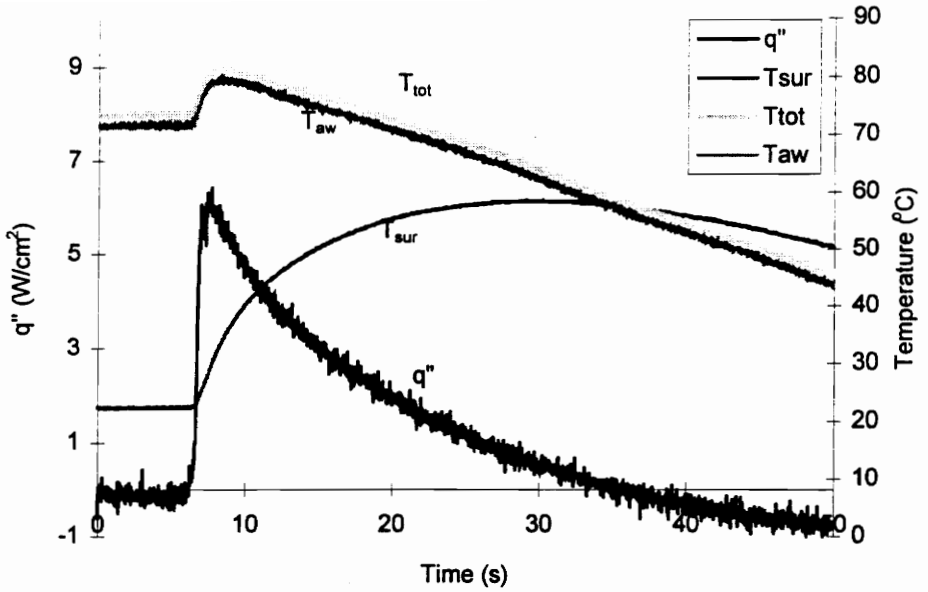


Figure A37. Example of Run For HFM-6 Gage 1 - Strut at Location 1 - Run #2

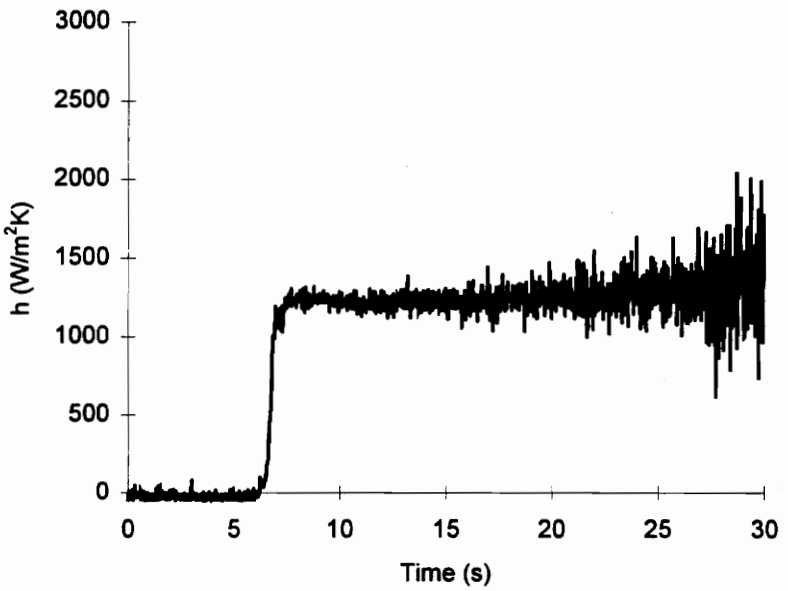


Figure A38. HTC Calculated From HFM-6 Gage 1 - Strut at Location 1 - Run #2

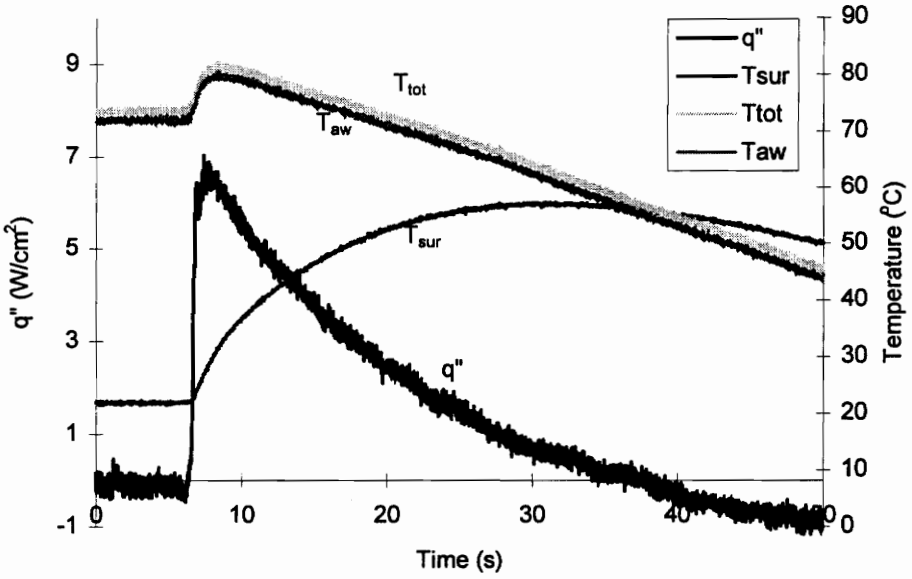


Figure A39. Example of Run For HFM-6 Gage 2 - Strut at Location 1 - Run #2

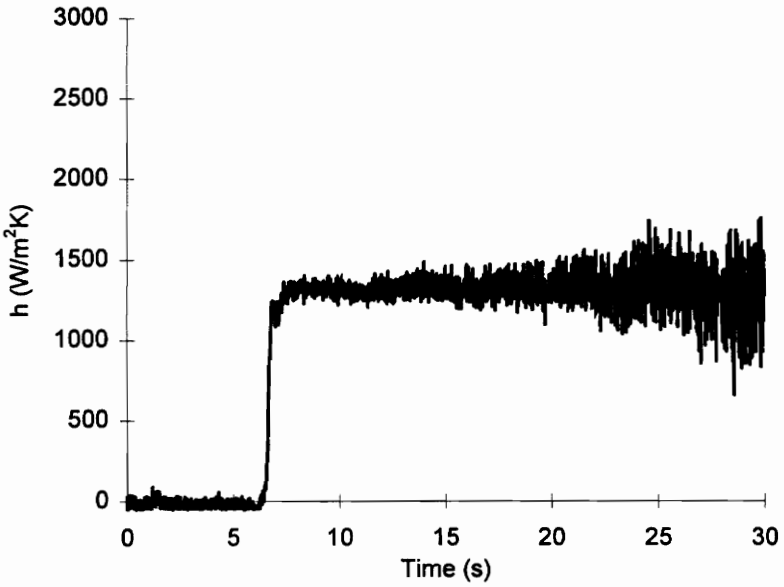


Figure A40. HTC Calculated From HFM-6 Gage 2 - Strut at Location 1 - Run #2

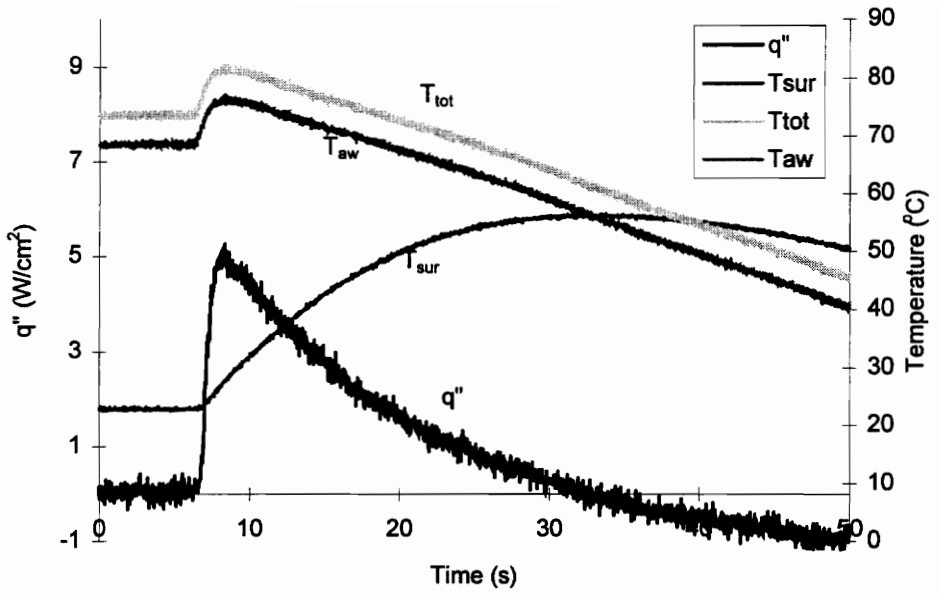


Figure A41. Example of Run For HFM-6 Gage 3 - Strut at Location 1 - Run #2

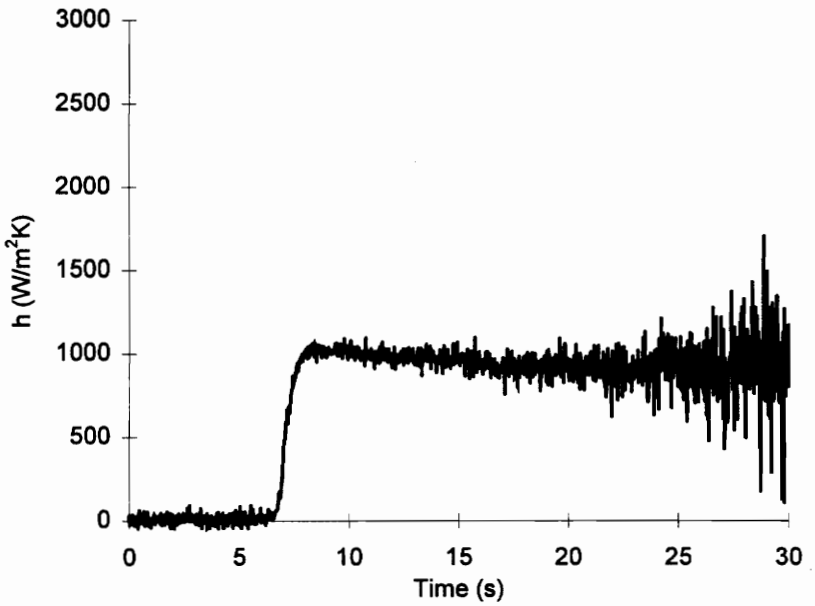


Figure A42. HTC Calculated From HFM-6 Gage 3 - Strut at Location 1 - Run #2

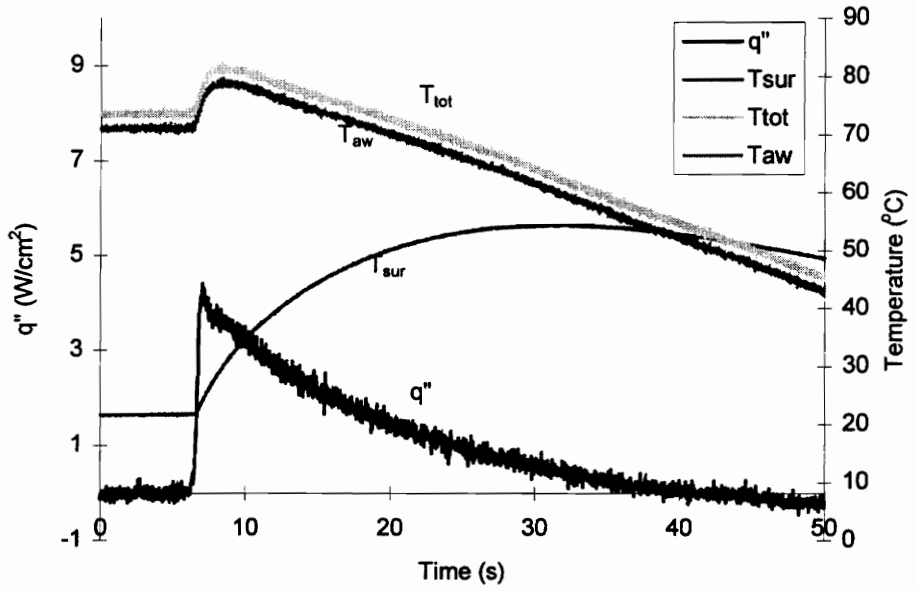


Figure A43. Example of Run For HFM-6 Gage 4 - Strut at Location 1 - Run #2

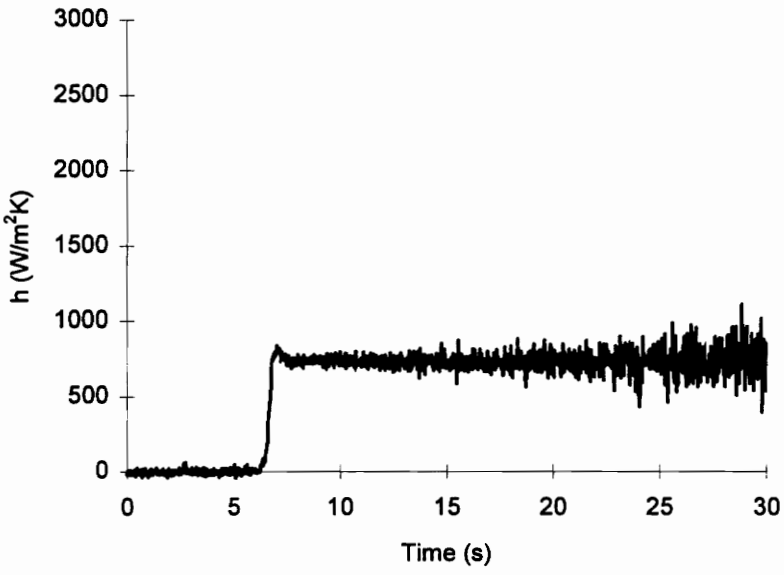


Figure A44. HTC Calculated From HFM-6 Gage 4 - Strut at Location 1 - Run #2

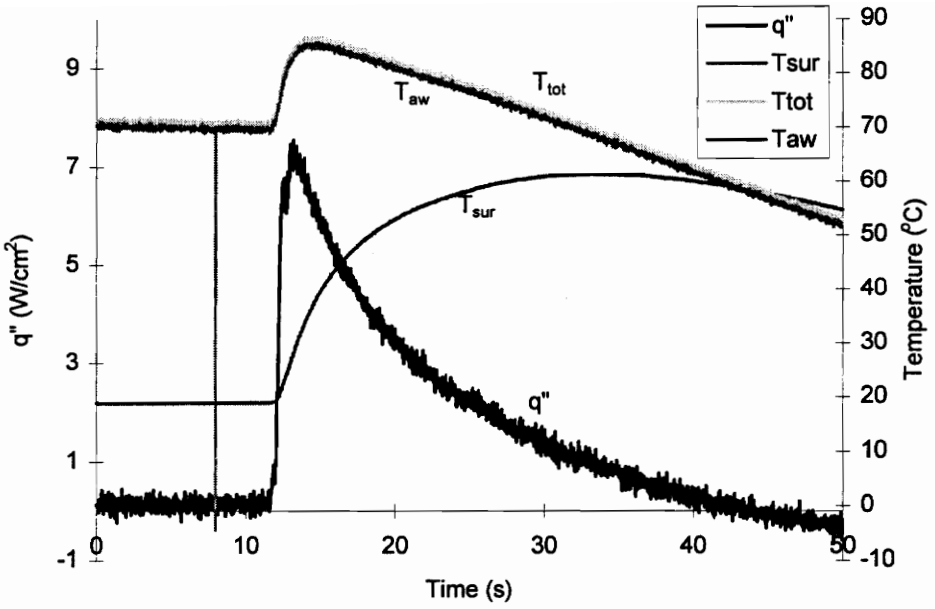


Figure A45. Example of Run For HFM-6 Gage 1 - Strut at Location 3- Run #1

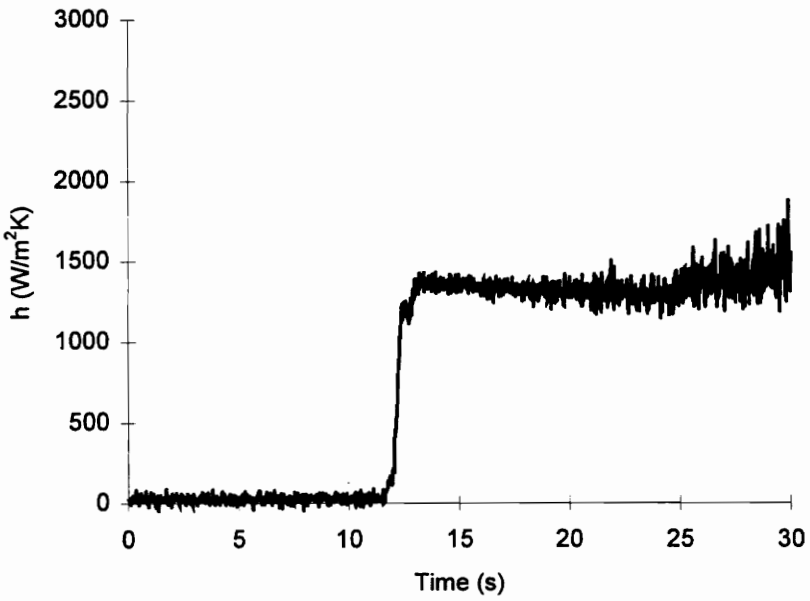


Figure A46. HTC Calculated From HFM-6 Gage 1 - Strut at Location 3 - Run #1

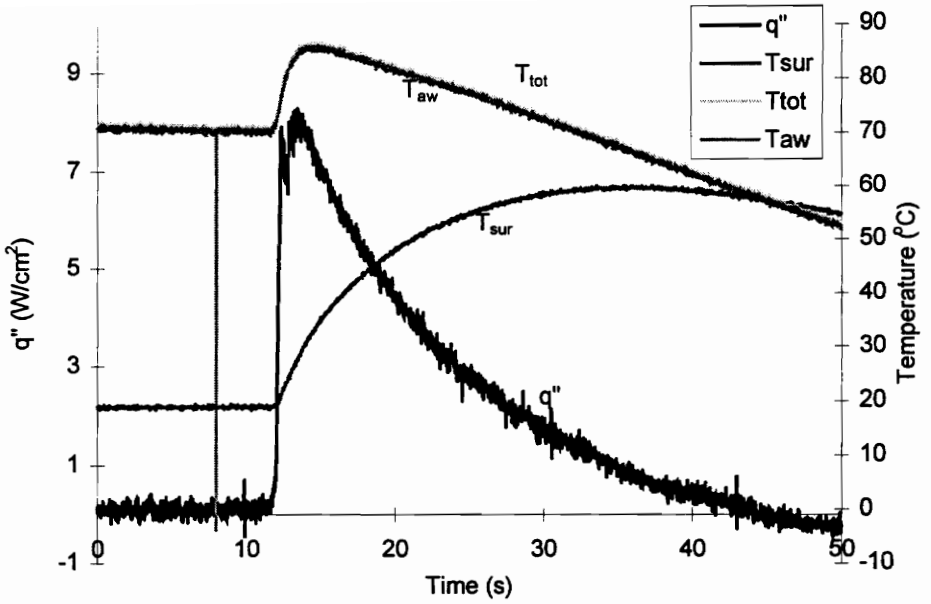


Figure A47. Example of Run For HFM-6 Gage 2 - Strut at Location 3- Run #1

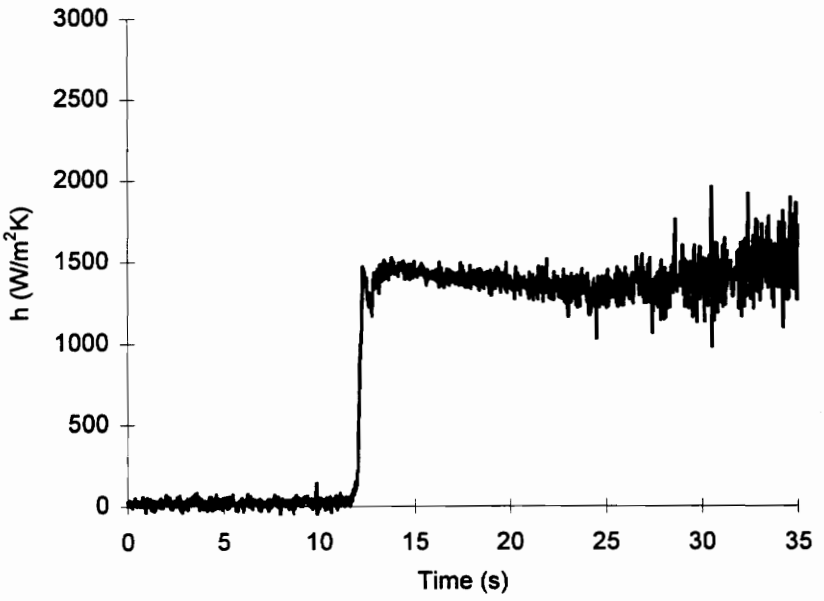


Figure A48. HTC Calculated From HFM-6 Gage 2 - Strut at Location 3 - Run #1

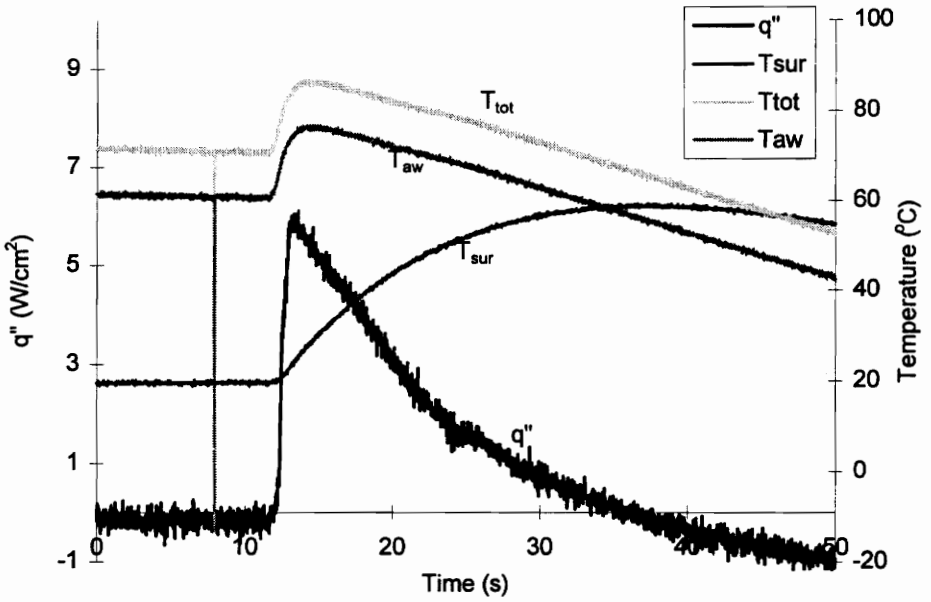


Figure A49. Example of Run For HFM-6 Gage 3 - Strut at Location 3- Run #1

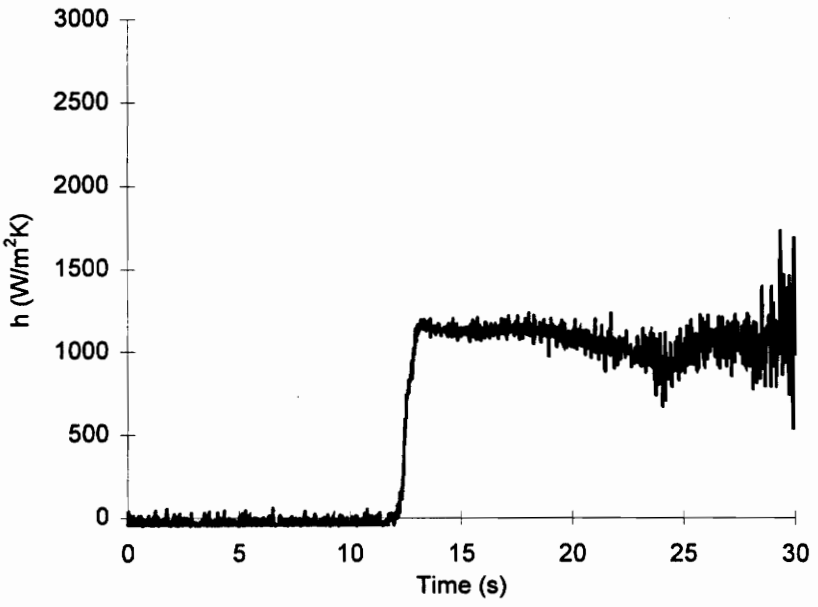


Figure A50. HTC Calculated From HFM-6 Gage 3 - Strut at Location 3 - Run #1

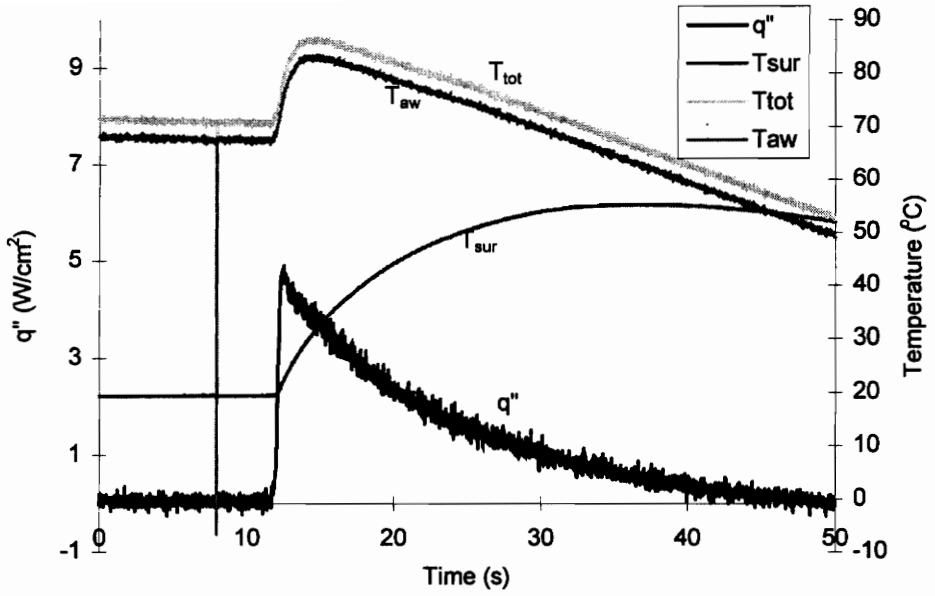


Figure A51. Example of Run For HFM-6 Gage 4 - Strut at Location 3- Run #1

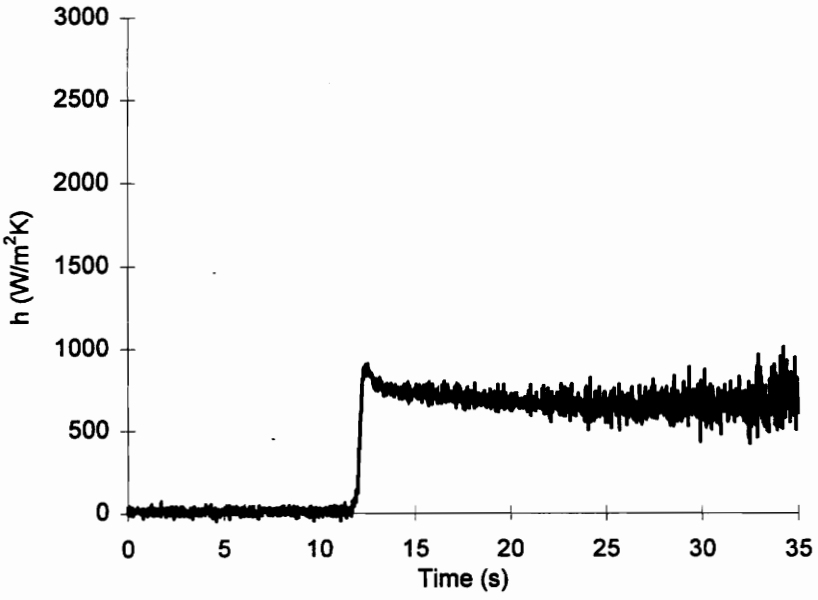


Figure A52. HTC Calculated From HFM-6 Gage 4 - Strut at Location 3 - Run #1

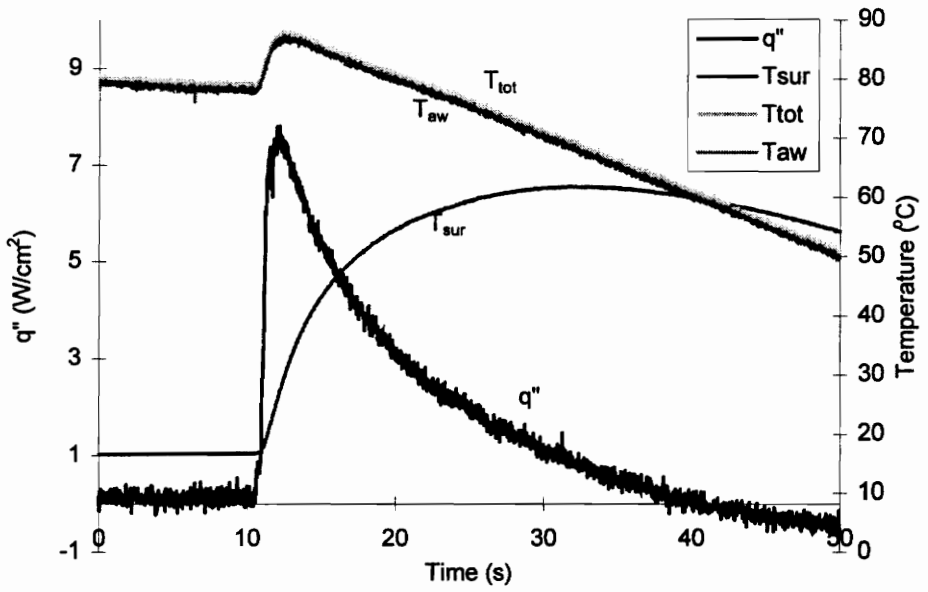


Figure A53. Example of Run For HFM-6 Gage 1 - Strut at Location 3- Run #2

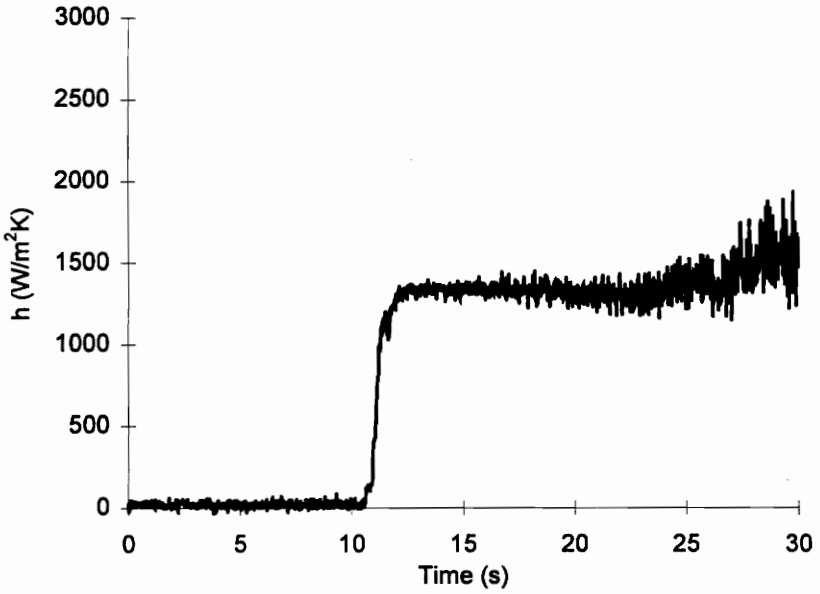


Figure A54. HTC Calculated From HFM-6 Gage 1 - Strut at Location 3 - Run #2

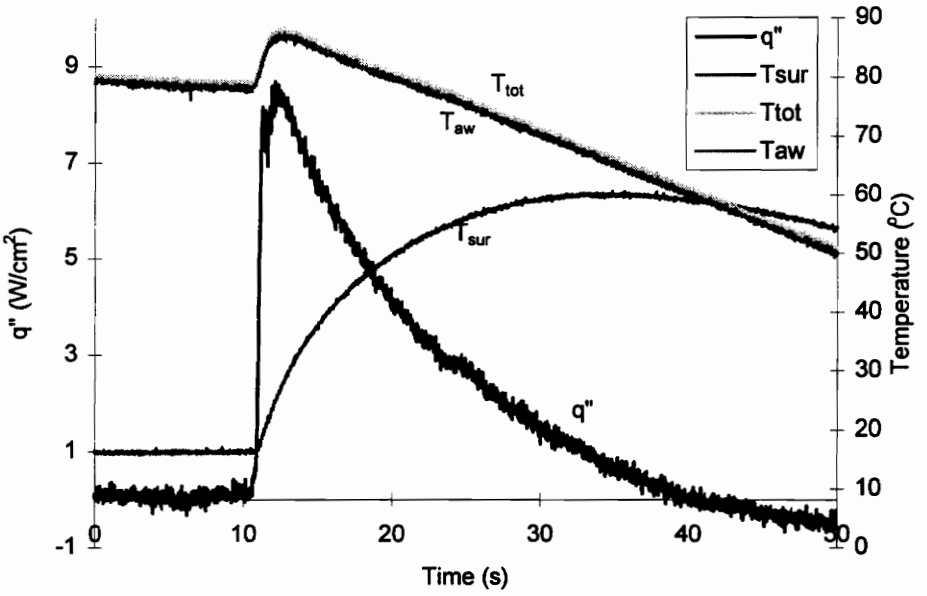


Figure A55. Example of Run For HFM-6 Gage 2 - Strut at Location 3- Run #2

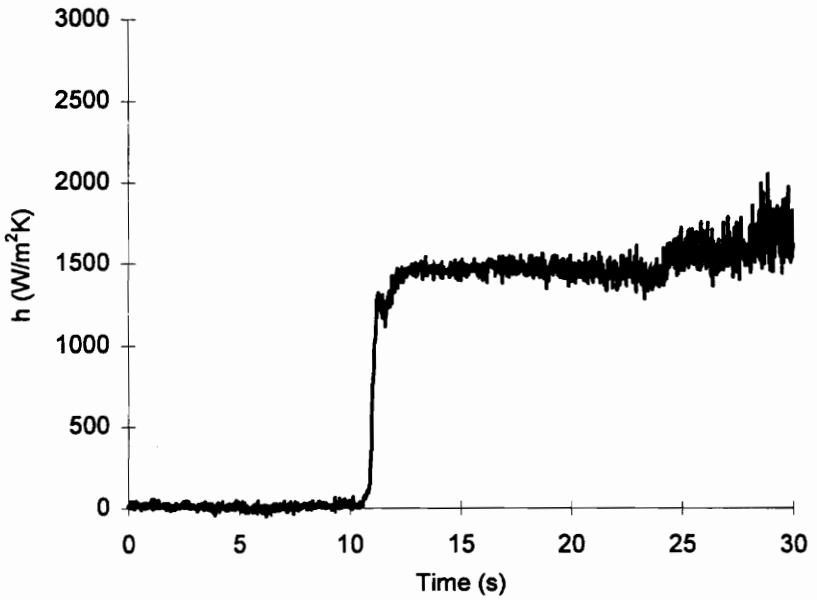


Figure A56. HTC Calculated From HFM-6 Gage 2 - Strut at Location 3 - Run #2

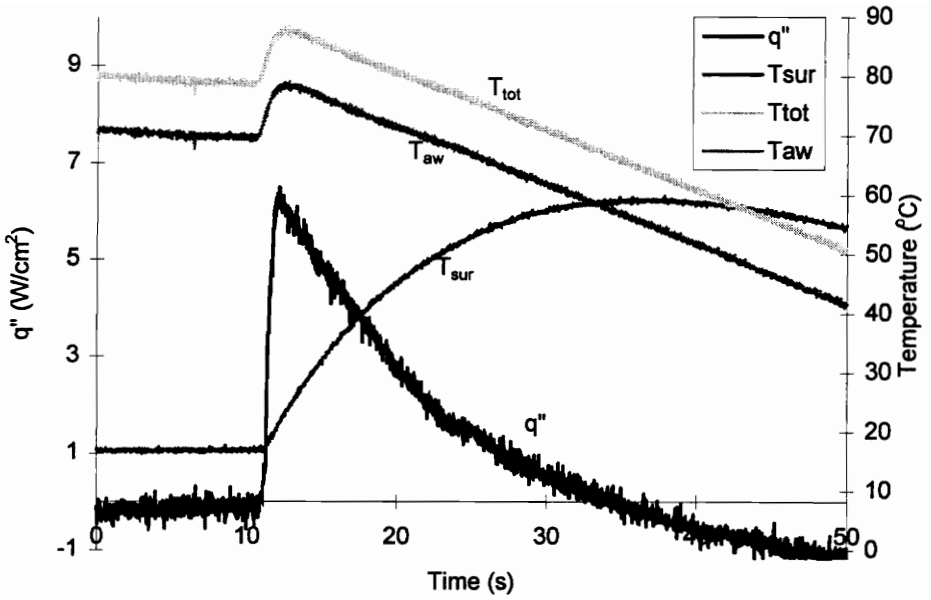


Figure A57 Example of Run For HFM-6 Gage 3 - Strut at Location 3- Run #2

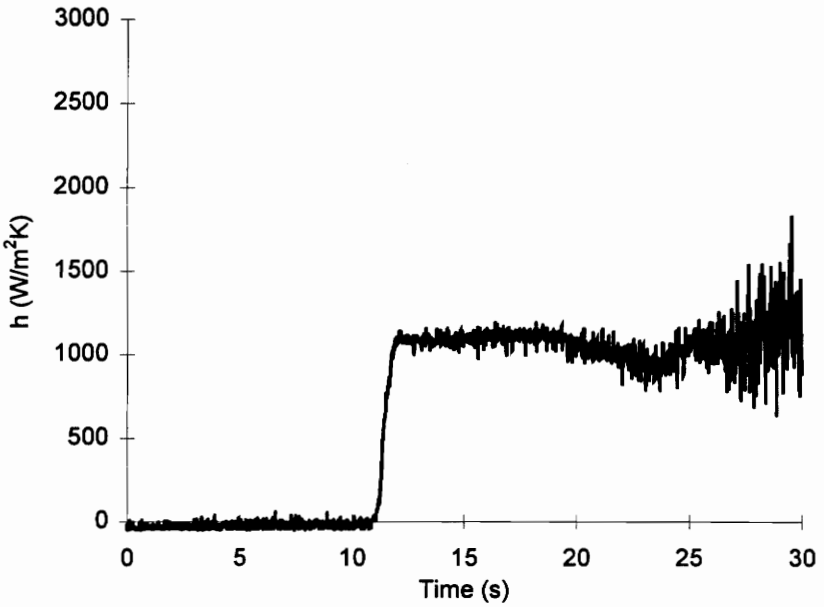


Figure A58. HTC Calculated From HFM-6 Gage 3 - Strut at Location 3 - Run #2

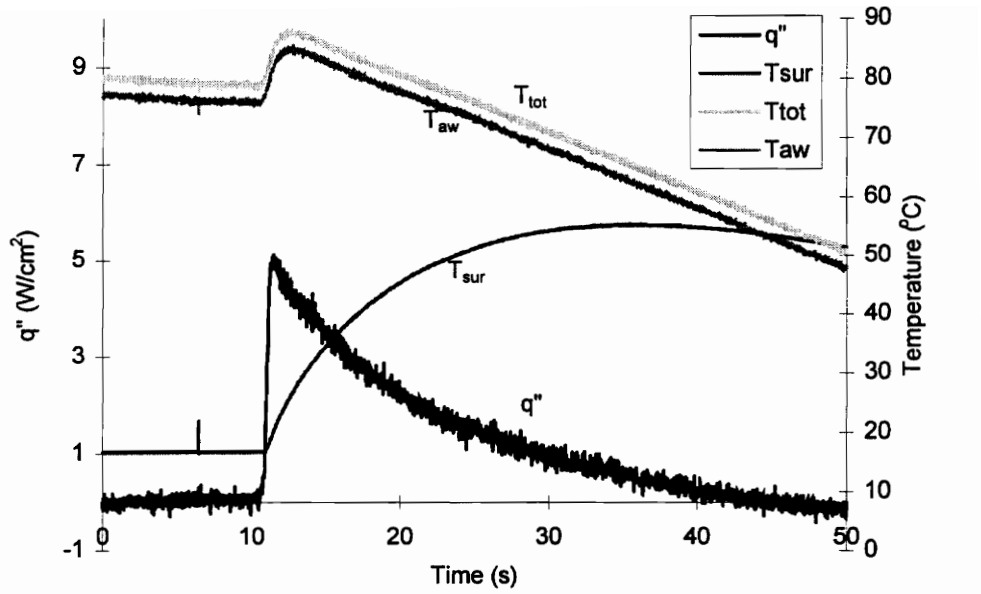


Figure A59. Example of Run For HFM-6 Gage 4 - Strut at Location 3- Run #2

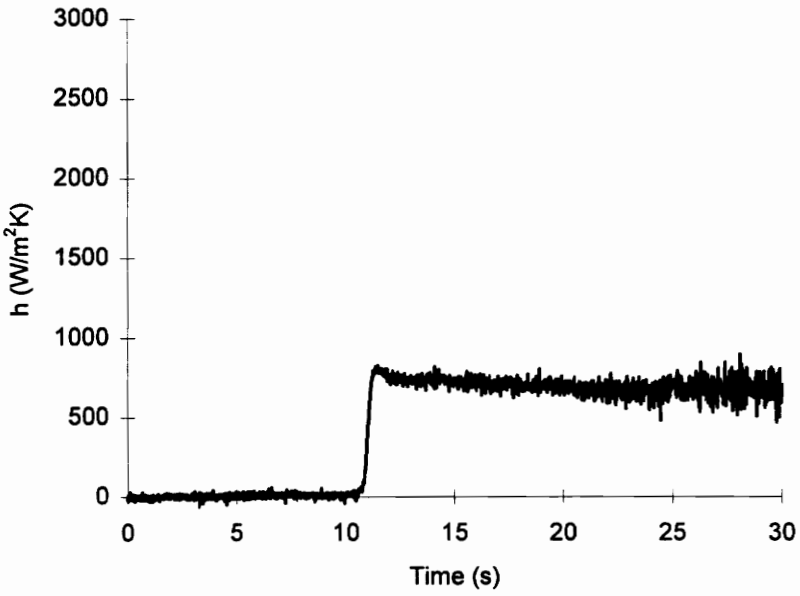


Figure A60. HTC Calculated From HFM-6 Gage 4 - Strut at Location 3 - Run #2

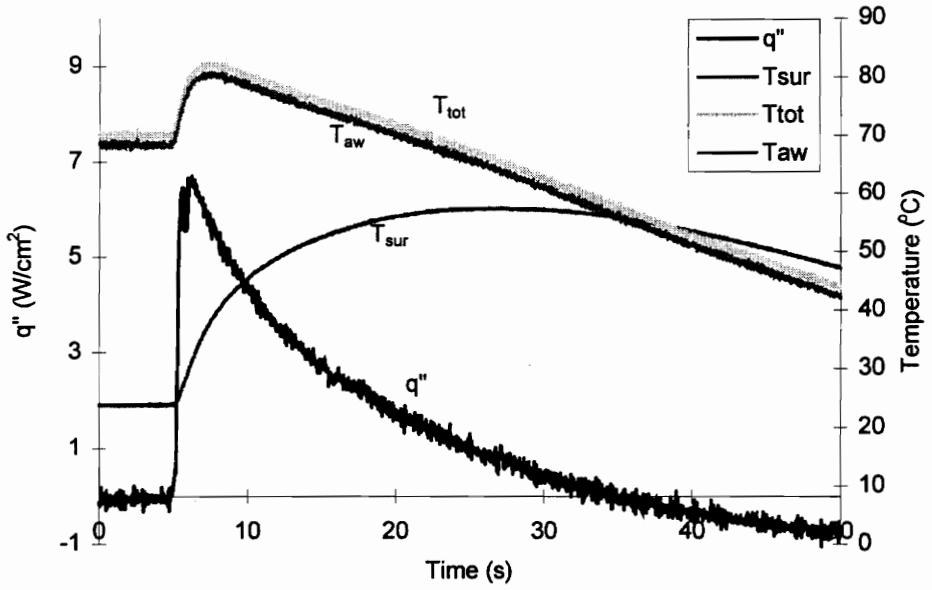


Figure A61. Example of Run For HFM-6 Gage 1 - Strut at Location 5 - Run #1

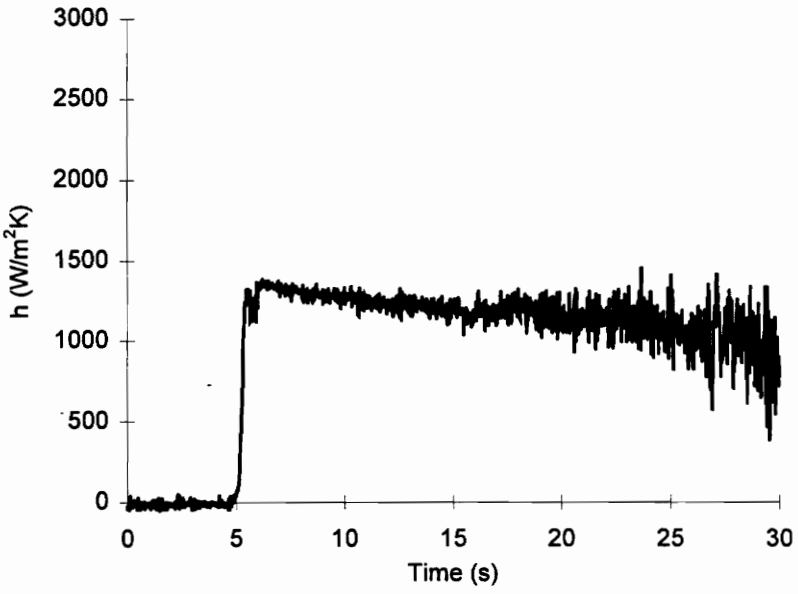


Figure A62. HTC Calculated From HFM-6 Gage 1 - Strut at Location 5 - Run #1

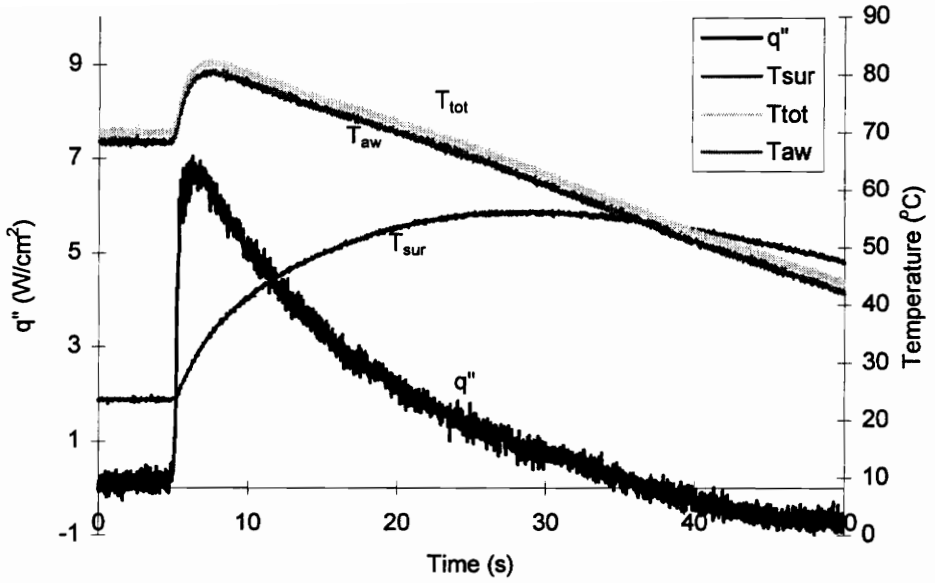


Figure A63. Example of Run For HFM-6 Gage 2 - Strut at Location 5 - Run #1

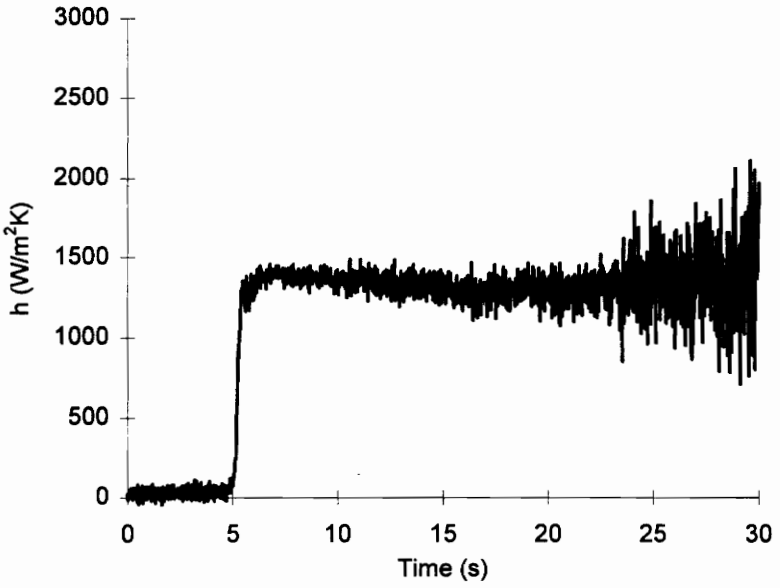


Figure A64. HTC Calculated From HFM-6 Gage 2 - Strut at Location 5 - Run #1

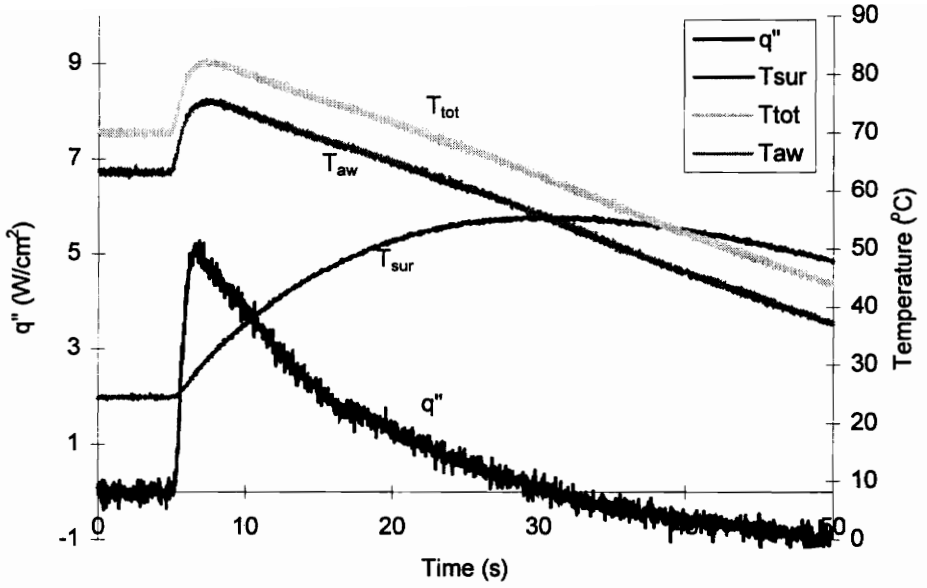


Figure A65. Example of Run For HFM-6 Gage 3 - Strut at Location 5 - Run #1

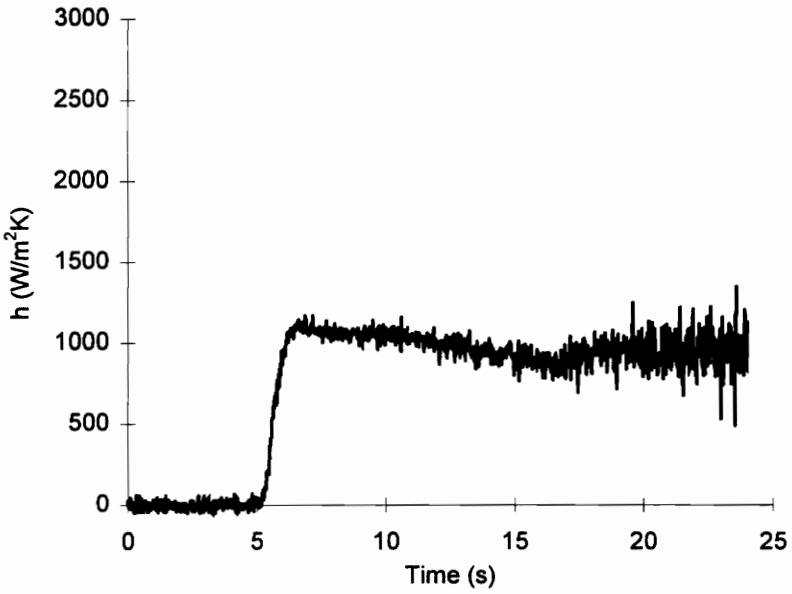


Figure A66. HTC Calculated From HFM-6 Gage 3 - Strut at Location 5 - Run #1

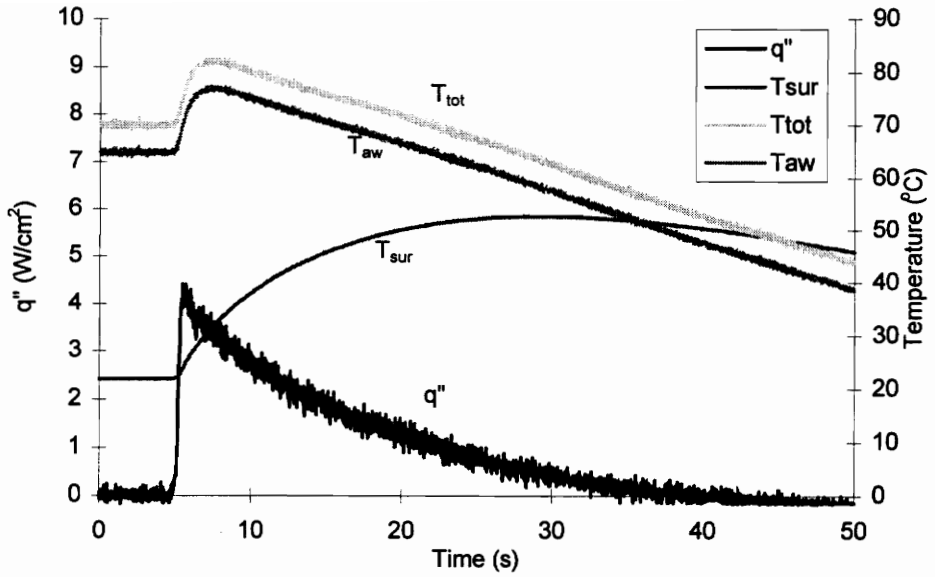


Figure A67. Example of Run For HFM-6 Gage 4 - Strut at Location 5 - Run #1

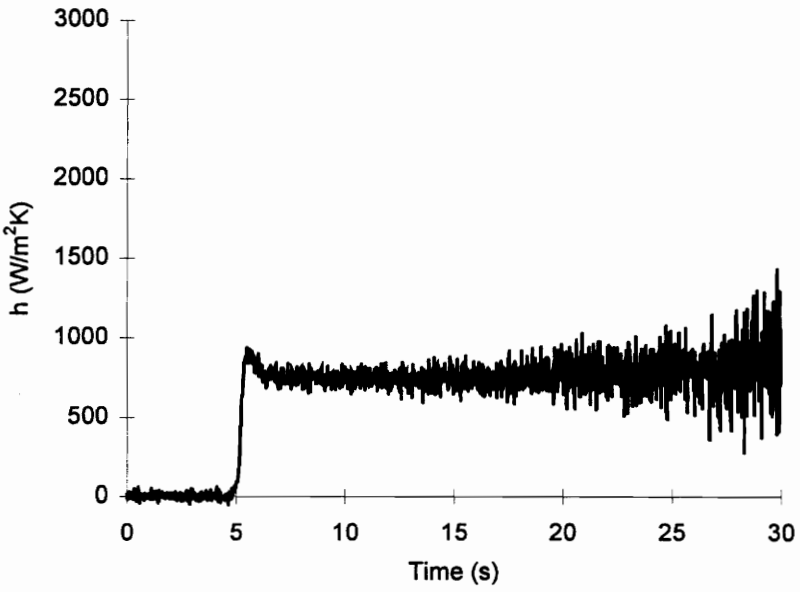


Figure A68. HTC Calculated From HFM-6 Gage 4 - Strut at Location 5 - Run #1

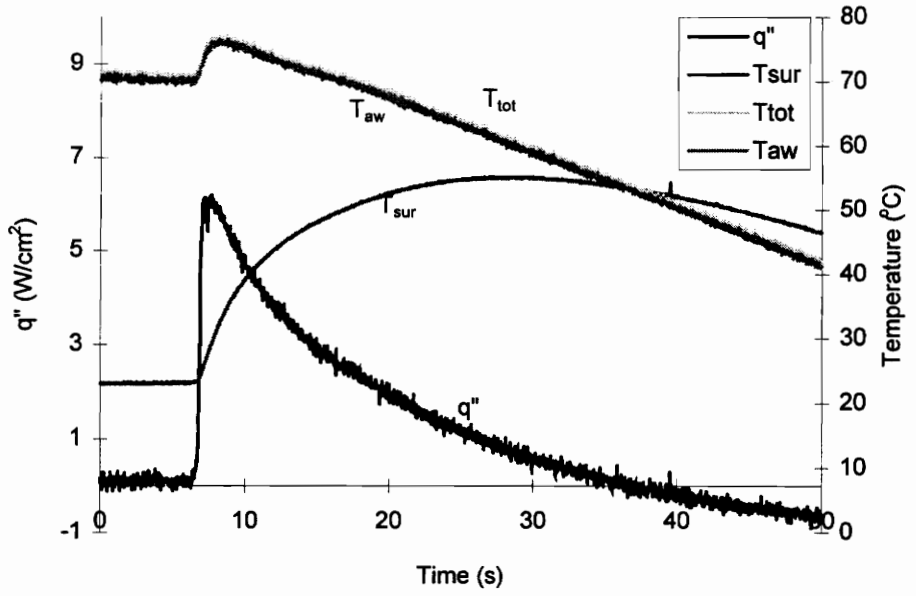


Figure A69. Example of Run For HFM-6 Gage 1 - Strut at Location 5 - Run #2

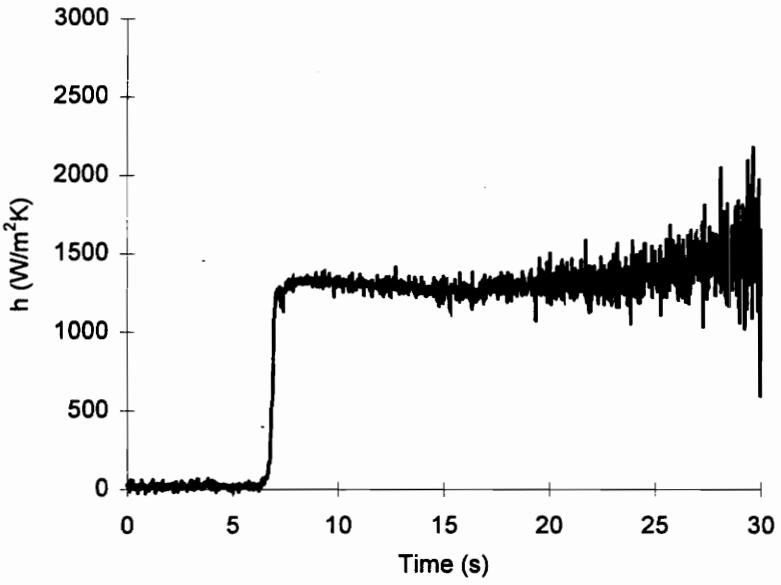


Figure A70. HTC Calculated From HFM-6 Gage 1 - Strut at Location 5 - Run #2

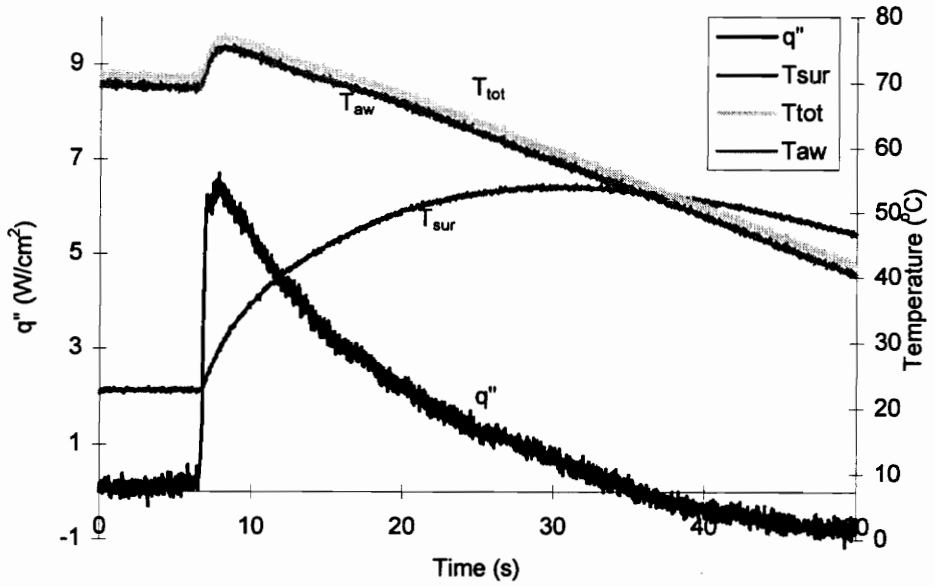


Figure A71. Example of Run For HFM-6 Gage 2 - Strut at Location 5 - Run #2

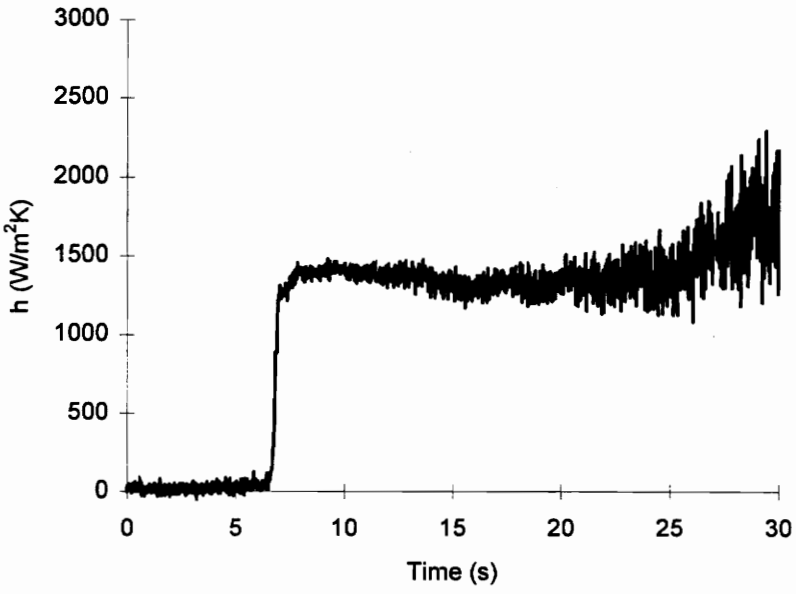


Figure A72. HTC Calculated From HFM-6 Gage 2 - Strut at Location 5 - Run #2

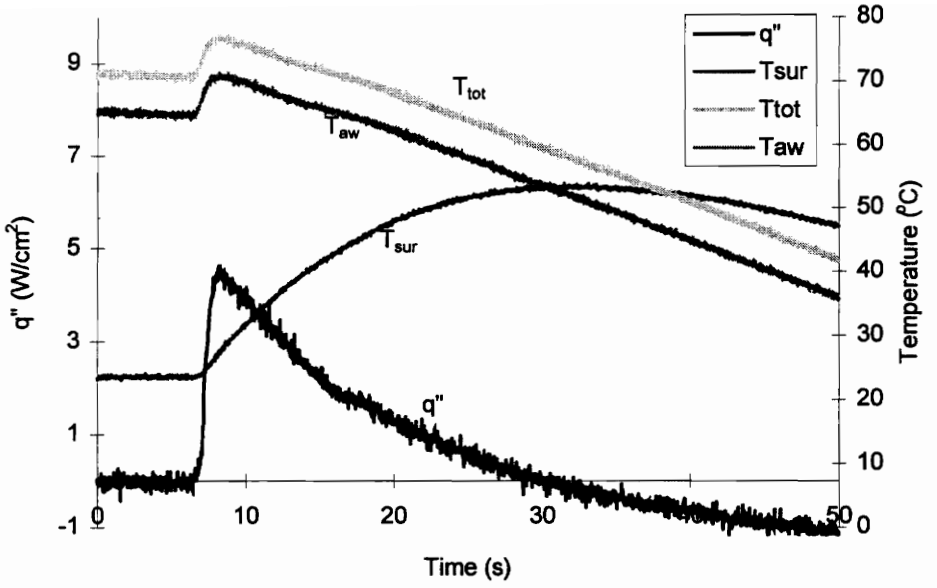


Figure A73. Example of Run For HFM-6 Gage 3 - Strut at Location 5 - Run #2

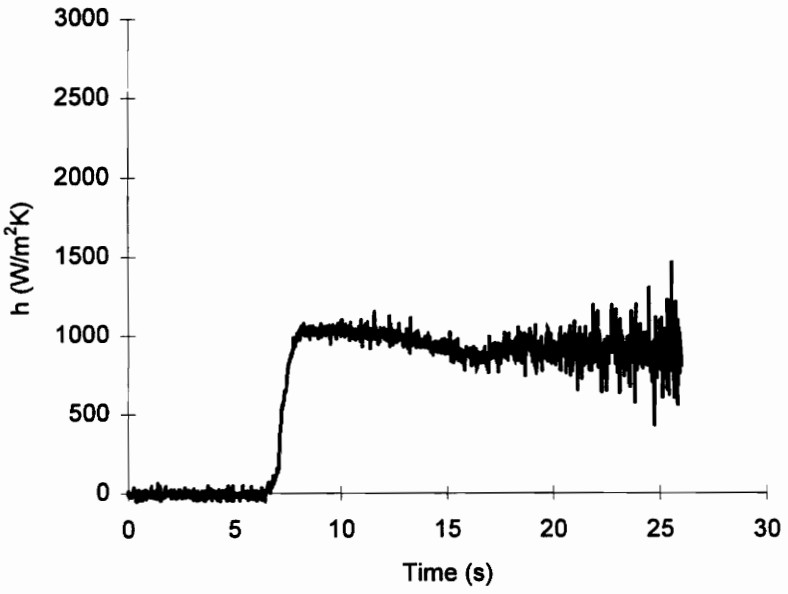


Figure A74. HTC Calculated From HFM-6 Gage 3 - Strut at Location 5 - Run #2

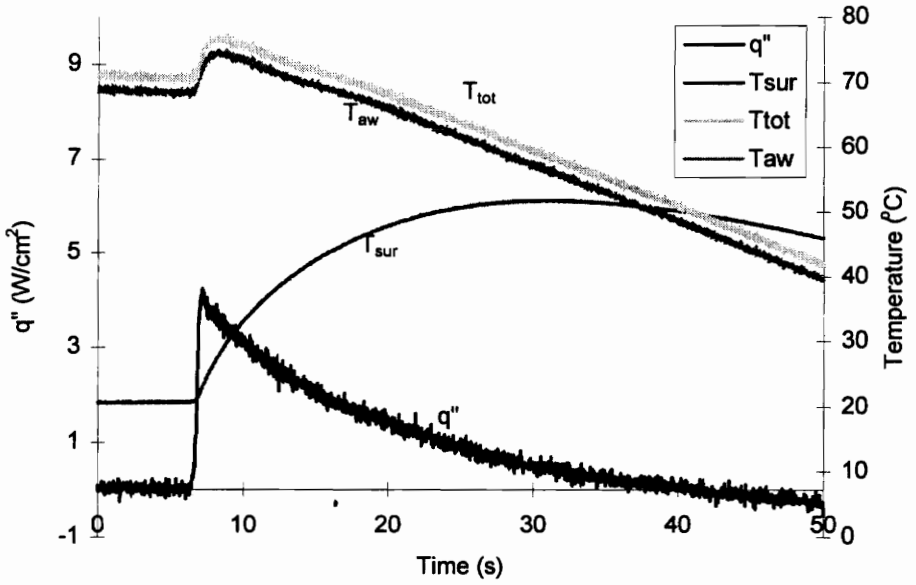


Figure A75. Example of Run For HFM-6 Gage 4 - Strut at Location 5 - Run #2

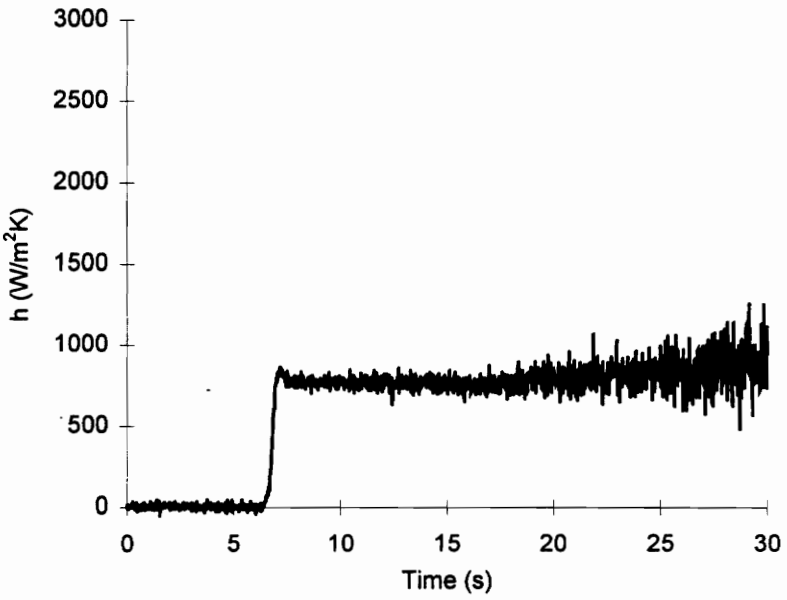


Figure A76. HTC Calculated From HFM-6 Gage 4 - Strut at Location 5 - Run #2

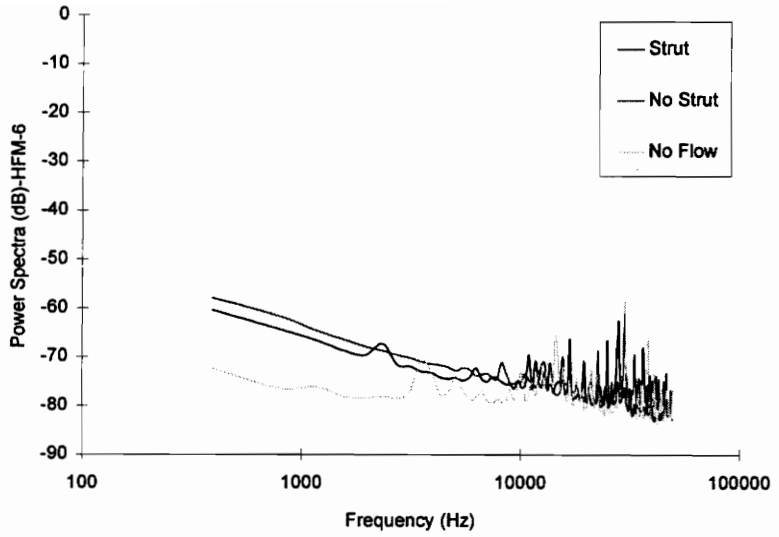


Figure A77. Power Spectra of No Strut and Strut at z/p=1.78 of Heat Flux Signal Sampled at 100 kHz (Gage 1)

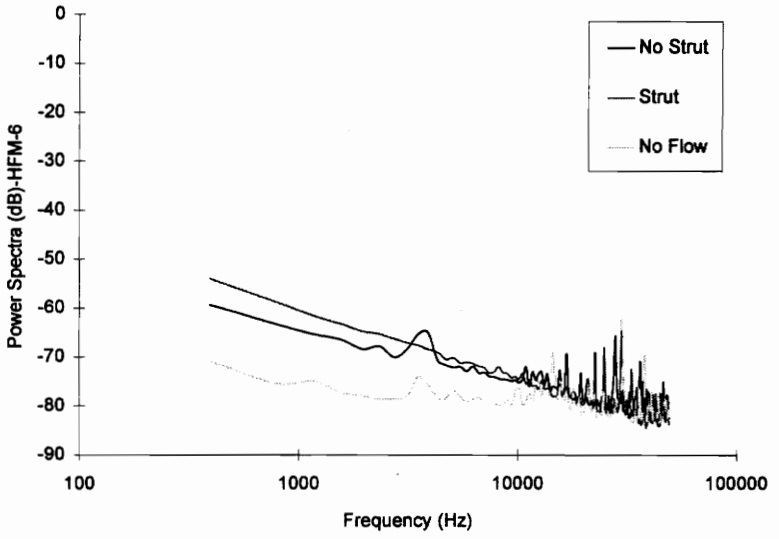


Figure A78. Power Spectra of No Strut and Strut at z/p=1.78 of Heat Flux Signal Sampled at 100 kHz (Gage 2)

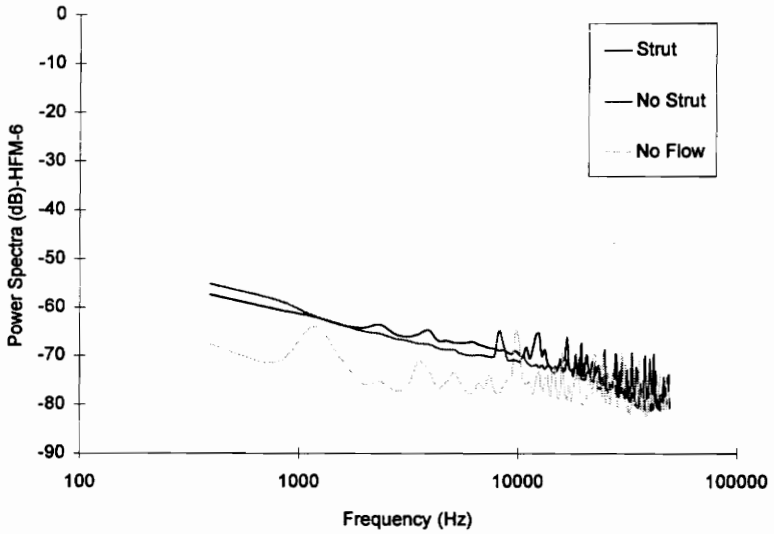


Figure A79. Power Spectra of No Strut and Strut at z/p=1.78 of Heat Flux Signal Sampled at 100 kHz (Gage 3)

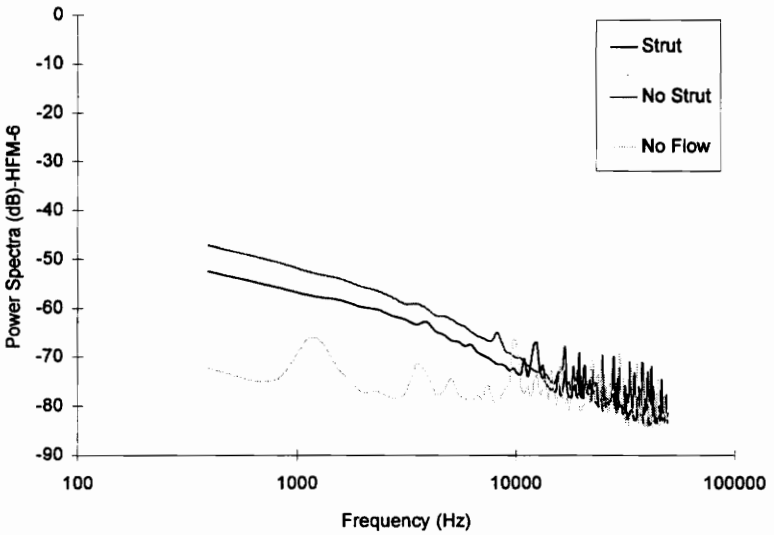


Figure A80. Power Spectra of No Strut and Strut at z/p=1.78 of Heat Flux Signal Sampled at 100 kHz (Gage 4)

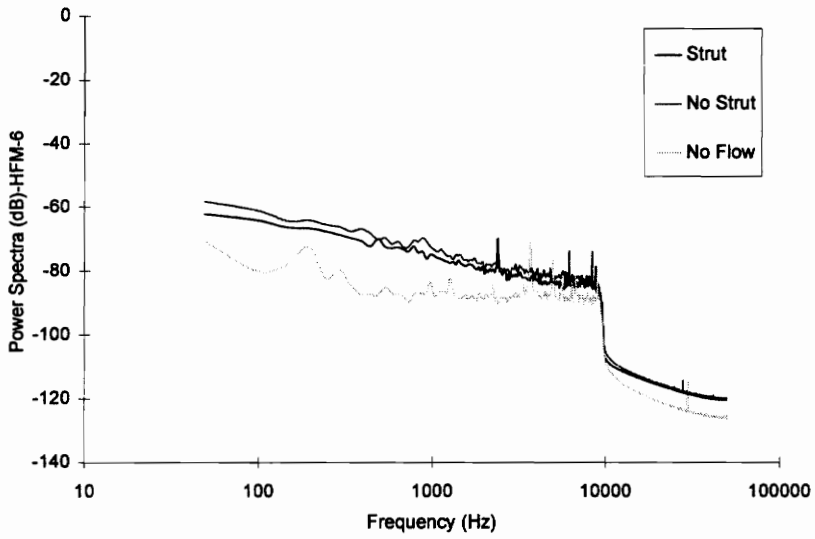


Figure A81. Filtered Power Spectra of No Strut and Strut at z/p=1.78 of Heat Flux Signal Sampled at 100 kHz (Gage 1)

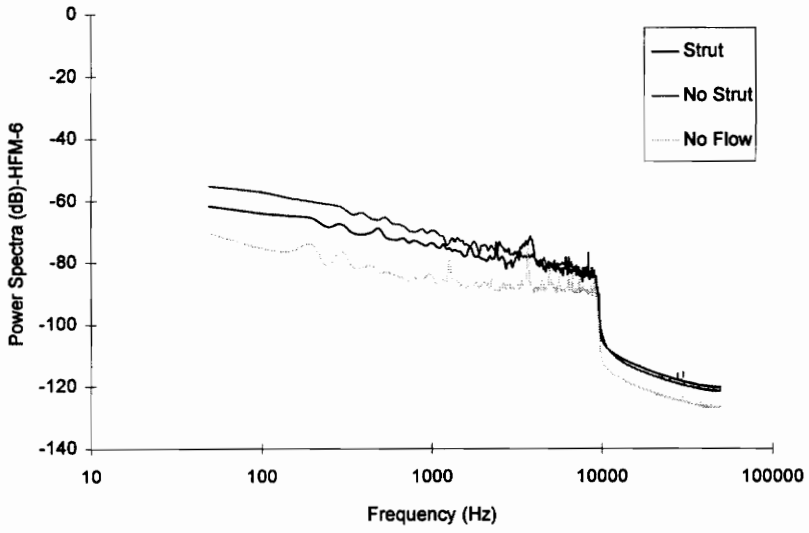


Figure A82. Filtered Power Spectra of No Strut and Strut at z/p=1.78 of Heat Flux Signal Sampled at 100 kHz (Gage 2)

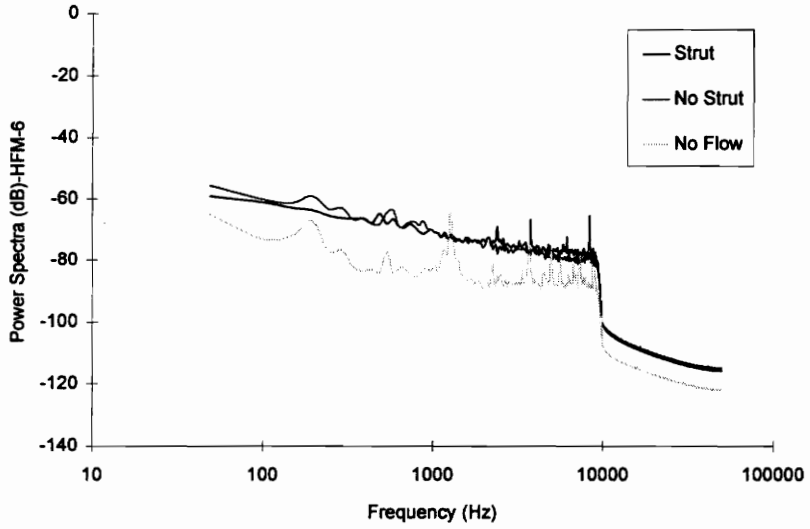


Figure A83. Filtered Power Spectra of No Strut and Strut at z/p=1.78 of Heat Flux Signal Sampled at 100 kHz (Gage 3)

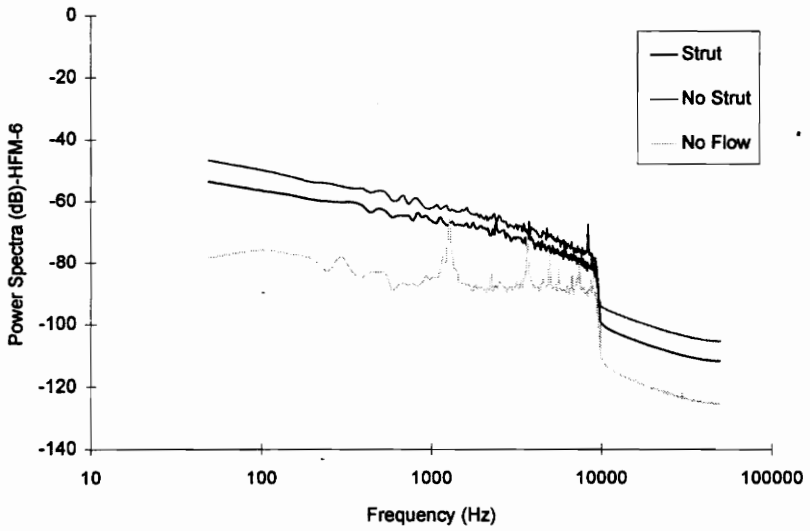


Figure A84. Filtered Power Spectra of No Strut and Strut at z/p=1.78 of Heat Flux Signal Sampled at 100 kHz (Gage 4)

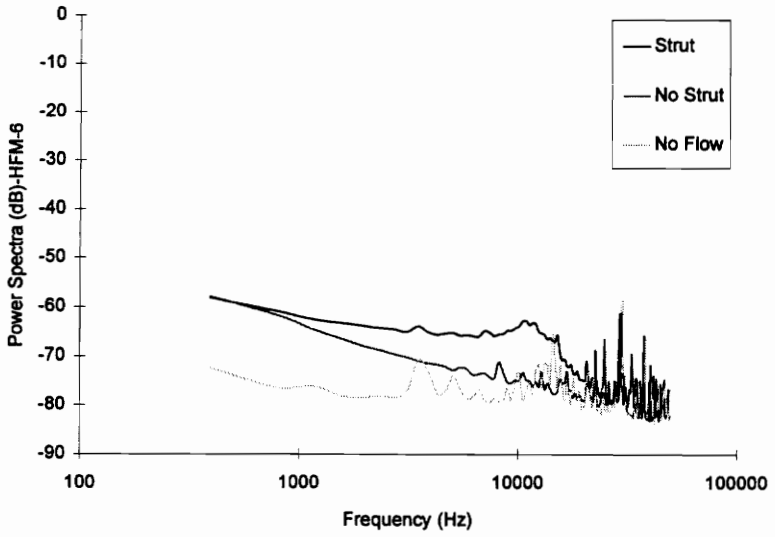


Figure A85. Power Spectra of No Strut and Strut at z/p=2.19 of Heat Flux Signal Sampled at 100 kHz (Gage 1)

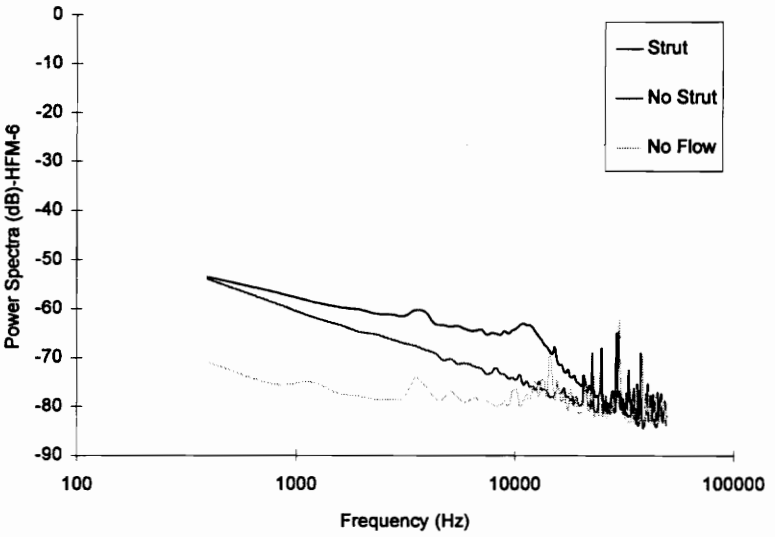


Figure A86. Power Spectra of No Strut and Strut at z/p=2.19 of Heat Flux Signal Sampled at 100 kHz (Gage 2)

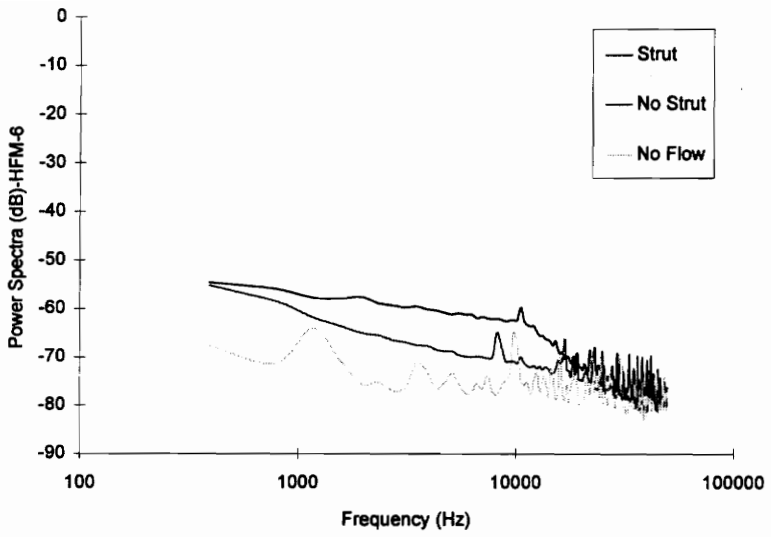


Figure A87. Power Spectra of No Strut and Strut at z/p=2.19 of Heat Flux Signal Sampled at 100 kHz (Gage 3)

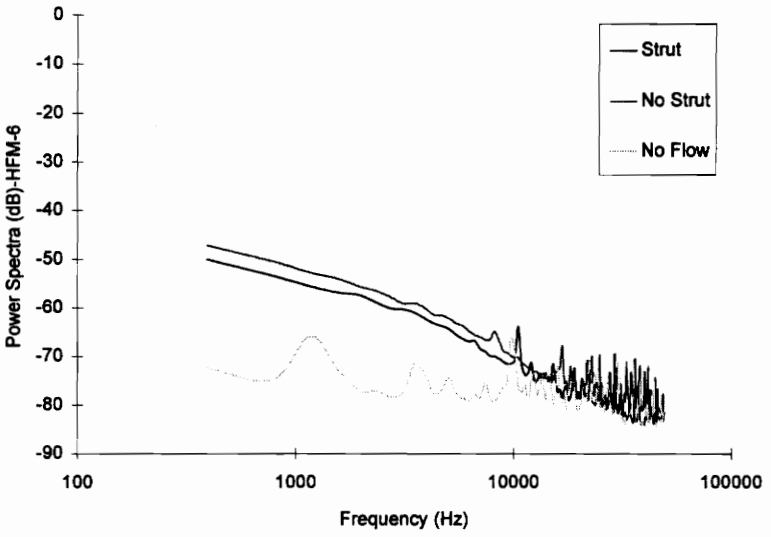


Figure A88. Power Spectra of No Strut and Strut at z/p=2.19 of Heat Flux Signal Sampled at 100 kHz (Gage 4)

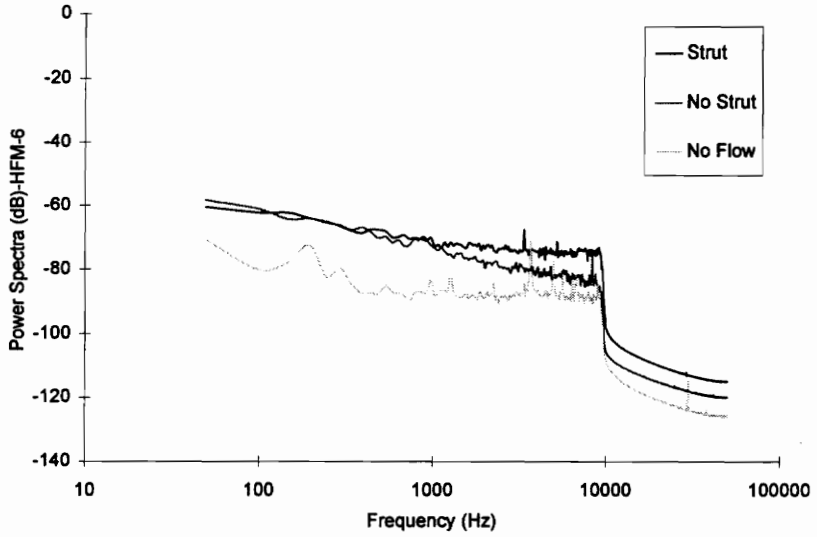


Figure A89. Filtered Power Spectra of No Strut and Strut at z/p=2.19 of Heat Flux Signal Sampled at 100 kHz (Gage 1)

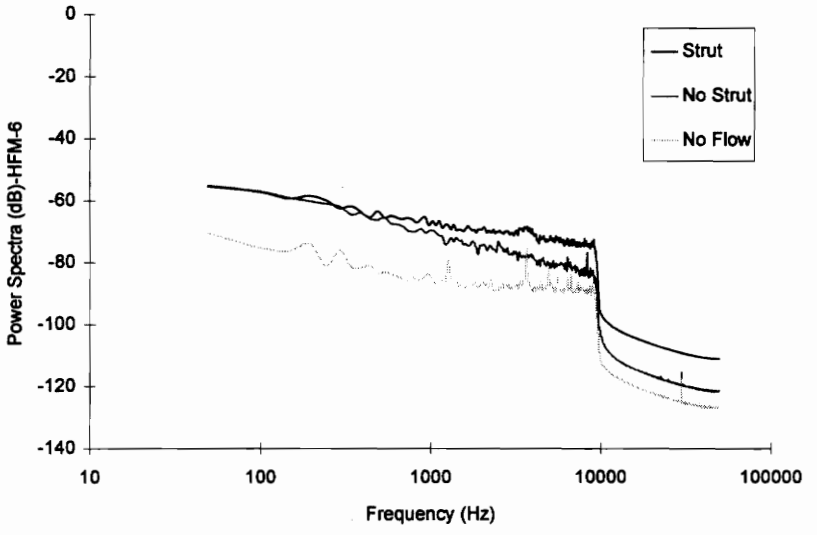


Figure A90. Filtered Power Spectra of No Strut and Strut at z/p=2.19 of Heat Flux Signal Sampled at 100 kHz (Gage 2)

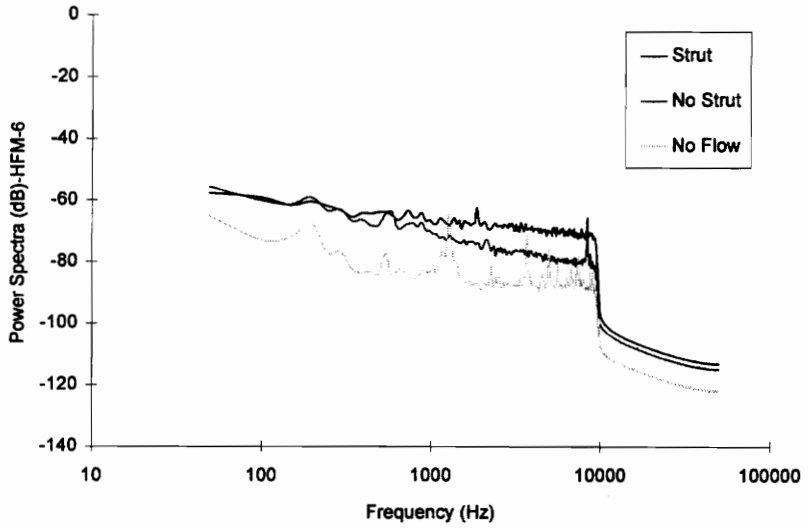


Figure A91. Filtered Power Spectra of No Strut and Strut at z/p=2.19 of Heat Flux Signal Sampled at 100 kHz (Gage 3)

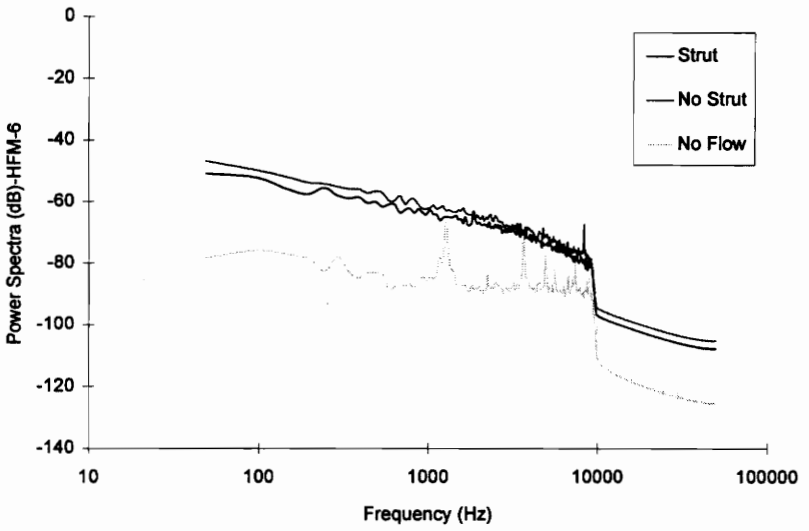


Figure A92. Filtered Power Spectra of No Strut and Strut at z/p=2.19 of Heat Flux Signal Sampled at 100 kHz (Gage 4)

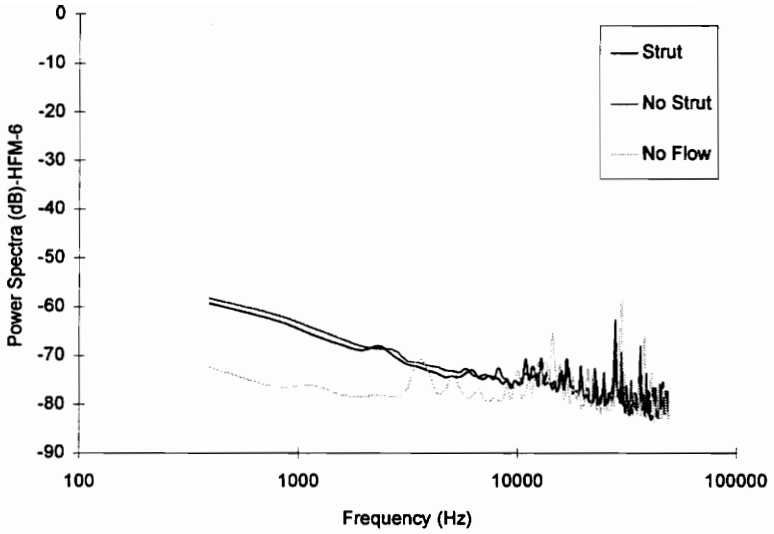


Figure A93. Power Spectra of No Strut and Strut at z/p=2.45 of Heat Flux Signal Sampled at 100 kHz (Gage 1)

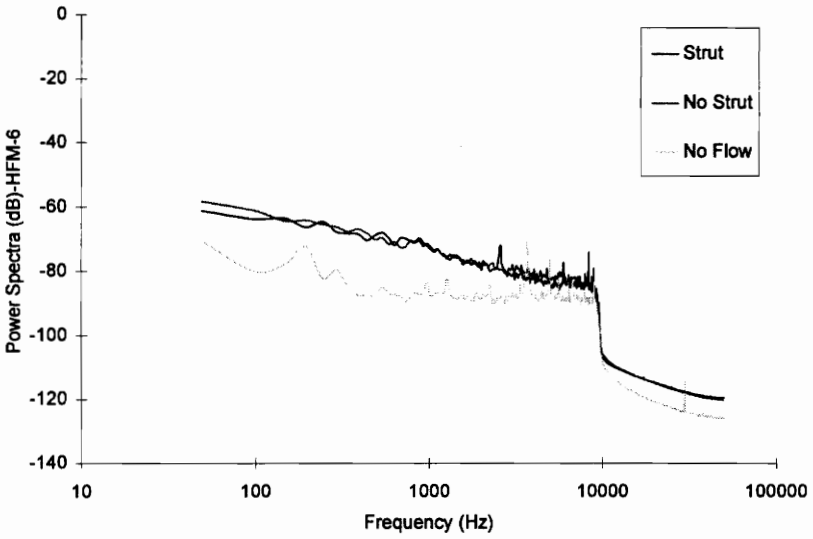


Figure A94. Filtered Power Spectra of No Strut and Strut at z/p=2.45 of Heat Flux Signal Sampled at 100 kHz (Gage 1)

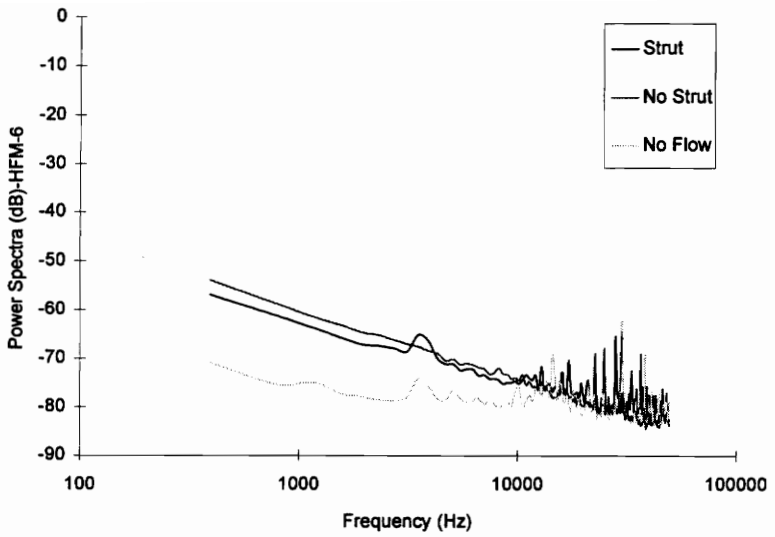


Figure A95. Power Spectra of No Strut and Strut at z/p=2.45 of Heat Flux Signal Sampled at 100 kHz (Gage 2)

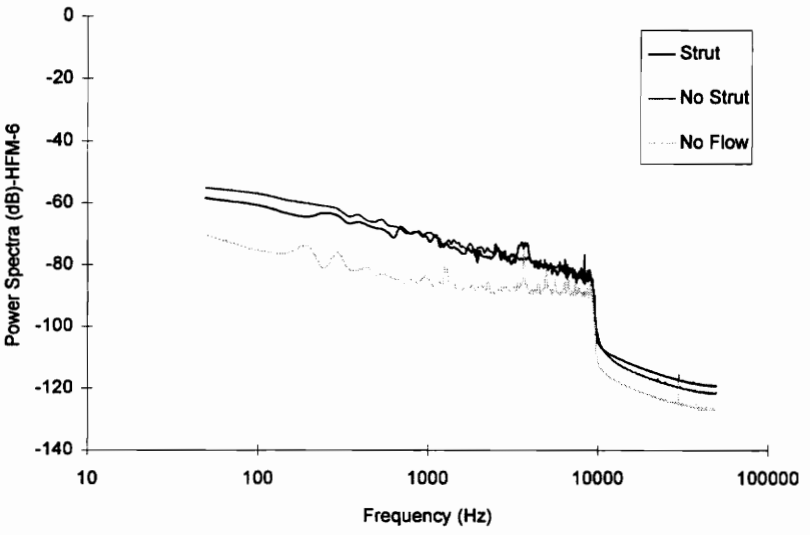


Figure A96. Filtered Power Spectra of No Strut and Strut at z/p=2.45 of Heat Flux Signal Sampled at 100 kHz (Gage 2)

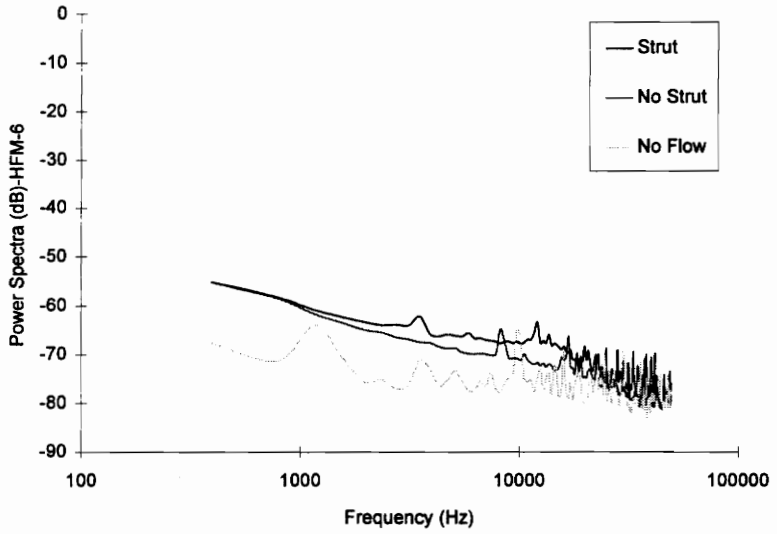


Figure A97. Power Spectra of No Strut and Strut at z/p=2.45 of Heat Flux Signal Sampled at 100 kHz (Gage 3)

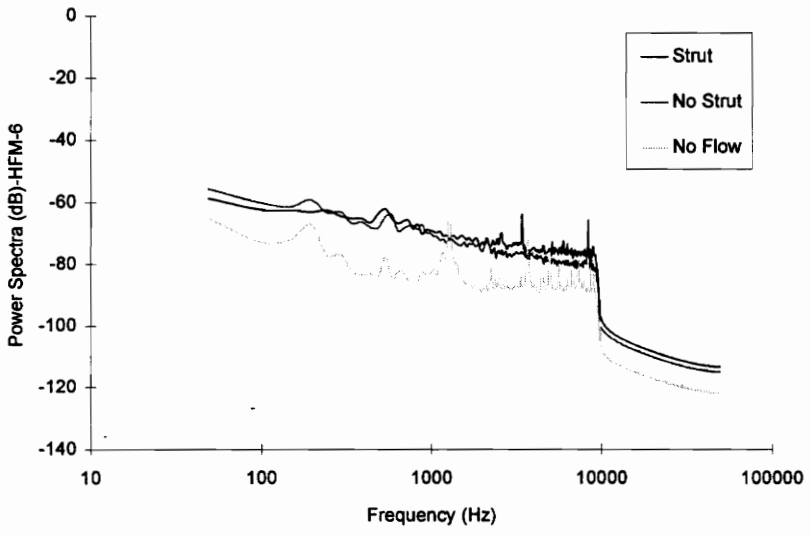


Figure A98. Filtered Power Spectra of No Strut and Strut at z/p=2.45 of Heat Flux Signal Sampled at 100 kHz (Gage 3)

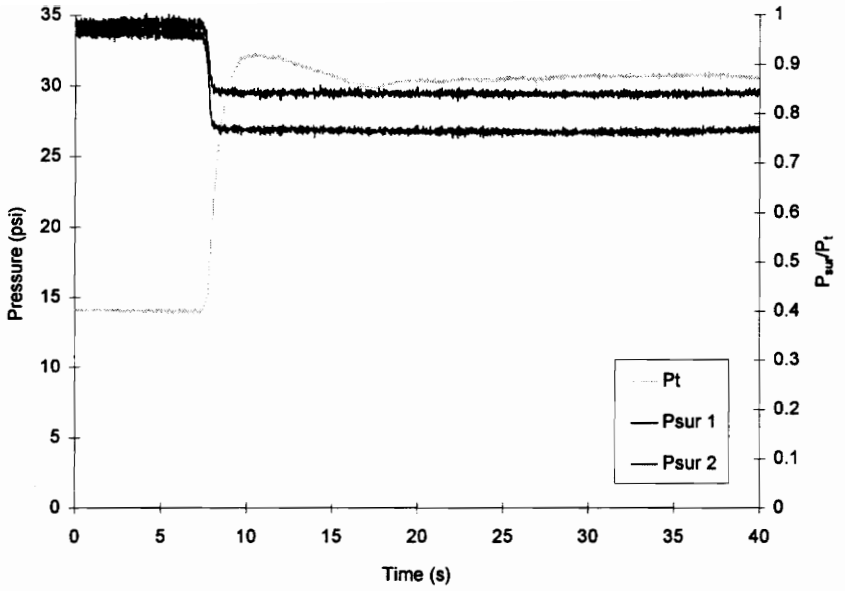


Figure A99. Total Pressure and Normalized Pressure for Strut at z/p=1.78 (Run #1)- Kulite 1 and Kulite 2

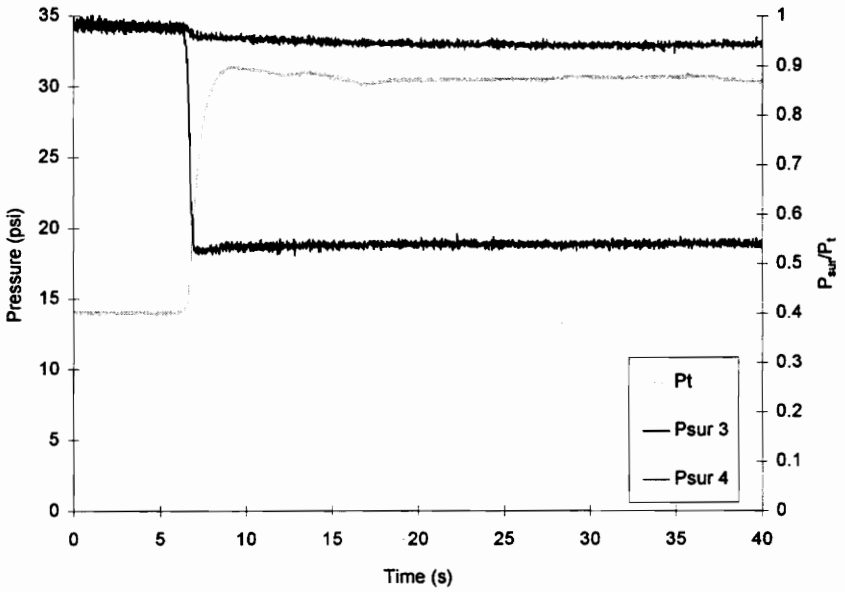


Figure A100. Total Pressure and Normalized Pressure for Strut at z/p=1.78 (Run #2)- Kulite 3 and Kulite 4

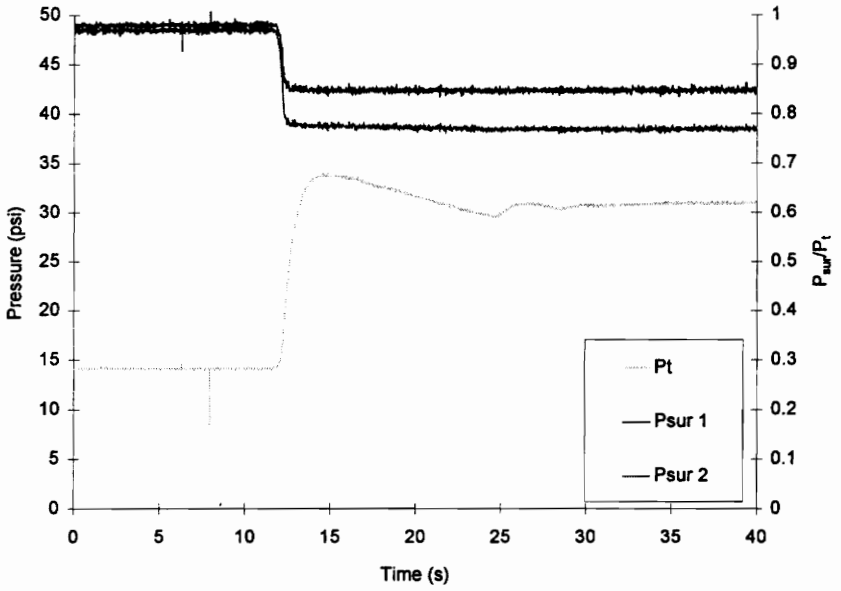


Figure A101. Total Pressure and Normalized Pressure for Strut at z/p=2.19 (Run #1)- Kulite 1 and Kulite 2

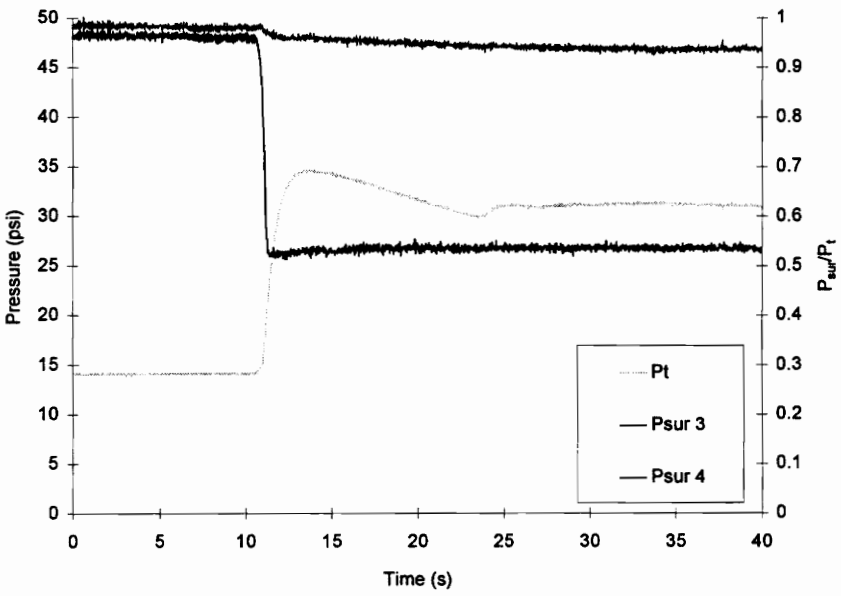


Figure A.102 Total Pressure and Normalized Pressure for Strut at z/p=2.19 (Run #2)- Kulite 3 and Kulite 4

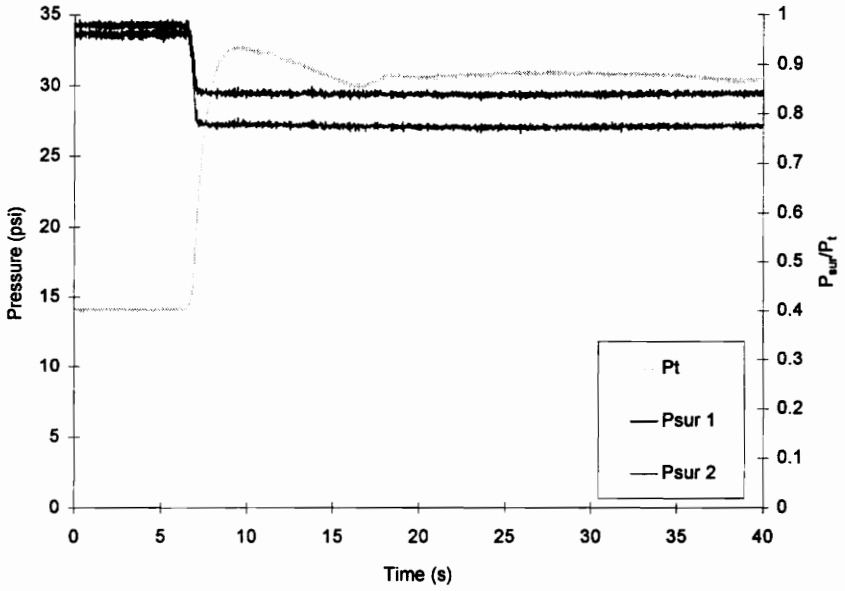


Figure A103. Total Pressure and Normalized Pressure for Strut at z/p=2.45 (Run #1)- Kulite 1 and Kulite 2

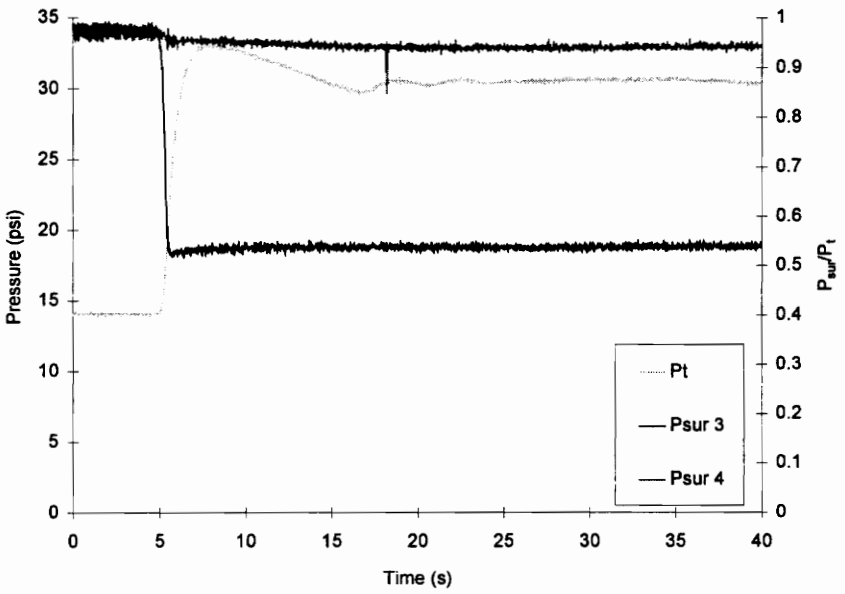


Figure A104. Total Pressure and Normalized Pressure for Strut at z/p=2.45 (Run #2)- Kulite 3 and Kulite 4

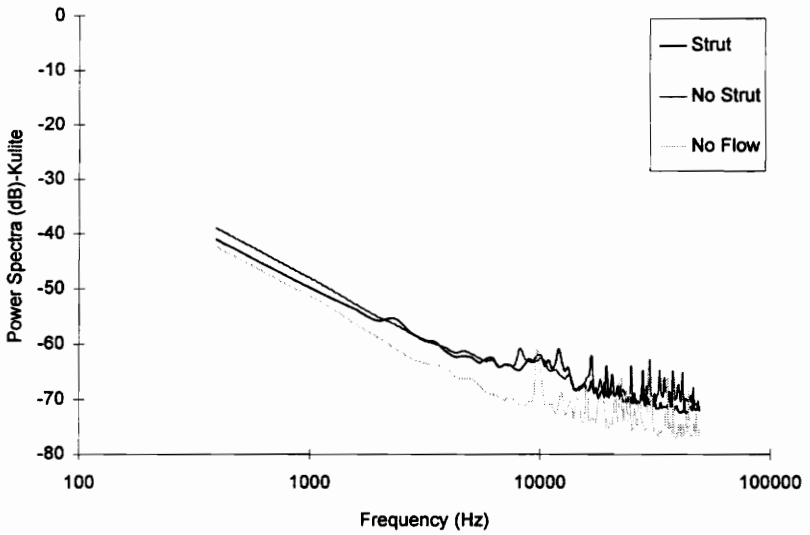


Figure A105. Power Spectra of No Strut and Strut at z/p=1.78 of Kulite Signal Sampled at 100 kHz (Gage 1)

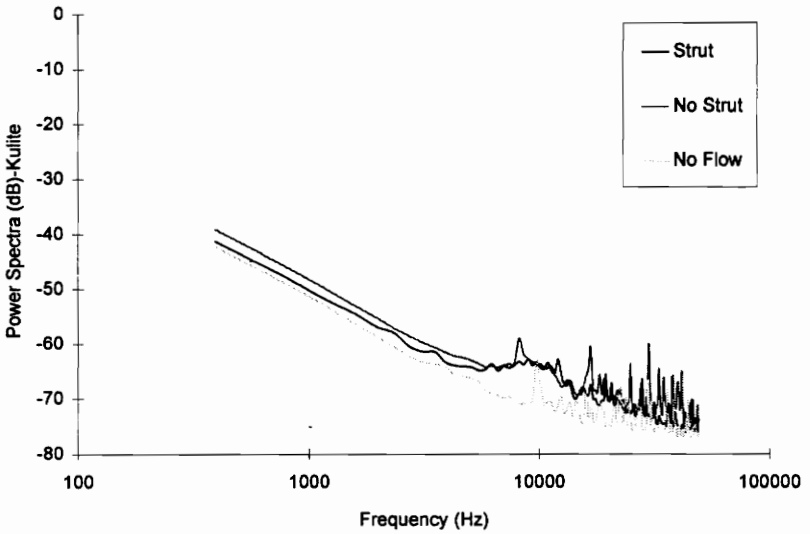


Figure A106. Power Spectra of No Strut and Strut at z/p=1.78 of Kulite Signal Sampled at 100 kHz (Gage 2)

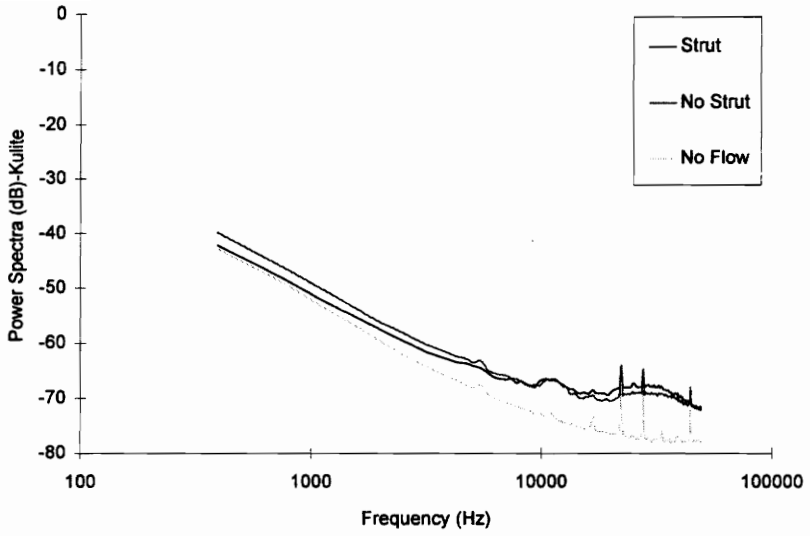


Figure A107. Power Spectra of No Strut and Strut at z/p=1.78 of Kulite Signal Sampled at 100 kHz (Gage 3)

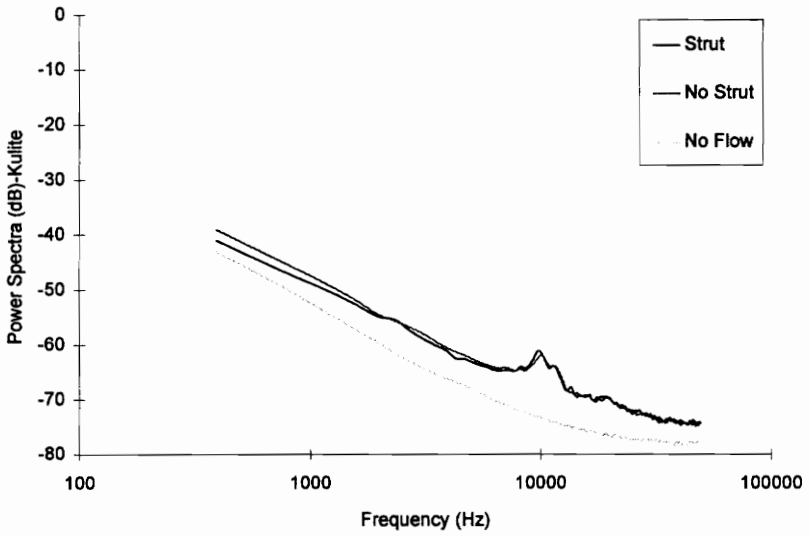


Figure A108. Power Spectra of No Strut and Strut at z/p=1.78 of Kulite Signal Sampled at 100 kHz (Gage 4)

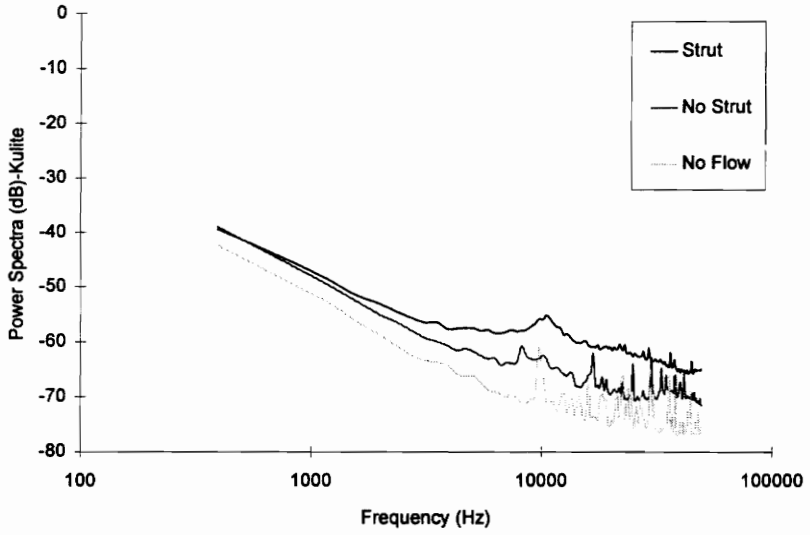


Figure A109. Power Spectra of No Strut and Strut at z/p=2.19 of Kulite Signal Sampled at 100 kHz (Gage 1)

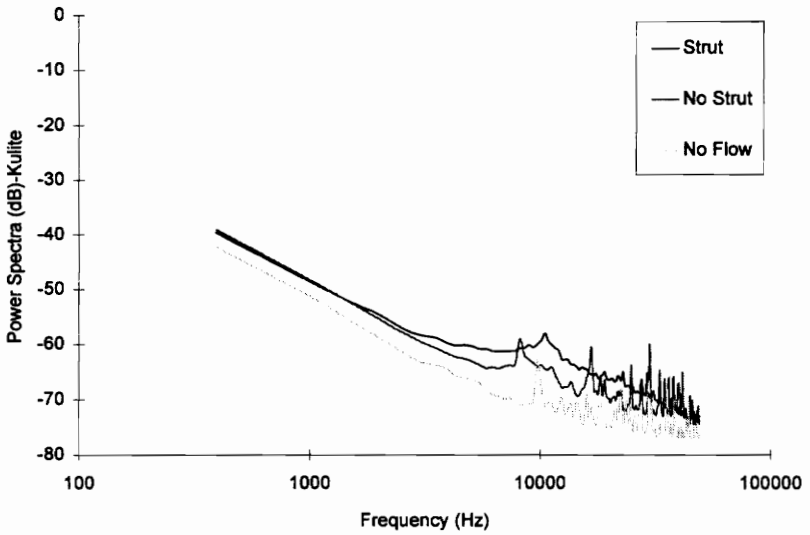


Figure A110. Power Spectra of No Strut and Strut at z/p=2.19 of Kulite Signal Sampled at 100 kHz (Gage 2)

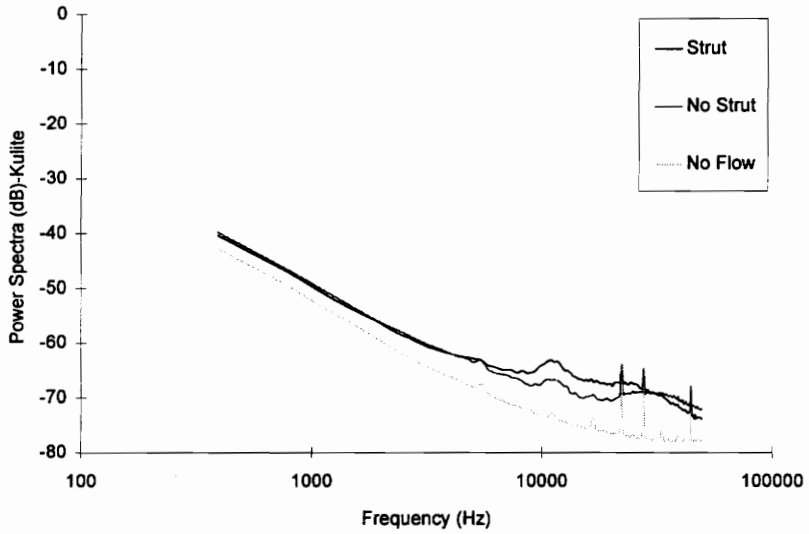


Figure A111. Power Spectra of No Strut and Strut at z/p=2.19 of Kulite Signal Sampled at 100 kHz (Gage 3)

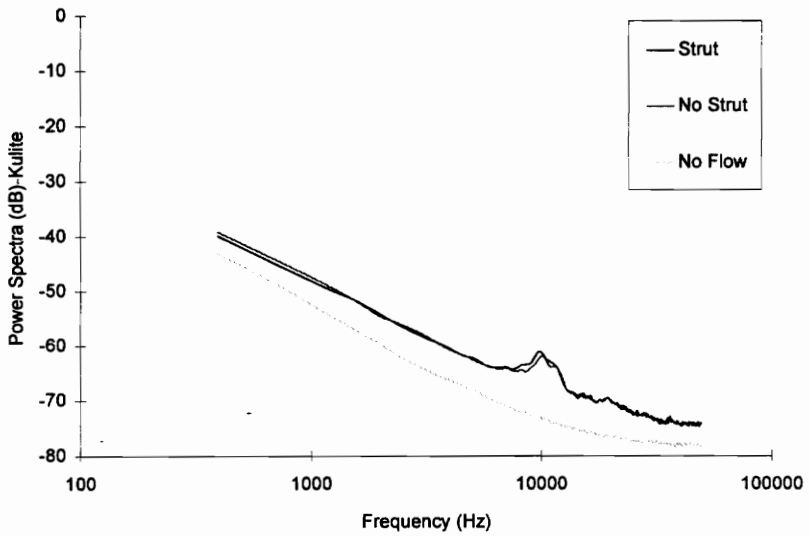


Figure A112. Power Spectra of No Strut and Strut at z/p=2.19 of Kulite Signal Sampled at 100 kHz (Gage 4)

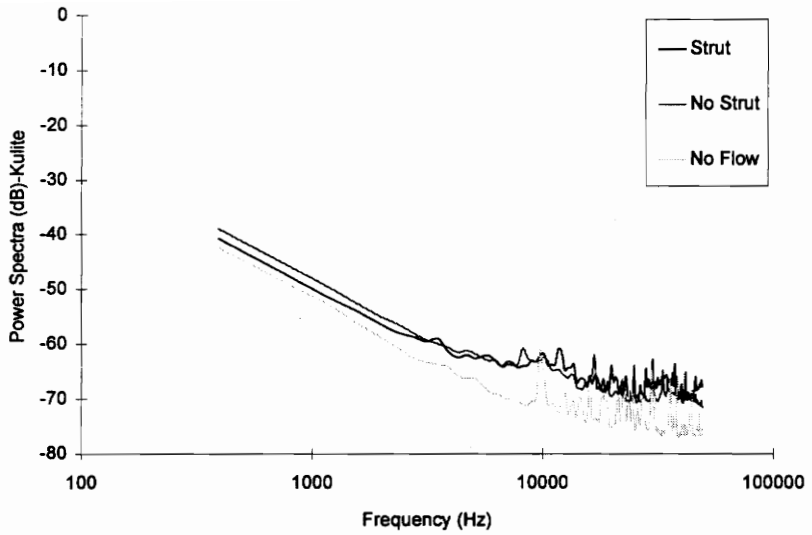


Figure A113. Power Spectra of No Strut and Strut at z/p=2.45 of Kulite Signal Sampled at 100 kHz (Gage 1)

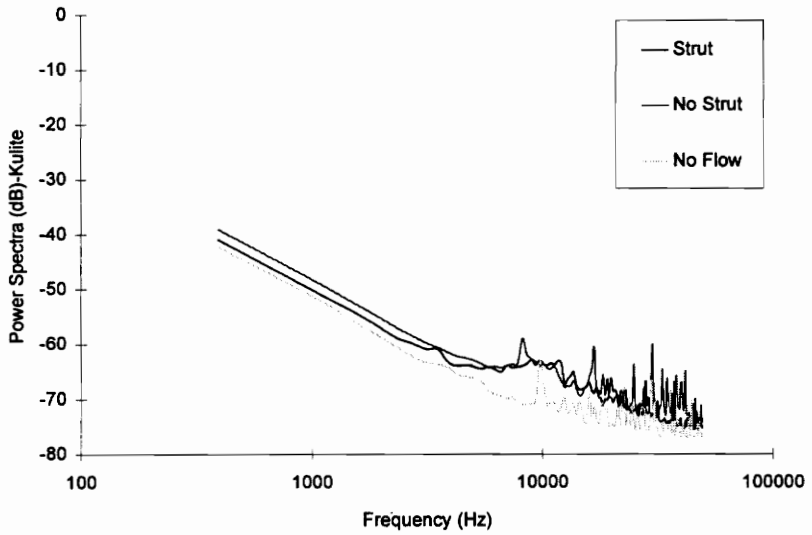


Figure A114. Power Spectra of No Strut and Strut at z/p=2.45 of Kulite Signal Sampled at 100 kHz (Gage 2)

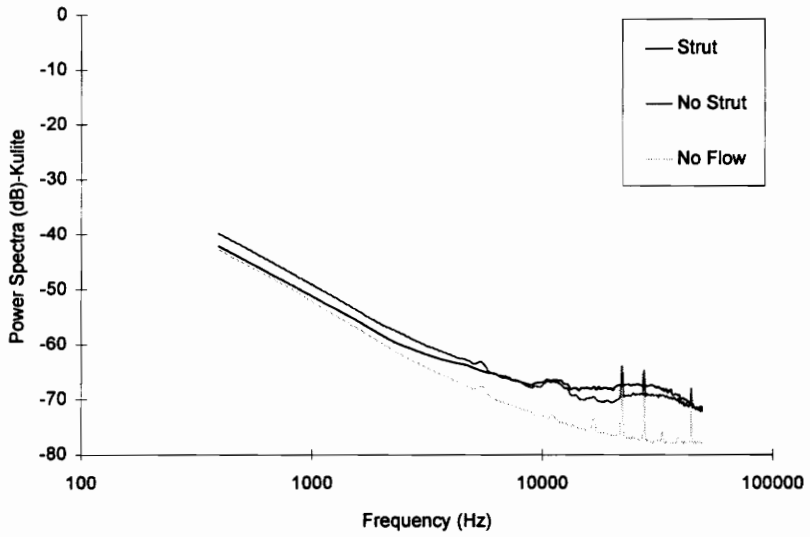


Figure A115. Power Spectra of No Strut and Strut at z/p=2.45 of Kulite Signal Sampled at 100 kHz (Gage 3)

# Appendix B

## FORTRAN and BASIC Programs

The following contains the FORTRAN programs used to reduce the data presented in this thesis and the BASIC program used to control the traversing mechanism and PSI system when acquirng pressure data.

FORTRAN programs:

**1). HWCAL.FOR**

**2). HWDAT.FOR**

**3). VELTUR.FOR**

**4). HFLUX.FOR**

**5). HFTURB.FOR**

**6). PSUR.FOR**

BASIC program:

**1). NEWOSR.BAS**

```
*****************************************************************************************************
*       HWCAL.FOR                                                                                   *
*       Written by Jamie H. Hale                                                                    *
*       Date 09/15/95                                                                               *
*                                                                                                   *
*       This program is designed to aid in the calibration of a hot-wire.  The program              *
*       reads in differential pressure, total pressure, total temperature, and hot-wire             *
*       voltage.  The are then manipulated through a series of equations to produce                 *
*       two output files.  One being a function of the Nusselt number and the other a               *
*       function of the Reynolds number.  These results can be used to determine                    *
*       the velocity of the flow from the hot-wire voltage.                                         *
*                                                                                                   *
*       Variables used are:                                                                         *
*       PMB.....Atmospheric pressure in millibars                                                   *
*       PATM.....Atmospheric pressure (kPa)                                                         *
*       DPV.....Differential Pressure signal (V)                                                    *
*       PTV.....Total Pressure signal (V)                                                           *
*       HWV.....Hot-wire signal (V)                                                                 *
*       TTV.....Total Temperature signal (V)                                                        *
*       OFFSDP.....Differential Pressure offset (V)                                                 *
*       PTPSIG.....Total Pressure (psig)                                                            *
*       PTKPA.....Total Pressure (kPa)                                                              *
*       DP.....Differential Pressure (kPa)                                                          *
*       PSKPA.....Static Pressure (kPa)                                                             *
*       V.....Total Temperature voltage (V)                                                         *
*       TSK.....Static Temperature (K)                                                              *
*       K.....Thermal Conductivity (W/m K)                                                          *
*       VIS.....Dynamic viscosity (Pa s)                                                            *
*       RHO.....Density (kg/m^3)                                                                    *
*       NUAPP.....Nusselt approximation                                                             *
*       UFS.....Free-stream velocity (m/s)                                                          *
*       G.....Specific heat ratio                                                                   *
*       R.....Universal gas constant (kJ/kg K)                                                      *
*       REAPP.....Reynolds approximation                                                            *
*       TIME.....(s)                                                                                *
*       TT.....Total Temperature (°C)                                                               *
*       TMK.....Mean Temperature (K)                                                                *
*****************************************************************************************************
      PROGRAM HWCAL
      REAL PMB,PATM,DPV,PTV,HWV,TTV,OFFSDP,
     &PTPSIG,PTKPA,DP,PSKPA,V,M,TSK,TW,K,TMK,VIS,RHO,
     &NUAPP,UFS,G,R,REAPP,TIME,TT

*****************************************************************************************************
*       Opening input data files and creating output files.                                         *
*****************************************************************************************************

      OPEN (UNIT=3,FILE='Differential Pressure Filename')
      OPEN (UNIT=8,FILE='Total Pressure Filename')
      OPEN (UNIT=7,FILE='Hot-Wire Filename')
      OPEN (UNIT=9,FILE='Total Temperature Filename')
```

```
      OPEN (UNIT=15,FILE='Output Filename 1')
      OPEN (UNIT=16,FILE='Output Filename 2')
      WRITE(15,40)
 40   FORMAT('TIME',5X,'UFS',6X,'REAPP',8X,'NUAPP')
      WRITE(16,45)
 45   FORMAT('TIME',5X,'TT',6X,'PTKPA',8X,'RHO')

*****************************************************************************************************************
*       Input atmospheric for run day in millibars and input differential pressure offfset                      *
*****************************************************************************************************************

      WRITE(*,*)'INPUT ATMOSPHERIC PRESSURE'
      READ(*,*) PMB
      WRITE(*,*)'INPUT DIFFERENTIAL PRESSURE OFFSET'
      READ(*,*) OFFSDP

*****************************************************************************************************************
*       Define properties of air and hot-wire.                                                                  *
*****************************************************************************************************************

      TW = 250.0
      G = 1.4
      R = 287.
      PATM = PMB*(1E5/(1000.0*1000.0))

*****************************************************************************************************************
*       Do loop to read ASCII files and convert voltage signals into meaningful results.  The IF                *
*       statement skips the data when the differential pressure is zero (tunnel not running) and                *
*       when the end of the file is completed.                                                                  *
*****************************************************************************************************************

      DO 10 I = 0, 4093
       TIME = 0.02*I
        READ(3,*) DPV
        READ(8,*) PTV
        READ(7,*) HWV
        READ(9,*) TTV
       IF(DPV .LE. 0.0)THEN
      GO TO 12
       ENDIF
       IF(I .GT. 4093)THEN
      GO TO 14
      ENDIF

*****************************************************************************************************************
*       Conversion equations for voltage signals                                                                *
*****************************************************************************************************************

          PTPSIG = -25.1976939 + 25.0938973*PTV
          PTKPA = PATM + PTPSIG*101.325/14.7
          DP = ((DPV+OFFSDP)/2.0)*101.325/14.7
```

```
      PSKPA = PTKPA - DP
      V = TTV*(1E6/100.)
      TT = 2.508355E-2*(V) +7.860106E-8*(V**2) -2.503131E-10*
     &(V**3)+8.315270E-14*(V**4) -1.228034E-17*(V**5) +9.804036E-22*
     &(V**6)-4.41303E-26*(V**7) +1.057734E-30*(V**8) +1.0527755E-35*
     &(V**9)
      WRITE(*,*) TT
      M = (((PTKPA/PSKPA)**((G-1.)/G) -1.)*(2./(G-1)))**.5
      TSK = (TT + 273.15)/(1. + ((G-1.)/2.)*(M**2.))
      TMK = ((TW + 273.15) + TSK)/2.
      K = 2.414E-2*((TMK/273.16)**(3./2.))*(473.16/(TMK + 200.))
      VIS = 1.716E-5*((TMK/273.16)**1.5)*(383.716/(TMK+110.556))
      RHO = (PSKPA*1000.)/(R*TSK)
      UFS = M*((G*R*TSK)**.5)
      NUAPP =((HWV/K)/(TMK - TSK))*((TMK/TSK)**(-0.17))
      REAPP = ((RHO*UFS)/VIS)**(.51)

*****************************************************************************************************************
*       Writing to output files opened above                                                                    *
*****************************************************************************************************************
     WRITE(15,30) TIME,UFS,REAPP,NUAPP
     WRITE(16,35) TIME,TT,PTKPA,RHO
30   FORMAT(1X,F6.3,2X,F11.6,2X,F11.6,2X,F11.6)
35   FORMAT(1X,F6.3,2X,F11.6,2X,F11.6,2X,F11.6)
12   CONTINUE
10   CONTINUE
14   STOP
     END
```

```
*****************************************************************************************************
*       HWDAT.FOR                                                                                   *
*       Written by Jamie H. Hale                                                                    *
*       Date 09/30/95                                                                               *
*                                                                                                   *
*       This program is designed to use the results from the calibration program to                 *
*       reduce the hot-wire data. The program needs the following input files: total                *
*       pressure, differential pressure, hot-wire voltage, total temperature, and lvdt              *
*       voltage. The lvdt voltage is needed to determine the position of the hot-wire               *
*       during the traverse. If a traverse is not employed this may be removed from                 *
*       the program. These signals are manipulated through a series of equations to                 *
*       produce three output files which contain various properties.                                *
*                                                                                                   *
*       Variables used are:                                                                         *
*                                                                                                   *
*       PMB.....Atmospheric pressure (mb)                                                           *
*       PATM.....Atmospheric pressure (kPa)                                                         *
*       DPVSUM.....Sum of Differential Pressure signal (V)                                          *
*       PTVSUM.....Sum of Total Pressure signal (V)                                                 *
*       HWVSUM.....Sum of Hot-wire signal (V)                                                       *
*       LVVSUM.....Sum of lvdt signal (V)                                                           *
*       TTVSUM.....Sum of Total Temperature signal (V)                                              *
*       DPV.....Differential Pressure signal (V)                                                    *
*       PTV.....Total Pressure signal (V)                                                           *
*       HWV.....Hot-wire signal (V)                                                                 *
*       LVV.....LVDT signal (V)                                                                     *
*       TTV.....Total Temperature signal (V)                                                        *
*       OFFSDP.....Differential Pressure offset (V)                                                 *
*       OFFSLV.....LVDT offset                                                                      *
*       DPAVG.....Average Differential Pressure signal (V)                                          *
*       PTAVG.....Average Total Pressure signal (V)                                                 *
*       HWVAVG.....Average Hot-wire signal (V)                                                      *
*       LVVAVG.....Average LVDT signal (V)                                                          *
*       TTVAVG.....Average Total Temperature (V)                                                    *
*       PTPSIG.....Total Pressure (psig)                                                            *
*       PTKPA.....Total Pressure (kPa)                                                              *
*       DP.....Differential Pressure (kPa)                                                          *
*       PSKPA.....Static Pressure (kPa)                                                             *
*       TT.....Total Temperature (°C)                                                               *
*       M.....Mach number                                                                           *
*       TSK.....Static temperature (K)                                                              *
*       TMK.....Mean Temperature (K)                                                                *
*       TW.....Hot-wire operating temperature                                                       *
*       K.....Thermal conductivity (W/m K)                                                          *
*       VIS.....Dynamic viscosity (Pa s)                                                            *
*       NUAPP.....Nusselt approximation                                                             *
*       UFS.....Free-stream velocity                                                                *
*       G.....Specific heat ratio                                                                   *
*       R.....Universal gas constant (kJ/kg K)                                                      *
*       RHO.....Density (kg/m^3)                                                                    *
*       RHOU.....Velocity-density combination                                                       *
```

```
*       TIME.....(s)                                                                    *
*       DIS.....Distance traversed (in)                                                 *
*********************************************************************************************************

      PROGRAM HWDAT
      REAL PMB,PATM,DPVSUM,PTVSUM,HWVSUM,LVVSUM,
     $TTVSUM,DPV,PTV,HWV,LVV,TTV,OFFSDP,OFFSLV,
     $DPVAVG,PTVAVG,HWVAVG,LVVAVG,TTVAVG,PTPSIG,PTKPA,DP,PSKPA,
     $DIS,TT,M,TSK,TW,K,TMK,VIS,RHO,NUAPP,UFS,G,R,RHOU,TIME

*********************************************************************************************************
*       Opening input data files and creating output files                              *
*********************************************************************************************************

      OPEN (UNIT=3,FILE='Differential Pressure Filename')
      OPEN (UNIT=4,FILE='Total Pressure Filename')
      OPEN (UNIT=7,FILE='Hot-wire Filename')
      OPEN (UNIT=8,FILE='LVDT Filename')
      OPEN (UNIT=9,FILE='Total Temperature Filename')
      OPEN (UNIT=15,FILE='Output File 1')
      OPEN (UNIT=16,FILE='Output File 2')
      OPEN (UNIT=17,FILE='Output File 3')

*********************************************************************************************************
*       Input atmospheric pressure in millibars for run day, differential pressure offset,  *
*       LVDT offset.                                                                    *
*********************************************************************************************************

      WRITE(*,*)'INPUT ATMOSPHERIC PRESSURE'
      READ(*,*) PMB
      WRITE(*,*)'INPUT DIFFERENTIAL PRESSURE OFFSET'
      READ(*,*) OFFSDP
      WRITE(*,*)'INPUT LVDT OFFSET'
      READ(*,*) OFFSLV

*********************************************************************************************************
*       Define properties of air and hot-wire                                           *
*********************************************************************************************************

      PATM = PMB*(1E5/(1000.0*1000.0))
      TW = 250.0
      G = 1.4
      R = 287.

*********************************************************************************************************
*       Do loop to read ASCII files and convert voltage signals into meaningful results.  *
*       The length of the loop may be changed to fit a particular file length.          *
*********************************************************************************************************

      DO 10 I = 0, 3275
       DPVSUM = 0.0
```

```
      PTVSUM = 0.0
      HWVSUM = 0.0
      LVVSUM = 0.0
      TTVSUM = 0.0
      TIME = 0.004*I

*****************************************************************************************************
*       Do loop to calculate the average signals over a short duration of time, before      *
*       preceeding to the other calculations.                                               *
*****************************************************************************************************

      DO 20 J = 1,20
        READ(3,*) DPV
        READ(4,*) PTV
        READ(7,*) HWV
        READ(8,*) LVV
        READ(9,*) TTV
        DPVSUM = DPVSUM + DPV + OFFSDP
        PTVSUM = PTVSUM + PTV
        HWVSUM = HWVSUM + HWV
        TTVSUM = TTVSUM + TTV
        LVVSUM = LVVSUM - LVV + OFFSLV
20    CONTINUE

*****************************************************************************************************
*       Calcuation of the average signals for the various inputs.  These will be used to    *
*       determine the other unknowns.                                                       *
*****************************************************************************************************

     DPVAVG = DPVSUM/20.0
     PTVAVG = PTVSUM/20.0
     HWVAVG = HWVSUM/20.0
     TTVAVG = TTVSUM/20.0
     LVVAVG = LVVSUM/20.0

*****************************************************************************************************
*       Conversion equations for voltage signals                                            *
*****************************************************************************************************

          PTPSIG = -25.1976939 + 25.0938973*PTVAVG
          PTKPA = PATM + PTPSIG*101.325/14.7
          DP = (DPVAVG/2.0)*101.325/14.7
          PSKPA = PTKPA - (DP)
          TT = TTVAVG*0.251718*1000 + 2.040301
          M = (((PTKPA/PSKPA)**((G-1.)/G) -1.)*(2./(G-1)))**.5
          TSK = (TT + 273.15)/(1. + ((G-1.)/2.)*(M**2.))
          TMK = ((TW + 273.15) + TSK)/2.
          K = 2.414E-2*((TMK/273.16)**1.5)*(473.16/(TMK + 200.))
          VIS = 1.716E-5*((TMK/273.16)**1.5)*(383.716/(TMK+110.556))
          RHO = (PSKPA*1000.)/(R*TSK)
          UFS = M*((G*R*TSK)**.5)
```

```
      DIS = -0.196656536E-1 + 0.885677135*LVVAVG
      NUAPP =(((HWVAVG**2)/K)/(TMK - TSK))*((TMK/TSK)**(-.17))

*****************************************************************************************************
*       Calibration equation obtained from the use of program HWCAL.FOR and a                      *
*       least squares line fitting program (FARNSFIT).                                             *
*****************************************************************************************************

      RHOU = ((3012.718795*NUAPP-1165.61744)**(1/0.51))*VIS

*****************************************************************************************************
*       Writing to output files opened above                                                       *
*****************************************************************************************************

   WRITE(15,30) DIS,UFS,RHO,RHOU
   WRITE(16,35) TIME,TT,PTKPA,M
   WRITE(17,40) DIS,RHOU
30  FORMAT(1X,F8.6,4X,F11.6,4X,F11.6,5X,F11.6)
35  FORMAT(1X,F6.3,4X,F11.6,5X,F11.6,4X,F10.8)
40  FORMAT(1X,F8.6,5X,F11.6)
10  CONTINUE
   END
```

```
**********************************************************************************************
*       VELTUR.FOR                                                                           *
*       Written by Jamie H. Hale                                                             *
*       Date 10/10/95                                                                        *
*                                                                                            *
*       The following program uses the results produced from the program HWDAT.FOR           *
*       and calculates the Turbulence intensity. The program reads in 2048 points and        *
*       calculates the turbulence for this set of data. This was done because the mean       *
*       velocity changes during the run (traverse).                                          *
*                                                                                            *
*       Variables used are:                                                                  *
*                                                                                            *
*       VEL.....Velocity (m/s)                                                               *
*       VELP.....Fluctuating component of velocity (m/s)                                     *
*       VELPS.....Fluctuating component of velocity squared (m/s)^2                          *
*       LV.....Distance (in)                                                                 *
*       VELSUM.....Sum of Velocitiy over 2048 points                                         *
*       VELAVG.....Average velocity over 2048 points                                         *
*       VLPSUM.....Sum of the squared fluctuating components (m/s)^2                         *
*       VLPAVG.....Average of the squared fluctuating components (m/s)^2                     *
*       TURB.....Turbulence intensity (RMS/Average)                                          *
*       RMS.....Root Mean Square                                                             *
*       LVSUM.....Sum of the LVDT signal (V)                                                 *
*       LVAVG.....Average LVDT signal (V)                                                    *
*       LVV.....LVDT signal (V)                                                              *
**********************************************************************************************

    PROGRAM VELTUR
    REAL VEL(2048),VELP(2048),VELPS(2048),LV(2048)
    REAL VELSUM,VELAVG,VLPSUM,VLPAVG,TURB1,RMS,LVSUM,LVAVG,LVV

**********************************************************************************************
*       Opening input files and creating output file                                         *
**********************************************************************************************

    OPEN (3,FILE='Velocity Filename')
    OPEN (4,FILE='LVDT Filename')
    OPEN (UNIT=18,FILE='Output Filename')

**********************************************************************************************
*       Outer do loop, this is dependent upon the input file size. For the case shown the    *
*       program will return 100 values of the turbulence intensity.                          *
**********************************************************************************************

    DO 10 I = 1, 100
    VELSUM = 0.0
    VELAVG = 0.0
    LVSUM = 0.0
    LVAVG = 0.0
```

```
*****************************************************************************************************
*       This do loop determines the number of data points to be read at a particular time.  *
*       The case below reads in 2048 points.  The input files are opened.  Each of the     *
*       velocity components are stored in memory and the average velocity is               *
*       determined.                                                                        *
*****************************************************************************************************

      DO 20 J = 1,2048
      READ(3,*) VELV
      READ(4,*) LVV
       VEL(J)=VELV
       VELSUM = VELSUM +VEL(J)
       LV(J)=-0.196656536E-1 + 0.885677135*(-LVV)
       LVSUM = LVSUM + LV(J)
20  CONTINUE
       VELAVG = VELSUM/2048.0
       VLPSUM = 0.0
       VLPAVG = 0.0
       LVAVG = LVSUM/2048.0

*****************************************************************************************************
*       This loop calcuates the fluctuating component of the velocity, then squares the    *
*       component, and determines an average for this component.  The RMS value            *
*       and turbulence intensity are then calculated.                                      *
*****************************************************************************************************

            DO 30 J = 1,2048
             VELP(J) = VEL(J) - VELAVG
             VELPS(J) = VELP(J)**2
             VLPSUM = VLPSUM + VELPS(J)
30  CONTINUE
       VLPAVG = VLPSUM/2048.0
       TURB = ((VLPAVG**.5)/VELAVG)*100.0
       RMS=VLPAVG**.5

*****************************************************************************************************
*       Writing to the output file opend above                                             *
*****************************************************************************************************

       WRITE(15,35)LVAVG,RMS,VELAVG,VLPSUM,TURB
35     FORMAT(1X,F8.6,1X,E14.7,1X,F11.7,1X,F11.7,1X,F11.7)
10  CONTINUE
    STOP
    END
```

```
*****************************************************************************************************
*       HFLUX.FOR                                                                                   *
*       Writtten by Jamie H. Hale                                                                   *
*       Date 10/28/95                                                                               *
*                                                                                                   *
*       This program is designed to calculate heat flux and surface temperature for                 *
*       four HFM-6 gages and total temperature.  The file opens four heat flux files,               *
*       four RTS files, and a total temperature file.  The results are writtten to two output       *
*       files.  For the case shown the program calculates 4094 values.                              *
*                                                                                                   *
*       Variables used are:                                                                         *
*                                                                                                   *
*       1.....Variable is associated with gage 1                                                    *
*       2.....Variable is associated with gage 2                                                    *
*       3.....Variable is associated with gage 3                                                    *
*       4.....Variable is associated with gage 4                                                    *
*       HF_V.....Heat Flux voltage (V)                                                              *
*       RTS_V.....Surface Temperature voltage (V)                                                   *
*       Q_.....Heat Flux (W/cm2)                                                                    *
*       TSUR_.....Surface Temperature (°C)                                                          *
*       SENS_.....Gage Sensitivity                                                                  *
*       TT.....Total Temperature (°C)                                                               *
*       TTV.....Total Temperature voltage                                                           *
*       HF_OFF.....Heat Flux offset acquired at beginning of run (V)                                *
*       RTS_OFF.....Surface Temperature offset acquired at beginning of day (V)                     *
*       RES_.....RTS ambient resistance (measured beginning of day)                                 *
*       GRTS_.....Surface Temperature gain setting for amplifier                                    *
*       GHFS_.....Heat Flux gain setting for amplifier                                              *
*       TIME..... (s)                                                                               *
*****************************************************************************************************

      PROGRAM HFLUX
      DIMENSION HF1V(4094),HF2V(4094),HF3V(4094),HF4V(4094),RTS1V(4094),
     &RTS2V(4094),RTS3V(4094),RTS4V(4094),Q1(4094),Q2(4094),Q3(4094),
     &Q4(4094),TSUR1(4094),TSUR2(4094),TSUR3(4094),TSUR4(4094),
     &SENS1(4094),SENS2(4094),SENS3(4094),SENS4(4094),TT(4094),TTV(4094)
      REAL HF1OFF,HF2OFF,HF3OFF,HF4OFF,RTS1OF,RTS2OF,RTS3OF,RTS4OF,
     &RES1,RES2,RES3,RES4,I,TIME

*****************************************************************************************************
*       Opening ASCII files.  Data is in one column.  Creating two output files.  File one          *
*       contains information for gages 1 and 2, and file two contains information for               *
*       gages 3 and 4.                                                                              *
*****************************************************************************************************

      OPEN (UNIT=2,FILE='Heat Flux Gage 1 Filename')
      OPEN (UNIT=3,FILE='Heat Flux Gage 2 Filename')
      OPEN (UNIT=4,FILE='Heat Flux Gage 3 Filename')
      OPEN (UNIT=7,FILE='Heat Flux Gage 4 Filename')
      OPEN (UNIT=8,FILE='Surface Temperature Gage 1 Filename')
      OPEN (UNIT=9,FILE='Surface Temperature Gage 2 Filename')
```

```
      OPEN (UNIT=10,FILE='Surface Temperature Gage 3 Filename')
      OPEN (UNIT=11,FILE='Surface Temperature Gage 4 Filename')
      OPEN (UNIT=12,FILE='Total Temperature Filename')
      OPEN (UNIT=13,FILE='Output Filename 1'')
      OPEN (UNIT=14,FILE='Output Filename 2'')

*****************************************************************************************************
*       Assignment of input filename with correct variable.                                         *
*****************************************************************************************************

      READ (2,*) HF1V
      READ (3,*) HF2V
      READ (4,*) HF3V
      READ (7,*) HF4V
      READ (8,*) RTS1V
      READ (9,*) RTS2V
      READ (10,*) RTS3V
      READ (11,*) RTS4V
      READ (12,*) TTV

*****************************************************************************************************
*       The heat flux values must be changed for each run.  The RTS offsets are the                 *
*       same for a particular day and the resistance values are the same for runs                   *
*       conducted on the same day.  The values for the gains are dependent upon the                 *
*       particular amplifier employed.  Typical values used for these variables are listed          *
*       beside the variables below.                                                                 *
*****************************************************************************************************

      I =100E-6
      HF1OFF=0.0075
      HF2OFF=0.04375
      HF3OFF=0.01775
      HF4OFF=-0.02775
      RTS1OF=0.009
      RTS2OF=0.042
      RTS3OF=0.042
      RTS4OF=0.035
      RES1=164.9
      RES2=174.5
      RES3=157.1
      RES4=90.6
      GRTS1=200.17
      GHF1=1012.0
      GRTS2=493.48
      GHF2=1036.0
      GRTS3=495.7
      GHF3=993.7
      GRTS4=496
      GHF4=1000.0

*****************************************************************************************************
*       Do loop used to calculate heat flux, surface temperature, and total temperature.            *
```

```
*       Each gage has a different surface temperature calibration equation and          *
*       calibrated sensitivity equation.  For different gages these equations would have to*
*       be modified.                                                                    *
*************************************************************************************************
    DO 4 J=1,4094
      TIME = .02*J -.02
      TSUR1(J)=2.9528*(((RTS1V(J)-RTS1OF)/(I*GRTS1))+RES1)-460.02
      TSUR2(J)=2.80929*(((RTS2V(J)-RTS2OF)/(I*GRTS2))+RES2)-463.673
      TSUR3(J)=3.2683*(((RTS3V(J)-RTS3OF)/(I*GRTS3))+RES3)-486.07
      TSUR4(J)=4.8765*(((RTS4V(J)-RTS4OF)/(I*GRTS4))+RES4)-415.47
      SENS1(J)=0.029*TSUR1(J) + 16.22
      SENS2(J)=0.0338*TSUR2(J) + 15.5
      SENS3(J)=0.035*TSUR3(J) + 21.33
      SENS4(J)=0.0355*TSUR4(J) + 23.09
      Q1(J)=((HF1V(J)-HF1OFF)*1E6)/(GHF1*SENS1(J))
      Q2(J)=((HF2V(J)-HF2OFF)*1E6)/(GHF2*SENS2(J))
      Q3(J)=((-HF3V(J)+HF3OFF)*1E6)/(GHF3*SENS3(J))
      Q4(J)=((-HF4V(J)+HF4OFF)*1E6)/(GHF4*SENS4(J))
       TT(J)=TTV(J)*0.251718*1000 +2.040301

*************************************************************************************************
*       Writing to output files opened above                                            *
*************************************************************************************************

       WRITE(13,30)TIME,Q1(J),TSUR1(J),TT(J),Q2(J),TSUR2(J)
       WRITE(14,30)TIME,Q3(J),TSUR3(J),TT(J),Q4(J),TSUR4(J)
30      FORMAT(1X,F6.3,1X,F8.5,1X,F8.5,1X,F8.5,1X,F8.5,1X,F8.5)
35      FORMAT(1X,F6.3,1X,F8.5,1X,F8.5,1X,F8.5,1X,F8.5,1X,F8.5)
4     CONTINUE
     STOP
     END
```

```
*****************************************************************************************************
*       HFTURB.FOR                                                                                  *
*       Written by Jamie H. Hale                                                                    *
*       Date 11/17/95                                                                               *
*                                                                                                   *
*       The following program is designed to calculate the turbulence intensity based on            *
*       the heat flux signal.  The program opens the files for four heat flux signals and           *
*       calculates a Tuq value every 2048 points.  The average heat flux signal                     *
*       diminishes during a run, therefore, calculating the turbulence intensity over a             *
*       short period of time and then averaging all these values produces better results            *
*       than determing one value for the entire run.  All quantities are in volts (V).              *
*                                                                                                   *
*       Variables used are:                                                                         *
*                                                                                                   *
*       1.....Variable is associated with gage 1                                                    *
*       2.....Variable is associated with gage 2                                                    *
*       3.....Variable is associated with gage 3                                                    *
*       4.....Variable is associated with gage 4                                                    *
*       Q_.....Heat Flux signal                                                                     *
*       Q_P.....Fluctuating component of heat flux                                                  *
*       Q_PS.....Fluctuating component of heat flux squared                                         *
*       Q_SUM.....Sum of heat flux signal over a distinct time (2048 points)                        *
*       Q_AVG.....Average heat flux signal over a distinct time (2048 points)                       *
*       Q_PSUM.....Sum of the squared fluctuating components                                        *
*       Q_PAVG.....Average of the squared fluctuating components                                    *
*       TURB_.....Turbulence intensity based on heat flux signal                                    *
*       RMSS_.....Root mean square value squared                                                    *
*       RMSUM_.....Sum of the root mean square for entire run                                       *
*       RMS_.....Root mean square for entire run                                                    *
*****************************************************************************************************

      PROGRAM HFTURB
     REAL Q1(2048),Q1P(2048),Q1PS(2048),Q2(2048),Q2P(2048),Q2PS(2048),
     &    Q3(2048),Q3P(2048),Q3PS(2048),Q4(2048),Q4P(2048),Q4PS(2048),
     &    Q1SUM,Q1AVG,Q1PSUM,Q1PAVG,Q2SUM,Q2AVG,Q2PSUM,Q2PAVG,
     &    Q3SUM,Q3AVG,Q3PSUM,Q3PAVG,Q4SUM,Q4AVG,Q4PSUM,Q4PAVG,TURB1,
     &    TURB2,TURB3,TURB4,RMSS1(100),RMSS2(100),RMSS3(100),RMSS4(100),
     &    RMSUM1,RMSUM2,RMSUM3,RMSUM4,RMS1,RMS2,RMS3,RMS4

*****************************************************************************************************
*       Opening heat flux ASCII files. The files contain data that is listed in a single            *
*       column.  Creating output files.                                                             *
*****************************************************************************************************

     OPEN (3,FILE='Heat Flux Gage 1 Filename')
     OPEN (4,FILE='Heat Flux Gage 2 Filename')
     OPEN (7,FILE='Heat Flux Gage 3 Filename')
     OPEN (8,FILE='Heat Flux Gage 4 Filename')
     OPEN (UNIT=15,FILE='Output Filename for Gage 1 Results')
     OPEN (UNIT=16,FILE='Output Filename for Gage 2 Results')
     OPEN (UNIT=17,FILE='Output Filename for Gage 3 Results')
```

```
      OPEN (UNIT=18,FILE='Output Filename for Gage 4 Results')

*****************************************************************************************************
*       Outer do loop, this is dependent upon the input file size.  For the case shown the  *
*       program will return 100 values of the turbulence intensity based on the heat        *
*       flux signal.  Initializing zeroes for the average and summation variables.          *
*****************************************************************************************************

      DO 10 I = 1, 100
      Q1SUM = 0.0
      Q1AVG = 0.0
      Q2SUM = 0.0
      Q2AVG = 0.0
      Q3SUM = 0.0
      Q3AVG = 0.0
      Q4SUM = 0.0
      Q4AVG = 0.0

*****************************************************************************************************
*       This do loop determines the number of data points to be read at a particular time.  *
*       The case below reads in 2048 points.  The input files are opened.  Each of the      *
*       heat flux components are stored in memory and the summation of the various          *
*       components is determined.                                                           *
*****************************************************************************************************

      DO 20 J = 1,2048
        READ(3,*) Q1V
        READ(4,*) Q2V
        READ(7,*) Q3V
        READ(8,*) Q4V
          Q1(J)=Q1V
          Q1SUM = Q1SUM + Q1(J)
          Q2(J)=Q2V
          Q2SUM = Q2SUM + Q2(J)
          Q3(J)=-Q3V
          Q3SUM = Q3SUM + Q3(J)
          Q4(J)=-Q4V
          Q4SUM = Q4SUM + Q4(J)
20    CONTINUE

*****************************************************************************************************
*       The average heat flux is determined for this particular time range.  Initializing   *
*       zeroes for the summation and average fluctuating components.                        *
*****************************************************************************************************

          Q1AVG = Q1SUM/2048.0
          Q1PSUM = 0.0
          Q1PAVG = 0.0
          Q2AVG = Q2SUM/2048.0
          Q2PSUM = 0.0
          Q2PAVG = 0.0
```

```
      Q3AVG = Q3SUM/2048.0
      Q3PSUM = 0.0
      Q3PAVG = 0.0
      Q4AVG = Q4SUM/2048.0
      Q4PSUM = 0.0
      Q4PAVG = 0.0

*****************************************************************************************************
*     This loop calcuates the fluctuating component of the heat flux, then squares the      *
*     component, and sums the squared fluctuating components over this particular      *
*     time period.  For the case shown over 2048 data points which corresponds to      *
*     0.02 seconds for a 100 kHz sampling frequency.                                   *
*****************************************************************************************************

        DO 30 J = 1,2048
            Q1P(J) = Q1(J) - Q1AVG
            Q1PS(J) = Q1P(J)**2
            Q1PSUM = Q1PSUM + Q1PS(J)
            Q2P(J) = Q2(J) - Q2AVG
            Q2PS(J) = Q2P(J)**2
            Q2PSUM = Q2PSUM + Q2PS(J)
            Q3P(J) = Q3(J) - Q3AVG
            Q3PS(J) = Q3P(J)**2
            Q3PSUM = Q3PSUM + Q3PS(J)
            Q4P(J) = Q4(J) - Q4AVG
            Q4PS(J) = Q4P(J)**2
            Q4PSUM = Q4PSUM + Q4PS(J)
30  CONTINUE

*****************************************************************************************************
*     Determination of the turbulence intensity based on the heat flux.                *
*****************************************************************************************************

      Q1PAVG = Q1PSUM/2048.0
      TURB1 = ((Q1PAVG**.5)/Q1AVG)*100.0
      RMSS1(I)=Q1PAVG
      Q2PAVG = Q2PSUM/2048.0
      TURB2 = ((Q2PAVG**.5)/Q2AVG)*100.0
      RMSS2(I)=Q2PAVG
      Q3PAVG = Q3PSUM/2048.0
      TURB3 = ((Q3PAVG**.5)/Q3AVG)*100.0
      RMSS3(I)=Q3PAVG
      Q4PAVG = Q4PSUM/2048.0
      TURB4 = ((Q4PAVG**.5)/Q4AVG)*100.0
      RMSS4(I)=Q4PAVG

*****************************************************************************************************
*     Writing to output files opend above                                              *
*****************************************************************************************************

      WRITE(15,35)RMSS1(I),Q1AVG,Q1PSUM,TURB1
```

```
      WRITE(16,35)RMSS2(I),Q2AVG,Q2PSUM,TURB2
      WRITE(17,35)RMSS3(I),Q3AVG,Q3PSUM,TURB3
      WRITE(18,35)RMSS4(I),Q4AVG,Q3PSUM,TURB4
35      FORMAT(1X,E14.7,1X,F11.7,1X,F11.7,1X,F11.7)
10  CONTINUE

*****************************************************************************************************
*       Initializing zero for the summation of the root mean square variable.                       *
*****************************************************************************************************

    RMSUM1=0.0
    RMSUM2=0.0
    RMSUM3=0.0
    RMSUM4=0.0

*****************************************************************************************************
*       Loop to sum the individual Root Mean Square values calculated by the program               *
*       which were stored in memory.  The summed value is then divided by the number               *
*       of values to determine on value for the entire run.  For this case the number or           *
*       values was 100.                                                                             *
*****************************************************************************************************
    DO 40 N=1,100
    RMSUM1=RMSUM1 + RMSS1(N)
    RMSUM2=RMSUM2 + RMSS2(N)
    RMSUM3=RMSUM3 + RMSS3(N)
    RMSUM4=RMSUM4 + RMSS4(N)
40  CONTINUE
    RMS1=RMSUM1**0.5/100.0
    RMS2=RMSUM2**0.5/100.0
    RMS3=RMSUM3**0.5/100.0
    RMS4=RMSUM4**0.5/100.0

*****************************************************************************************************
*       Output is written to the screen                                                             *
*****************************************************************************************************

    WRITE(*,*) RMS1,RMS2,RMS3,RMS4
   STOP
   END
```

```
************************************************************************************************
*       PSUR.FOR                                                                               *
*       Written by Jamie H. Hale                                                               *
*       Date 11/14/95                                                                          *
*                                                                                              *
*       This program is designed to calculate the surface pressure along a turbine             *
*       from Kulite signals which are inserted into the blade at various locations on the      *
*       suction and pressure surfaces. The file opens four Kulite files. The results are       *
*       written to two output files. For the case shown the program calculates 4094            *
*       values.                                                                                *
*                                                                                              *
*       Variables used are:                                                                    *
*                                                                                              *
*       1.....Variable is associated with Kulite 1                                             *
*       2.....Variable is associated with Kulite 2                                             *
*       3.....Variable is associated with Kulite 3                                             *
*       4.....Variable is associated with Kulite 4                                             *
*       KL_.....Kulite signal (V)                                                              *
*       PTV.....Total Pressure signal (V)                                                      *
*       PSUR_.....Surface Pressure (psi)                                                       *
*       PTPSIG.....Total Pressure (psig)                                                       *
*       TIME.....(s)                                                                           *
*       PATM.....Atmospheric Pressure (psi)                                                    *
*       PMB.....Atmospheric Pressure (mb)                                                      *
*       GKUL.....Kulite amplifier gain setting
************************************************************************************************

  PROGRAM PSUR
   REAL KL1V(4094),KL2V(4094),KL3V(4094),KL4V(4094),
  &PTV(4094),PSUR1(4094),PSUR2(4094),PSUR3(4094),
  &PSUR4(4094),PTPSIG(4094),TIME

************************************************************************************************
*       Opening ASCII files. Data is in one column. Creating two output files. File one        *
*       contains information for gages 1 and 2, and file two contains information for          *
*       gages 3 and 4.                                                                         *
************************************************************************************************

    OPEN (UNIT=2,FILE='C:\USERS\JAMIE\KULRUNS\RUN23\KL1R23.ASC')
    OPEN (UNIT=3,FILE='C:\USERS\JAMIE\KULRUNS\RUN23\KL2R23.ASC')
    OPEN (UNIT=4,FILE='C:\USERS\JAMIE\KULRUNS\RUN13\KL3R13.ASC')
    OPEN (UNIT=7,FILE='C:\USERS\JAMIE\KULRUNS\RUN13\KL4R13.ASC')
    OPEN (UNIT=8,FILE='C:\USERS\JAMIE\KULRUNS\RUN23\PTR23.ASC')
    OPEN (UNIT=14,FILE='C:\USERS\JAMIE\KULRUNS\RUN23\PSUR23.DAT')
    OPEN (UNIT=15,FILE='C:\USERS\JAMIE\KULRUNS\RUN23\PSUR23.DAT')

************************************************************************************************
*       Assignment of input filename with correct variable.                                    *
************************************************************************************************

     READ (2,*) KL1V
```

```
      READ (3,*) KL2V
      READ (4,*) KL3V
      READ (7,*) KL4V
      READ (8,*) PTV

*****************************************************************************************************
*       The following values must be changed to meet test conditions.  Atmospheric      *
*       pressure changes and the gain may be set at different values on the amplifier.   *
*****************************************************************************************************
       PMB =945.3
       PATM = PMB*(1E5/(1000.0*1000.0))*(14.7/101.325)
       GKUL=50.0

*****************************************************************************************************
*       Do loop used to calculate surface pressure. Each gage has a different calibration *
*       equation.  For different gages these equations would have to be modified.         *
*****************************************************************************************************

     DO 4 J=1,4094
        TIME = J*.02 - .02
        PSUR1(J)=(KL1V(J)*1000.0)/(2.680*GKUL) + PATM
        PSUR2(J)=(KL2V(J)*1000.0)/(2.307*GKUL) + PATM
        PSUR3(J)=(KL3V(J)*1000.0)/(1.541*GKUL) + PATM
        PSUR4(J)=(KL4V(J)*1000.0)/(2.411*GKUL) + PATM
        PTPSIG(J) = 25.0938973*PTV(J) - 25.1976939  + PATM

*****************************************************************************************************
*       Writing to output files opened above                                              *
*****************************************************************************************************

       WRITE(14,30)TIME,PSUR1(J),PSUR2(J),PTPSIG(J)
       WRITE(15,30)TIME,PSUR3(J),PSUR4(J),PTPSIG(J)
30     FORMAT(1X,F6.3,1X,F8.5,1X,F8.5,1X,F8.5,1X,F8.5)
4      CONTINUE
      STOP
      END
```

```
10 '*********************************************************************
20 '*       Program NEWOSR.BAS                                          *
30 '*       A/D Block Scan Mode and PSI Pressure Measurement*
40 '* MetraByte Corp. & PSI                Rev. 2.00  7-12-87     *
50 '* with Todd Bushlow, Fei T. Kwok, and R. L. Campbell          *
60 '*                                                               *
70 '*********************************************************************
80 '
90 CLEAR, 59000! 'reduce workspace to 48K
100 SCREEN 0,0,0 : CLS : KEY OFF : WIDTH 80
110 DIM A$(30),B$(30),TU$(30),TD$(30),TRAV(1000)
120 FALSE=0:TRUE=NOT FALSE:XOFF$=CHR$(19):XON$=CHR$(17)
130 CLOSE
140 DEF SEG:WIDTH "COM1:",255:DEF SEG
150 CM$="COM1:9600,N,8,1"
160 OPEN CM$ AS #1
170 PAUSE=FALSE
180 B$=CHR$(13):GOSUB 3980:GOSUB 3980
190 PRINT:PRINT "Reset PSI system"
250 'INPUT "Enter traverse UP command";TU$
260 TU$="V40 D840 Z1 R1 V50 D840 Z0 R1
270 'INPUT "Enter traverse DOWN command";TD$
280 B$=TU$+CHR$(13):GOSUB 3980 'send traverse up command
1050 GOSUB 2590    ' setup psi system  I1,C1,F1
1070 PRINT:PRINT "Hit any key to begin. . ."
1080 IF INKEY$="" THEN 1080
1200 B$="Y1":GOSUB 3980:PRINT:PRINT "Traverse up"   'start traverse up
1340 PRINT "PSI system taking data. . ."
1470 GOSUB 3180  'set PSI system going  D2
1690 PRINT:PRINT "Collecting . . ."
1810 CLOSE #1 'close COM1: file
2120 '
2130 '---------------- STEP 12 ----------------------------------------
2140 'Receive pressure data from PSI system
2150 GOSUB 3830  ' service request  SRQ
2160 GOSUB 3330  ' psi data reduction  F2
2170 GOSUB 3400  ' write out psi data to file  O6
2180 '
2190 END
2560 '
2570 '=============== PSI SUBROUTINES ==================================
2580 '
2590 IBINIT1 = 59000!
2600 IBINIT2 = 59003!
2610 BLOAD "bib.m",IBINIT1
2620 CALL
IBINIT1(IBFIND,IBTRG,IBCLR,IBPCT,IBSIC,IBLOC,IBPPC,IBBNA,IBONL,IBRSC,IBSRE,IBRSV,I
BPAD,IBSAD,IBIST,IBDMA,IBEOS,IBTMO,IBEOT,IBRDF,IBWRTF)
2630 CALL
IBINIT2(IBGTS,IBCAC,IBWAIT,IBPOKE,IBWRT,IBWRTA,IBCMD,IBCMDA,IBRD,IBRDA,IBSTOP,
IBRPP,IBRSP,IBDIAG,IBXTRC,IBRDI,IBWRTI,IBRDIA,IBWRTIA,IBSTA%,IBERR%,IBCNT%)
```

```
2640 DIM J(5),K(3),BYTE(3),CAL(3,112),COEFF(3,112),PARAMETER(21)
2650 DIM PERIOD(18),VOLTS(3,112)
2660 DIM BUFFER$(40)
2670 A1%=10: A2%=0: A3%=0 : A4%=0 : A5%=0 : A6%=0
2680 B%=8
2690 C=.0001 : D%=25: E=.01: F%=3 : G%=5: H%=3
2700 CH=A1%+A2%+A3%+A4%+A5%+A6% : SEN=CH/G% : BITS%=14
2710 BOARD$="DACU" : CALL IBFIND(BOARD$,DACU%)
2720 CLS : PRINT "780B SYSTEM TEST" : PRINT
2730 INPUT "Total time (sec)";TIME
2740 INPUT "Number of data frames averaged per measurement set ";B%
2750 INPUT "Number of measurement sets";D%
2752 IF D%>255 THEN PRINT" D% IS TOO BIG": GOTO 2720
2755 INPUT "time for taking one measurement set (sec)";MTIME
2760 TSET = TIME/ D%
2770 E%=INT((TSET-MTIME)/.01)
2775 IF E%<1 THEN PRINT" E% < 1   CHECK INITIALIZATION" : GOTO 2720
2776 IF E%>9999 THEN PRINT" E% BIG,  CHECK INITIALIZATION" : GOTO 2720
2780 T1=A1%*.0001
2790 C%=INT((MTIME-T1*B%)/B%/.00001)
2800 IF C%<1 THEN PRINT" C% < 1  CHECK INITIALIZATION": GOTO 2720
2810 IF C%>9999 THEN PRINT" C% BIG, CHECK INITIALIZATION": GOTO 2720
2820 PRINT"B%=";B%
2825 PRINT"C%=";C%
2830 PRINT"D%=";D%
2840 PRINT"E%=";E%
2850 PRINT:PRINT "Hit Enter to calibrate . . ."
2855 A$=INKEY$ : IF A$="" THEN 2855
2860 GOSUB 2930  'I1
2870 GOSUB 3110  'C1
2880 GOSUB 3260  'F1
2890 RETURN
2900 '$$$$$$$$$$$$$$$$$$$$$$$$$$$$$
2910 '$$$$$ I1:  Initialization $$$$$
2920 '$$$$$$$$$$$$$$$$$$$$$$$$$$$$$
2930 CMD$="I1" : GOSUB 3940
2940 PARAMETER(1)=INT(A1%/100) : PARAMETER(2)=A1%-INT(A1%/100)*100
2950 PARAMETER(3)=INT(A2%/100) : PARAMETER(4)=A2%-INT(A2%/100)*100
2960 PARAMETER(5)=INT(A3%/100) : PARAMETER(6)=A3%-INT(A3%/100)*100
2970 PARAMETER(7)=INT(A4%/100) : PARAMETER(8)=A4%-INT(A4%/100)*100
2980 PARAMETER(9)=INT(A5%/100) : PARAMETER(10)=A5%-INT(A5%/100)*100
2990 PARAMETER(11)=INT(A6%/100) : PARAMETER(12)=A6%-INT(A6%/100)*100
3000 PARAMETER(13)=B%
3010 PARAMETER(14)=INT(C%/100) : PARAMETER(15)=C%-INT(C%/100)*100
3020 PARAMETER(16)=D%
3030 PARAMETER(17)=INT(E%/100) : PARAMETER(18)=E%-INT(E%/100)*100
3040 PARAMETER(19)=F% : PARAMETER(20)=G% : PARAMETER(21)=H%
3050 OUTP$="I1" : CALL IBWRT(DACU%,OUTP$)
3060 FOR X=1 TO 21 : OUTP$=CHR$(PARAMETER(X)) : CALL IBWRT(DACU%,OUTP$)
3070 NEXT X: GOSUB 3950: RETURN
3080 '$$$$$$$$$$$$$$$$$$$$$$$$$$$$
```

```
3090 '$$$$$ C1:  Calibration $$$$$
3100 '$$$$$$$$$$$$$$$$$$$$$$$$$$$$
3110 CMD$="C1" : GOSUB 3940
3120 OUTP$="C1" : CALL IBWRT(DACU%,OUTP$)
3130 GOSUB 3830  'SRQ
3140 GOSUB 3950 : RETURN
3150 '$$$$$$$$$$$$$$$$$$$$$$$$$$$$$$$$$$$$$$$$
3160 '$$$$$ D2:  Average Data Acquisition $$$$$
3170 '$$$$$$$$$$$$$$$$$$$$$$$$$$$$$$$$$$$$$$$$
3180 CMD$="D2" : GOSUB 3940
3190 OUTP$="D2" : CALL IBWRT(DACU%,OUTP$)
3200 GOSUB 3750  'Trigger acquisition
3210 GOSUB 3950
3220 RETURN
3230 '$$$$$$$$$$$$$$$$$$$$$$$$$$$$$$$$$$
3240 '$$$$$ F1:  Cal Data Reduction $$$$$
3250 '$$$$$$$$$$$$$$$$$$$$$$$$$$$$$$$$$$
3260 CMD$="F1" : GOSUB 3940
3270 OUTP$="F1" : CALL IBWRT(DACU%,OUTP$)
3280 GOSUB 3830  'SRQ
3290 GOSUB 3950 : RETURN
3300 '$$$$$$$$$$$$$$$$$$$$$$$$$$$$$$$$$$$$$$$$
3310 '$$$$$ F2:  Acquisition Data Reduction $$$$$
3320 '$$$$$$$$$$$$$$$$$$$$$$$$$$$$$$$$$$$$$$$$
3330 CMD$="F2" : GOSUB 3940
3340 OUTP$="F2" : CALL IBWRT(DACU%,OUTP$)
3350 GOSUB 3830  'SRQ
3360 GOSUB 3950 : RETURN
3370 '$$$$$$$$$$$$$$$$$$$$$$$$$$$$$$$$
3380 '$$$$$ O6:  Input ASCII Data $$$$$
3390 '$$$$$$$$$$$$$$$$$$$$$$$$$$$$$$$$
3400 CMD$="O6" : GOSUB 3940
3410 OUTP$="O6" : CALL IBWRT(DACU%,OUTP$)
3420 PRINT:PRINT "Reading pressure data"
3430 GOSUB 3655  'input pressure data
3440 OPEN "a:PRSWRK" FOR INPUT AS #1
3445 OPEN "a:PRES" FOR OUTPUT AS #2
3446 IF EOF(1) THEN 3600
3450 PRES$=INPUT$(11,#1)
3460 WRITE #2,VAL(PRES$)
3470 GOTO 3446
3600 PRINT
3620 GOSUB 3950 : RETURN
3630 '$$$$$$$$$$$$$$$$$$$$$$$$$$$$$$$$$$$$$$$$$$$$$$$$$$$$$$$$$$$$$$$$$$$$$$$
3640 '$$$$$ DATA_INPUT:  Input Measurement Data From DACU $$$$$
3650 '$$$$$$$$$$$$$$$$$$$$$$$$$$$$$$$$$$$$$$$$$$$$$$$$$$$$$$$$$$$$$$$$$$$$$$$
3655 FLNAME$ = "a:prswrk"
3660 CALL IBRDF(DACU%,FLNAME$)
3710 PRINT:RETURN
3720 '$$$$$$$$$$$$$$$$$$$$$$$$$$$$$$$$$$$$$$$$
3730 '$$$$$ TRIGGER:  Initiate Acquisition $$$$$
```

```
3740 '$$$$$$$$$$$$$$$$$$$$$$$$$$$$$$$$$$$$$$$$$$
3750 IF H%<>7 THEN 3780
3760 PRINT "Press any key for SOFTWARE TRIGGER"
3770 IF INKEY$="" THEN 3770 ELSE CLS
3780 IF H%<=7 THEN OUTP$=CHR$(13) : CALL IBWRT(DACU%,OUTP$)
3790 RETURN
3800 '$$$$$$$$$$$$$$$$$$$$$$$$$$$$$$$$$$$$$$
3810 '$$$$$ SRQ:  DACU Service Request $$$$$
3820 '$$$$$$$$$$$$$$$$$$$$$$$$$$$$$$$$$$$$$$
3830 RQSWAIT%=&H800 : CALL IBWAIT(DACU%,RQSWAIT%)
3840 CALL IBRSP(DACU%,SPOLL%)
3850 IF SPOLL%-64 =13 THEN 3750
3860 RETURN
3870 '$$$$$$$$$$$$$$$$$$$$$$$$$$$$$$$$$$$$$$$$$$$$$$$$$$$$$$$$
3880 '$$$$$ EXTRACT-BYTE:  Extract data from GPIB input $$$$$
3890 '$$$$$$$$$$$$$$$$$$$$$$$$$$$$$$$$$$$$$$$$$$$$$$$$$$$$$$$$
3900 BUFLINE=0 : SEGMENT$=""
3910 IF STARTPOS > 255 THEN BUFLINE=BUFLINE+1 : STARTPOS=STARTPOS-255 : GOTO
3910
3920 FOR BUILDSEG=1 TO WANTLEN :
SEGMENT$=SEGMENT$+MID$(BUFFER$(BUFLINE),STARTPOS+BUILDSEG-1,1) : IF
STARTPOS+BUILDSEG=256 THEN BUFLINE=BUFLINE+1 : STARTPOS=1-BUILDSEG
3930 NEXT BUILDSEG : RETURN
3940 CXPOS=POS(0) : CYPOS=CSRLIN : LOCATE 1,60 : PRINT CMD$; : LOCATE
CYPOS,CXPOS : RETURN
3950 CXPOS=POS(0) : CYPOS=CSRLIN : LOCATE 1,60 : PRINT SPACE$(19); : LOCATE
CYPOS,CXPOS : RETURN
3960 'That's it
3970 '------------------------------------------------------------
3980 'TALK TO TRAVERSE
3990 FOR JJ=1 TO LEN(B$)
4000 PRINT #1,MID$(B$,JJ,1);
4010 IF EOF(1) THEN 4100
4020 IF LOC(1)>128 THEN PAUSE=TRUE:PRINT#1,XOFF$;
4030 A$=INPUT$(LOC(1),#1)
4040 FOR II=1 TO LEN(A$)
4050 A1$=MID$(A$,II,1)
4060 IF (ASC(A1$)<31 AND A1$<>CHR$(13)) OR A1$=CHR$(127) THEN 4100
4070 NEXT II
4080 IF LOC(1)>0 THEN 4100
4090 IF PAUSE THEN PAUSE=FALSE:PRINT#1,XON$;
4100 NEXT JJ
4110 RETURN
4120 '------------------------------------------------------------
4130 'Check input buffer
4140 IF EOF(1) THEN 4230
4150 IF LOC(1)>128 THEN PAUSE=TRUE:PRINT#1,XOFF$;
4160 A$=INPUT$(LOC(1),#1)
4170 FOR II=1 TO LEN(A$)
4180 A1$=MID$(A$,II,1)
4190 IF (ASC(A1$)<31 AND A1$<>CHR$(13)) OR A1$=CHR$(127) THEN 4230
```

```
4200 NEXT II
4210 IF LOC(1)>0 THEN 4230
4220 IF PAUSE THEN PAUSE=FALSE:PRINT#1,XON$;
4230 RETURN
```

# Appendix C

## Hot-Wire Anemometer Calibration

The first step in calibrating the hot wire is to set the controls on the IFA 100 flow analyzer. The cable operating resistance must be known. This is accomplished by placing a shorting plug into the probe support and measuring the resistance of the cable according to the IFA 100 manual. After determining the cable resistance the probe resistance at room temperature must then be determined. This is simply accomplished by replacing the shorting plug by the hot-wire anemometer probe and repeating the steps outlined in the manual. The recommended operating temperature for this particular probe was 250°C. Knowing the two resistances, the operating temperature, and the temperature coefficient, the operating resistance for the probe can be calculated from the following formula:

$$R_{op} = \left[1 + \alpha\left(T_m - T_r\right)\right] \cdot R_r \qquad [C1]$$

The operating resistance is know entered into the analyzer. For most of the hot-wires used in these experiments this produced overheat ratios of approximately 1.9. The gain is set at one and the offset is set at zero. The final setting for the analyzer is the filter setting, which for the calibration of the hot-wire is set a 20 Hz.

Two hot-wire anemometer probes were used in these experiments. The calibration conditions and all other pertinent data for calibrating the hot-wire is listed in Table C1 below.

**Table C1 Hot Wire Calibration Data**

| | Hot Wire Probe #1 | Hot Wire Probe #2 |
|---|---|---|
| Cable Resistance ($R_c$) | .593 Ω | .520 Ω |
| Probe Resistance ($R_r$) | 5.635 Ω | 4.536 Ω |
| Operating Resistance ($R_{op}$) | 11.007 Ω | 8.918 Ω |
| Reference Temperature ($T_r$) | 24°C | 20°C |
| Overheat Ratio | 1.95 | 1.96 |
| Atmospheric Pressure | 94.71 kPa | 94.89 kPa |

The general procedure to calibrate a hot-wire is to place the wire in a known velocity jet flow and adjust the hot-wire signal. This is achieved by adjusting the bridge and frequency compensation knobs on the analyzer while monitoring the response of a test square wave on an oscilloscope screen. Instead of placing the hot-wire in a jet flow the wire was placed in the wind tunnel test section. This was performed due to the fact that the velocity of the flow entering the test section is in excess of 100 m/s which approaches compressible conditions. The tunnel was run and the wire was adjusted using the above procedures until the desired frequency response was achieved.

The next step in the calibration process is to calibrate voltage from the hot-wire with the inlet velocity flow into the test section. To accomplish this the following data had to be recorded: hot-wire voltage, total temperature, total pressure, and static pressure. The LeCroy Waveform Recorder was used to acquire the above signals. The sampling rated used for this calibration was 50 Hz. The LeCroy set-up can be seen in Table C2. To reduce the data for the hot-wire calibration, a FORTRAN program, HWCAL, was written (refer to Appendix B). The first step is to calculate the Mach number from the given data utilizing the following formula:

$$M = \left[ \left( \left( \frac{P_t}{P_s} \right)^{\gamma - 1/\gamma} - 1 \right) \left( \frac{2}{\gamma - 1} \right) \right]^{1/2} \qquad [C2]$$

**Table C2 Hot-wire calibration (LeCroy set-up)**

| | Channel 1 | Channel 2 | Channel 3 | Channel 4 |
|---|---|---|---|---|
| **Name** | **Hot Wire (HW)** | **Differ. Press. (DP)** | **Total Press. (PT)** | **Total Temp. (TT)** |
| Full Scale V | 10 | 10 | 4 | .4 |
| Offset Volts | -2 | 0 | -2 | -.2 |
| Coupling | +DC | +DC | +DC | +DC |
| Segment Size | 4K | 4K | 4K | 4K |
| Period | 20 ms | 20 ms | 20 ms | 20 ms |

Once the Mach number has been calculated the static temperature can be determined

$$T_s = \frac{T_t}{\left( 1 + \left( \frac{\gamma - 1}{2} \right) M^2 \right)} \qquad [C3]$$

Certain air properties must be determined next. The thermal conductivity and the dynamic viscosity of the air are calculated from the following equations respectively:

$$k = 2.414x10^{-2} \left( \frac{T_f}{273.15} \right)^{3/2} \left( \frac{473.15}{T_f + 200} \right) \qquad [C4]$$

$$\mu = 1.716x10^{-5} \left( \frac{T_f}{273.15} \right)^{3/2} \left( \frac{383.716}{T_f + 110.556} \right) \qquad [C5]$$

where $T_f$ is the film temperature calculated from equation 3.16. The next step in the calibration process is to calculate the air density

$$\rho = \frac{P_s}{RT_s} \qquad [C6]$$

and then calculate the free-stream velocity

$$U_{fs} = M\sqrt{T_s R\gamma} \qquad [C7]$$

The next step in the process is to manipulate the data so that equation 3.18 can be used to create a calibration curve. To accomplish this, however, we must first approximate the Nusselt and Reynolds numbers. The following equations were taken from King (1959).

$$Nu = \frac{hd_w}{k} \qquad [C8]$$

The heat transfer coefficient for the flow over the wire can be calculated from the following formula:

$$h = \left( \frac{\left(V^2/R_w\right)}{\left(\pi d_w l_w\right)\left(T_f - T_s\right)} \right) \qquad [C9]$$

This means that the Nusselt number can be represented by the following equation:

$$Nu = \left( \frac{\left(V^2/R_w\right)}{\left(\pi d_w l_w\right)\left(T_f - T_s\right)} \right)\left(\frac{d_w}{k}\right) \qquad [C10]$$

The Reynolds number is represented by the ensuing equation

$$\mathrm{Re} = \frac{\rho U d_w}{\mu} \qquad [C11]$$

Equations C10 and C11 can now be substituted into equation 3.18 to yield the succeeding formula:

$$\left(\frac{\left(V^2 d_w / R_w k\right)}{\left(\pi d_w l_w\right)\left(T_f - T_s\right)}\right)\left(\frac{T_f}{T_s}\right)^{-0.17} = 0.48\left(\frac{\rho U d_w}{\mu}\right)^{0.51} \qquad [C12]$$

The preceding equation can be simplified into a simpler form if the subsequent assumptions are made. The wire length, diameter, and resistance are all a constant and can be removed from the equation. This in turn provides a new constant to be determined by performing the calibration. The resulting equation is as follows:

$$\left(\frac{\left(V^2/k\right)}{\left(T_f - T_s\right)}\right)\left(\frac{T_f}{T_s}\right)^{-0.17} = A\left(\frac{\rho U}{\mu}\right)^{0.51} + B \qquad [C13]$$

## RESULTS

The FORTRAN program, HWCAL, calculated the Nusselt and Reynolds number approximations as well as other pertinent information. The total pressure ($P_t$), the free-stream velocity ($U_{fs}$), the total temperature ($T_t$), and the density ($\rho$) was plotted for each of the calibration runs for the two separate hot-wire probes. These plots can be seen in the following pages (refer to Figures C1.1 through C4.2). Figures C1.1 and C1.2 show the variation of the free-stream velocity for the run. In each run the free-stream velocity approaches 130 m/s and stabilizes at this point before starting its descent.

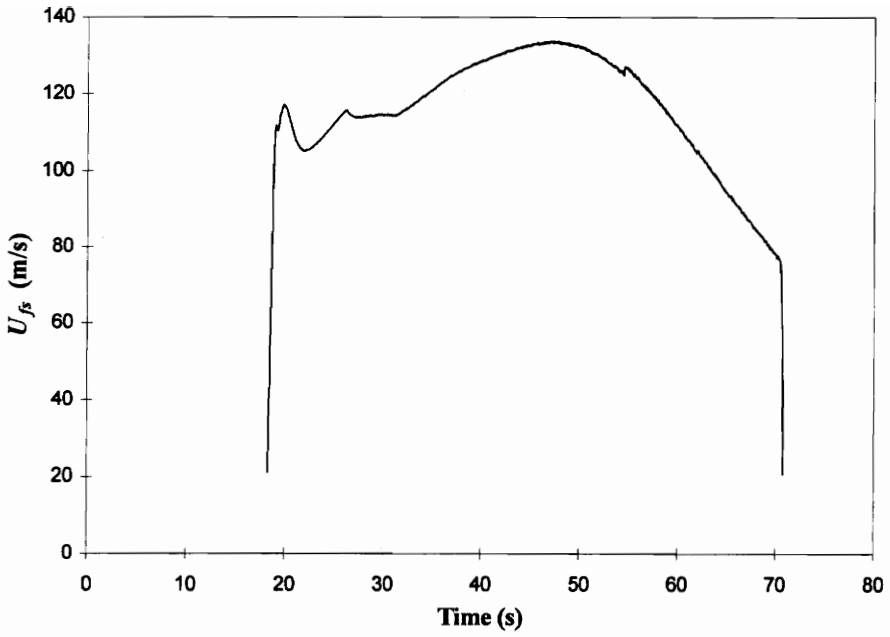


Figure C1.1 Velocity distribution - Hot-Wire Calibration run of Probe #1

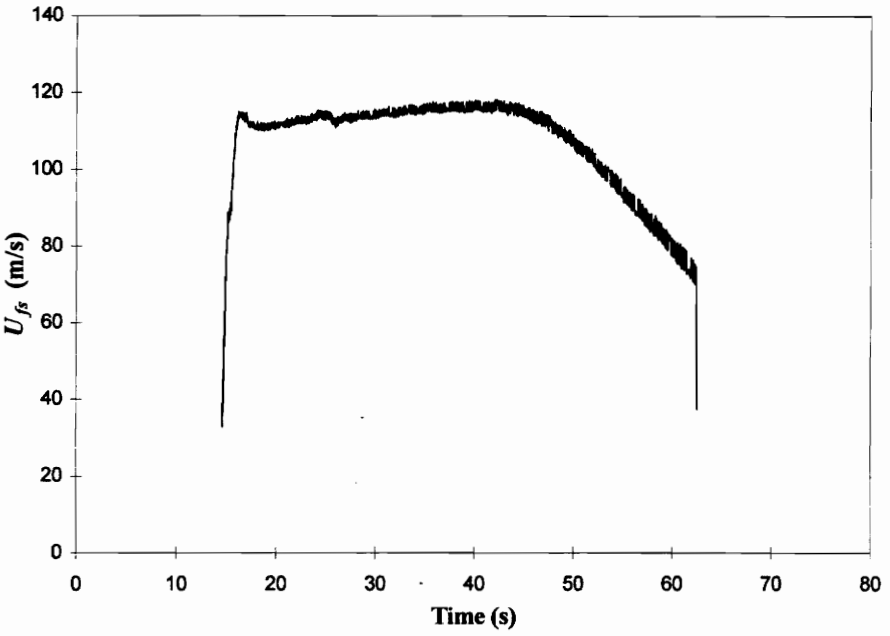


Figure C1.2 Velocity distribution-Hot-Wire Calibration of Probe #2

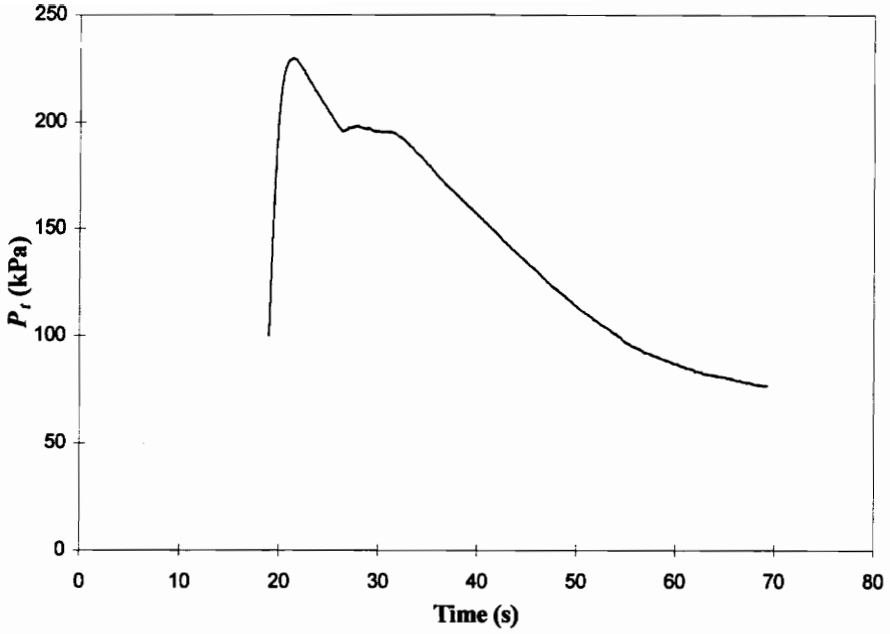


Figure C2.1 Total Pressure distribution-Hot-Wire Calibration of Probe #1

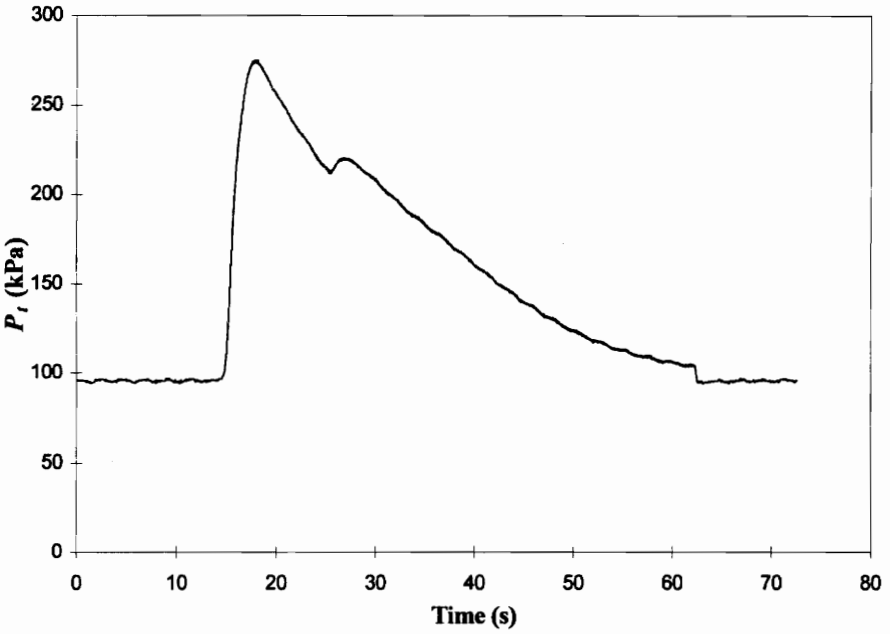


Figure C2.2 Total Pressure distribution-Hot-Wire Calibration of Probe #2

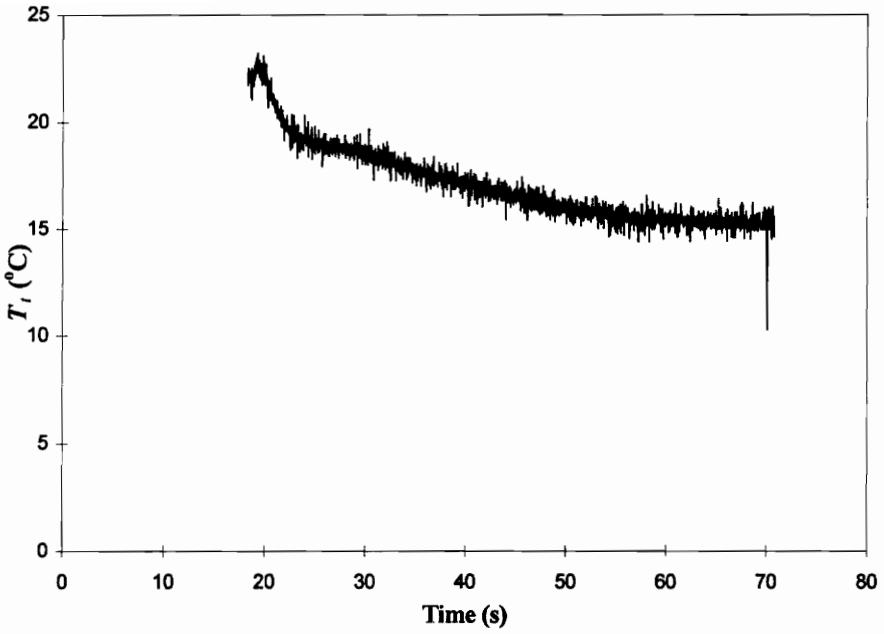


Figure C3.1 Total Temperature distribution-Hot-Wire Calibration of Probe #1

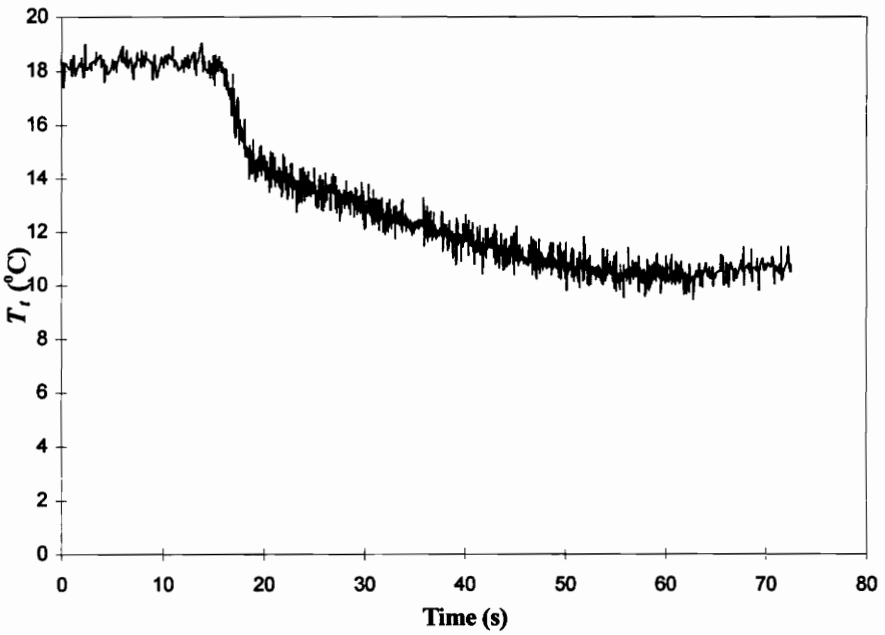


Figure C3.2 Total Temperature distribution-Hot-Wire Calibration of Probe #2

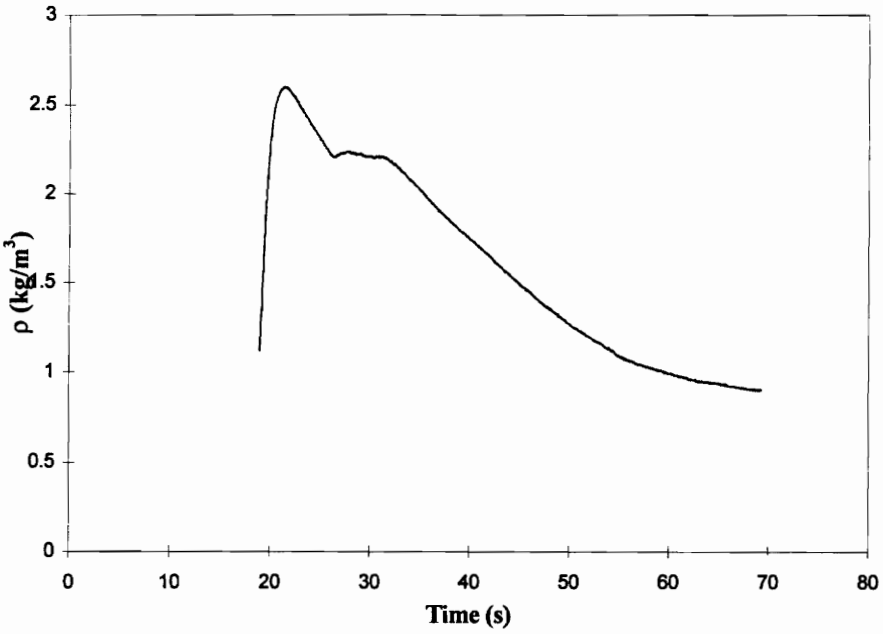


Figure C4.1 Density distribution-Hot-Wire Calibration of Probe #1

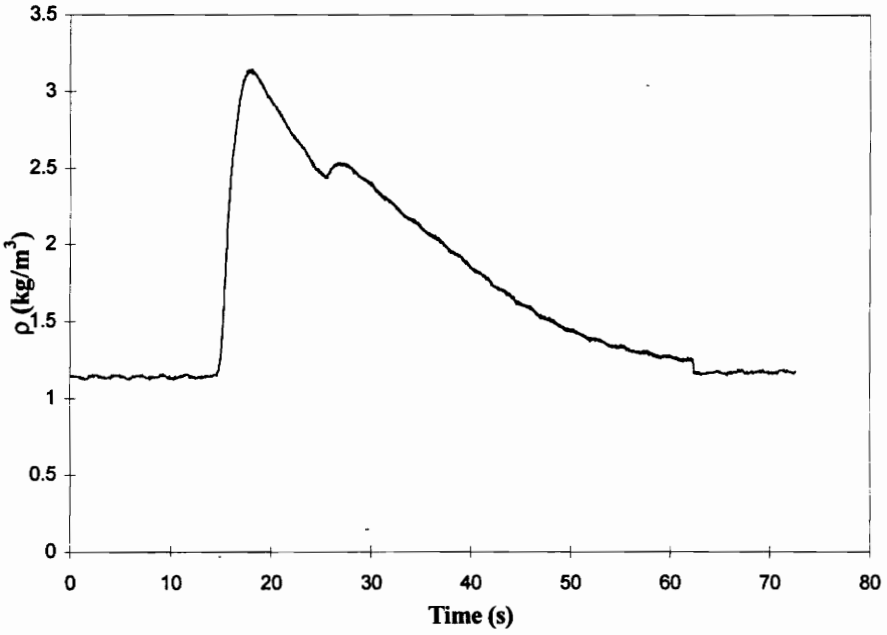


Figure C4.2 Density distribution-Hot-Wire Calibration of Probe #2

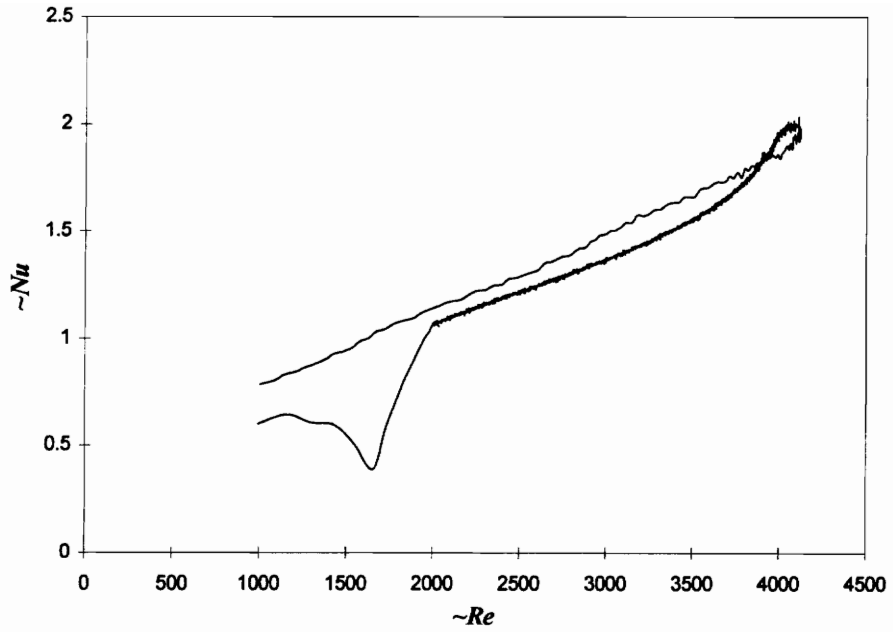


Figure C5.1 Nusselt-Reynolds distribution-Hot-Wire Calibration of Probe #1

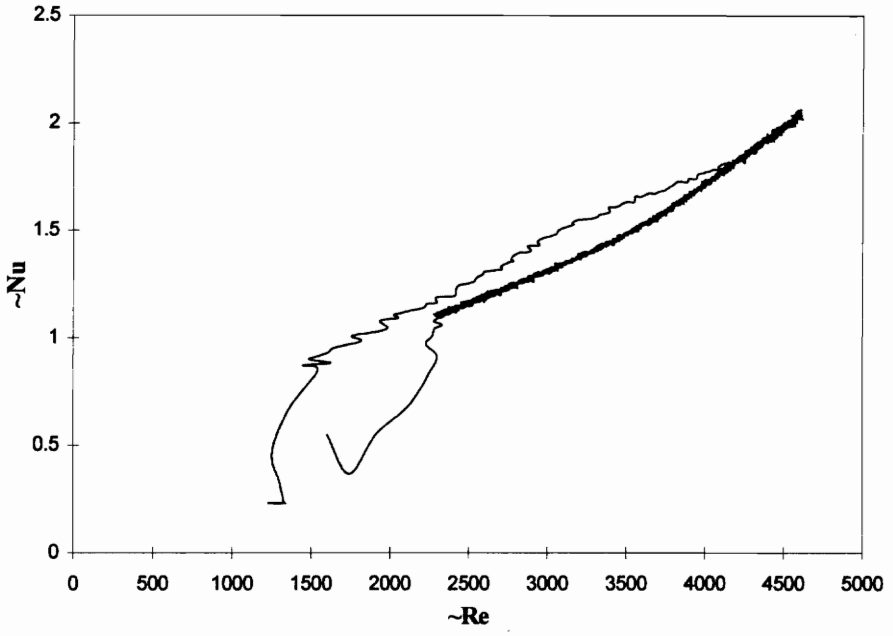


Figure C5.2 Nusselt-Reynolds distribution-Hot-Wire Calibration of Probe #2

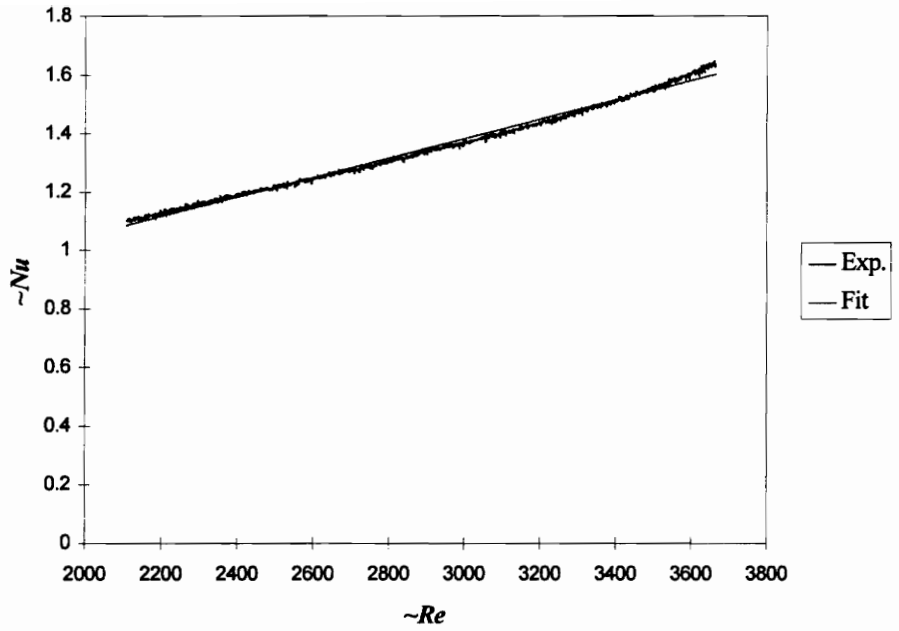


Figure C6.1 Nusselt-Reynolds Curve Fit-Hot-Wire Calibration of Probe #1

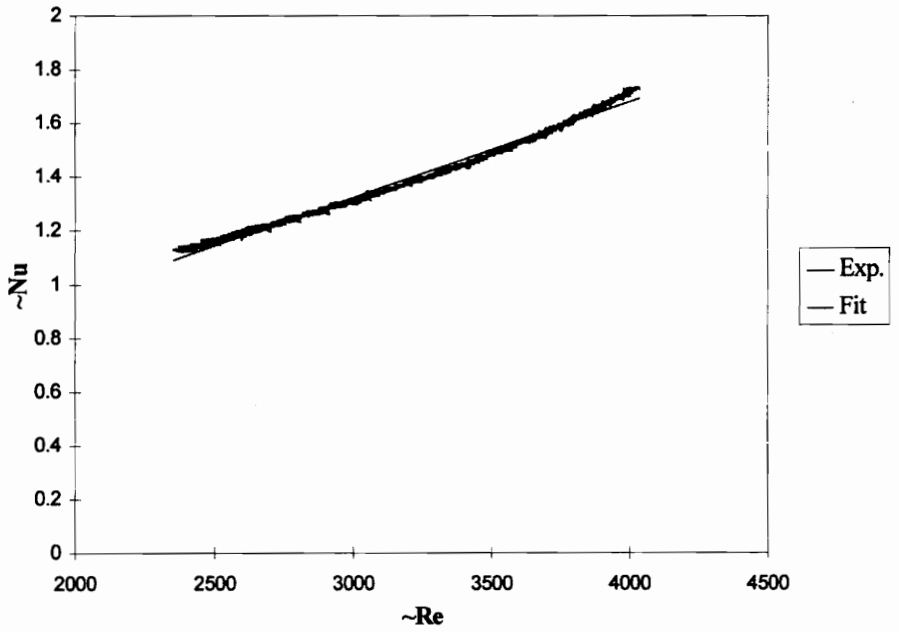


Figure C6.2 Nusselt-Reynolds Curve Fit-Hot-Wire Calibration of Probe #2

This is the point where the calibration data is acquired. There are a couple of reasons why this area of the run is chosen. The first being the fact that there is very little variation in the total temperature in this region of the run. This is very important because the calibration of the hot wire is very sensitive to variations in the temperature of the flow. Another moderately important consideration is the density of the flow being relatively constant for the calibration. There is some small variation in the density, however, it is only minor and should not affect the results drastically. Figures C5.1 and C5.2 show the Nusselt-Reynolds plot for the entire run. A small segment of this data, corresponding to the time when the total temperature and density is relatively constant, and when there is ample variation in the velocity of the flow, is used to fit a calibration equation of the form of equation C13. The data was inputted into a line fitting program, FARNSFIT, which utilizes the method of least squares to fit a line to the data. The program also yields statistical information to gain better confidence in the results. The following calibration equations were produced for the two probes:

$$\left(\frac{(V^2/k)}{(T_f - T_s)}\right)\left(\frac{T_f}{T_s}\right)^{-0.17} = 0.331926100x10^{-3}\left(\frac{\rho U}{\mu}\right)^{0.51} + 0.386898851 \qquad [C14]$$

$$\left(\frac{(V^2/k)}{(T_f - T_s)}\right)\left(\frac{T_f}{T_s}\right)^{-0.17} = 0.357786263x10^{-3}\left(\frac{\rho U}{\mu}\right)^{0.51} + 0.249702073 \qquad [C15]$$

Table C3 shows the statistical analysis provided by the program. For both of the calibrations the root mean square error and the standard deviation error is less than 2% which is well within acceptable limits. The other useful piece of statistical

**Table C3 Statistical Results for Calibration Equations**

| | Hot-Wire Probe #1 | Hot-Wire Probe #2 |
|---|---|---|
| Rms Error % | 1.345 | 1.827 |
| Std. Error % | 1.346 | 1.830 |
| Maximum Error % | 4.650 | 5.781 |
| Coeff. of Determination $R^2$ | 0.9925 | 0.9889 |

information is the coefficient of determination $R^2$. Both of the calibrations produce a coefficient of determination which approaches unity. This means a good linear relationship in the data exists, and modeling the data as a linear equation was correct.

If the assumption is made that the flow entering the test section is incompressible then the velocity can be calculated using the calibration equations above. This assumption is questionable since the Mach number entering the blade is approximately 0.36. Therefore, in certain instances the results will be presented as the velocity, $U$, and in other instances they will be presented as the product of the density and the velocity, $\rho U$. Equations C13 and C14 can be manipulated to yield the following equations which may be utilized to determine the density-velocity profile:

$$\rho U = \mu\left(3012.718795\left(\frac{(V^2/k)}{(T_f - T_s)}\right)\left(\frac{T_f}{T_s}\right)^{-0.17} - 1165.61744\right)^{(1/0.51)} \qquad [C15]$$

$$\rho U = \mu\left(2794.964769\left(\frac{(V^2/k)}{(T_f - T_s)}\right)\left(\frac{T_f}{T_s}\right)^{-0.17} - 697.9084968\right)^{(1/0.51)} \qquad [C16]$$

Again if the density is assumed to be constant, incompressible, then the velocity of the flow can be determined by moving the density to the opposite side of the equation and solving for the velocity alone.

# Appendix D

## Uncertainty Analysis

Several factors effect the uncertainty in a particular measurement. The heat flux measurements were influenced by the following: LeCroy accuracy, gain uncertainty, bias uncertainty of calibration, and zero error. The LeCroy accuracy and gain uncertainty are not easily quantified, and were assumed to be negligible. The bias uncertainty from the calibration was provided from the manufacturer, ± 10%. When comparing the various heat transfer coefficients from the different runs the bias uncertainty can be disregarded. The bias uncertainty is present in all the runs and is assumed to be constant from run to run. When comparing the heat transfer coefficients the gage precision uncertainty is of major importance. The errors related to zeroing the heat flux signal appear to be the dominant factor in determining the gage precision uncertainty.

To determine the uncertainty in the measurements the zero level offsets were entered into a spreadsheet. These values were then divided into two sections since the data was collected on two different days. The results for gage 2 will be presented here. The other gages produced similar results. The standard deviation was determined for six of the runs conducted on day one and it was determined for four of the runs conducted on day two. The values were 0.016955 V and 0.013008 V, respectively. A 95% confidence interval was then determined for different days. These values were 0.013567 V and 0.012748 V, respectively. An average 95% confidence interval was determined from the preceding values. The 95 % confidence interval for gage 2 zero offsets was determined to be 0.013164 V.

The signal from the heat flux gage varies between 0.2 and 0.3 V during a typical run. With this information the gage precision uncertainty can be determined. Using an average value of .25 V for a typical run, the following uncertainty was determined for

gage 2, ± 5%. Therefore, the uncertainty in the heat transfer measurements is ± 5%. The data and results are tabulated in Table D1.

**Table D1 Uncertainty Analysis Data**

| Day One-Zero Offsets (V) | Day Two-Zero Offsets (V) |
|---|---|
| 0.01375 | 0.0195 |
| 0.03 | 0.0275 |
| 0.04375 | 0.04955 |
| 0.04725 | 0.03775 |
| 0.0575 | |
| 0.05875 | |
| **Standard Deviation** | **Standard Deviation** |
| .016955 | 0.013008 |
| **95 % Confidence Interval** | **95 % Confidence Interval** |
| 0.013567 | 0.012748 |

# Vita

The author of this document was born in Richlands, Virginia on March 16, 1971. He and his family have lived in Honaker, Virginia the authors entire life. Growing up in a small coal town in Southwest Virginia molded him into the type of person he is today. He enjoys the simple things in life, and is especially attracted to outdoor activities such as fishing and hunting. After graduating from Honaker High School in June of 1989, he began his studies in engineering at Southwest Virginia Community College. The author attended the community college for two years, and during his summer and Christmas breaks he worked at Consolidation Coal Company. Upon graduating from the community college in May of 1991 the author was faced with the decision of where to continue his undergraduate education. The answer was obvious after visiting the Virginia Tech campus. Virginia Tech offered everything the author was looking for in a University. They had an excellent Mechanical Engineering department, and an array of outdoor activities to occupy the author's "spare time". In May of 1994, he graduated *magna cum laude* with a Bachelor of Science degree in Mechanical Engineering. The following fall, he started his graduate work at Virginia Tech working as a graduate research assistant for Dr. Wing Ng. On April 4, 1996 the author defended this work, and on April 12, 1996 he plans to be married to a very special woman, Susan Renea Puckett. They plan to move to Kingsport, Tennessee where the author has accepted a position with Eastman Chemical Company in the Process Engineering division.

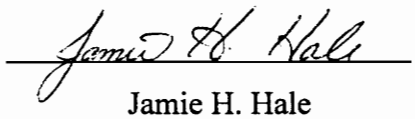

Jamie H. Hale